Technical Report No. 147

The Rectangular Cavity Slot Antenna With Homogenous Isotropic Loading

A. T. Adams

COOLEY ELECTRONICS LABORATORY

Department of Electrical Engineering
The University of Michigan

United States Air Force
Air Force Systems Command
Aeronautical Systems Division
Contract No. AF 33(657)-10607
Wright-Patterson Air Force Base, Ohio

March, 1964

Technical Report No. 147

5549-7-T

THE RECTANGULAR CAVITY SLOT ANTENNA WITH HOMOGENEOUS ISOTROPIC LOADING

by

A. T. Adams

Approved by John A. M. Lyon

COOLEY ELECTRONICS LABORATORY
Department of Electrical Engineering
The University of Michigan
Ann Arbor

Submitted in partial fulfillment of the requirements for
the degree of Doctor of Philosophy in
The University of Michigan

March 1964

ACKNOWLEDGMENTS

The author wishes to acknowledge the valuable help and encouragement of his thesis chairman, Professor John A. M. Lyon, as well as the assistance of the committee members. This report is based upon work performed on Contract No. AF 33(657)-10607. Those who assisted in the performance of the work on this project were D. K. Adams, R. M. Kalafus, J. C. Palais, W. B. Ribbens and A. I. Simanyi.

TABLE OF CONTENTS

TABLE OF CONTENTS (Cont.)

LIST OF TABLES

LIST OF ILLUSTRATIONS

LIST OF ILLUSTRATIONS (Cont.)

LIST OF ILLUSTRATIONS (Cont.)

LIST OF ILLUSTRATIONS (Cont.)

LIST OF ILLUSTRATIONS (Cont.)

LIST OF SYMBOLS

Symbol	Description	Reference
Π	Hertzian electric potential function	Eq. 2.1
Π^*	Hertzian magnetic potential function	Eq. 2.1
$\psi(xy)$	potential function	Eq. 2.6
k	material wave number	Eq. 2.1
k_o	free space wave number	Eq. 2.12
Γ_{mn}	propagation constant	Eq. 2.8
A_{mn}	mode coefficients	Eq. 2.8
B_{mn}	mode coefficients	Eq. 2.8
R	dominant mode reflection coefficient for E_x	Eq. 2.10
F	electric vector potential	Eq. 2.14
μ	relative permeability	Eq. 2.19
ϵ_r	relative permittivity	Eq. 2.20
ϵ_{mn}	number	Eq. 2.26
$G_1(x, y, \xi, \eta)$	kernel function	Eq. 2.30
D	integral function	Eq. 2.35
Y/Y_o	normalized admittance function	Eq. 2.33
G/Y_o	normalized conductance function	Eq. 2.33
B/Y_o	normalized susceptance function	Eq. 2.33
x, y, z	field point coordinates	Eq. 2.12
ξ, η, z	source point coordinates	Eq. 2.12
$\lambda, \mu, \delta, \nu$	transformed coordinates	Eq. 2.47
C_1, D_1	free space cutoff functions	Eq. 2.49
r, θ	polar coordinates	Eq. 2.51
θ_1	angle of the diagonal of the integration rectangle	Eq. 2.53

Symbol	Description	Reference
λ_1, δ_1	small rectangle dimensions	Eq. 2.53
Q	relative size of small rectangle	Eq. 2.54
f, g, d	angle functions	Eq. 2.57
a, b	rectangular waveguide dimensions	Fig. 3(a)
$F_1(\theta_1)$	configuration function	Eq. 2.65
$a_1, a_2, b_1, b_2, d_1, d_2$	iris dimensions	Fig. 7(a)
$\frac{Y_1}{Y_o}, \frac{Y_2}{Y_o}$	compound iris admittance functions	Eq. 3.5
$\frac{Y_a(d_1, d_2)}{Y_o}$	normalized aperture admittance for rectangular waveguide of dimensions d_1, d_2	Eq. 3.10
C_{fghl}	quadruple integral functions	Eq. 4.5
D_{mn}	linear equation coefficients	Eq. 4.12
Y_{mn}/Y_o	mode admittance functions	Eq. 4.20
Δ	determinant of coefficients	Eq. 4.22
C_m, D_m	free space cutoff functions	Eq. 4.26
R_{fgfg}	self reflection coefficient for (f, g) mode	Eq. 5.1
D_{fghl}	linear equation coefficients	Sec. 4.4
R_r, R_i	real and imaginary parts of the dominant mode reflection coefficient	Eq. 5.12
$R_{fgfg(r)}$	real part of self reflection coefficient for (f, g) mode	Eq. 5.20
$R_{fgfg(i)}$	imaginary part of self reflection coefficient for (f, g) mode	Eq. 5.20
$G_2(x, y, \xi, \eta)$	kernel functions	Eq. 5.30
$G_3(x, y, \xi, \eta)$	kernel functions	Eq. 5.31
$G_4(x, y, \xi, \eta)$	kernel functions	Eq. 5.32
R_m	reflection coefficient--H_x--dual problem	Eq. 5.24
R_e	reflection coefficient--E_y--dual problem	Eq. 5.26
V_i	mode voltages	Eq. 5.33

LIST OF SYMBOLS (Cont.)

Symbol	Description	Reference
Y_i	mode admittances	Eq. 5.33
λ_o	free space wavelength	Eq. 6.1
B_p	probe susceptance	Fig. 22
B'_p	transformed probe susceptance	Fig. 22
G'_p	transformed probe conductance	Fig. 22
G_p	transformed probe conductance	Fig. 22
B'_s	transformed short susceptance	Fig. 22
B_a	aperture susceptance	Fig. 22
G_a	aperture conductance	Fig. 22
$\|T\|^2$	squared magnitude of the transmission coefficient	Eq. 7.1
K	conductance-susceptance ratio	Eq. 7.2
B_I	iris susceptance	Eq. 7.3
$\overline{P}_L$	time average power dissipated	Eq. B.3
$\overline{P}_r$	time average power radiated	Eq. B.3
$\epsilon', \epsilon'', \mu', \mu''$	material constants	Eq. B.3
$\|R\|$	magnitude of reflection coefficient	Eq. B.4
θ_r	argument of reflection coefficient	Eq. B.4
α_{10}	real part of propagation constant	Eq. B.4
β_{10}	imaginary part of propagation constant	Eq. B.4
$\|A\|^2$	field constant for Region No. 2	Eq. B.5
$*$	indicates complex conjugate except when used in Π^*	Eq. B.10
R_s	surface resistivity	Eq. B.11

ABSTRACT

The rectangular cavity slot antenna, with dielectric or magnetic loading, and with a compound iris in the aperture plane, is analyzed utilizing variational techniques to derive accurate design guides for efficiency, bandwidth, and resonant frequency. The problem is broken up into several steps. First, the admittance of a loaded semi-infinite waveguide opening out into an infinite ground plane is analyzed using variational techniques. The normalized admittance is computed for a variety of values of μ_r, ϵ_r, b/a, and frequency. Next, the effect of the compound iris is analyzed. A stationary expression is obtained for the admittance of a loaded semi-infinite waveguide opening out into an infinite ground plane, with a compound iris in the aperture plane. This expression is evaluated using two different approximations of aperture field. It is shown, and verified by experiment, that the errors incurred are not serious. Finally, the effect of the feed and the finite length of the cavity are taken into account by, respectively, perturbation techniques and network transformations.

The effect of higher order modes is analyzed and shown to be minor. The results are generalized to take into account any incident higher mode. Experimental results include:

(1) Experimental verification of variational data.

(2) Measurements of aperture field.

(3) Comparison of theoretical and experimental values of bandwidth, efficiency, and resonant frequency, and beam pattern for several models loaded with ferrite powder, solid ferrite, and solid dielectric.

(4) Measurement of the effect of applied d-c magnetic field. It is shown that a solid ferrite model with a bandwidth of 2% can be tuned over a greater than 30% bandwidth.

General conclusions concerning the use of material loaded antennas are discussed. In all cases discussed, the admittance is proportional to μ_r times an integral which depends only on the product $\mu_r \epsilon_r$. For a given size reduction, or $\mu_r \epsilon_r$ product, an optimum value

of μ_r, which can be predicted, exists. The optimum value may improve bandwidth by a factor as large as 2:1 over purely dielectric loading. Similarly, for equal loss tangents, efficiency is also improved.

The analysis provides an accurate method of predicting the characteristics of loaded cavity antennas and of choosing a material for optimum antenna characteristics. The primary contributions are:

1. The derivation of accurate simplified design techniques for rectangular cavity slot antennas and the optimization of antenna characteristics.

2. Two contributions to mathematical techniques for variational calculations.

(a) Discussion and example of the use of two forms of electric field in a single variational expression.

(b) A proof that, in the problem at hand, the forbidden modes do not contribute to the admittance calculation.

3. General conclusions concerning the limitations and potentialities of loaded antennas.

4. Practical realization of several loaded cavity antennas of reduced size.

5. Two contributions to measurement techniques including (a) the measurement of aperture admittance using a wedged transition and (b) a proposed new method of measuring dielectric constant.

CHAPTER 1

INTRODUCTION

The idea of loading an antenna with dielectric or magnetic material has a certain natural appeal, yet relatively few loaded antennas are in use today. This condition arises not because loaded antennas lack useful applications, but because accurate design procedures are not available. There are many practical difficulties in the experimental use of material loading. Without accurate design guides, chances of arriving at a suitable design are not very good. In this study, the general subject of electrically small antennas will be treated. Particular emphasis will be placed upon obtaining practical antennas from the analysis of a class of electrically small dielectric or ferrite loaded structures. General conclusions concerning the potentialities and limitations of loaded antennas will be discussed.

There are several intuitive ideas about electrically small antennas that have proved useful in this study. For example, small antennas may be regarded as less "sensitive" than large antennas, in that the smaller antenna extracts less power from an incident wave. However, upon comparing the half-wave resonant dipole with the infinitesimal dipole [Fig. 1(a) and (b)] , one finds that they have essentially the same directivity. They differ primarily in their radiation impedance. The half-wave dipole has a resonant impedance of 73 ohms and a fairly low Q. The small dipole looks like a small resistor and a small capacitor in series, so it requires external tuning to yield its full available gain. When tuned, however, the small dipole has a relatively high Q. Therefore, one of the main differences between a resonant dipole and a small dipole is bandwidth. Moreover, conductor loss is far more significant for the small dipole. The ratio R_L/R_R [Fig. 1(c)] becomes large for small antennas, resulting in low efficiency. The reason for this is that R_R depends critically on the electrical size of the antenna (for a small dipole R_R is proportional to the square of its electrical length $k\ell$), whereas R_L depends primarily on the skin depth and the current distribution, both of which change relatively slowly with frequency (skin depth is roughly proportional to the -1/2 power of frequency). Thus a second import-

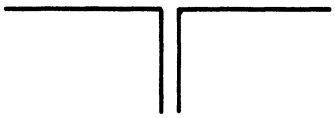

Fig. 1(a). Resonant dipole.

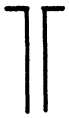

Fig. 1(b). Electrically small dipole.

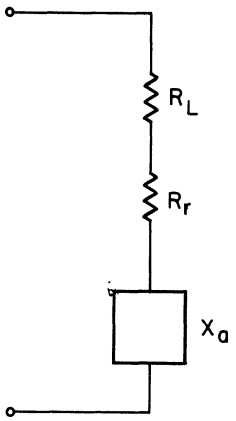

R_L = LOSS RESISTANCE
R_r = RADIATION RESISTANCE

$$EFF = \frac{R_r}{R_L + R_r}$$

Fig. 1(c). Antenna equivalent circuit.

ant difference between a resonant dipole and a small dipole is efficiency.

Some of these distinctions may be made in an alternate manner in terms of equivalent spherical transmission lines.[1,2,3,4] The field solution to any antenna problem can be expressed in terms of a complete orthogonal set of spherical line modes, each with a characteristic impedance defined in terms of the ratio of transverse electric and magnetic fields. In spherical line modes, a phenomenon similar to a cutoff effect exists, in that the ratio of the imaginary to the real part of the characteristic impedance approaches large values as the wave is confined to restricted dimensions, that is, if we consider an orthogonal set of spherical line modes with a common origin, the ratio of the imaginary to the real part of the characteristic impedance approaches infinity as r, the distance from the origin, approaches zero.

This effect is shown in Fig. 1(d) (extracted from Ref. 4) which shows a plot of the real (R_n) and the imaginary (X_n) parts of the characteristic impedance of the TM_{on} spherical line modes as a function of the electrical distance (kr) from the origin. Since the electrically small dipole pattern is identical to that of the lowest order (n = 1) radiating

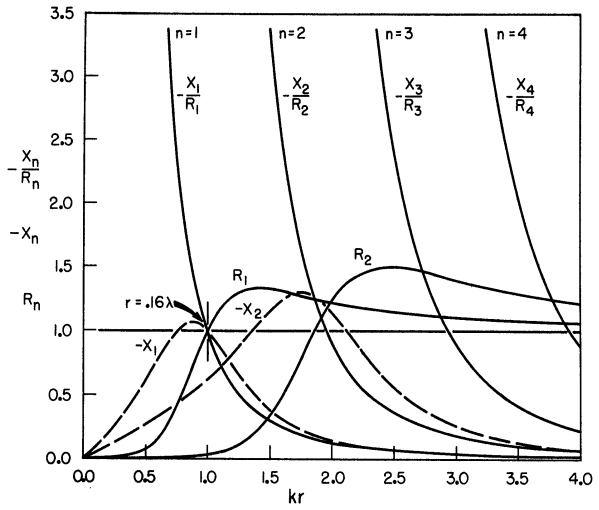

Fig. 1(d). Spherical line mode characteristic impedances.

spherical line mode, we may consider that coupling from the dipole to the higher order spherical line modes is negligible; thus the equivalent circuit of the small dipole may be represented in terms of a junction between a TEM spherical transmission line (the dipole) and the lowest order radiating spherical transmission line. The reflection coefficient at such a junction depends on (1) the ratio X_1/R_1 and (2) the characteristic impedance of the TEM transmission line. The effect of the ratio X_1/R_1 represents the basic limitations of electrically small antennas. Any attempt to launch a spherical line mode in a restricted space (kr small) automatically leads to a large X_1/R_1 ratio. The effect of the characteristic impedance of the TEM transmission line is one over which we have some degree of control and this control is used to optimize the reflection coefficient in a similar problem (Section 7. 1). Thus a basic limitation of an electrically small antenna is noted in that it must convert energy to a highly reactive free space spherical line mode.

Figure 1(e) shows three types of antennas with, respectively, material, inductive and capacitive loading. All three types have proven useful in improving antenna characteristics.[5] It is important at this point to distinguish between circuit and field effects. If these three types of loading merely add series or parallel reactance to the circuit, they are of no more use than the antenna of Fig. 1(f) with a tuner inserted in the transmission line. This suggests a critical test for any electrically small loaded antenna, namely, a comparison of efficiency and bandwidth with the loading removed and a tuner inserted in the input line.

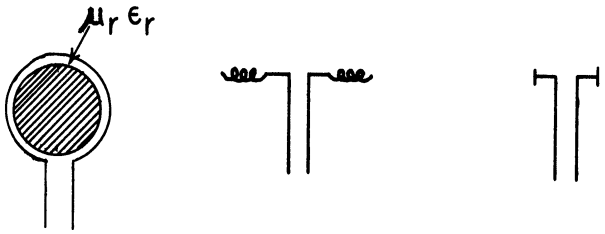

Fig. 1(e). Loaded antennas.

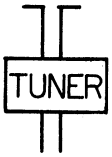

Fig. 1(f). Tuning effects.

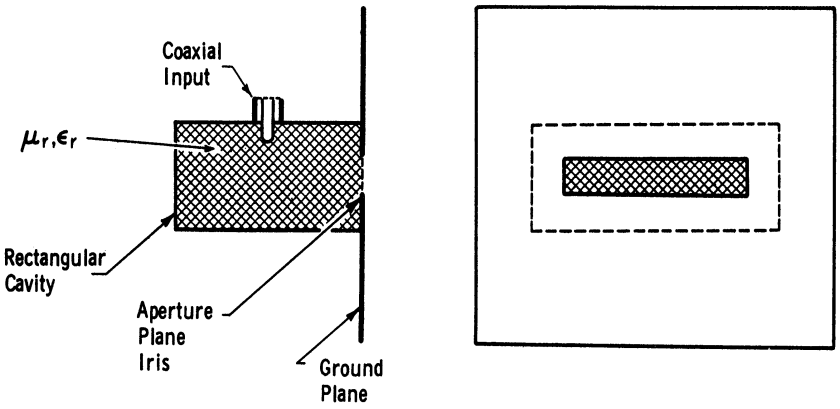

Fig. 1(g). A rectangular cavity slot antenna.

Some of these effects are brought out more clearly in a study of the loaded antenna of Fig. 1(g), which shows a probe-fed loaded rectangular waveguide opening out into a ground plane. The reflection coefficient at the aperture can be analyzed in some detail and its effect on the antenna bandwidth and efficiency predicted. This antenna has the advantages of (1) flush mounting and (2) a single-lobed radiation pattern. It can be shown, for this antenna, that loading leads to a definite advantage in the reduction of aperture reflection coefficient.

1.1 Historical Background

The literature on electrically small antennas is extensive. Interest has centered around two antenna characteristics, namely, directivity and size. Interest in increasing the directivity of antennas of a given size has led to discussions of "supergain" antennas in the literature. Several writers showed that an arbitrarily large directivity could be obtained with sources confined to a finite area or volume. This was puzzling to many, since antenna designers had realized for some time that some sort of natural limitation on antenna directivity existed. For example, experience had shown that, for a given antenna size, directivity exceeding that of a uniformly illuminated antenna was difficult to achieve.

Schelkunoff[6] and W. W. Hansen[7] were among those who first realized that arbitrarily large directivity could be obtained in theory. Bouwkamp and de Bruijn[8] proved that the directivity of a linear current distribution of fixed length can be made arbitrarily large by proper adjustment of the amplitude and phase of the current. H. J. Riblet[9] proved the analogous theorem for a two-dimensional current distribution and noted the discrepancy between theory and experiment. T. T. Taylor[10] showed that the behavior of the solution of the wave equation in spherical coordinates indicated severe practical difficulties in realizing high directivity with antennas confined to a small volume. He noted that an extremely sharp increase in reactive energy occurs as size is reduced below that of a critical "cutoff sphere." This effect corresponds to the rapid change of X_n/R_n noted before in Fig. 1(d). Associated with an antenna of high directivity will be a spherical line mode of large n and a cutoff sphere of large kr. Taylor also pointed out that such "superdirective" antennas require extremely rapid space variations of source amplitude and phase.

The discussion and analyses[11, 12] stimulated by these papers established the fact that supergain antennas are theoretically realizable, in that it is always possible to specify the source distribution necessary to produce the required far field pattern. This is evident from the Fourier transform relationship between aperture field and far field.[13] Attempts to realize supergain antennas have encountered the following difficulties:

1. The realization of the required rapid phase and amplitude variations of the source is difficult, particularly when the associated mechanical tolerances are considered.

2. Even if the proper source distribution can be realized, the severe restric-

tions noted by Taylor lead to high Q, narrow bandwidth, and low efficiency. Despite these severe difficulties, it has proven useful in some cases to accept some of these limitations in return for modest improvements in gain. An example is found in Hansen-Woodyard arrays.[14]

The history of supergain antennas may be described as an attempt to obtain high directivity with an antenna of moderate size. Alternatively, it may be described as the attempt to reduce the size of a high gain antenna while maintaining the directivity constant. A related problem is that of reducing the size of a low gain antenna while maintaining the directivity constant. While the same basic restrictions apply, they are less severe when only modest gain is required. The curve for the lowest order spherical mode changes [Fig. 1(d)] less rapidly than do those of the higher order modes; a size reduction of a given fraction results in a smaller ratio of imaginary to real parts of the impedance for a lower order mode. Thus the bandwidth and efficiency restrictions are less severe for the lower order modes. Several studies of the basic limitations of electrically small antennas have been made.[1,2,3,10,15-17]

Early in the history of microwave antennas, experiments were made with dielectric and magnetic loaded antennas in the hope of improving antenna performance or reducing antenna size.[18] Many of these experiments yielded negative results; only a few were successful. Two notable successes were the "loopstick" antenna[19] and dielectric rod antennas.[20] The loopstick antenna had increased "pickup" compared with a loop of the same dimensions without a ferrite rod, if, in both cases a capacitor in a tuned circuit connected between the antenna and receiver was adjusted for maximum receiver output. The dielectric rod antenna had a small cross-section area compared with a horn of the same gain.

It became evident that some of the simpler intuitive ideas were not adequate for the explanation of the effects associated with material loading. For instance, simple concepts associated with the shrinkage of wavelength $\lambda = \lambda_o / \sqrt{\mu_r \epsilon_r}$ were inadequate, as were attempts to explain the impedance behavior simply in terms of increasing series inductance by a factor of μ_r or capacitance by a factor of ϵ_r or in terms of a simple loaded quarter wave transformer[21] between the input transmission line and free space. Similarly, simple concepts associated with low frequency behavior may not be applicable to high frequency effects

(Chapter 7). As a further example, one unfamiliar with the limitations of electrically small antennas might assume that the use of material with $\mu_r = \epsilon_r$ would provide a reflectionless transition to free space. This is not the case; the reflection coefficient depends primarily on the free space electrical size of the antenna.

The explanation of the behavior of the dielectric rod required the solution of the wave equation in cylindrical coordinates. Explanations of the behavior of the loopstick antenna have utilized the solution of the wave equation in cylindrical, spherical, and prolate spheroidal coordinates. There has developed a divergence of opinion on the usefulness of material loading, stemming largely from encouraging mathematics, generally discouraging experiment, and the failure of loaded antenna problems to yield to simple analysis or intuition.

1.2 Review of the Literature

Since the early days of radar, a number of theoretical studies of loaded antennas have been made utilizing classical methods[22-29] to treat separable geometries, such as the loop antenna loaded with a ferrite sphere,[23-27] cylinder,[22] or spheroid,[22,23] the biconical antenna loaded with a ferrite sphere[24,29] and the small dipole loaded with a ferrite sphere.[28] These studies have certain characteristics in common. They all show resonant increases in radiation resistance, indicating the possibility of increased efficiency. Because of the difficulties inherent in dealing with Bessel and Legendre functions of complex arguments, most of these results have not been extended to take efficiency and bandwidth for lossy media into account. In addition, any antenna whose dimensions are infinitesimal at any point[24,28,29] is not suited to efficiency analysis because of infinite energy storage, which results in zero efficiency for any finite σ, ϵ'', or μ''. Thus, the classical studies have aroused considerable interest in loading of antennas. However, because of their highly idealized nature, and the complexity of the mathematics, it has not been possible to answer in detail these basic questions:

(1) For a given metal conductivity, what material characteristics are necessary to improve efficiency?

(2) Can bandwidth be increased?

(3) What types of trade-off are possible between bandwidth, size, and efficiency?

Variational techniques have been used to analyze a number of antennas, both

loaded and unloaded.[30-39] Lewin[30] has derived a stationary expression for the impedance of a waveguide (unloaded) radiating out into free space and has plotted curves for G and B as a function of waveguide dimensions. Many of the mathematical techniques used in this thesis are similar to those used throughout Lewin's book. Cohen, Crowley, and Levis[36] have solved the same problem, taking dielectric loading into account, and have published data on admittance for several values of b/a. The impedance of an unloaded rectangular waveguide opening out into an infinite ground plane has been studied by several other methods.[40,41] In Volume 10 of the Rad. Lab. Series,[42] the impedance of a waveguide opening out into a restricted space is analyzed for several different geometries. Levine and Papas[31] have analyzed the admittance of an unloaded coaxial line opening out into an infinite ground plane (circular diffraction antenna). Galejs[33,34] has made a theoretical analysis of the dielectric loaded annular slot antenna utilizing variational techniques. He has also analyzed the impedance properties of a dielectric loaded rectangular cavity antenna feeding a thin slot in an infinite ground plane. M. H. Cohen[36] studied transient phenomena to analyze the Q of cavity antennas and compared theoretical and experimental data on cavity Q for a square waveguide cavity. A number of analyses of loaded cavity antennas have been made utilizing other techniques. Counter[43] has analyzed a loaded cavity by considering the cavity to be half of a closed (parent) cavity, with fields identical in the two cases. Tector[44] has made an experimental investigation of air loaded cavity antennas. Recently, integral transform and Wiener-Hopf techniques have been applied to loaded and unloaded antennas;[45-48] much of this literature might be included under the subject of "Surface Wave Antennas."

Under the impetus of these theoretical approaches, several types of dielectric and ferrite loaded antennas have evolved.[49-58] The use of materials with relative permeability and relative permittivity greater than one provides an additional degree of freedom in the parameters μ_r, ϵ_r. It would indeed be surprising if optimum results were always obtained with $\mu_r = \epsilon_r = 1$. However, the use of material loading is limited. No panacea is provided for small antenna problems.

1.3 Statement of the Problem

A particular type of material loaded antenna, shown in Fig. 1(g) is analyzed in this paper. The antenna is a rectangular cavity, fed by any one of a number of coaxial probe

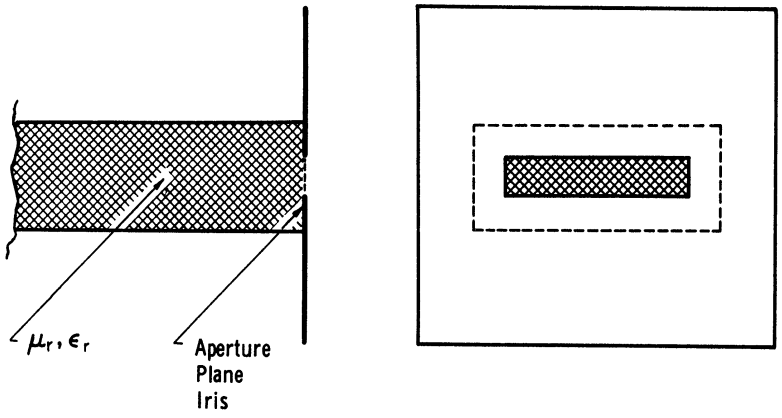

Fig. 2. Material loaded rectangular waveguide radiator with aperture plane iris.

arrangements, and opening out into a ground plane. A compound iris is located in the aperture plane. This antenna is studied by means of the model shown in Fig. 2. This model consists of a semi-infinite waveguide loaded with material of characteristics μ_r, ϵ_r opening out into an infinite ground plane, with a compound iris in the aperture plane. The problem is further simplified by analyzing the antenna of Fig. 3(a) (no iris in the aperture plane) and then taking the compound iris into account with a separate calculation. The input admittance is analyzed by variational techniques. The finite length of the antenna shown in Fig. 1 is taken into account by simple transmission-line calculations. The effects of the particular type of feed is taken into account by perturbation calculations. The finite size of the ground plane has little effect on the admittance, bandwidth, efficiency, and resonant frequency, although its effect on the E plane beam pattern is significant. Predictions of bandwidth, efficiency, impedance, resonant frequency, and beam pattern show good agreement with experimental data.

In Chapter 2, a stationary expression for the normalized aperture admittance of the antenna of Fig. 3(a) is obtained. The dominant mode aperture field approximation is made and the expression is reduced to a double integral form suitable for computation. This expression is evaluated by computer for a variety of values of μ_r, ϵ_r, b/a (ratio of waveguide dimensions), and frequency, with increments small enough to allow accurate interpolation. Approximate expressions are obtained for large values of $\mu_r\epsilon_r$. In Chapter 3, the compound iris is analyzed by variational techniques. The compound iris problem is split into two problems, one of which is solved in the literature and the other of which can be

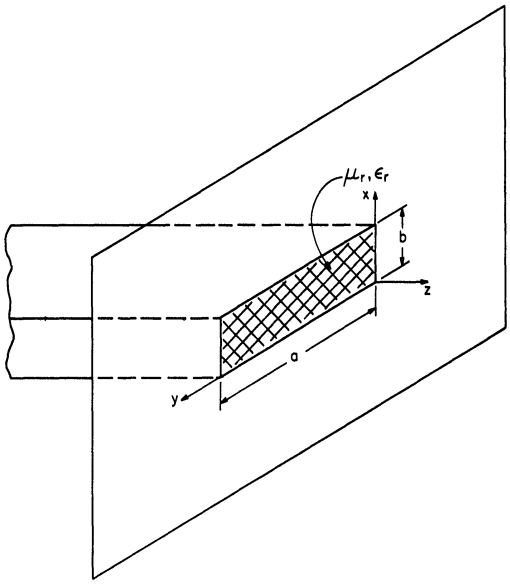

Fig. 3(a). Material loaded rectangular waveguide radiator.

related to the problem already solved in Chapter 2. The solution of the problem of Chapter 2 below dominant mode cutoff is required in some cases. In Chapter 4, the effect of higher order modes is analyzed. A general expression for the aperture field, involving an infinite number of higher order modes with unknown coefficients, is substituted into the variational expression. Using the condition for stationarity, an infinite number of simultaneous linear equations in the unknown mode coefficients is obtained. An expression for the admittance in terms of a linear combination of the unknown mode coefficients is obtained. The infinite set of equations is truncated for certain specific choices of higher order modes and computation of the mode coefficients and the correction term for admittance is carried out. Certain modes are forbidden by symmetry considerations and it is shown that these modes have no effect on the variational expression for admittance. In Chapter 5, certain generalizations of the method are considered. Among these are:

(1) other modes incident

(2) other cylindrical geometries

(3) below cutoff effects.

It is noted that variational expressions can be obtained for any mode incident. These expressions all have a form which consists of μ_r times a double integral which is a function only of

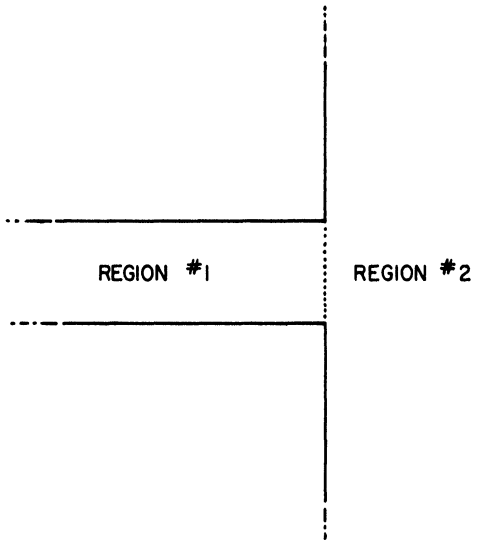

Fig. 3(b). Regions of a boundary value problem.

$\mu_r \epsilon_r$. In Chapter 6, experimental results are described. The variational admittance data of the antenna of Fig. 3(a) are verified experimentally for several values of ϵ_r. The admittance of the antenna of Fig. 2 is verified experimentally for both inductive and capacitive irises. Simplified methods for predicting bandwidth, efficiency, resonant frequency, and beam pattern are described and compared with experimental results for several dielectric and ferrite loaded models. Aperture field measurements of several ferrite loaded waveguide models are described.

The results of the analysis and experiments indicate that gross assumptions may be made concerning aperture field, feed admittance, feed location, modes present in the cavity, and the application of transmission-line theory without serious inaccuracy in the results. Chapter 7 contains general conclusions concerning the limitations and potentialities of material loaded antennas.

CHAPTER 2

RADIATION FROM A WAVEGUIDE FILLED WITH ISOTROPIC FERRITE MATERIAL

2.1 Introduction

This chapter outlines the first steps in the solution by a variational technique of the radiating characteristics of a material loaded antenna. The physical configuration is shown in Fig. 1(g). The antenna consists of a rectangular loaded cavity open on one end, fed by a coaxial probe arrangement, and opening out into a ground plane, with a compound iris located in the aperture plane. The problem can be simplified to the antenna of Fig. 2 by (a) perturbational techniques taking the feed configuration into account and (b) network transformations to take into account the finite size of the cavity. The antenna of Fig. 2 consists of a semi-infinite waveguide with a dominant mode wave incident from the left and a compound iris located in the aperture plane. The problem can be further simplified to the antenna of Fig. 3(a). In Chapter 3, it will be shown that corrections can be made to the solution of the antenna of Fig. 3(a) to take into account the compound iris in the aperture plane.

Consider the antenna of Fig. 3(a). The rectangular waveguide is semi-infinite and extends from $z = -\infty$ to $z = 0$. The waveguide is completely filled with isotropic, homogeneous material of characteristics μ_r, ϵ_r. The assumption that the material is isotropic and linear is equivalent in most ferrite materials to assumptions that

(a) the applied d-c magnetic field is zero, and

(b) the signal is small compared with the saturation magnetization.

The flange is assumed to be infinite in x and y directions. It will be shown later that the finite size of the flange has only a minor effect on impedance properties, resonant frequency, bandwidth, and efficiency, although its effect on beam pattern may be significant. It is not necessary to assume that the frequency of excitation and the size of the waveguide are chosen so that all waveguide modes except the dominant (TE_{10}) mode are cut off, although the network transformations introduced later are more reliable in this region.

Assume a dominant mode wave incident from the left. It will be shown later that the analysis can be generalized to take into account any incident mode.

Information sought includes the complex dominant mode reflection coefficient and the aperture fields as a function of μ_r, ϵ_r, and frequency. The far field beam pattern, the bandwidth, the efficiency, the resonant frequency, and the maximum effective aperture of the finite radiator of Fig. 1 are also of interest.

Assuming that there is no E_y, the fields can be derived from Hertzian vectors Π^* of magnetic type with a single component in the y direction. The problem is split up into two regions [Fig. 3(b)], Region No. 1 including the semi-infinite waveguide and Region No. 2 including the half space $z > 0$. In each region a general solution is constructed.

2.2 General Field Solutions

2.2.1 Region No. 1--Waveguide Fields. The fields in the waveguide satisfy the wave equation for the Hertzian potentials:

$$\begin{aligned} (\nabla^2 + k^2)\, \Pi \;(x,y,z) &= 0 \\ (\nabla^2 + k^2)\, \Pi^* (x,y,z) &= 0 \end{aligned} \tag{2.1}$$

where the electric and magnetic fields are:

$$\begin{aligned} \underline{E} &= \nabla \times \nabla \times \Pi - j\omega\mu\, \nabla \times \Pi^* \\ \underline{H} &= j\omega\epsilon\, \nabla \times \Pi + \nabla \times \nabla \times \Pi^* \end{aligned} \tag{2.2}$$

If we expand the above expressions in rectangular coordinates, it becomes apparent that, if

$$\Pi_x^* = \Pi_z^* = \Pi = 0 \;, \tag{2.3}$$

E_y will be zero and all of the other components will in general be nonzero. Similarly, if $\Pi_x = \Pi_z = \Pi^* = 0$ then H_y will be zero and all other components will in general be nonzero. This corresponds to the fact that the total field can be broken up into LSE (longitudinal section electric) modes and LSH (longitudinal section magnetic) modes derived from, respectively Π_y^* and Π_y vectors. Similarly the total field could be broken up into LSE and LSH modes derived from Hertzian magnetic and electric vectors in the x direction, or into TM and TE modes derived from Hertzian magnetic and electric vectors in the z direction.

In our problem, since there is no E_y, the fields can be derived from a Hertzian magnetic vector Π_y^*. The fields are then

$$\begin{aligned} \underline{E} &= -j\omega\mu \nabla \times \Pi_y^* \hat{y} \\ \underline{H} &= \nabla \times \nabla \times \Pi_y^* \hat{y} \end{aligned} \tag{2.4}$$

Solving for Π_y^*:

$$(\nabla^2 + k^2)\, \Pi_y^* \quad \hat{y} = 0 \tag{2.5}$$

where

$$\Pi_y^* = \psi(x,y)\, e^{\pm \Gamma z}$$

$$(\nabla^2 + k^2)\, \psi(x,y)\, e^{\pm \Gamma z}$$

$$\left[\frac{\partial^2}{\partial x^2} + \frac{\partial^2}{\partial y^2} + (k^2 + \Gamma^2) \right] \psi(x,y) = 0$$

$$(\nabla_\tau + k_c^2)\, \psi(x,y) = 0$$

where

$$\nabla_\tau = \frac{\partial^2}{\partial x^2} + \frac{\partial^2}{\partial y^2}$$

$$(\nabla_\tau^{\,2} + k_c^2)\, X(x)\, Y(y) = 0$$

$$\frac{\ddot{X}}{x} + \frac{\ddot{Y}}{y} = -k_c^{\,2}$$

$$\frac{\ddot{X}}{x} + k_c^2 = -\frac{\ddot{Y}}{y} = k_y^2$$

$$\ddot{X} + (k_c^2 - k_y^2)\, X = 0 = \ddot{X} + k_x^2\, X$$

$$\ddot{Y} + k_y^2 Y = 0$$

$$\psi(x,y) = \left\{ \begin{matrix} \cos k_x X & \cos k_y y \\ \sin k_x X & \sin k_y y \end{matrix} \right\} \tag{2.6}$$

Applying boundary conditions to $\psi(x,y)$:

$$\psi(x,y) = \{\sin k_y y\}\{\cos k_x x\} \tag{2.7}$$

$$\Pi_1^* = \sum_{m=0}^{\infty} \sum_{n=0}^{\infty} \frac{A_{mn}}{\Gamma_{mn}} \sin \frac{m\pi y}{a} \cos \frac{n\pi x}{b} e^{\Gamma_{mn} z}$$

$$+ \sum_{m=0}^{\infty} \sum_{n=0}^{\infty} \frac{B_{mn}}{\Gamma_{mn}} \sin \frac{m\pi y}{a} \cos \frac{n\pi x}{b} e^{-\Gamma_{mn} z} \tag{2.8}$$

We have chosen the mode coefficients to be A_{mn}/Γ_{mn} for convenience.

$$\Gamma_{mn}^2 = (k_c)_{mn}^2 - k^2, \quad \Gamma_{mn} = j\beta_{mn}$$

$$k_y = \frac{m\pi}{a}$$

$$k_x = \frac{n\pi}{b}$$

$$k_c^2 = k_x^2 + k_y^2 = \frac{m^2\pi^2}{a^2} + \frac{n^2\pi^2}{b^2}$$

$$k^2 = \omega^2 \mu\epsilon$$

$$\Gamma_{mn}^2 = \frac{m^2\pi^2}{a^2} + \frac{n^2\pi^2}{b^2} - \omega^2 \mu\epsilon$$

with the assumption of a single dominant mode wave incident from the left, this becomes:

$$\Pi_1^* = \sum_{m=0}^{\infty} \sum_{n=0}^{\infty} \frac{A_{mn}}{\Gamma_{mn}} \sin \frac{m\pi y}{a} \cos \frac{n\pi x}{b} e^{\Gamma_{mn} z} + \frac{B_{10}}{\Gamma_{10}} \sin \frac{\pi y}{a} e^{-\Gamma_{10} z} \tag{2.9}$$

we make the following choices to simplify the form of E_{x1}:

$$B_{10} = \frac{1}{\omega\mu\beta_{10}} \quad \text{(implies a choice of the magnitude of the incident wave)}$$

$$A_{10} = \frac{-R}{\omega\mu\beta_{10}}$$

R = reflection coefficient for dominant mode E_x.

with these definitions:

$$\Pi_1^* = \frac{1}{-j\omega\mu}\left[\frac{(e^{-\Gamma_{10}z} - R\, e^{\Gamma_{10}z})}{\Gamma_{10}} \sin\frac{\pi y}{a} + \sum_{m=1}^{\infty}\sum_{n=0}^{\infty'} \frac{A_{mn}}{\Gamma_{mn}} \sin\frac{m\pi y}{a} \cos\frac{n\pi x}{b}\, e^{\Gamma_{mn}z}\right] \quad (2.10)$$

$$E_{x1} = \left(e^{-\Gamma_{10}z} + R\, e^{\Gamma_{10}z}\right)\sin\frac{\pi y}{a} - \sum_{m=1}^{\infty}\sum_{n=0}^{\infty'} A_{mn} \sin\frac{m\pi y}{a} \cos\frac{n\pi x}{b}\, e^{\Gamma_{mn}z} \quad (2.11)$$

where the prime on the double summation indicates that the 1, 0 term has already been removed.

2.2.2 Region No. 2--Fields in Half Space. The Hertzian potential in Region No. 2 may be expressed as:

$$\Pi_2^*(x,y,z) = -\frac{1}{2j\omega\mu_o\pi}\int_o^a\int_o^b f(\xi,\eta)\,\frac{e^{-jkr}}{r}\,d\xi\,d\eta \quad (2.12)$$

where $r = \sqrt{(x-\xi)^2 + (y-\eta)^2 + z^2}$, the distance between source and field point, and $f(\xi,\eta)$ is an arbitrary source function. It can be shown[59,60] that:

$$f(\xi,\eta) = E_x(\xi,\eta) \quad (2.13)$$

where

$$E_x(\xi,\eta) = E_x(\xi,\eta,0)$$

An alternate method of deriving the potential function is as follows: The aperture fields can

be replaced with a magnetic current sheet $\underline{M}_s = \underline{E} \times \underline{n}$ backed by a conductor.[61]

Then the method of images can be used to replace the original problem with a magnetic current sheet $\underline{M}_s = 2\underline{E} \times \underline{n}$. In this case our only sources are magnetic sources, so that the fields can be derived from an electric vector potential F.[62]

$$E = -\nabla \times F \tag{2.14}$$

$$\underline{F} = \frac{1}{4\pi} \int_0^a \int_0^b \underline{M} \frac{e^{-jkr}}{r} \, ds$$

$$= \frac{1}{4\pi} \int_0^a \int_0^b 2\underline{E} \times \underline{n} \frac{e^{-jkr}}{r} \, dx \, dy \tag{2.15}$$

$$\underline{F} = -\left(\frac{1}{2\pi} \int_0^a \int_0^b E_x \frac{e^{-jkr}}{r} \, dx \, dy \right) \cdot \hat{y}$$

$$F_y = -\frac{1}{2\pi} \int_0^a \int_0^b E_x \frac{e^{-jkr}}{r} \, dx \, dy \tag{2.16}$$

$$F_z = F_x = 0 \tag{2.17}$$

The F functions used here are related by a constant to the Π^* functions, just as the vector potential A is related by a constant to the vector potential Π.

$$E = +\nabla \times \left(\frac{1}{2\pi} \int_0^a \int_0^b E_x \frac{e^{-jkr}}{r} \, dx \, dy \right) \cdot \hat{y} \tag{2.18}$$

This definition of the electric field agrees with that derived from the Hertzian potential function Π_2^*. It is interesting to note here that the planar geometry greatly simplifies the analysis. If the geometry of the plate was such that image method could not be used, then the representation of the fields would involve the Green's function for that geometry instead of the free space Green's function used here.

2.3 Derivation of Variational Expression for Admittance

In this section the E_x and H_y fields are equated at the boundary between Regions 1 and 2, the unknown mode coefficients A_{mn} are eliminated, and an integral equation for the

aperture field $E_x(x,y)$ is obtained. Then a variational expression for the normalized aperture admittance $Y/Y_0 = (1-R)/(1+R)$ is obtained from the integral equation.

Boundary Conditions

We have already included the boundary condition that tangential E fields go to zero on the plate in our expression for Π_2^* [Eq. (2.12)].

$$\frac{\partial \Pi_1^*}{\partial z} = \frac{\partial \Pi_2^*}{\partial z} \frac{1}{\mu_r} \tag{2.19}$$

$$\frac{\partial \Pi_1^*}{\partial x} = \frac{\partial \Pi_2^*}{\partial x} \frac{1}{\epsilon_r \mu_r} \tag{2.20}$$

$$\frac{\partial^2 \Pi_1^*}{\partial y \partial x} = \frac{\partial^2 \Pi_2^*}{\partial y \partial x} \tag{2.21}$$

$$\left(\frac{\partial^2}{\partial y^2} + k^2 \right) \Pi_1^* = \left(\frac{\partial^2}{\partial y^2} + k_o^2 \right) \Pi_2^* \tag{2.22}$$

$$\frac{\partial^2 (\Pi_1^* - \Pi_2^*)}{\partial y \partial x} = 0 \tag{2.23}$$

where μ_r, ϵ_r are relative permeability and relative permittivity.

$$\epsilon = \epsilon_r \epsilon_o$$

$$\mu = \mu_r \mu_o$$

We wish to form the quantity (1-R/1+R). Differentiation with respect to z yields a 1+R term and differentiation with respect to x or y yields a 1-R term. We will use boundary conditions (2.19) and (2.22).

$E_{x1} = E_{x2}$ (at z = 0):

$$E_x(x,y) = \left[(1+R) \sin \frac{\pi y}{a} - \sum_{m=1}^{\infty} \sum_{n=0}^{\infty}{}' A_{mn} \sin \frac{m\pi y}{a} \cos \frac{n\pi x}{b} \right] \tag{2.24}$$

Multiplying Eq. (2.24) by $\sin \pi y/a$ and integrating over the aperture:

$$(1+R) = \frac{2}{ab} \int_0^a \int_0^b E_x(\xi,\eta) \sin \frac{\pi\eta}{a} \, d\xi \, d\eta \tag{2.25}$$

multiplying Eq. (2.24) by $\sin \frac{m'\pi y}{a} \cos \frac{n'\pi x}{b}$ and integrating over the aperture:

$$\int_0^a \int_0^b E_x(\xi,\eta) \sin \frac{m'\pi\eta}{a} \cos \frac{n'\pi\xi}{b} \, d\xi \, d\eta = - A_{m'n'} \frac{ab}{4\epsilon_{m'n'}} \tag{2.26}$$

where

$$\epsilon_{mn} = \frac{1}{2} \quad (n=0)$$

$$= 1 \quad (n \neq 0)$$

switching from primed to unprimed notation:

$$A_{mn} = \frac{-4\epsilon_{mn}}{ab} \int_0^a \int_0^b E_x(\xi,\eta) \sin \frac{m\pi\eta}{a} \cos \frac{n\pi\xi}{b} \, d\xi \, d\eta \tag{2.27}$$

$\underline{H_{y1} = H_{y2}}$ at $z = 0$:

$$- \frac{1}{j\omega\mu} \left[\left(k^2 - \frac{\pi^2}{a^2} \right) \sin \frac{\pi y}{a} \left(\frac{1-R}{\Gamma_{10}} \right) \right.$$

$$\left. + \left(\frac{\partial^2}{\partial y^2} + k^2 \right) \sum_{m=1}^{\infty} {\sum_{n=0}^{\infty}}' \frac{A'_{mn}}{\Gamma_{mn}} \sin \frac{m\pi y}{a} \cos \frac{n\pi x}{b} \right]$$

$$= \frac{-1}{2\pi j\omega\mu_o} \left[\int_0^a \int_0^b E_x(\xi,\eta) \left(\frac{\partial^2}{\partial y^2} + k_o^2 \right) \frac{e^{-jk_o r}}{r} \, d\xi \, d\eta \right] \tag{2.28}$$

Substituting for A_{mn} from (2.27):

$$\frac{1}{2\pi}\int_0^a\int_0^b E_x(\xi,\eta)\left(\frac{\partial^2}{\partial y^2}+k_o^2\right)\frac{e^{-jk_o r}}{r}\,d\xi\,d\eta$$

$$= -\sin\frac{\pi y}{a}\,\frac{(1-R)\,\Gamma_{10}}{\mu_r} - \sum_{m=1}^{\infty}\sum_{n=0}^{\infty}{}'\,\frac{4\epsilon_{mn}}{ab\mu_r\Gamma_{mn}}\left[\int_0^a\int_0^b E_x(\xi,\eta)\right.$$

$$\left.\sin\frac{m\pi\eta}{a}\cos\frac{n\pi\xi}{b}\,d\xi\,d\eta\right]\left(\frac{\partial^2}{\partial y^2}+k^2\right)\sin\frac{m\pi y}{a}\cos\frac{n\pi x}{b} \qquad (2.29)$$

Interchanging the order of summation and integration and transposing:

$$\int_0^a\int_0^b E_x(\xi,\eta)\underbrace{\left[\left(\frac{\partial^2}{\partial y^2}+k_o^2\right)\left(\frac{e^{-jk_o r}}{2\pi r}\right)+\left(\frac{\partial^2}{\partial y^2}+k^2\right)\sum_{m=1}^{\infty}\sum_{n=0}^{\infty}{}'\,\frac{4\epsilon_{mn}}{ab\mu_r\Gamma_{mn}}\sin\frac{m\pi\eta}{a}\cos\frac{n\pi\xi}{b}\sin\frac{m\pi y}{a}\cos\frac{n\pi x}{b}\right]}_{G_1(x,y,\xi,\eta)}d\xi\,d\eta$$

$$= -\sin\frac{\pi y}{a}\,\frac{(1-R)\Gamma_{10}}{\mu_r} \qquad (2.30)$$

$$\int_0^a\int_0^b E_x(\xi,\eta)\,G_1(x,y,\xi,\eta)\,d\xi\,d\eta = -\sin\frac{\pi y}{a}\,\frac{(1-R)\Gamma_{10}}{\mu_r} \qquad (2.31)$$

Multiplying by $E_x(x,y)$ and integrating over the aperture:

$$1-R = -\frac{\mu_r\int_0^a\int_0^b\int_0^a\int_0^b E_x(x,y)\,E_x(\xi,\eta)\,G_1(x,y,\xi,\eta)\,dx\,dy\,d\xi\,d\eta}{\Gamma_{10}\int_0^a\int_0^b E_x(x,y)\sin\frac{\pi y}{a}\,dx\,dy} \qquad (2.32)$$

Dividing (2.32) by (2.25):

$$\frac{1-R}{1+R} = \frac{-ab\mu_r}{2\Gamma_{10}}\,\frac{\int_0^a\int_0^b\int_0^a\int_0^b E_x(x,y)\,G_1(x,y,\xi,\eta)\,E_x(\xi,\eta)\,dx\,dy\,d\xi\,d\eta}{\left[\int_0^a\int_0^b E_x(x,y)\sin\frac{\pi y}{a}\,dx\,dy\right]^2} = \frac{Y}{Y_o} = \frac{G}{Y_o}+\frac{jB}{Y_o} \qquad (2.33)$$

This is the final variational expression for the input admittance. Upon setting $\mu = \mu_o$, $\epsilon = \epsilon_o$, this expression agrees with Lewin.[63] It will now be shown that this expression is stationary.

Proof of Stationarity:

Elimination of R from Eqs. (2.25) and (2.31):

$$\int_0^a \int_0^b E_x(\xi,\eta)\, G_1(x,y,\xi,\eta)\, d\xi\, d\eta = -\sin\frac{\pi y}{a}\,\frac{(1-R)\Gamma_{10}}{\mu_r}$$

$$= -\sin\frac{\pi y}{a}\,\frac{\Gamma_{10}}{\mu_r}\left(-\frac{2}{ab}\int_0^a\int_0^b E_x(\xi,\eta)\,\sin\frac{\pi\eta}{a}\,d\xi\,d\eta + 2\right) \tag{2.34}$$

$$\int_0^a \int_0^b E_x(\xi,\eta)\, G_1(x,y,\xi,\eta)\, d\xi\, d\eta = -\frac{2\Gamma_{10}}{\mu_r}\sin\frac{\pi y}{a}\left(1-\frac{D}{ab}\right) \tag{2.35}$$

where

$$D = \int_0^a\int_0^b E_x(\xi,\eta)\,\sin\frac{\pi\eta}{a}\,d\xi\,d\eta = \int_0^a\int_0^b E_x(x,y)\,\sin\frac{\pi y}{a}\,dx\,dy$$

This is an integral equation for $E_x(\xi,\eta)$. Consider small variations $\delta E_x(\xi,\eta)$ from the correct value as determined by (2.35). Taking the first variation of (2.33) gives:

$$\delta y = -\frac{ab\mu_r}{2\Gamma_{10}}\,\delta\left(\frac{\int_0^a\int_0^b\int_0^a\int_0^b E_x(x,y)\,E_x(\xi,\eta)\,G_1(x,y,\xi,\eta)\,dx\,dy\,d\xi\,d\eta}{\left[\int_0^a\int_0^b E_x(x,y)\,\sin\frac{\pi y}{a}\,dx\,dy\right]^2}\right)$$

$$= -\frac{ab\mu_r}{2\Gamma_{10}}\,\delta\left(\frac{\text{num}}{\text{denom}}\right) = -\frac{ab\mu_r}{2\Gamma_{10}}\left[\frac{\delta(\text{num})\,\text{denom} - \text{num}\,\delta(\text{denom})}{(\text{denom})^2}\right] \tag{2.36}$$

$$\delta(\text{num}) = \int_0^a\int_0^b\int_0^a\int_0^b E_x(\xi,\eta)\,\delta E_x(x,y)\,G_1(x,y,\xi,\eta)\,dx\,dy\,d\xi\,d\eta$$

$$+ \int_0^a\int_0^b\int_0^a\int_0^b \delta E_x(\xi,\eta)\,E_x(x,y)\,G_1(x,y,\xi,\eta)\,dx\,dy\,d\xi\,d\eta$$

$$\delta(\text{denom}) = 2\left(\int_0^a\int_0^b E_x(x,y)\sin\frac{\pi y}{a}\,dx\,dy\right)$$

$$\left(\int_0^a\int_0^b \delta E_x(x,y)\sin\frac{\pi y}{a}\,dx\,dy\right)$$

Symmetry of $G_1(x,y,\xi,\eta)$:

$$G_1(x,y,\xi,\eta) = \left(\frac{\partial^2}{\partial y^2}+k_o^2\right)\frac{e^{-jk_o r}}{2\pi r}$$

$$+\left(\frac{\partial^2}{\partial y^2}+k^2\right)\left(\sum_{m=1}^{\infty}\sum_{n=0}^{\infty}{}'\frac{4\epsilon_{mn}}{ab\mu_r\Gamma_{mn}}\sin\frac{m\pi\eta}{a}\cos\frac{n\pi\xi}{b}\sin\frac{m\pi y}{a}\cos\frac{n\pi x}{b}\right)$$

G_1 is symmetrical in x,ξ and y,η: $G_1(x,y,\xi,\eta) = G_1(\xi,\eta,x,y)$ because

$$\frac{e^{-jk_o r}}{2\pi r} \quad\text{and}\quad \sum_{m=1}^{\infty}\sum_{n=0}^{\infty}{}'\frac{4\epsilon_{mn}}{ab\mu_r\Gamma_{mn}}\sin\frac{m\pi\eta}{a}\cos\frac{n\pi\xi}{b}\sin\frac{m\pi y}{a}\cos\frac{n\pi x}{b}$$

are symmetrical and differentiation twice with respect to y introduces either constant multipliers or multipliers of form $(y-\eta)^2$. Therefore

$$\delta(\text{num}) = 2\int_0^a\int_0^b\int_0^a\int_0^b E_x(\xi,\eta)\,\delta E_x(x,y)\,G_1(x,y,\sigma,\eta)\,dx\,dy\,d\xi\,d\eta$$

$$\delta y = \frac{-ab\mu_r}{2\Gamma_{10}D^4}\left[2D^2\left(\int_0^a\int_0^b\int_0^a\int_0^b E_x(\xi,\eta)\,\delta E_x(x,y)\,G_1(x,y,\xi,\eta)\,dx\,dy\,d\xi\,d\eta\right)\right.$$

$$-2D\left(\int_0^a\int_0^b\int_0^a\int_0^b E_x(\xi,\eta)\,E_x(x,y)\,G_1(x,y,\xi,\eta)\,dx\,dy\,d\xi\,d\eta\right)$$

$$\left.\left(\int_0^a\int_0^b \delta E_x(\xi,\eta)\sin\frac{\pi\eta}{a}\,d\xi\,d\eta\right)\right] \qquad (2.37)$$

Evaluating the individual terms from (2.35):

$$\int_0^a \int_0^b E_x(\xi,\eta)\, G_1(x,y,\xi,\eta)\, d\xi\, d\eta = \sin\frac{\pi y}{a}\left(\frac{-2\Gamma_{10}}{\mu_r}\right)\left(1-\frac{D}{ab}\right) \tag{2.38}$$

Multiplying by $\delta E_x(x, y)\, 2D^2$ and integrating over the aperture:

$$2D^2 \int_0^a \int_0^b \int_0^a \int_0^b E_x(\xi,\eta)\, \delta E_x(x,y)\, G_1(x,y,\xi,\eta)\, dx\, dy\, d\xi\, d\eta$$

$$= -\frac{4D^2\Gamma_{10}}{\mu_r}\left(1-\frac{D}{ab}\right)\int_0^a \int_0^b \sin\frac{\pi y}{a}\, \delta E_x(x,y)\, dx\, dy \tag{2.39}$$

Multiplying (2.35) by $E(x, y)$, integrating over the aperture, and multiplying by

$2D \int_0^a \int_0^b \delta E_x(\xi,\eta) \sin\frac{\pi\eta}{a}\, d\xi\, d\eta$:

$$2D \int_0^a \int_0^b \int_0^a \int_0^b E_x(\xi,\eta)\, E_x(x,y)\, G_1(x,y,\xi,\eta)\, dx\, dy\, d\xi\, d\eta \left(\int_0^a \int_0^b \delta E_x(\xi,\eta) \sin\frac{\pi\eta}{a}\, d\xi\, d\eta\right)$$

$$= \frac{-4\Gamma_{10}D^2}{\mu_r}\left(1-\frac{D}{ab}\right)\left(\int_0^a \int_0^b \delta E_x(\xi,\eta) \sin\frac{\pi\eta}{a}\, d\xi\, d\eta\right) \tag{2.40}$$

Substitution of (2.39) and (2.40) into (2.37):

$$\delta y = 0 \tag{2.41}$$

Therefore Eq. (2.33) is stationary with respect to small variations of $E_x(x,y)$ about its correct value.

A variational expression for the input admittance of a material loaded rectangular waveguide opening out into an infinite ground plane has been obtained. The next step is the evaluation of this expression for a given aperture field.

2.4 Evaluation of Variational Expression for Admittance

2.4.1 Reduction From Quadruple Integral to Double Integral. In this section the variational expression for admittance will be evaluated assuming that $E_x = \sin\frac{\pi y}{a}$. This

assumption will be justified in later sections both by experimental measurements of aperture field and by the results of higher order approximations.

Substituting $E_x = \sin \frac{\pi y}{a}$ into (2.33) gives:

$$\frac{Y}{Y_o} = \frac{G}{Y_o} + \frac{jB}{Y_o} = \frac{-ab\mu_r \int_o^a \int_o^b \int_o^a \int_o^b E_x(x,y)\, E_x(\xi,\eta)\, G_1(x,y,\xi,\eta)\, dx\, dy\, d\xi\, d\eta}{2\Gamma_{10} \left[\int_o^a \int_o^b E_x(x,y) \sin \frac{\pi y}{a}\, dx\, dy \right]^2} \tag{2.33}$$

$$= \frac{-2\mu_r}{\Gamma_{10} ab} \int_o^a \int_o^b \int_o^a \int_o^b \sin \frac{\pi y}{a} \sin \frac{\pi \eta}{a}\, G_1(x,y,\xi,\eta)\, dx\, dy\, d\xi\, d\eta \tag{2.42}$$

$$= \frac{-2\mu_r}{\Gamma_{10} ab} \int_o^a \int_o^b \int_o^a \int_o^b \sin \frac{\pi y}{a} \sin \frac{\pi \eta}{a} \left(\frac{\partial^2}{\partial y^2} + k_o^2 \right) \left(\frac{e^{-jk_o r}}{2\pi r} \right) dx\, dy\, d\xi\, d\eta \tag{2.43}$$

Replacing $\partial^2 / \partial y^2$ with $-\partial^2 / \partial y\, \partial \eta$ and integrating twice by parts with respect to y and η gives:

$$u = \frac{\sin \pi\eta}{a} \sin \frac{\pi y}{a} \qquad dV = \frac{\partial^2}{\partial y\, \partial \eta} \left(\frac{e^{-jk_o r}}{2\pi r} \right)$$

$$du = \frac{\pi}{a} \sin \frac{\pi \eta}{a} \cos \frac{\pi y}{a}\, dy \qquad V = \frac{\partial}{\partial \eta} \left(\frac{e^{-jk_o r}}{2\pi r} \right)$$

$$\frac{Y}{Y_o} = -\int_o^b dx \int_o^b d\xi \int_o^a d\eta \int_o^a \sin \frac{\pi y}{a} \sin \frac{\pi \eta}{a} \frac{+\partial^2}{\partial y\, \partial \eta} \left(\frac{e^{-jk_o r}}{2\pi r} \right) dy$$

$$= -\int_o^b dx \int_o^b d\xi \int_o^a d\eta \left\{ \left[+ \sin \frac{\pi \eta}{a} \sin \frac{\pi y}{a} \frac{\partial}{\partial \eta} \left(\frac{e^{-jk_o r}}{2\pi r} \right) \right]_o^a \right.$$

$$\left. - \int_o^a \frac{\partial}{\partial \eta} \frac{e^{-jk_o r}}{2\pi r} \left(\frac{\pi}{a} \right) \sin \frac{\pi \eta}{a} \cos \frac{\pi y}{a}\, dy \right\}$$

$$= \frac{\pi}{a} \int_o^b dx \int_o^b d\xi \int_o^a dy \int_o^a \sin \frac{\pi \eta}{a} \cos \frac{\pi y}{a} \frac{\partial}{\partial \eta} \left(\frac{e^{-jk_o r}}{2\pi r} \right) d\eta \tag{2.44}$$

$$u = \sin\frac{\pi\eta}{a}\cos\frac{\pi y}{a} \qquad dV = \frac{\partial}{\partial\eta}\left(\frac{e^{-jk_o r}}{2\pi r}\right)d\eta$$

$$du = \frac{\pi}{a}\cos\frac{\pi\eta}{a}\cos\frac{\pi y}{a} \qquad V = \frac{e^{-jk_o r}}{2\pi r}$$

$$= \frac{\pi}{a}\int_o^b dx \int_o^b d\xi \int_o^a dy\left\{\left[\frac{e^{-jk_o r}}{2\pi r}\sin\frac{\pi\eta}{a}\cos\frac{\pi y}{a}\right]_o^a - \int_o^a \frac{\pi}{a}\cos\frac{\pi\eta}{a}\cos\frac{\pi y}{a}\frac{e^{-jk_o r}}{2\pi r}\,d\eta\right\}$$

$$= -\frac{\pi^2}{a^2}\int_o^a\int_o^b\int_o^a\int_o^b \cos\frac{\pi\eta}{a}\cos\frac{\pi y}{a}\frac{e^{-jk_o r}}{2\pi r}\,dx\,dy\,d\xi\,d\eta \tag{2.45}$$

$$\frac{Y}{Y_o} = \frac{-\mu_r}{\Gamma_{10}ab}\int_o^a\int_o^b\int_o^a\int_o^b \frac{e^{-jk_o r}}{2\pi r}\left[\left(k_o^2 - \frac{\pi^2}{a}\right)\cos\frac{\pi}{a}(y-\eta) - \left(k_o^2 + \frac{\pi^2}{a^2}\right)\cos\frac{\pi}{a}(y+\eta)\right]dx\,dy\,d\xi\,d\eta \tag{2.46}$$

At this point we note that r is a function only of the differences of variables $(y-\eta)$ and $(x-\xi)$. If, therefore, we make a transformation to sum and difference variables, we will be able to integrate over the sum variables, leaving a double integral in the difference variables. This is an essential step because the quadruple integral is not practical for numerical computation.

Now introduce the change of variables:

$$y-\eta = \lambda \qquad x-\xi = \sigma$$

$$y+\eta = a+\mu \qquad x+\xi = b+\nu \tag{2.47}$$

This transformation consists of a 45^o rotation of coordinates, a translation, and a linear magnification of $\sqrt{2}$ (see Appendix A). The transformation is shown in Fig. 4.

$$\frac{Y}{Y_o} = \frac{-4\mu_r}{\Gamma_{10}ab}\int_o^a d\lambda \int_o^b \frac{e^{-jk_o\sqrt{\lambda^2+\sigma^2}}}{2\pi\sqrt{\lambda^2+\sigma^2}}\,d\sigma \int_o^{a-\lambda} d\mu \int_o^{b-\sigma}\left(k_o^2 - \frac{\pi^2}{a^2}\right)\cos\frac{\pi\lambda}{a} + \left(k_o^2 + \frac{\pi^2}{a^2}\right)\cos\frac{\pi\mu}{a}\,d\nu$$

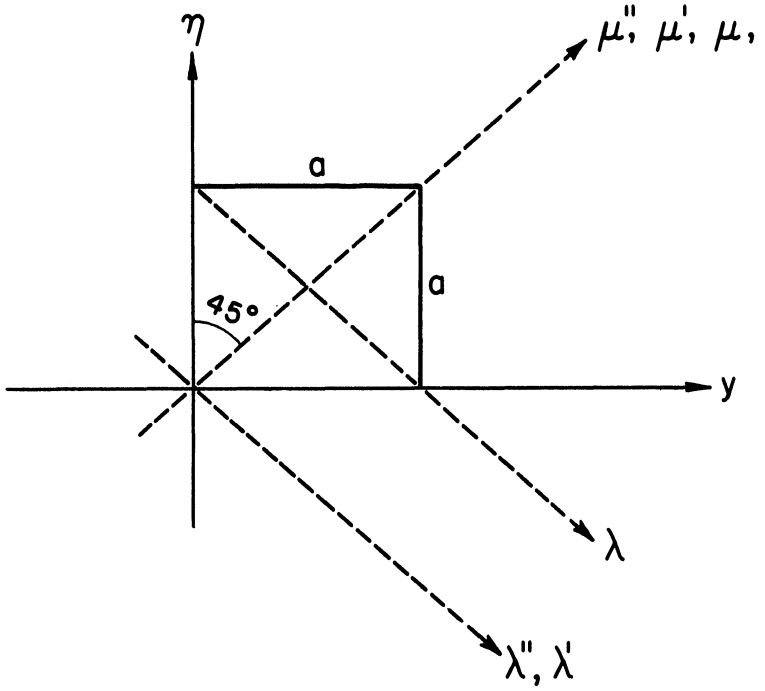

Fig. 4. Coordinate transformation.

$$= \frac{-4\mu_r}{\Gamma_{10}ab} \int_0^a \int_0^b (b-\sigma) \left[(a-\lambda)\left(k_o^2 - \frac{\pi^2}{a^2}\right) \cos\frac{\pi\lambda}{a} + \frac{a}{\pi}\left(k_o^2 + \frac{\pi^2}{a^2}\right) \sin\frac{\pi\lambda}{a} \right] \frac{e^{-jk_o\sqrt{\lambda^2+\sigma^2}}}{2\pi\sqrt{\lambda^2+\sigma^2}} \, d\lambda \, d\sigma$$

$$= \frac{G}{Y_o} + \frac{jB}{Y_o} \tag{2.48}$$

This expression also agrees with Lewin[64] after setting $\mu = \mu_o$, $\epsilon = \epsilon_o$. The integrand has a singularity at the origin. The contribution of the area near the origin is significant, as shown by a computer printout, so it cannot be neglected. The next section will be concerned with the evaluation of the contribution of the small area near the origin. The double integral expression (2.48) would be suitable for numerical integration were it not for the singularity at the origin.

2.4.2 Elimination of Singularity in the Normalized Admittance Function.

Separating (2.48) into its real and imaginary parts gives:

$$\frac{G}{Y_o} = \frac{2\mu_r(k_o^2a^2 - \pi^2)}{\pi^2a^2b\sqrt{k^2a^2 - \pi^2}} \int_0^a \int_0^b \left[(b-\sigma)\,\pi(a-\lambda)\cos\frac{\pi\lambda}{a} + a\frac{C_1}{D_1}\sin\frac{\pi\lambda}{a} \right] \frac{\sin k_o\sqrt{\lambda^2+\sigma^2}}{\sqrt{\lambda^2+\sigma^2}} \, d\sigma \, d\lambda \tag{2.49}$$

$$\frac{B}{Y_o} = \frac{2\mu_r(k_o^2a^2 - \pi^2)}{\pi^2 a^2 b\sqrt{k^2a^2 - \pi^2}} \int_o^a \int_o^b \left[(b-\sigma)\,\pi(a-\lambda)\cos\frac{\pi\lambda}{a} + a\frac{C_1}{D_1}\sin\frac{\pi\lambda}{a} \right] \frac{\cos k_o\sqrt{\lambda^2+\sigma^2}}{\sqrt{\lambda^2+\sigma^2}}\, d\sigma\, d\lambda \tag{2.50}$$

where

$$C_1 = k_o^2a^2 + \pi^2$$

$$D_1 = k_o^2a^2 - \pi^2$$

transforming to polar coordinates:

$$\lambda = r\cos\theta$$

$$\sigma = r\sin\theta$$

$$\frac{G}{Y_o} = \frac{2\mu_r(k_o^2a^2 - \pi^2)}{\pi^2 a^2 b\sqrt{k^2a^2 - \pi^2}} \left\{ \int_o^{\theta_1} \int_o^{a\sec\theta} (b - r\sin\theta) \left[\pi(a - r\cos\theta)\cos\left(\frac{\pi r\cos\theta}{a}\right) + a\frac{C_1}{D_1}\sin\left(\frac{\pi r\cos\theta}{a}\right) \right] \sin k_o r\, dr\, d\theta \right.$$

$$\left. + \int_{\theta_1}^{\pi/2} \int_o^{b\csc\theta} (b - r\sin\theta) \left[\pi(a - r\cos\theta)\cos\left(\frac{\pi r\cos\theta}{a}\right) + a\frac{C_1}{D_1}\sin\left(\frac{\pi r\cos\theta}{a}\right) \right] \cos k_o r\, dr\, d\theta \right\} \tag{2.51}$$

$$\frac{B}{Y_o} = \frac{2\mu_r(k_o^2a^2 - \pi^2)}{\pi^2 a^2 b\sqrt{k^2a^2 - \pi^2}} \left\{ \int_o^{\theta_1} \int_o^{a\sec\theta} (b - r\sin\theta) \left[\pi(a - r\cos\theta)\cos\left(\frac{\pi r\cos\theta}{a}\right) + a\frac{C_1}{D_1}\sin\left(\frac{\pi r\cos\theta}{a}\right) \right] \cos k_o r\, dr\, d\theta \right.$$

$$\left. + \int_{\theta_1}^{\pi/2} \int_o^{b\csc\theta} (b - r\sin\theta) \left[\pi(a - r\cos\theta)\cos\left(\frac{\pi r\cos\theta}{a}\right) + a\frac{C_1}{D_1}\sin\left(\frac{\pi r\cos\theta}{a}\right) \right] \cos k_o r\, dr\, d\theta \right\} \tag{2.52}$$

The transformation from rectangular to polar coordinates eliminates the singularity in the double integration in x and y occurring at the origin. The integration in r can now be carried out to give a single integral in θ. However, this single integral has a singularity at $k_o a = \pi\cos\theta$. Moreover, the formulation is quite complicated. The double integration in θ and r has the advantage of having no singularities. However, if we split the rectangular area into sections of equal increments in r and θ, the irregular shaped areas remaining require weighting factors which vary with the ratio b/a. Thus the polar coordinate forms do not appear to have significant advantage over the rectangular form. Accordingly,

both the rectangular and the polar forms have been used. The integral has been split up into two parts. For the first, a small rectangular area including the origin, approximations are made for small λ/a, σ/b and the integration is carried out explicitly using the polar forms. For the remaining area, the integration is evaluated by computer using the rectangular form. The two contributions are then added.

The evaluation of the integral for a small area including the origin proceeds as follows:

Evaluation of G:

$$\frac{G}{Y_o} = \frac{2\mu_r(k_o^2a^2 - \pi^2)}{\pi^2 a^2 b\sqrt{k^2a^2 - \pi^2}} \left\{ \int_o^{\theta_1} \int_o^{\lambda_1 \sec\theta} (b - r\sin\theta)\left[(a - r\cos\theta)\left(\frac{\pi r\cos\theta}{a}\right) + \frac{a\frac{C_1}{D_1}}{\pi}\right.\right.$$

$$\left.\sin\left(\frac{\pi r\cos\theta}{a}\right)\right]\sin k_o r\, dr\, d\theta$$

$$\left. + \int_{\theta_1}^{\pi/2} \int_o^{\sigma_1 \csc\theta} (b - r\sin\theta)\left[(a - r\cos\theta)\cos\left(\frac{\pi r\cos\theta}{a}\right) + \frac{a\frac{C_1}{D_1}}{\pi}\sin\left(\frac{\pi r\cos\theta}{a}\right)\right]\sin k_o r\, dr\, d\theta\right\}$$

(2.53)

where

$\theta_1 = \tan^{-1} b/a$

$\lambda_1 = Qa$, $\sigma_1 = Qb$. In the computations for Fig. 5, $Q = .05$.

λ_1 and σ_1 are the dimensions of the small rectangular area including the origin.

Let

$$\cos\left(\frac{\pi r\cos\theta}{a}\right) = 1 - \frac{\pi^2 r^2\cos^2\theta}{2a^2}$$

$$\sin k_o r = k_o r$$

Integration yields:

$$\frac{G}{Y_o} = \frac{2\mu_r(k_o^2a^2 - \pi^2)(ka)}{\pi\sqrt{k^2a^2 - \pi^2}} \frac{b}{a}\sqrt{\frac{\mu_r}{\epsilon_r}} \left[Q^2 + \left(\frac{\frac{C_1}{D_1} - 2}{2}\right) Q^3 - \left(\frac{5.57 + \frac{C_1}{D_1}}{4}\right) Q^4 + 2.06Q^5 - .616Q^6\right] \tag{2.54}$$

where

$Q = \lambda_1/a = \sigma_1/b$ and the rectangle of integration has sides of length λ_1 and σ_1

$$\frac{G}{Y_o} \approx \frac{2\mu_r(k_o^2a^2 - \pi^2)(ka)}{\pi\sqrt{k^2a^2 - \pi^2}} \frac{b}{a}\sqrt{\frac{\mu_r}{\epsilon_r}}\, Q^2 \qquad \text{(for small Q)} \tag{2.55}$$

This represents the contribution to the total value of G of the small rectangular area including the origin.

Evaluation of B:

$$\frac{B}{Y_o} = \frac{2\mu_r(k_o^2a^2 - \pi^2)}{\pi\sqrt{k^2a^2 - \pi^2}} \left\{\left[f - \frac{b}{a}f\right] Q + \left[\frac{\left(\frac{C_1}{D_1} - 1\right) f}{2} - \frac{a}{2b}(d-1)\right.\right.$$

$$\left. + g\frac{b}{2a} + \frac{1}{2}\frac{b^2}{a^2}\left(\frac{C_1}{D_1} - 1\right)\left(\frac{a}{b}d - 1\right)\right] Q^2 + \left[-\frac{f}{12}(2\pi^2 + k_o^2a^2) + \frac{g}{12}\frac{b^3}{a^3}(k_o^2a^2 - \pi^2)\right.$$

$$\left.\left. \frac{\left(\frac{C_1}{D_1} - 1\right)}{3}\left[\frac{a}{b}(d-1) + \frac{b^2}{a^2}\left(\frac{a}{b}d - 1\right)\right] - \frac{1}{12}\frac{bd}{a}(2k_o^2a^2 - \pi^2)\right] Q^3\right\} \tag{2.56}$$

$$\frac{B}{Y_o} \approx \frac{2\mu_r(k_o^2a^2 - \pi^2)}{\pi\sqrt{k^2a^2 - \pi^2}} \left[f - \frac{b}{a}g\right] Q \qquad \text{(for small Q)} \tag{2.57}$$

where

$$f = \log \tan \left(\frac{\theta_1}{2} + \frac{\pi}{4} \right)$$

$$g = \log \tan \frac{\theta_1}{2}$$

$$d = \sqrt{\frac{b^2}{a^2} + 1} = \sec \theta_1$$

This represents the contribution to the total value of B of the small rectangular area including the origin.

A computer program was prepared to evaluate and combine the contributions to B and G of the large and small areas. Results are shown in Figs. 5(a)-(j). This represents the basic aperture admittance data from which later calculations of bandwidth, efficiency, and resonant frequency will be made. Each figure represents a given choice of μ_r, ϵ_r. The data is plotted versus normalized frequency F_N ($F_N = ka/\pi$, $F_N = 1$ at cutoff). As expected, the ratio B/G increases rapidly with the $\mu_r\epsilon_r$ product, indicating a rapidly increasing reflection coefficient. Near cutoff, both B/Y_0 and G/Y_0 change rapidly with frequency because of the factor $1/\sqrt{k^2a^2 - \pi^2}$ in Eqs. (2.49), (2.50). The behavior of B/Y_0 with frequency is approximately that of a series resonant L-C circuit resonant at cutoff frequency ($F_N = 1$). The data of Fig. 5(a) agrees with Lewin's data for the unloaded waveguide radiator.[65]

As a check on the computation, two different increments were used in the integration and their results compared. The maximum error in the imaginary part of the admittance was .7 percent. The integration in G involves positive and negative parts which nearly cancel as the $\mu_r\epsilon_r$ product becomes large. Correspondingly the error in the real part of the admittance increased to a maximum of 2.5 percent at $\mu_r = \epsilon_r = 10$. It is estimated that the computation is accurate to within a few percent.

Normalization of the Data:

For all the data presented, μ_r is equal to ϵ_r. However, each figure with a given μ_r and ϵ_r may be expanded to give a family of figures with the same $\mu_r\epsilon_r$ product but

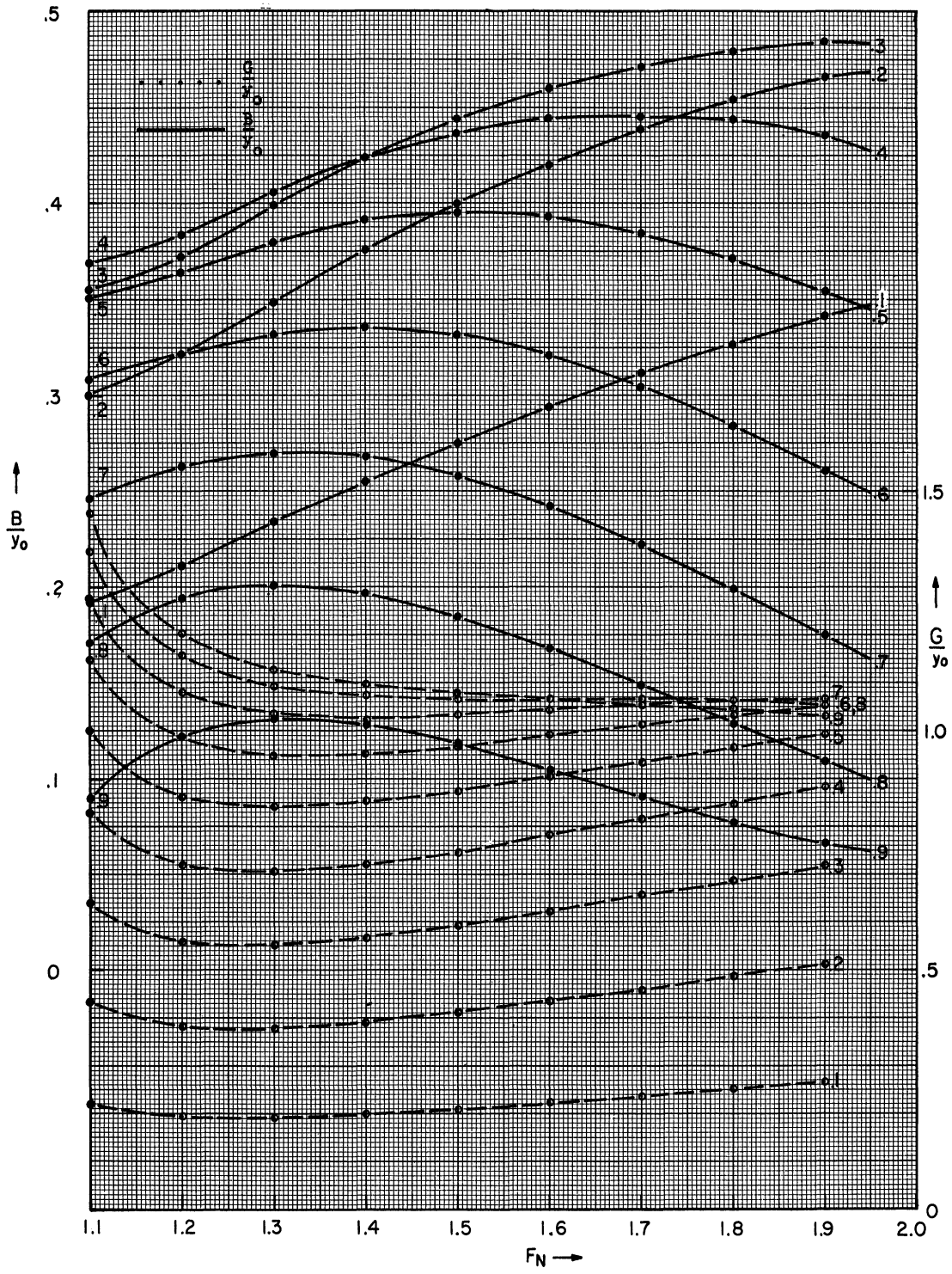

Fig. 5. Aperture admittance of a loaded waveguide radiator (F_N = 1.0 at cutoff). (a) $\mu_r = \epsilon_r = 1.0$.

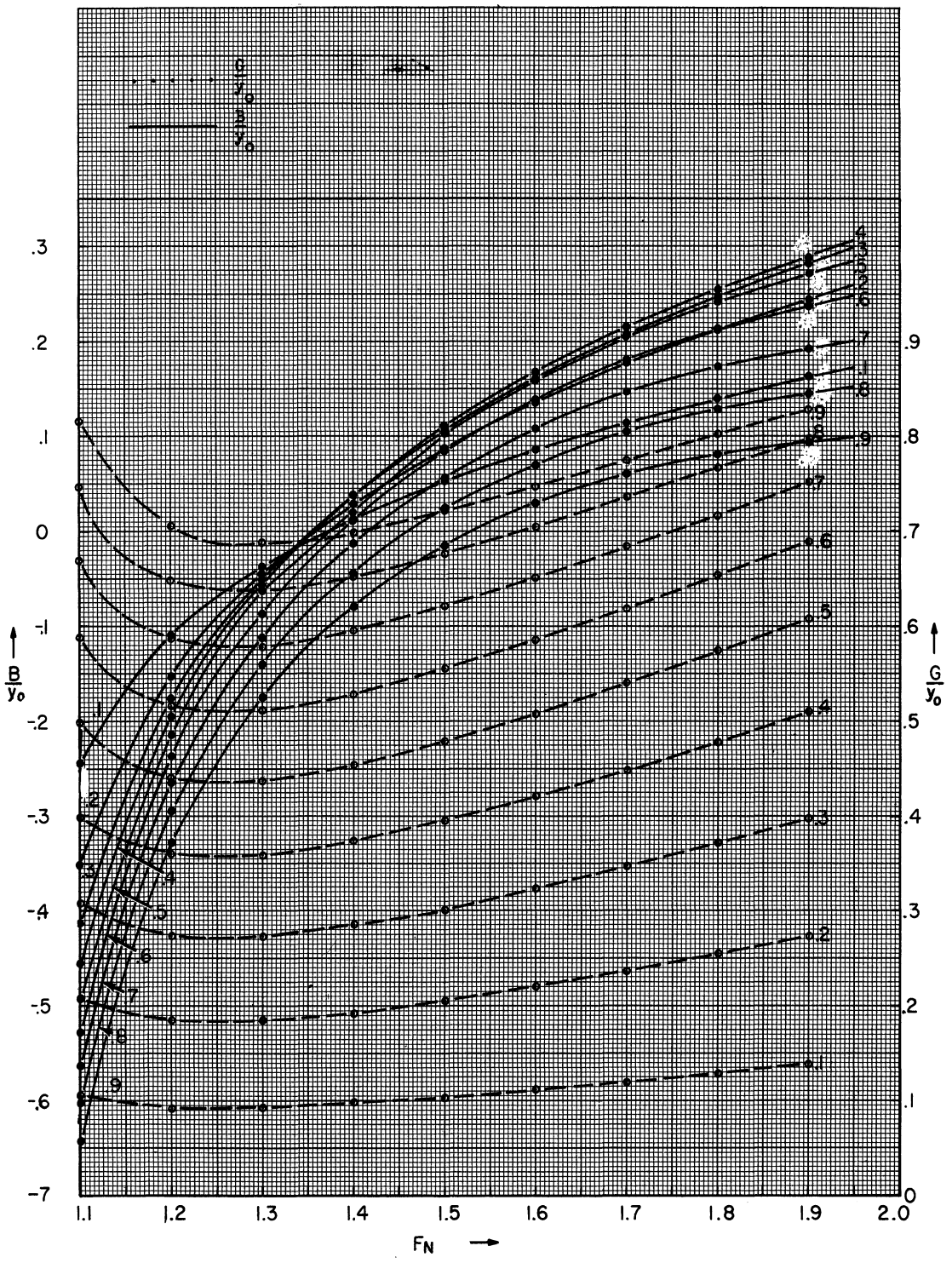

Fig. 5. Aperture admittance of a loaded waveguide radiator (F_N = 1.0 at cutoff). (b) $\mu_r = \epsilon_r = 1.5$.

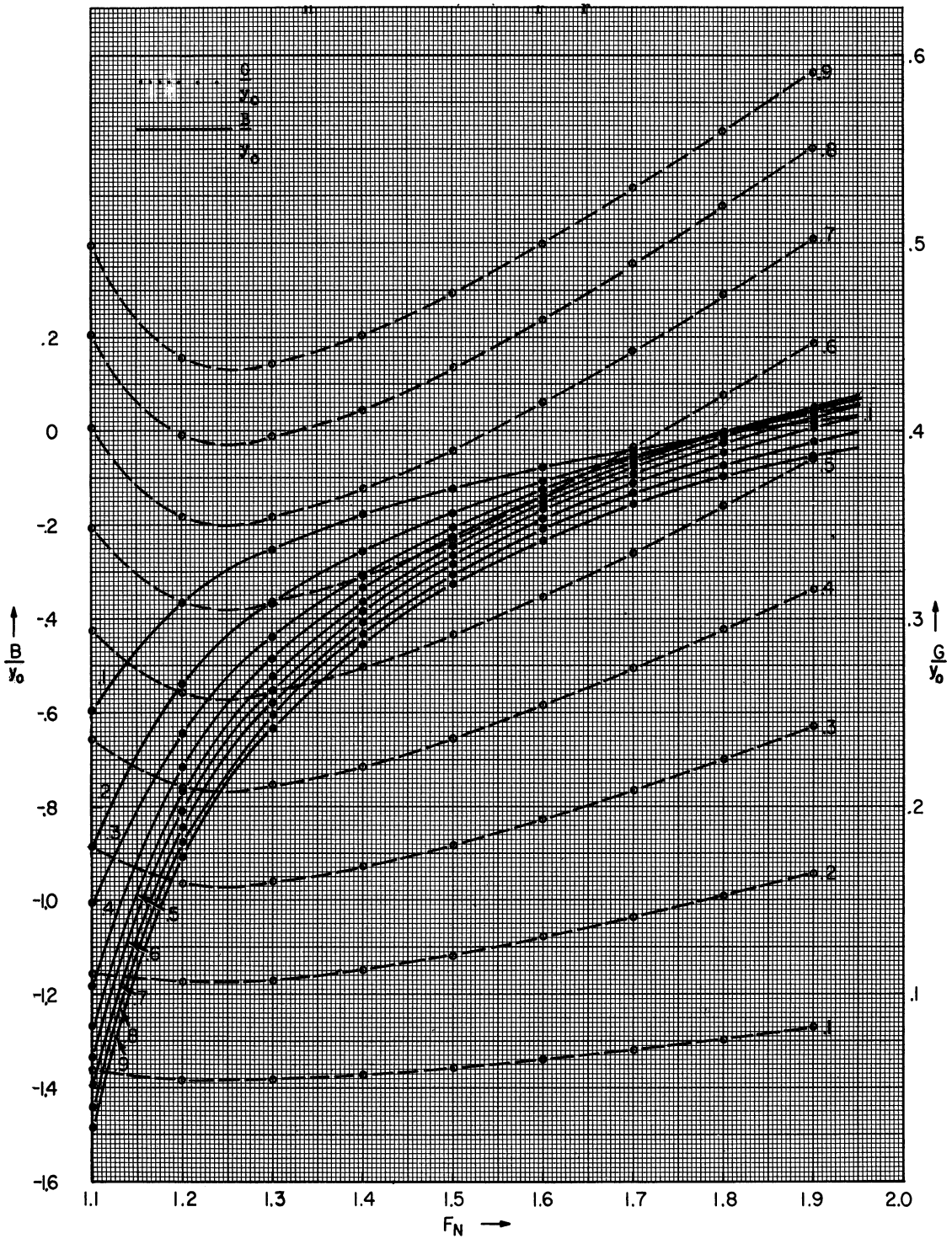

Fig. 5. Aperture admittance of a loaded waveguide radiator (F_N = 1.0 at cutoff). (c) $\mu_r = \epsilon_r$ = 2.0.

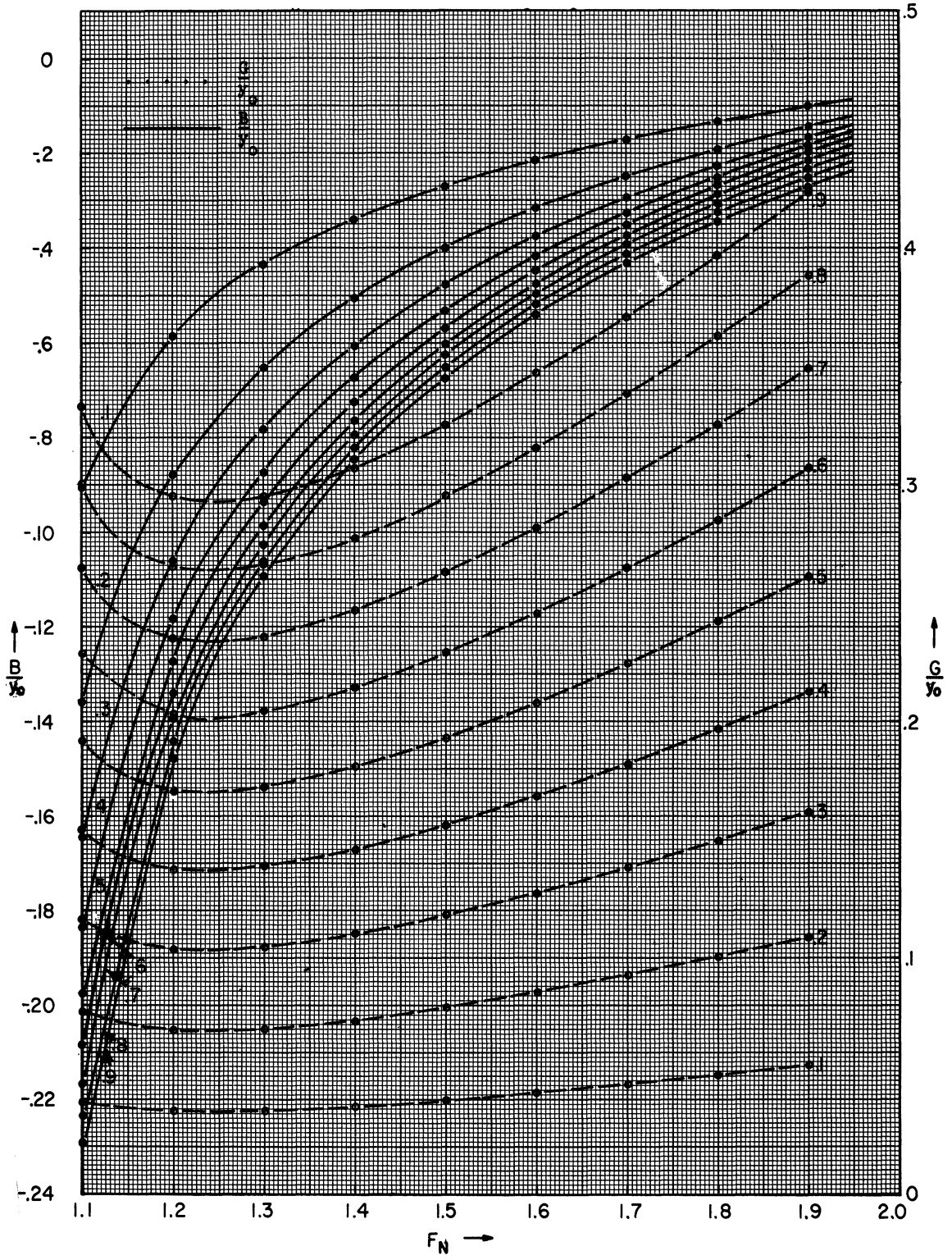

Fig. 5. Aperture admittance of a loaded waveguide radiator (F_N = 1.0 at cutoff). (d) $\mu_r = \epsilon_r = 2.5$.

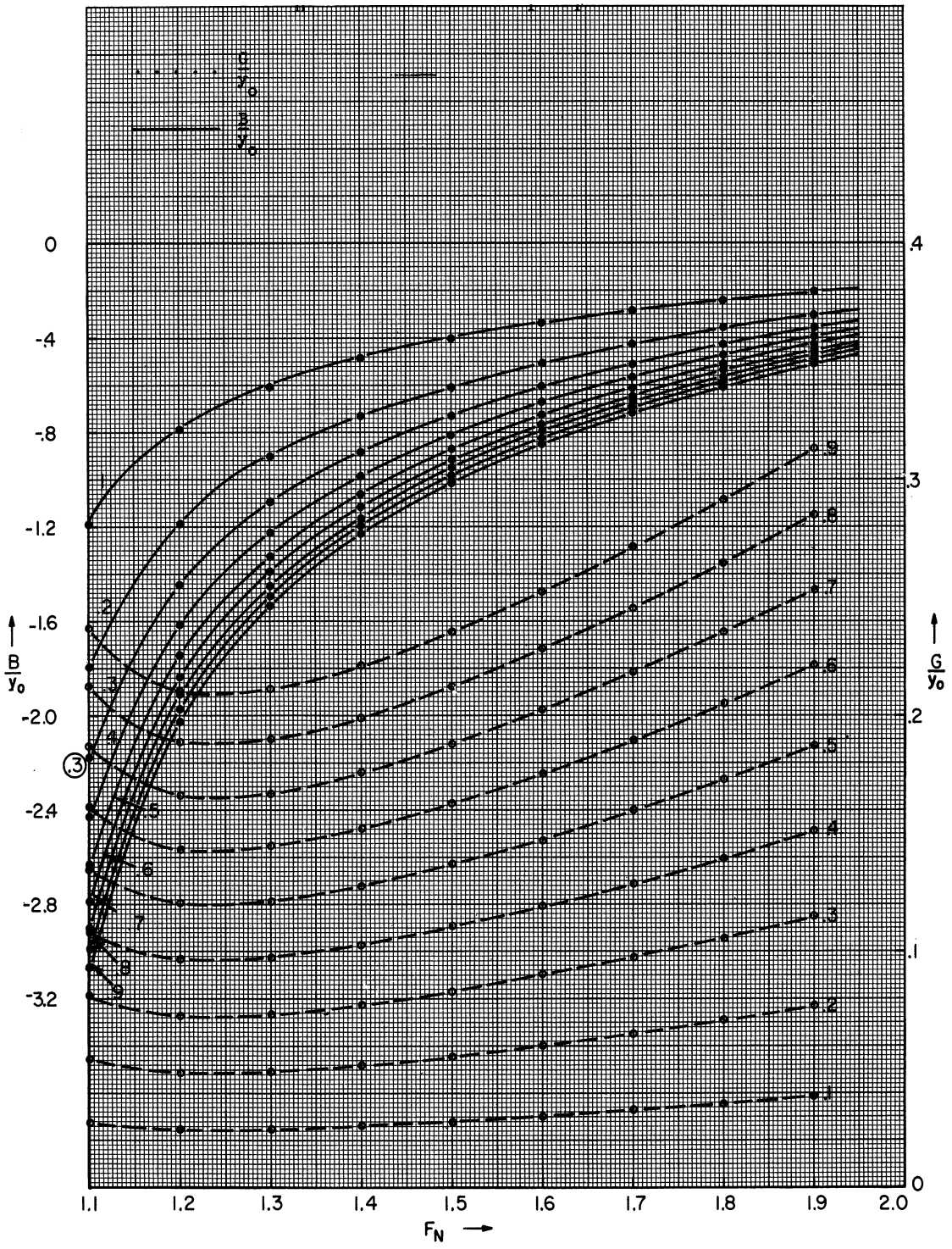

Fig. 5. Aperture admittance of a loaded waveguide radiator (F_N = 1.0 at cutoff). (e) $\mu_r = \epsilon_r = 3.0$.

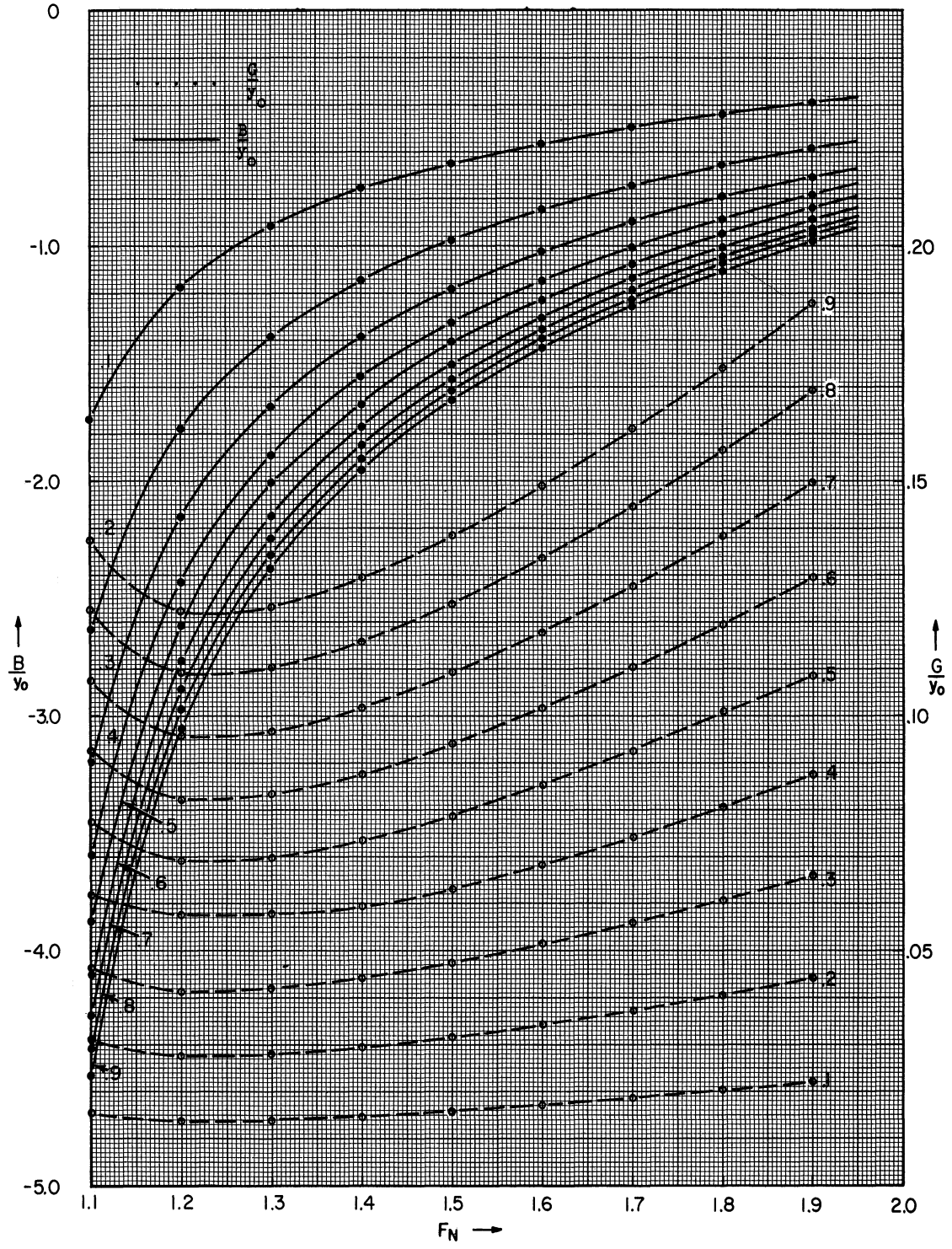

Fig. 5. Aperture admittance of a loaded waveguide radiator (F_N = 1.0 at cutoff). (f) $\mu_r = \epsilon_r = 4.0$.

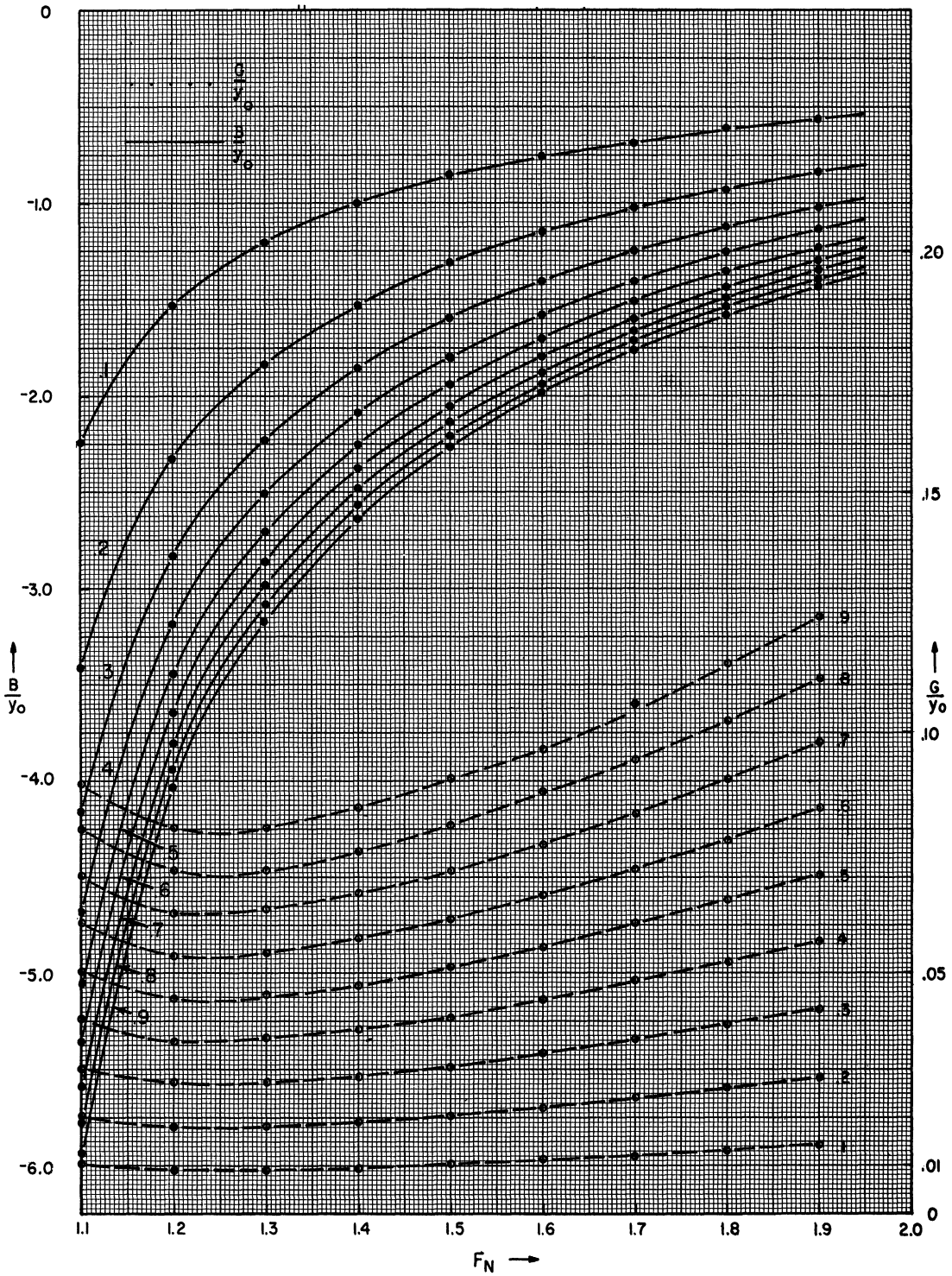

Fig. 5. Aperture admittance of a loaded waveguide radiator (F_N = 1.0 at cutoff). (g) $\mu_r = \epsilon_r = 5.0$.

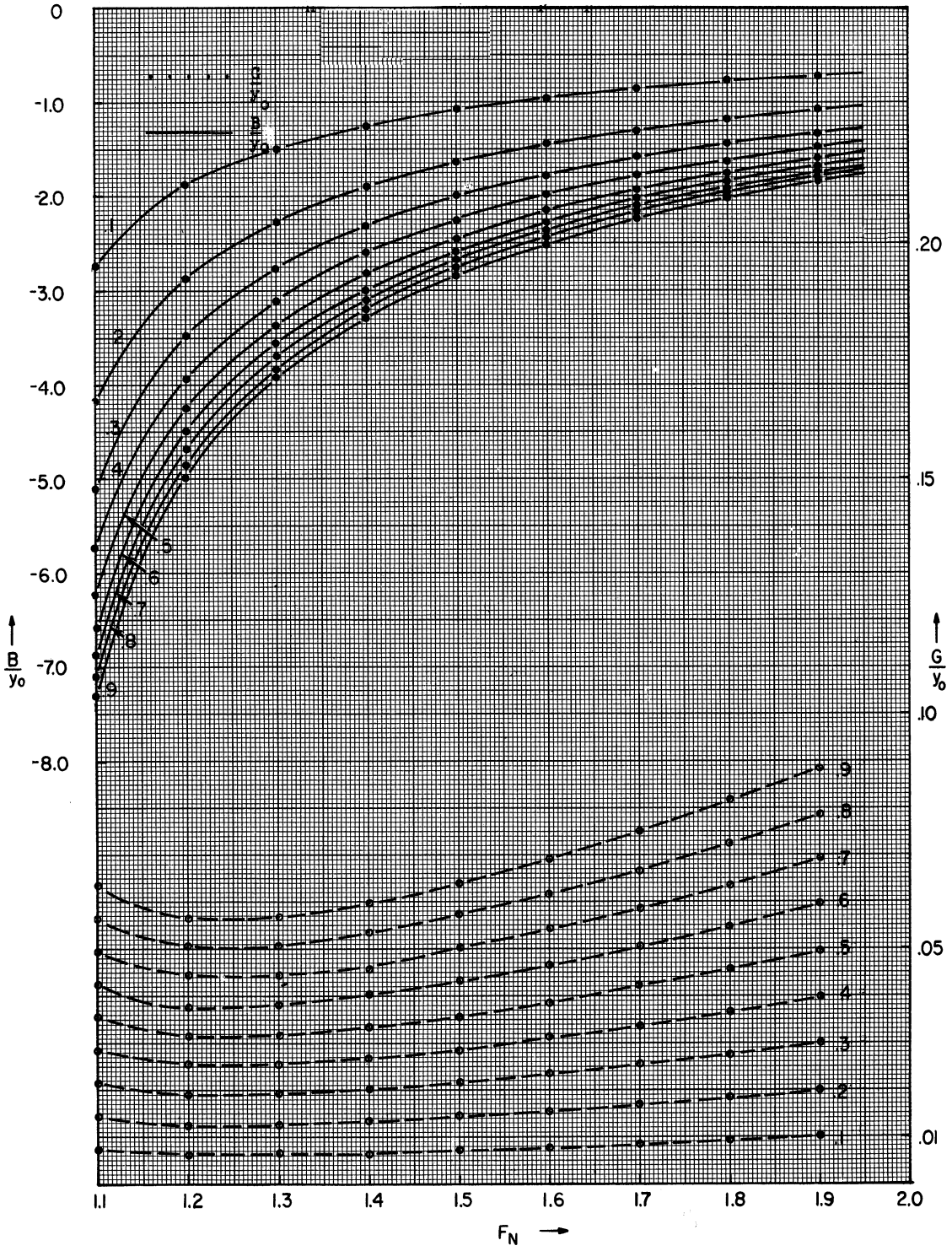

Fig. 5. Aperture admittance of a loaded waveguide radiator (F_N = 1.0 at cutoff). (h) $\mu_r = \epsilon_r = 6.0$.

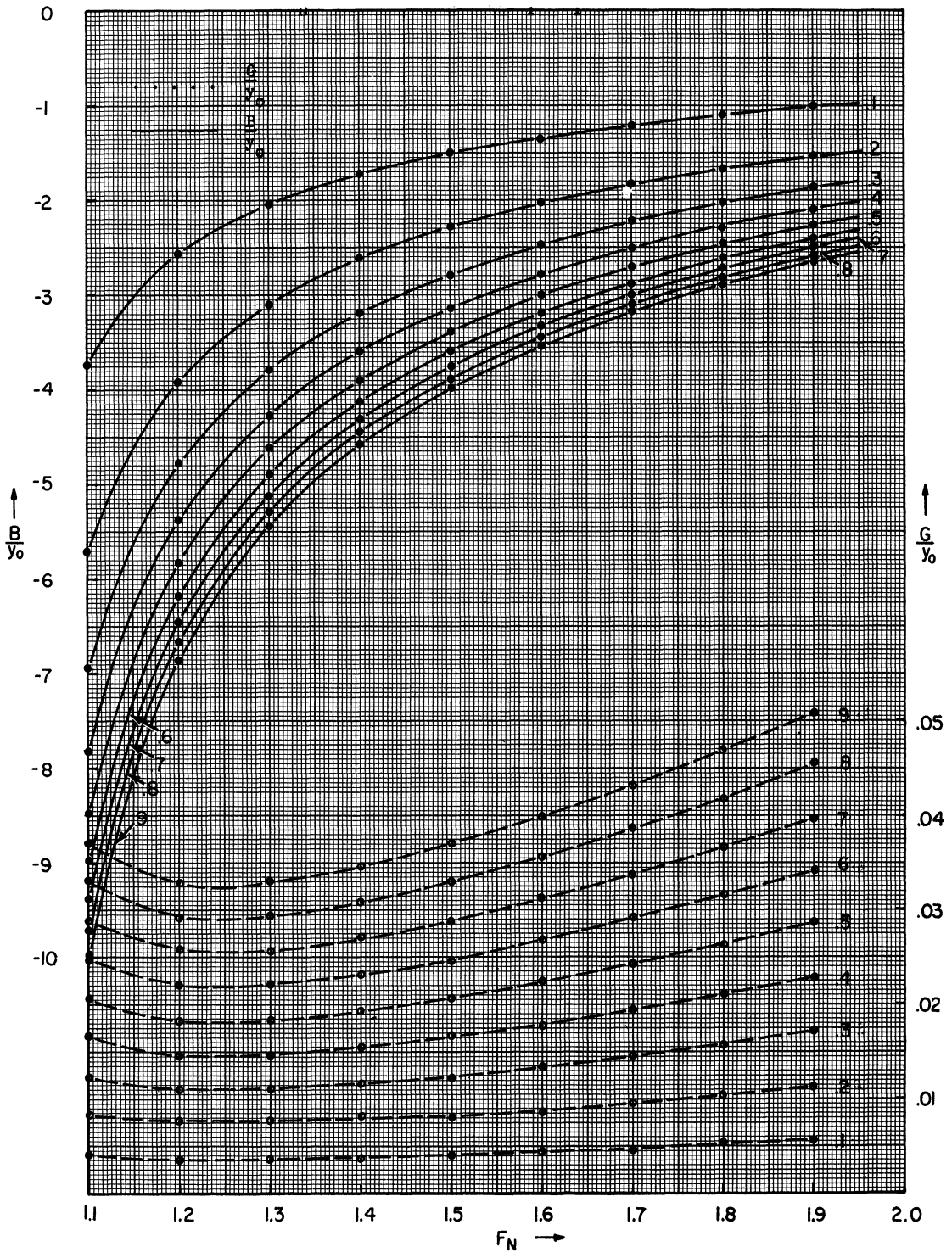

Fig. 5. Aperture admittance of a loaded waveguide radiator (F_N = 1.0 at cutoff). (i) $\mu_r = \epsilon_r = 8.0$.

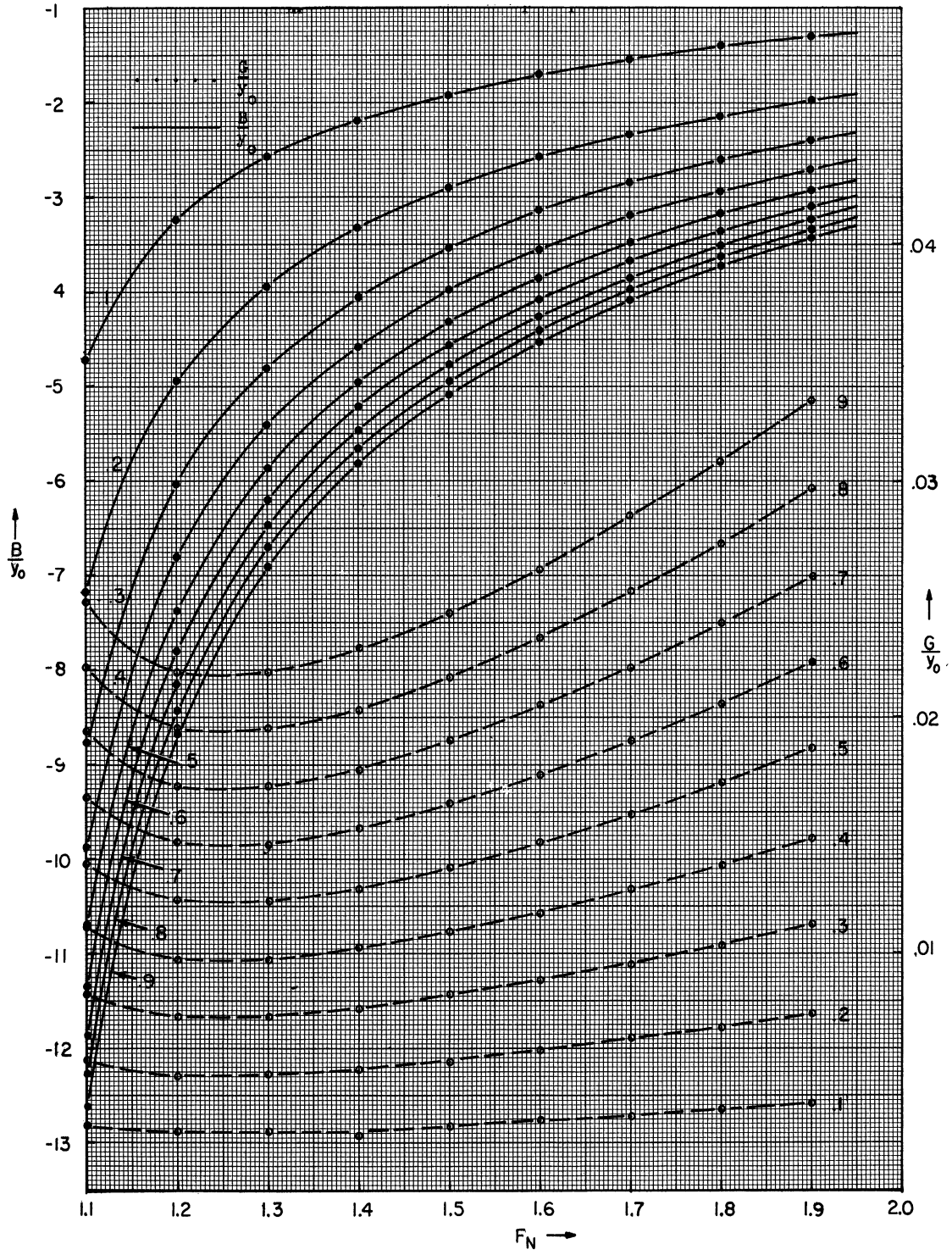

Fig. 5. Aperture admittance of a loaded waveguide radiator (F_N = 1.0 at cutoff). (j) $\mu_r = \epsilon_r = 10.0$.

different μ_r/ϵ_r ratios. This additional data is obtained by multiplying the real and imaginary parts of the admittance by μ_r(actual)/μ_r(figure). For instance, Fig. 5(e) can be converted to ($\mu_r = 4.5$, $\epsilon_r = 2$) by multiplying B and G by 4.5/3.0.

The basic data shown in Fig. 5 is checked (a) by a direct measurement of admittance and (b) indirectly by measurements of resonant frequency. The experimental checks are described in Chapter 6.*

2.4.3 Normalized Admittance for Small Apertures. For electrically small apertures ($k_o a$ small), or, alternatively, for moderate values of ka and large values of $\mu_r \epsilon_r$ (such as in Fig. 5(j)), the results for the real part of the impedance decrease in accuracy due to the fact that the integration involves negative and positive parts which nearly cancel. This section will remedy this inaccuracy by integrating the expression for admittance using approximation for $\cos k_o r$ and $\sin k_o r$. In addition, the asymptotic expressions derived will provide some insight into the behavior of the admittance functions. The approximations:

$$\begin{aligned} \sin X &= X - X^3/3! \\ \cos X &= 1 - X^2/2! \end{aligned} \qquad (2.58)$$

where $X = k_o \sqrt{\lambda^2 + \sigma^2}$ were used. These small angle approximations can be made for large μ_r and ϵ_r because the aperture is now small in terms of air wavelengths.

Evaluation of G:

$$\frac{G}{Y_o} = \frac{2\mu_r(k_o^2 a^2 - \pi^2)\, k_o}{a^2 b\, \pi^2 \sqrt{k^2 a^2 - \pi^2}} \int_0^a \int_0^b (b-\sigma) \left[\pi(a-\lambda) \cos \frac{\pi\lambda}{a} + a \frac{C_1}{D_1} \sin \frac{\pi\lambda}{a}\right] \left[1 - \frac{k_o^2(\lambda^2 + \sigma^2)}{6}\right] d\sigma\, d\lambda \qquad (2.59)$$

Integration gives:

$$\frac{G}{Y_o} = \frac{2\mu_r(k_o^2 a^2 - \pi^2)}{\pi^3 \sqrt{k^2 a^2 - \pi^2}} \left\{(k_o b)\left(\frac{C_1}{D_1} + 1\right) - \frac{(k_o b)^3}{36\pi^2}\left[\left(\frac{C_1}{D_1} + 1\right)\pi^2 + \frac{3a^2}{b^2}\left[(\pi^2 - 4)\left(\frac{C_1}{D_1} + 3\right) - 2\pi^2\right]\right]\right\} \qquad (2.60)$$

$$\frac{G}{Y_o} \longrightarrow \frac{4}{\sqrt{k^2 a^2 - \pi^2}} \left(\frac{ka}{\pi}\right)^3 \left(\frac{b}{a}\right) \frac{1}{\mu_r^{1/2} \epsilon_r^{3/2}} \qquad \text{(for small } k_o b) \qquad (2.61)$$

*It should be noted that experimental verification is limited to a narrow range of values. It has been suggested that, at points where $|1-R| \ll 1$, the higher order fields may dominate, thereby invalidating the assumption of dominant mode aperture field.

Evaluation of B:

$$\frac{B}{Y_o} = \frac{2\mu_r(k_o^2a^2 - \pi^2)}{a^2b\,\pi\sqrt{k^2a^2 - \pi^2}} \int_o^a \int_o^b (b-\sigma)\left[(a-\lambda)\cos\frac{\pi\lambda}{a} + \frac{a\frac{C_1}{D_1}}{\pi}\sin\frac{\pi\lambda}{a}\right]\frac{1}{\sqrt{\lambda^2+\sigma^2}}\,d\sigma\,d\lambda \tag{2.62}$$

Transform to polar coordinates:

$$\lambda = r\cos\theta$$

$$\sigma = r\sin\theta$$

$$\frac{B}{Y_o} = \frac{2\mu_r(k_o^2a^2 - \pi^2)}{a^2b\,\pi\;\; k^2a^2 - \pi^2}\left\{\int_o^{\theta_1}\int_o^{a\sec\theta}(b-r\sin\theta)\left[(a-r\cos\theta)\cos\left(\frac{\pi r\cos\theta}{a}\right) + \frac{a\frac{C_1}{D_1}}{\pi}\sin\left(\frac{\pi r\cos\theta}{a}\right)\right]dr\,d\theta\right.$$

$$\left. + \int_{\theta_1}^{\pi/2}\int_o^{b\csc\theta}(b-r\sin\theta)\left[(a-r\cos\theta)\cos\left(\frac{\pi r\cos\theta}{a}\right) + \frac{a\frac{C_1}{D_1}}{\pi}\sin\left(\frac{\pi r\cos\theta}{a}\right)\right]dr\,d\theta\right\} \tag{2.63}$$

where

$$\theta_1 = \tan^{-1} b/a$$

Integration gives:

$$\frac{B}{Y_o} = \frac{2\mu_r}{\pi\sqrt{k^2a^2 - \pi^2}}\left\{2\left(1 - \frac{C_1}{D_1}\right)\log\tan\left(\frac{\theta_1}{2} + \frac{\pi}{4}\right) + \frac{a}{b}\left(2 + \frac{C_1}{D_1}\right)(1 - \sec\theta)\right.$$

$$+ \int_{\theta_1}^{\pi/2}\left\{\frac{a}{b}\tan\theta\sec\theta\left[1 - \cos\left(\frac{\pi b\,\mathrm{ctn}\,\theta}{a}\right)\right] + \sec\theta\left[\left(2 + \frac{C_1}{D_1}\right)\left[\cos\left(\frac{\pi b\,\mathrm{ctn}\,\theta}{a}\right)\right.\right.\right.$$

$$\left.\left.\left. - \frac{a}{b\pi}\tan\theta\sin\left(\frac{\pi b\,\mathrm{ctn}\,\theta}{a}\right)\right] + \left(1 - \frac{C_1}{D_1}\right)\left[1 - \cos\left(\frac{\pi b\,\mathrm{ctn}\,\theta}{a}\right)\right]\right]\right\}\,d\theta\Bigg\} \tag{2.64}$$

For small $k_o a$, $\frac{C_1}{D_1} \longrightarrow -1$

$$\frac{B}{Y_o} \rightarrow \frac{\mu_r \pi}{\sqrt{k^2 a^2 - \pi^2}} \; F_1(\theta_1) \tag{2.65}$$

where

$$\theta_1 = \tan^{-1} b/a$$

$$\frac{2}{\pi^2} F_1(\theta_1) = 4 \log \tan \left(\frac{\theta_1}{2} + \frac{\pi}{4} \right) - \frac{a}{b} (\sec \theta_1 - 1)$$

$$+ \int_{\theta_1}^{\pi/2} \frac{a}{b} \tan \theta \sec \theta \left[1 - \cos \left(\frac{\pi b \operatorname{ctn} \theta}{a} \right) \right] d\theta$$

$$+ \int_{\theta_1}^{\pi/2} \sec \theta \left[\cos \left(\frac{\pi b \operatorname{ctn} \theta}{a} \right) - \frac{a}{b\pi} \tan \theta \sin \left(\frac{\pi b \operatorname{ctn} \theta}{a} \right) \right] d\theta$$

$$+ \int_{\theta_1}^{\pi/2} 2 \sec \theta \left[1 - \cos \left(\frac{\pi b \operatorname{ctn} \theta}{a} \right) \right] d\theta \tag{2.66}$$

For small $k_o a$:

$$\frac{B}{G} \rightarrow - \frac{\pi}{4} \frac{a}{b} \frac{F_1(\theta_1)}{\left(\frac{k_o a}{\pi} \right)^3} \tag{2.67}$$

Figure 6(a) shows the approximate form of $F_1(\theta_1)$, which was extrapolated from the computer data for Fig. 5(j) ($\mu_r = \epsilon_r = 10$). A check with additional computer data for $\mu_r = \epsilon_r = 100$ shows good agreement (within 2 percent) with the curve for $F_1(\theta_1)$. Figures 6(b) and 6(c) compare computer data for admittance with the asymptotic forms (Eqs. 2.60 and 2.65) for G/Y_o and B/Y_o. Figure 6(b) shows that the accuracy of the approximate expression (2.60) increases rapidly with increasing $\mu_r \epsilon_r$. At $\mu_r \epsilon_r = 6.25$, the error is approximately 7 percent for the particular case shown in Fig. 6(b). Further checks on the conductance G/Y_o for other values of b/a between .1 and .9, and values of ka/π between 1.1 and 2.0 show a maximum error less than 10 percent over these ranges.

Figure 6(c) shows the accuracy of the asymptotic expression (2.65) for B/Y_o. This expression is somewhat less accurate than (2.60); the error does not approach 10 per-

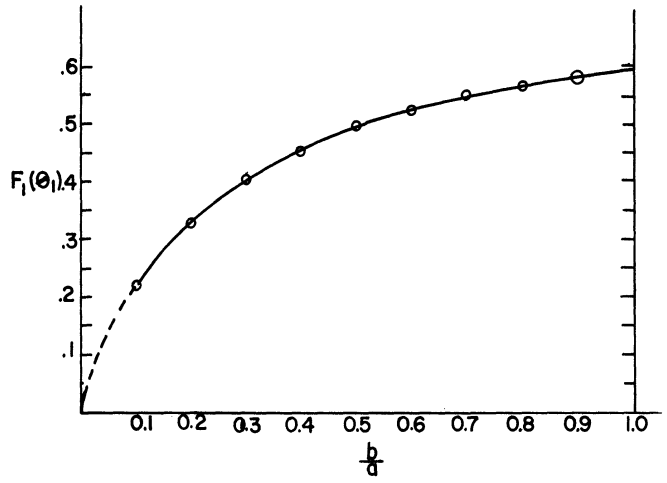

Fig. 6(a). $F_1(\theta_1)$.

cent until $\mu_r \epsilon_r \approx 36$.

The form of the asymptotic expressions for B/Y_0 and G/Y_0 allows us to draw some conclusions regarding basic limitations of this type of antenna. For instance, the curve for $F_1(\theta_1)$ has roughly the shape of $K(b/a)^{1/2}$, where K is a constant.

When this type of dependence is assumed, Eqs. 2.60, 2.65, and 2.67 become:

$$\frac{G}{Y_0} \approx \frac{K_1 \mu_r}{\sqrt{k^2 a^2 - \pi^2}} \left(\frac{k_0 a}{\pi}\right)^3 \left(\frac{b}{a}\right) \tag{2.68}$$

$$\frac{B}{Y_0} \approx \frac{K_2 \mu_r}{\sqrt{k^2 a^2 - \pi^2}} \left(\frac{b}{a}\right)^{1/2} \tag{2.69}$$

$$\frac{B}{G} \approx K_3 \left(\frac{a}{b}\right)^{1/2} \cdot \frac{1}{\left(\frac{k_0 a}{\pi}\right)^3} \tag{2.70}$$

B/G is a basic quantity, sometimes referred to as the Q of an antenna, in analogy to the Q of a tuned circuit. As noted before, B/G is closely related to the inverse of the fractional bandwidth. B/G is proportional to $(a/b)^{1/2}$; thus reducing b by a factor of 4 will reduce band-

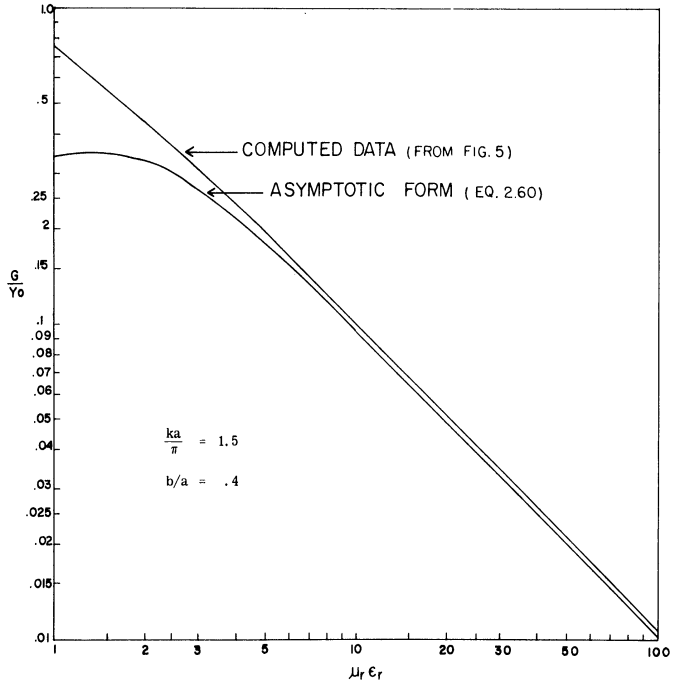

Fig. 6(b). Comparison of asymptotic expression ($k_0 a << \pi$) for G/Y_0 with computer data.

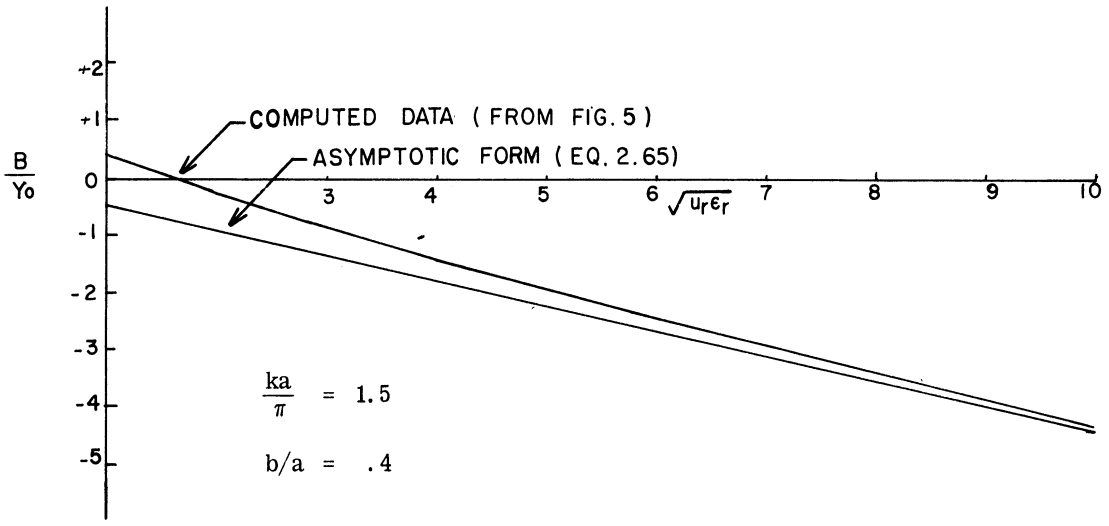

COMPARISON OF ASYMPTOTIC EXPRESSION ($k_0 a << \pi$) FOR B/Y_0 WITH COMPUTER DATA

width by a factor of about 2. This indicates that the price paid for b-dimension size reduction is not too severe, in contrast with a-dimension size reduction. It is further noted that the ratio B/G depends only on the free space electrical size of the antenna, and is unaffected by the material used. However, as noted before, the magnitudes of B/Y_0 and G/Y_0 are directly proportional to μ_r. A more complete discussion of these concepts and their relation to the general limitations is carried out in Chapter 7.

CHAPTER 3

THE COMPOUND IRIS

3.1 Introduction

This chapter is concerned with the effect on the radiating properties of an inductive, capacitive, or compound iris located in the aperture plane of the ferrite loaded waveguide radiator. The configuration is shown in Fig. 7(a) for the general case of the compound iris. For the inductive iris $b_1 = 0$, $b_2 = b$. For the capacitive iris $a_1 = 0$, $a_2 = a$. Figure 3(b) shows the division of the problem into two regions, Region No. 1 (waveguide) and Region No. 2 (half-space).

A variational expression for the normalized admittance is developed and shown to be stationary with respect to small variations of the aperture field about the correct value as determined by the defining integral equation. The development proceeds in a manner similar to that of Chapter 2 for the admittance of the loaded open-ended waveguide.

Once the variational expression is derived, it is noted that the admittance expression is not amenable to simple evaluation, even with a simple assumption of aperture field, due to the fact that the part of the admittance associated with the second term of $G_1(x, y, \xi, \eta)$ involves a slowly converging infinite series involving sine and cosine terms not orthogonal over the aperture. In order to evaluate the expression for the normalized aperture admittance, two different assumptions of trial field are used. The use of two different assumptions of trial field makes it possible to reduce the admittance to two terms, one of which is related to the admittance of the same iris in an infinite waveguide, and the other of which is related to the admittance of a loaded waveguide of reduced dimensions radiating out into half-space. Stationarity is destroyed for the imaginary part of the admittance. That accurate results are still to be expected can be shown by appealing to related variational expressions.

3.2 Derivation of Variational Expression for Admittance

The representations of the fields in Region No. 1 (waveguide) and Region No. 2 (half-space) are the same as those of Chapter 2.

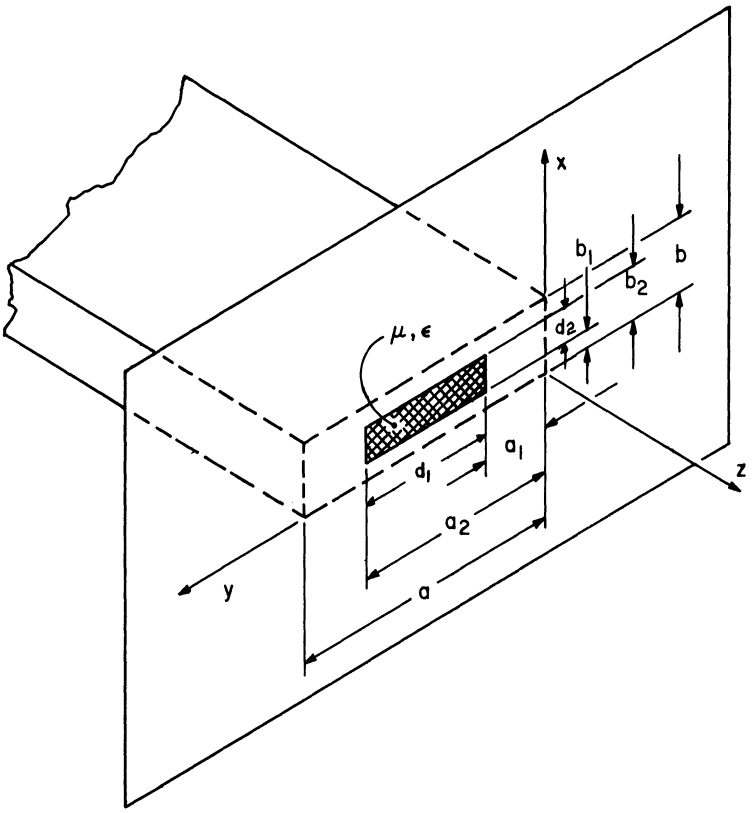

Fig. 7(a). Compound iris in the aperture plane of a material-loaded waveguide radiator.

$$\Pi_1^* = \frac{1}{-j\omega\mu}\left[\frac{\left(e^{-\Gamma_{10}z} - R\,e^{-\Gamma_{10}z}\right)}{\Gamma_{10}}\sin\frac{\pi y}{a} + \sum_{m=1}^{\infty}{}' \sum_{n=0}^{\infty} \frac{A_{mn}}{\Gamma_{mn}}\sin\frac{m\pi y}{a}\cos\frac{n\pi x}{b}\,e^{\Gamma_{mn}z}\right] \quad (3.1)$$

$$\Pi_2^* = -\frac{1}{2\pi j\omega\mu_o}\int_o^a\int_o^b E_x(\xi,\eta)\,\frac{e^{-jkr}}{r}\,d\xi\,d\eta \quad (3.2)$$

The only differences are (1) the coefficients A_{mn} have different values and (2) $E_x(\xi,\eta) = 0$ on iris.

A development parallel to that of Section 2.3 yields a final variational expression:

$$\frac{1-R}{1+R} = \frac{Y}{Y_o} = -\frac{ab\mu_r}{2\Gamma_{10}} \frac{\int_{a_1}^{a_2}\int_{b_1}^{b_2}\int_{a_1}^{a_2}\int_{b_1}^{b_2} E_x(x,y)\, E_x(\xi,\eta)\, G_1(x,y,\xi,\eta)\, dx\, dy\, d\xi\, d\eta}{\left[\int_{a_1}^{a_2}\int_{b_1}^{b_2} E(x,y) \sin\frac{\pi y}{a}\, dx\, dy\right]^2} \tag{3.3}$$

and a defining integral equation:

$$\int_{a}^{a_2}\int_{b_1}^{b_2} E_x(\xi,\eta)\, G_1(x,y,\xi,\eta)\, d\xi\, d\eta = \frac{-2\Gamma_{10}}{\mu_r} \sin\frac{\pi y}{a}\left(1 - \frac{\int_{a_1}^{a_2}\int_{b_1}^{b_2} E_x(\xi,\eta) \sin\frac{\pi\eta}{a}\, d\xi\, d\eta}{ab}\right) \tag{3.4}$$

Using the defining integral equation above, and a development parallel to that of Section 2.3, it may be shown that Eq. (3.3) is stationary with respect to small variations about its correct value.

Equation (3.3) involves, because of the second term of G_1, a slowly converging infinite series consisting of $\sin\frac{m\pi y}{a}$ and $\cos\frac{n\pi x}{b}$ terms which are not orthogonal over the aperture. Thus the integrals associated with these terms will not drop out as was the case in Chapter 2. The following sections are concerned with the simplifications of Eq. (3.3) to a form suitable for computation.

3.3 The Compound Iris

$$\frac{Y}{Y_o} = -\frac{ab\mu_r}{2\Gamma_{10}} \frac{\int_{a_1}^{a_2}\int_{b_1}^{b_2}\int_{a_1}^{a_2}\int_{b_1}^{b_2} E_x(x,y)\, E_x(\xi,\eta)\, G_1(x,y,\xi,\eta)\, dx\, dy\, d\xi\, d\eta}{\left[\int_{a_1}^{a_2}\int_{b_1}^{b_2} E_x(x,y) \sin\frac{\pi y}{a}\, dx\, dy\right]^2} = \frac{Y_1}{Y_o} + \frac{Y_2}{Y_o}$$

$$\frac{Y_1}{Y_o} = -\frac{ab\mu_r}{2\Gamma_{10}} \frac{\int_{a_1}^{a_2}\int_{b_1}^{b_2}\int_{a_1}^{a_2}\int_{b_1}^{b_2} E_x(x,y)\, E_x(\xi,\eta) \left[\sum_{m=1}^{}\sum_{n=0}^{}{}' \frac{\left(k^2 - \frac{m^2\pi^2}{a^2}\right) 4\epsilon_{mn}}{ab\mu_r\Gamma_{mn}} \sin\frac{m\pi\eta}{a}\cos\frac{n\pi\xi}{b}\sin\frac{m\pi y}{a}\cos\frac{n\pi x}{b}\right] dx\,dy\,d\xi\,d\eta}{\left[\int_{a_1}^{a_2}\int_{b_1}^{b_2} E_x(x,y)\sin\frac{\pi y}{a}\,dx\,dy\right]^2}$$

$$\frac{Y_1}{Y_o} = -\frac{\frac{2(j)}{\beta_{10}}\sum_{m=1}^{\infty}\sum_{n=0}^{\infty}{}' \frac{\epsilon_{mn}\left(\frac{m^2\pi^2}{a^2} - k^2\right)}{\Gamma_{mn}} \left[\int\int E_x(x,y)\sin\frac{m\pi y}{a}\cos\frac{n\pi x}{b}\,dx\,dy\right]^2}{\left[\int_{a_1}^{a_2}\int_{b_1}^{b_2} E_x(x,y)\sin\frac{\pi y}{a}\,dx\,dy\right]^2} \qquad (3.5)$$

This expression has the same form as one-half of the admittance of the compound iris in an infinite waveguide loaded with material of characteristics μ_r, ϵ_r.[66] In particular, if the aperture field $E_x(x,y)$ is identical in the two cases (infinite waveguide and semi-infinite waveguide with infinite ground plane), then Y_1 reduces to one-half of the admittance of the compound iris in an infinite waveguide. The admittance of the compound iris in an infinite waveguide has been calculated by Lewin.[67] The addition of material with characteristics μ_r, ϵ_r does not change the normalized admittance if frequency is changed (or if the linear dimensions are reduced by $\sqrt{\mu_r\epsilon_r}$) so as to maintain f/f_c. Y_a/Y_o will now be evaluated for the compound iris:

$$\frac{Y_2}{Y_o} = -\frac{ab\mu_r}{2\Gamma_{10}} \frac{\int_{a_1}^{a_2}\int_{b_1}^{b_2}\int_{a_1}^{a_2}\int_{b_1}^{b_2} E_x(x,y)\, E_x(\xi,\eta)\left[\frac{\partial^2}{\partial y^2} + k_o^2\right]\frac{e^{-jk_o r}}{2\pi r}\,dx\,dy\,d\xi\,d\eta}{\left[\int_{a_1}^{a_2}\int_{b_1}^{b_2} E_x(x,y)\sin\frac{\pi y}{a}\,dx\,dy\right]^2} \qquad (3.6)$$

At this point we assume that $E_x(x,y)$ is separable $= E_x(x)\, E_x(y)$.

Integrating twice by parts with respect to y and η gives:

$$\frac{Y_2}{Y_o} = -\frac{ab\mu_r}{2\Gamma_{10}} \frac{\left[k_o^2 \int_{a_1}^{a_2}\int_{b_1}^{b_2}\int_{a_1}^{a_2}\int_{b_1}^{b_2} E_x(x,y)\, E_x(\xi,\eta)\, \frac{e^{-jk_o r}}{2\pi r}\, dx\, dy\, d\xi\, d\eta - \int_{a_1}^{a_2}\int_{b_1}^{b_2}\int_{a_1}^{a_2}\int_{b_1}^{b_2} E_x(x)\, E_x(\xi)\, E'_x(y)\, E'_x(\eta)\, \frac{e^{-jk_o r}}{2\pi r}\, dx\, dy\, d\xi\, d\eta\right]}{\left[\int_{a_1}^{a_2}\int_{b_1}^{b_2} E_x(x,y) \sin\frac{\pi y}{a}\, dx\, dy\right]^2} \tag{3.7}$$

where

$$E'_x(y) = \frac{\partial E_x(y)}{\partial y}$$

$$E'_x(\eta) = \frac{\partial E_x(\eta)}{\partial \eta}$$

in

$$\begin{aligned} y' &= y - a_1 \qquad x' = x - b_1 \qquad a_2 - a_1 = d_1, \qquad r' = r \\ \eta' &= \eta - a_1 \qquad \xi' = \xi - b_1 \qquad b_2 - b_1 = d_2 \end{aligned} \tag{3.8}$$

$$\frac{Y_2}{Y_o} = -\frac{ab\mu_r}{2\Gamma_{10}} \frac{\int_0^{d_1}\int_0^{d_2}\int_0^{d_1}\int_0^{d_2} E_x(x',y')\, E_x(\xi',\eta') \left[\frac{\partial^2}{\partial y'^2} + k_o^2\right] \frac{e^{-jk_o r}}{2\pi r}\, dx'\, dy'\, d\xi'\, d\eta'}{\left[\int_0^{d_1}\int_0^{d_2} E_x(x',y') \sin\frac{\pi(y'+a_1)}{a}\, dx'\, dy'\right]^2} \tag{3.9}$$

This form bears some similarity to the dominant mode approximation to the aperture admittance of a loaded waveguide of dimensions d_1 and d_2 radiating into half space [see Eq. (2.33)].

Let $Y_A(d_1, d_2)/Y_o$ be the normalized aperture admittance of a rectangular waveguide with broad dimension d_1, narrow dimension d_2, material loading μ_r, ϵ_r, radiating into half space.

With the assumption of dominant mode aperture field:

$$\frac{Y_A(d_1,d_2)}{Y_o} = -\frac{d_1^2 d_2 \mu_r}{2j\sqrt{k^2 d_1^2 - \pi^2}} \frac{\int_0^{d_1}\int_0^{d_2}\int_0^{d_1}\int_0^{d_2} E_x(x,y)\, E_x(\xi,\eta) \left[\frac{\partial^2}{\partial y^2} + k_o^2\right] \frac{e^{-jk_o r}}{2\pi r}\, dx\, dy\, d\xi\, d\eta}{\left[\int_0^{d_1}\int_0^{d_2} E_x(x,y) \sin\frac{\pi y}{a}\, dx\, dy\right]^2} \tag{3.10}$$

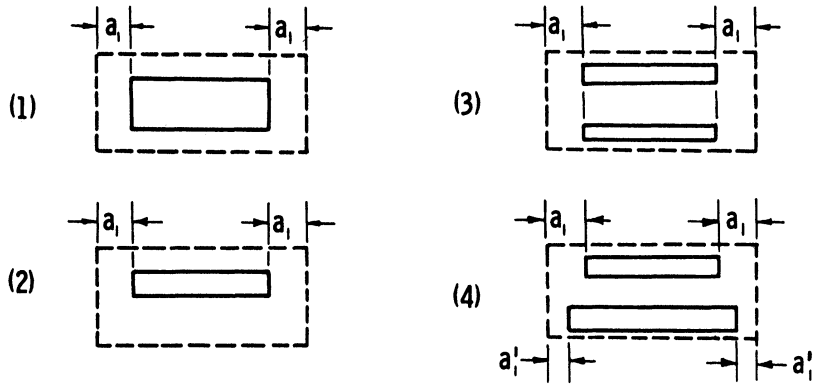

Fig. 7(b). Compound irises.

In certain cases, it may be reasonable to assume that the aperture fields for $Y_A(d_1, d_2)/Y_o$ and Y_2/Y_o are identical. This would be a reasonable assumption for the cases shown in Fig. 7(b), which include all symmetric irises as well as irises asymmetric in x, and multiple irises each one of which is symmetric in y.

Cases where the iris is asymmetric in y would have to be treated separately with particular assumptions of aperture field in Eq. (3.7).

$$\frac{Y_2}{Y_A(d_1, d_2)} = \frac{a^2 b}{d_1^2 d_2} \frac{\sqrt{k^2 d_1^2 - \pi^2}}{\sqrt{k^2 a^2 - \pi^2}} \frac{\left[\int_0^{d_1}\int_0^{d_2} E_x(x,y) \sin \frac{\pi y}{a}\right]^2}{\left[\int_0^{d_1}\int_0^{d_2} E_x(x',y') \sin \frac{\pi(y'+a_1)}{a}\, dx'\, dy'\right]^2} \tag{3.11}$$

Let

$$E_x(x,y) = \sin \frac{\pi}{d_1}(y - a_1) \tag{3.12}$$

in the aperture of the compound iris.

$$Y_2 = \left[\frac{\pi^2}{16}\left(\frac{a^2}{d_1^2}\right)\left(\frac{b}{d_2}\right)\frac{\sqrt{k^2 d_1^2 - \pi^2}}{\sqrt{k^2 a^2 - \pi^2}}\left(1 - \frac{d_1^2}{a^2}\right)^2 \csc^2 \frac{\pi a_1}{a}\right] \cdot Y_A(d_1, d_2) \tag{3.13}$$

Thus Y_2 can be expressed as the product of an algebraic factor which is a function of the iris dimensions times $Y_A(d_1, d_2)$, which is the normalized aperture admittance of a rectangular

waveguide with broad dimension d_1, narrow dimension d_2, ferrite loading μ_r, ϵ_r radiating into half space [see Fig. 3(a)].

The real and imaginary parts of $Y_A(d_1, d_2)/Y_0$ approach infinity as $kd_1 \longrightarrow \pi$ because of the factor $1/\sqrt{k^2 d_1^2 - \pi^2}$ in $Y_A(d_1, d_2)/Y_0$. The factor $\sqrt{k^2 d_1^2 - \pi^2}/\sqrt{k^2 a^2 - \pi^2}$ cancels the poles at $kd_1 = \pi$ and produces poles in the real and imaginary parts of Y_2/Y_0 at $ka = \pi$ (the cutoff of the actual waveguide used) as would be expected.

Thus, the admittance of the compound iris has been reduced to two terms Y_1/Y_0 and Y_2/Y_0. Y_1/Y_0 can be related to the admittance of the same compound iris in an infinite waveguide and Y_2/Y_0 can be related to the admittance of a waveguide of reduced dimensions d_1, d_2, radiating into half-space. However, in order to evaluate the separate expressions, it may be necessary to use two different approximations to the aperture field because aperture field assumptions convenient for the evaluation of Y_1/Y_0 may not be convenient for the evaluation of Y_2/Y_0. This, of course, destroys the stationarity, since Y_1/Y_0 and Y_2/Y_0 are not individually stationary. Y_1/Y_0 is stationary with respect to small variations about the value as defined by the integral equation for the iris in the infinite waveguide, but is not stationary with respect to small variations about the true value as defined by the integral equation (3. 12) for the iris in the waveguide radiating into half-space. This implies that results derived from different assumptions may not be as accurate as results derived from a single assumption of aperture field, although different assumptions of aperture field are sometimes used in variational expressions without comment.[68] Consider the approximation:

$$\frac{Y}{Y_0} = \frac{Y_1(E_1)}{Y_0} + \frac{Y_2(E_2)}{Y_0} \qquad (E_1(x, y) \neq F_2(x, y))$$

At first glance, such an approximation (using two different values of aperture field) might appear to lack most of the advantages of a variational expression since the proof of stantionarity is no longer valid. However, it may be shown that most of the advantages of the variational method are retained because of the stationarity of Y_1/Y_0 with respect to the defining integral equation for the infinite waveguide case.

Consider the Inductive Iris:

A convenient assumption for the evaluation of Y_2/Y_0 is $E_x = \sin \frac{\pi}{d_1} (y - a_1)$ which reduces Y_2/Y_0 to the waveguide half-space problem without an iris in the aperture plane. Now consider the expression for Y_1/Y_0, which is identical in form to 1/2 the admittance of the same iris in an infinite waveguide, with, however, different defining integral equations for, respectively, the infinite waveguide case and the problem under consideration. If we use the same assumption $E_x = \sin \frac{\pi}{d_1} (y - a_1)$ in Y_1/Y_0, we would expect good results because of stationarity. It is not convenient to use this approximation, but it may be argued that the results, if we used $E_x = \sin \frac{\pi}{d_1} (y - a_1)$ would be close to those obtained with Schwinger's[69] approximation, which is often used to evaluate the admittance of the inductive iris. The primary reason for using the Schwinger transformation is to obtain an infinite series which is orthogonal over the aperture and which is summable. Typical results show a difference of only a few percent between upper and lower bounds. Because of the stationary property of the admittance of the inductive iris in the infinite waveguide, we would expect that the assumption $E_x = \sin \frac{\pi}{d_1} (y - a_1)$ would also give very good answers for the admittance of the inductive iris in the infinite waveguide. It is not convenient to use this assumption in the expression for Y_1/Y_0 but it may be argued that the results for Y_1/Y_0 would be close to those obtained with Schwinger approximation.

Comparing the result of using a single approximation $E_{x2} = \sin \frac{\pi}{d_1} (y - a_1)$ in both Y_1/Y_0 and Y_2/Y_0 with the result of using E_{x2} in Y_2/Y_0 and E_{x1} (Schwinger's approximation) in Y_1/Y_0, we see that Y_2/Y_0 is identical and Y_1/Y_0 is very close, in the two cases. Thus we have argued that the individual terms Y_1/Y_0 and Y_2/Y_0 are accurately evaluated. Similar arguments would apply to the capacitive and inductive irises.

It should be noted that the above limitations apply only to the imaginary part of the impedance $Y/Y_0 = Y_1/Y_0 + Y_2/Y_0$. Since $\delta y = 0$, the real and imaginary parts of the admittance must separately be stationary ($\delta G = \delta B = 0$). If (a) $E_x(xy)$ is real and (b) higher

order modes are cut off, then Y_1/Y_o will be purely imaginary. The only contribution to the real part of the admittance comes then from Y_2/Y_o. As long as only one assumption is used for $E_x(x, y)$ in Y_2/Y_o, the stationary property of the real part is preserved.

3.4 Special Cases--Inductive and Capacitive Irises

Consider the special cases of the inductive and the capacitive iris. These special cases introduce a higher degree of symmetry in the infinite waveguide case than they do in the problem under study. Therefore, the forms for Y_1/Y_o do not reduce to the corresponding infinite waveguide admittance forms without further assumptions.

3.4.1 Inductive Iris.

$$\frac{Y}{Y_o} = -\frac{ab\mu_r}{\left[\int_{a_1}^{a_2}\int_{o}^{b} E_x(x,y)\sin\frac{\pi y}{a}\,dx\,dy\right]^2}\int_{a_1}^{a_2}\int_{o}^{b}\int_{a_1}^{a_2}\int_{o}^{b} E_x(x,y)\,E_x(\xi,\eta)\,G_1(x,y,\xi,\eta)\,dx\,dy\,d\xi\,d\eta = \frac{Y_1}{Y_o}+\frac{Y_2}{Y_o} \tag{3.14}$$

Let us assume that $E_x(x, y)$ is independent of x. This is a reasonable assumption since the physical configuration of the inductive obstacle does not vary with x.

$$\begin{aligned} E_x(x,y) &= E_x(y) \\ E_x(\xi,\eta) &= E_x(\eta) \end{aligned} \tag{3.15}$$

$$\frac{Y_1}{Y_o} = \frac{\int_{a_1}^{a_2}\int_{a_1}^{a_2} E_x(y)\,E_x(\eta)\sum_{m=2}^{\infty}\frac{\Gamma_{mo}}{\Gamma_{10}}\sin\frac{m\pi y}{a}\sin\frac{m\pi\eta}{a}\,dy\,d\eta}{\left[\int_{a_1}^{a_2} E_x(y)\sin\frac{\pi y}{a}\,dy\right]^2} \tag{3.16}$$

The equation above is similar to the normalized admittance of an inductive iris in an infinite waveguide.[71,72] If the aperture electric field $E_x(y)$ is assumed to be the same as in the waveguide case, then Y_1/Y_o is equal to one-half the normalized admittance of the inductive iris in the waveguide case.

The expression for Y_2/Y_o reduces immediately to

$$\frac{Y_2}{Y_o} = \left[\frac{\pi^2(1-d_1^2/a^2)^2 \sqrt{k^2d_1^2-\pi^2}}{16\sqrt{k^2a^2-\pi^2}\cos^2\frac{\pi d_1}{2a}} \left(\frac{a^2}{d_1^2}\right) \right] Y_A(d_1, b) \tag{3.17}$$

3.4.2 Capacitive Iris.

$$\frac{Y}{Y_o} = -\frac{ab\mu_r}{2\Gamma_{10}} \frac{\int_o^a \int_{b_1}^{b_2} \int_o^a \int_{b_1}^{b_2} E_x(x,y)\, E_x(\xi,\eta)\, G_1(x,y,\xi,\eta)\, dx\, dy\, d\xi\, d\eta}{\left[\int_o^a \int_{b_1}^{b_2} E_x(x,y) \sin\frac{\pi y}{a}\, dx\, dy\right]^2} = \frac{Y_1}{Y_o} + \frac{Y_2}{Y_o} \tag{3.18}$$

assume that $E_x(x,y)$ is separable $= E_x(x)\, E_x(y)$

$$\frac{Y_1}{Y_o} = -\frac{ab\mu_r}{2\Gamma_{10}} \sum_{m=1} \sum_{n=0}' \frac{4\epsilon_{mn}\left(k^2 - \frac{m^2\pi^2}{a^2}\right)}{ab\mu_r\Gamma_{10}} \int_o^a \int_o^a E_x(y)\, E_x(\eta) \sin\frac{m\pi y}{a} \sin\frac{m\pi\eta}{a}\, d\eta\, dy$$

$$\frac{\left[\int_{b_1}^{b_2} \int_{b_1}^{b_2} E_x(x)\, E_x(\xi) \cos\frac{n\pi\xi}{b} \cos\frac{n\pi x}{b}\, dx\, d\xi\right]}{\left[\int_o^a E_x(y) \sin\frac{\pi y}{a} \int_{b_1}^{b_2} E_x(x)\, dx\right]^2}$$

Let

$$E_x(y) = \sin\frac{\pi y}{a} \tag{3.19}$$

Then the integration in y and η yields a contribution only if m = 1. $\epsilon_{mn} = 1$ for all terms.

$$\frac{Y_1}{Y_o} = \frac{2\Gamma_{10} \sum_{n=1}^{\infty} \frac{1}{\Gamma_{1n}} \int_{b_1}^{b_2} \int_{b_1}^{b_2} E_x(x)\, E_x(\xi) \cos\frac{n\pi\xi}{b} \cos\frac{n\pi x}{b}\, dx\, d\xi}{\left[\int_{b_1}^{b_2} E_x(x)\, dx\right]^2} \tag{3.20}$$

This term is equal to one-half the normalized admittance of a capacitive iris in an infinite waveguide if the fields $E_x(x)$ are identical in the two cases.

The expression for Y_2/Y_o reduces immediately to:

$$\frac{Y_2}{Y_o} = \left(\frac{b}{d_2}\right) \frac{Y_A(a, d_2)}{Y_o} \tag{3.21}$$

where $Y_A(\,)/Y_o$ is as defined in Section 3.3. The theoretical formulations (3.17) and (3.21) of this chapter for the admittance of a loaded waveguide radiator with an iris in the aperture plane are compared with experimental results in Chapter 6.

Figures 8 and 9 include additional data on the admittance of a loaded rectangular radiator [Fig. 3(a)] including (a) data below (1,0) mode cutoff necessary for the evaluation of (3.17), and (b) data above (2,0) mode cutoff.

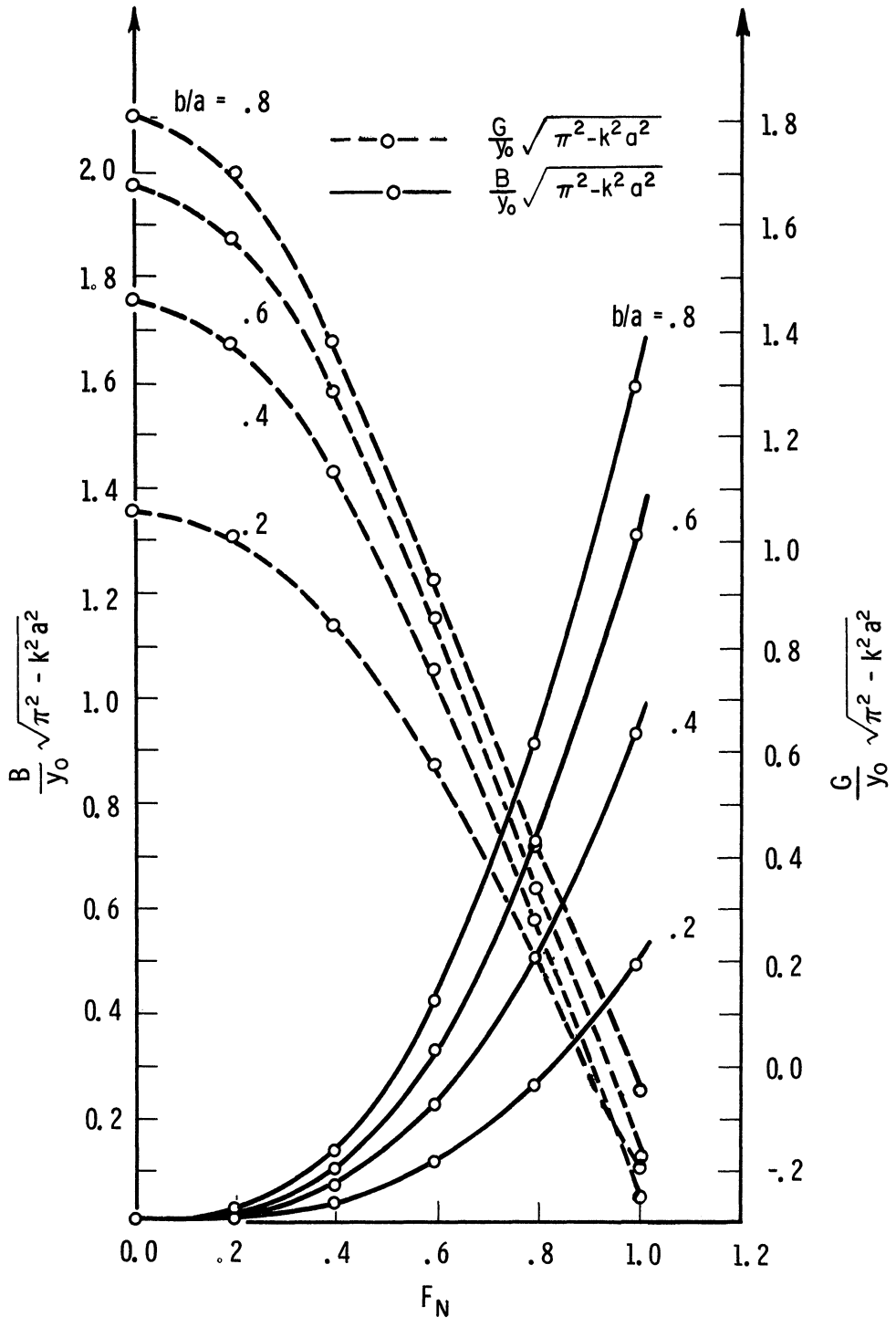

Fig. 8(a) Aperture admittance of a loaded waveguide radiator below cutoff ($F_N = 1.0$ at cutoff). (a) $\mu_r = \epsilon_r = 1.0$.

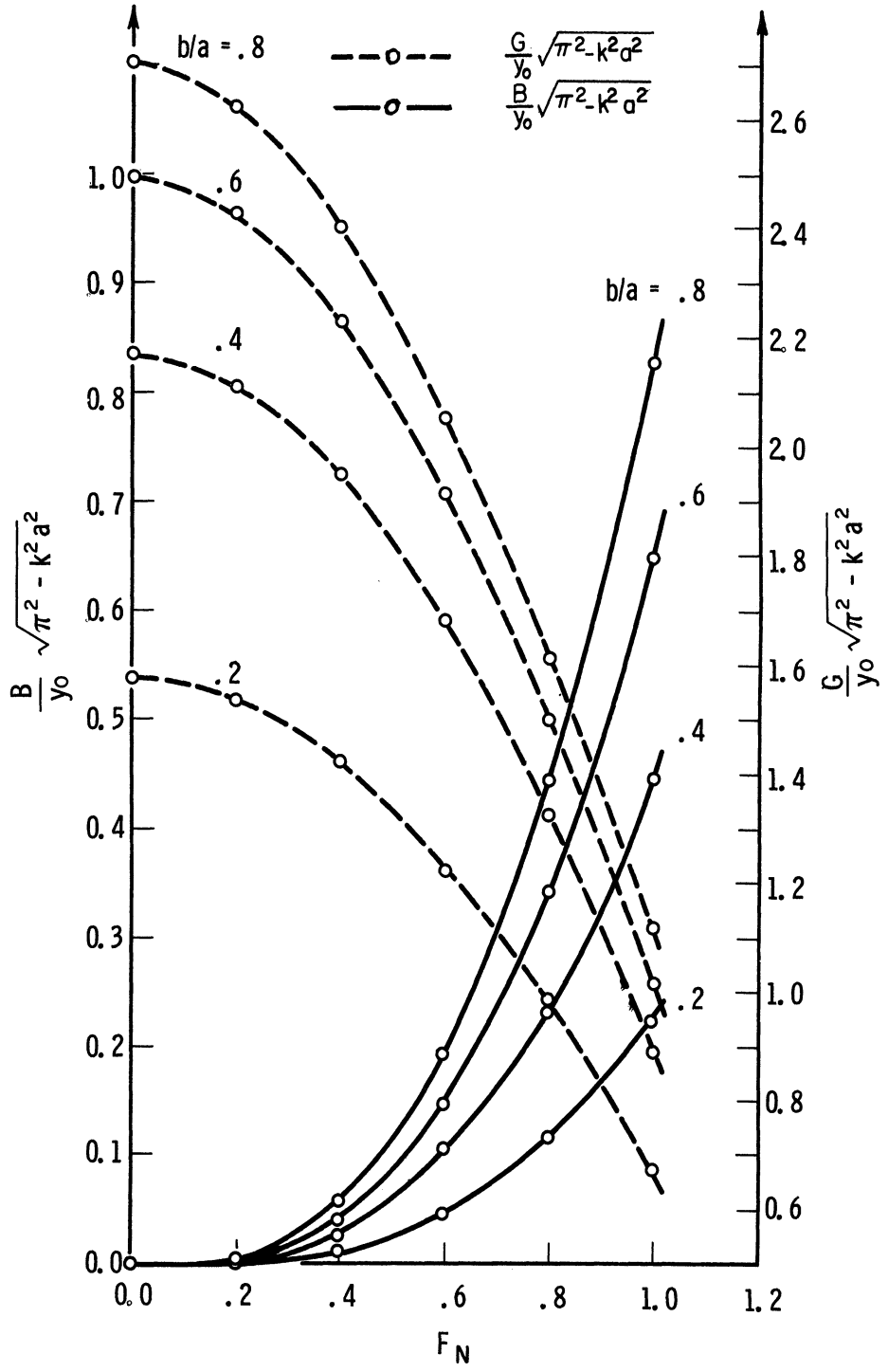

Fig. 8(b) Aperture admittance of a loaded waveguide radiator below cutoff ($F_N = 1.0$ at cutoff). (b) $\mu_r = \epsilon_r = 1.5$.

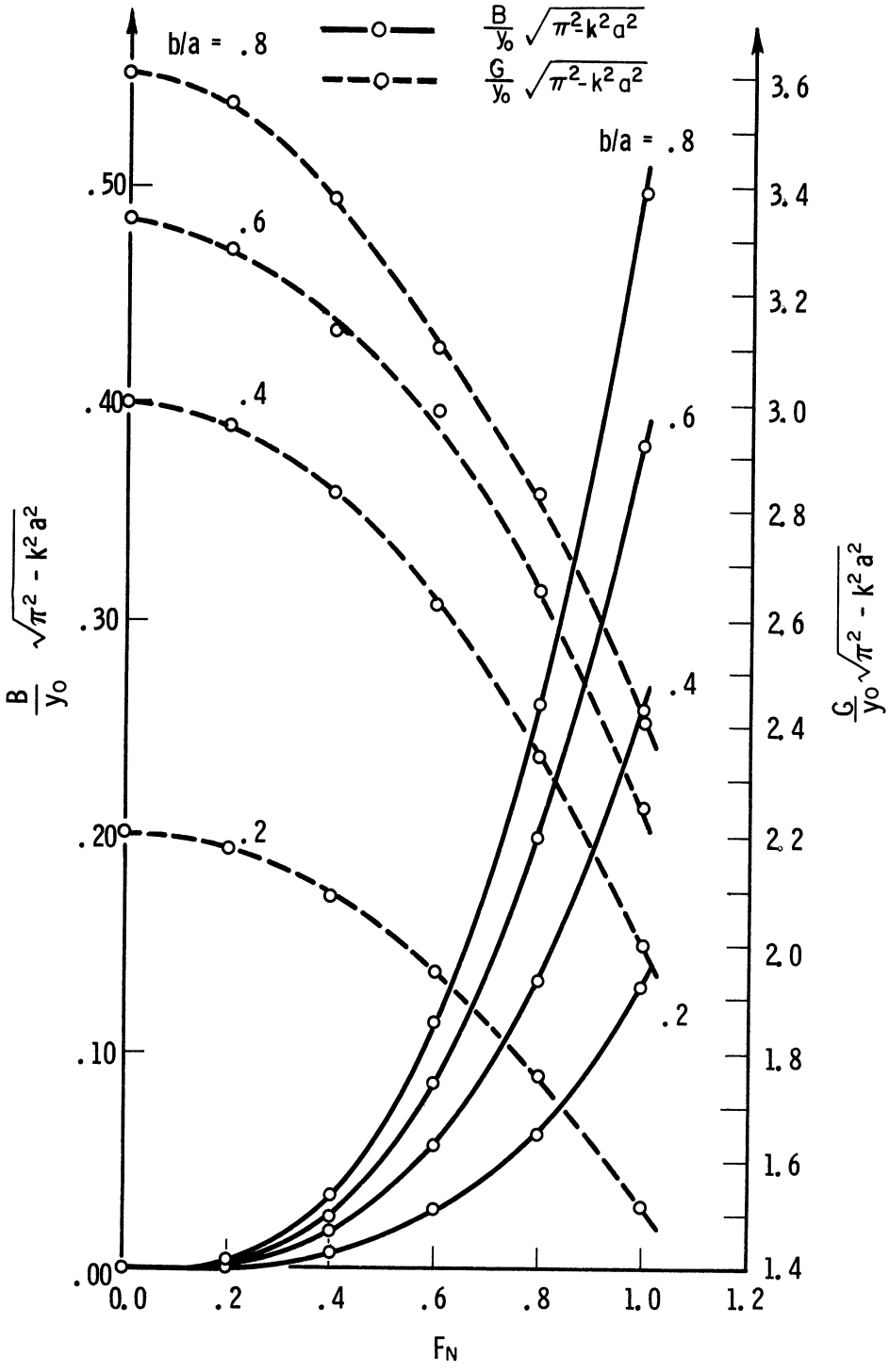

Fig. 8(c) Aperture admittance of a loaded waveguide radiator below cutoff (F_N = 1.0 at cutoff). (c) $\mu_r = \epsilon_r = 2.0$.

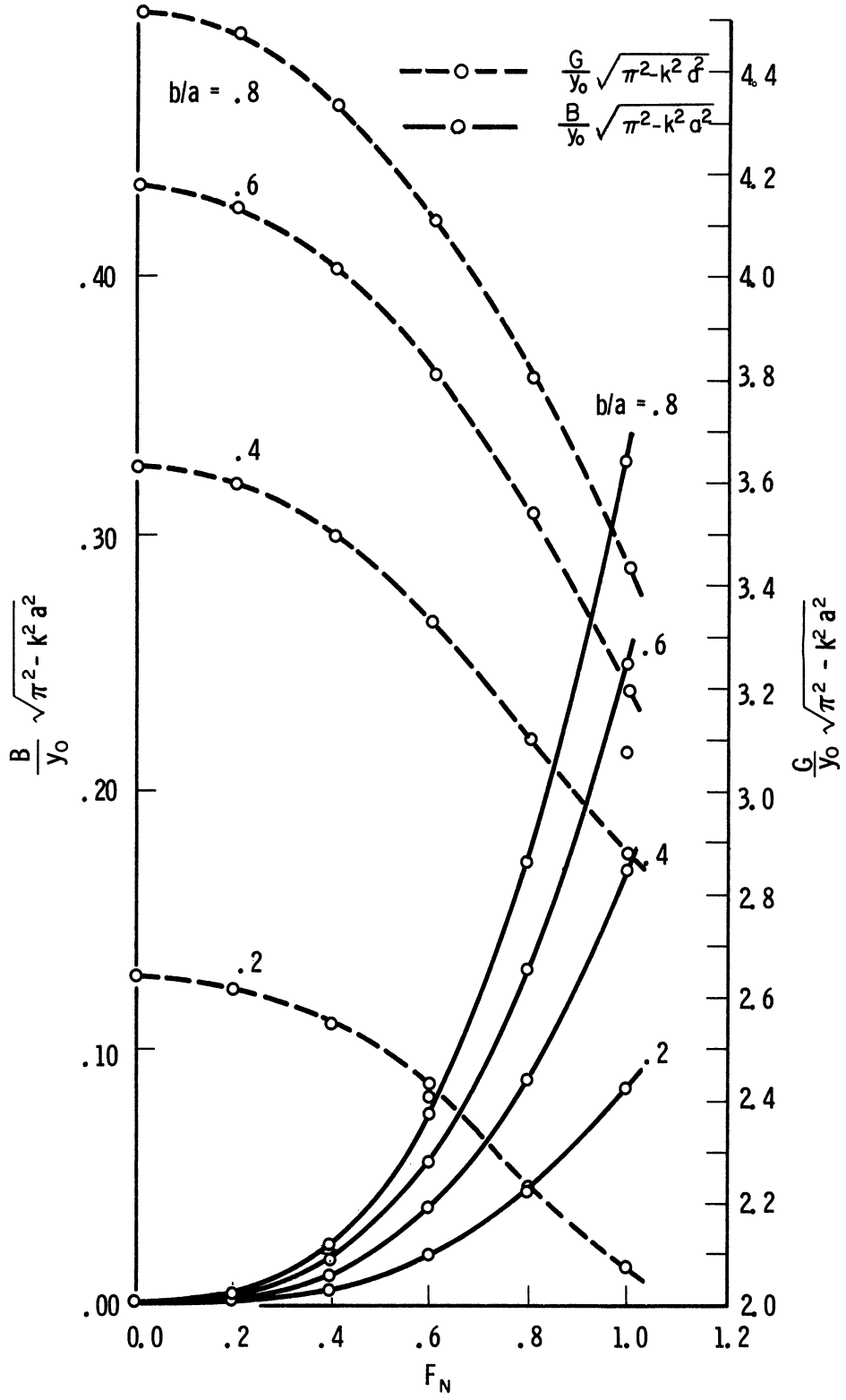

Fig. 8(d) Aperture admittance of a loaded waveguide radiator below cutoff (F_N = 1.0 at cutoff). (d) $\mu_r = \epsilon_r = 2.5$.

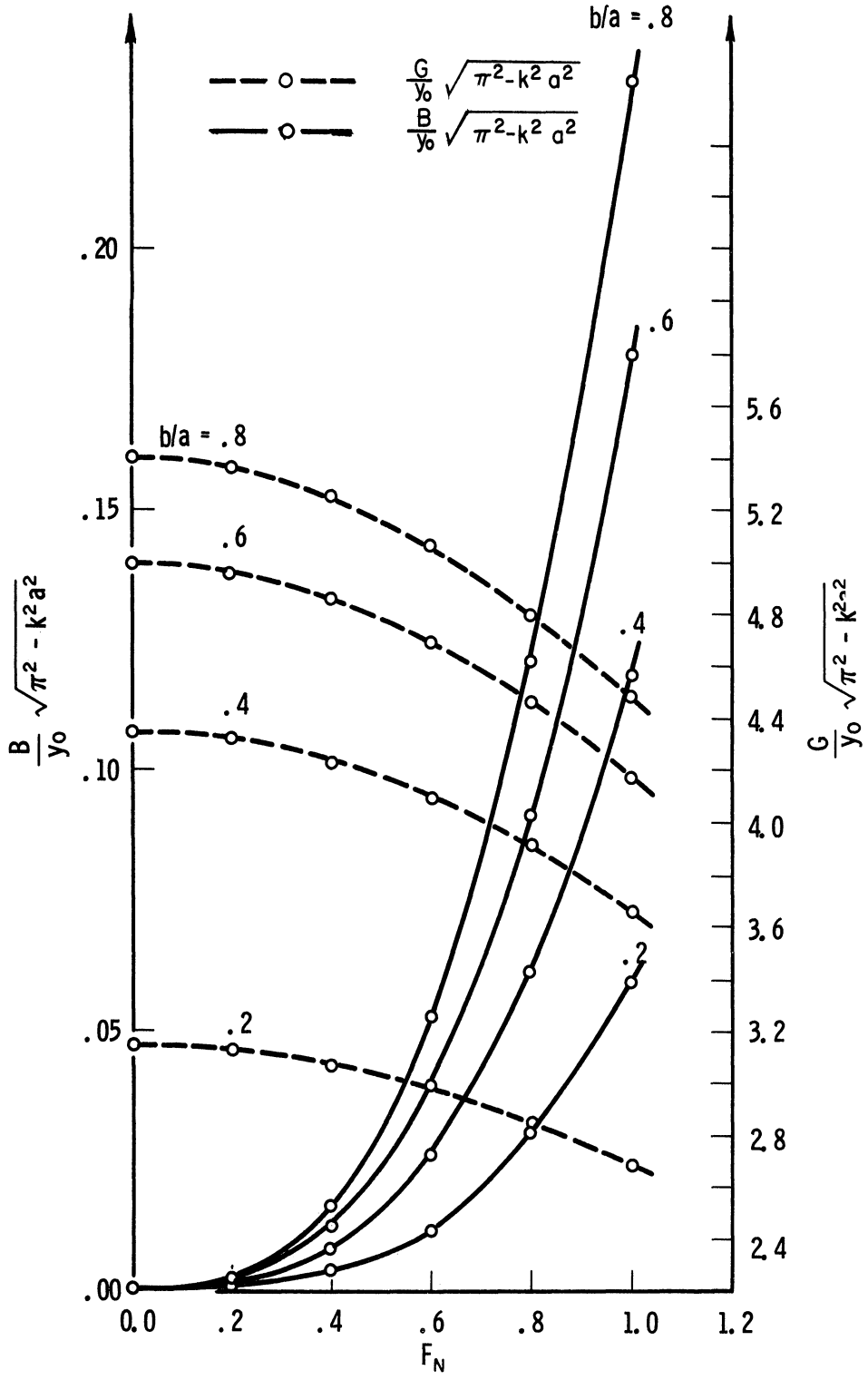

Fig. 8(e) Aperture admittance of a loaded waveguide radiator below cutoff (F_N = 1.0 at cutoff). (e) $\mu_r = \epsilon_r = 3.0$.

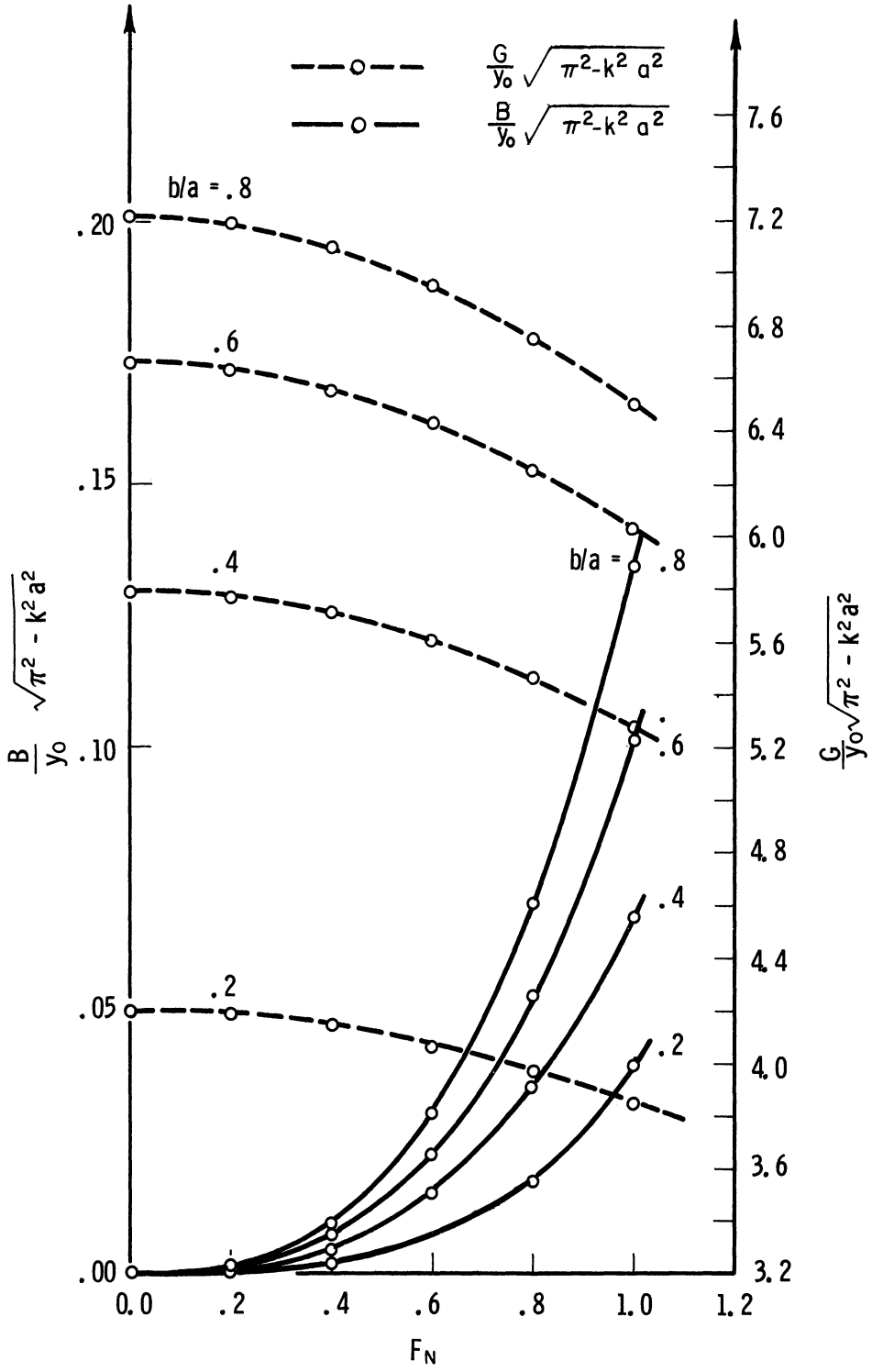

Fig. 8(f) Aperture admittance of a loaded waveguide radiator below cutoff ($F_N = 1.0$ at cutoff). (f) $\mu_r = \epsilon_r = 4.0$.

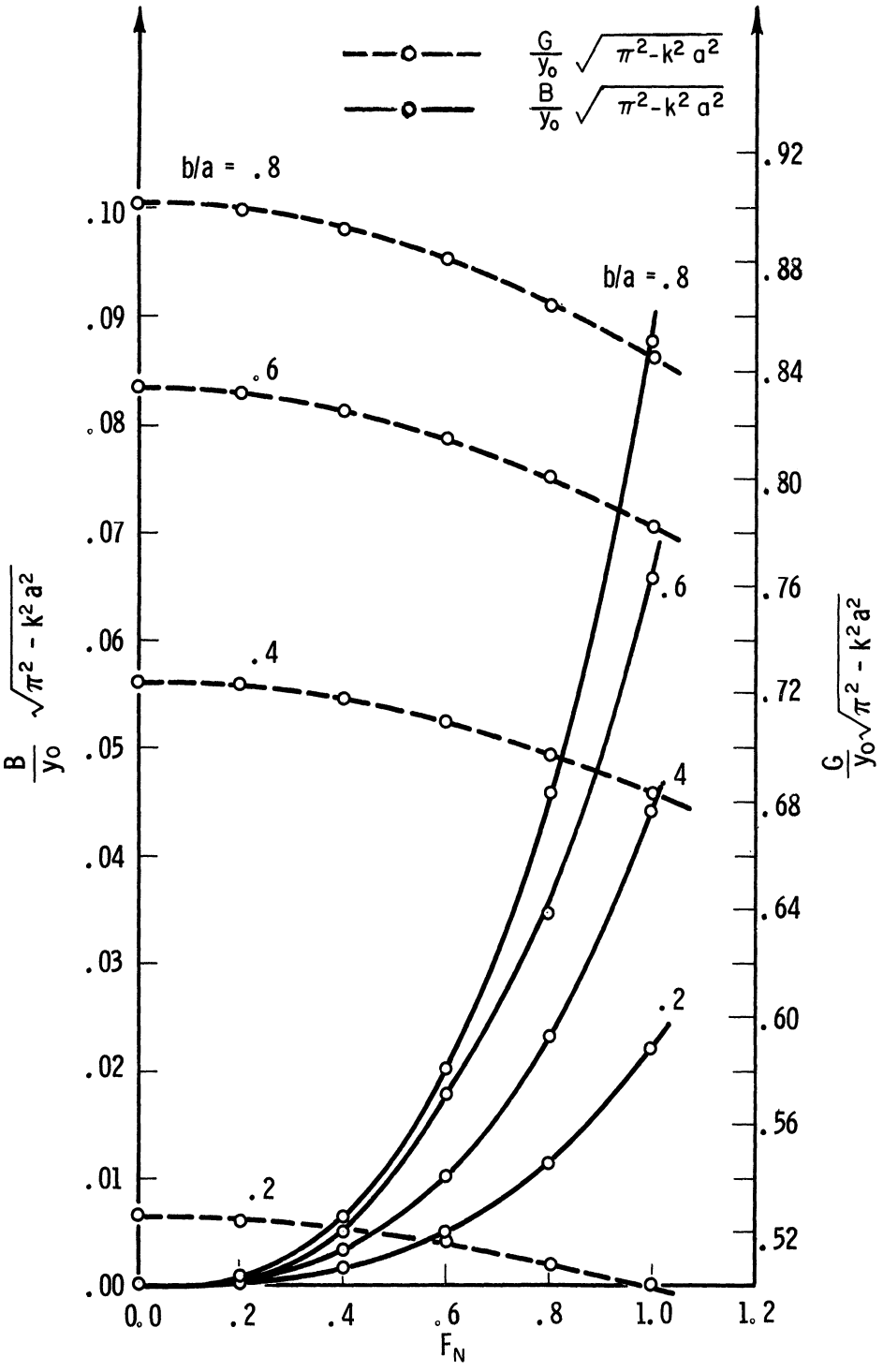

Fig. 8(g) Aperture admittance of a loaded waveguide radiator below cutoff (F_N = 1.0 at cutoff). (g) $\mu_r = \epsilon_r = 5.0$.

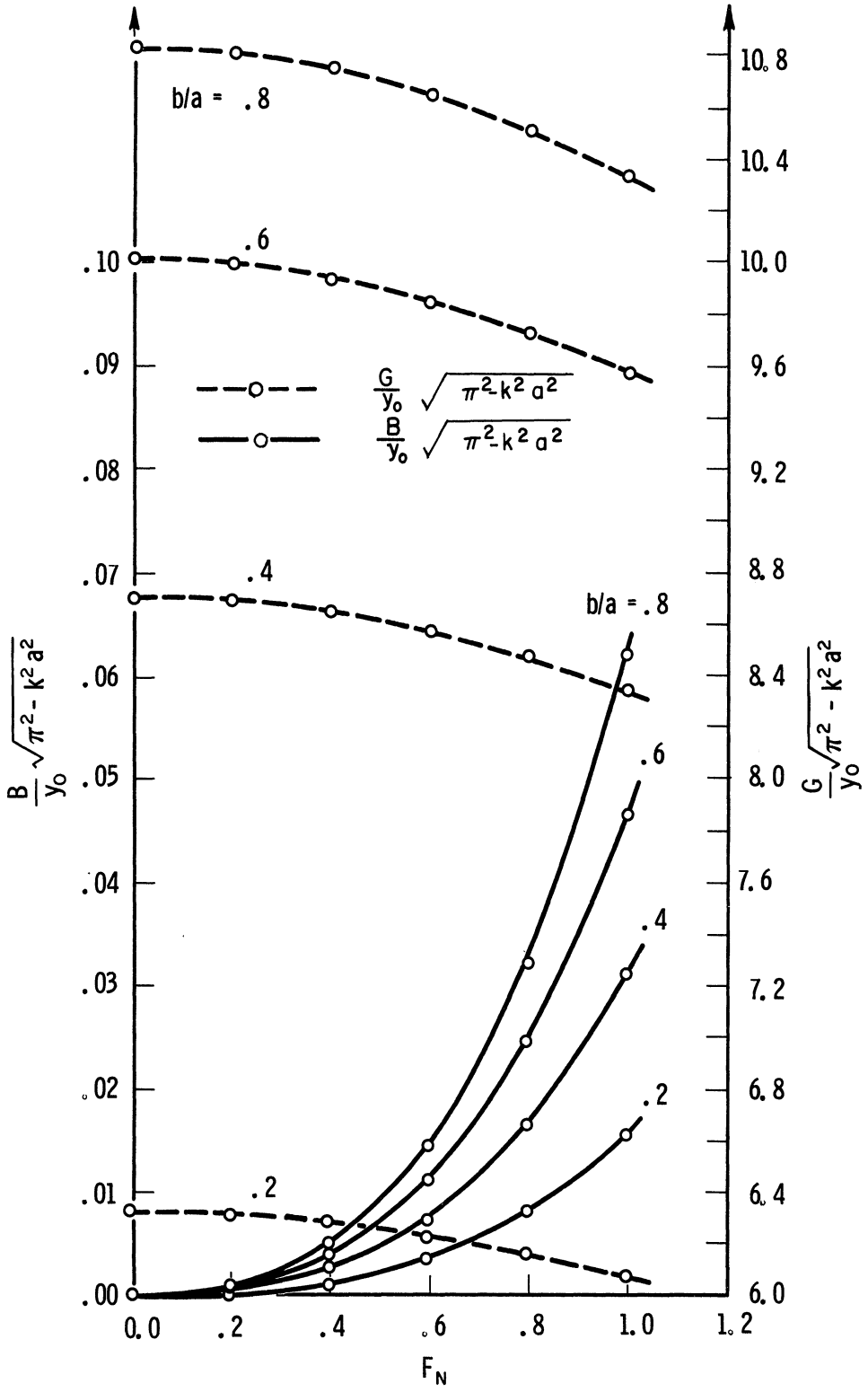

Fig. 8(h) Aperture admittance of a loaded waveguide radiator below cutoff (F_N = 1.0 at cutoff). (h) $\mu_r = \epsilon_r = 6.0$.

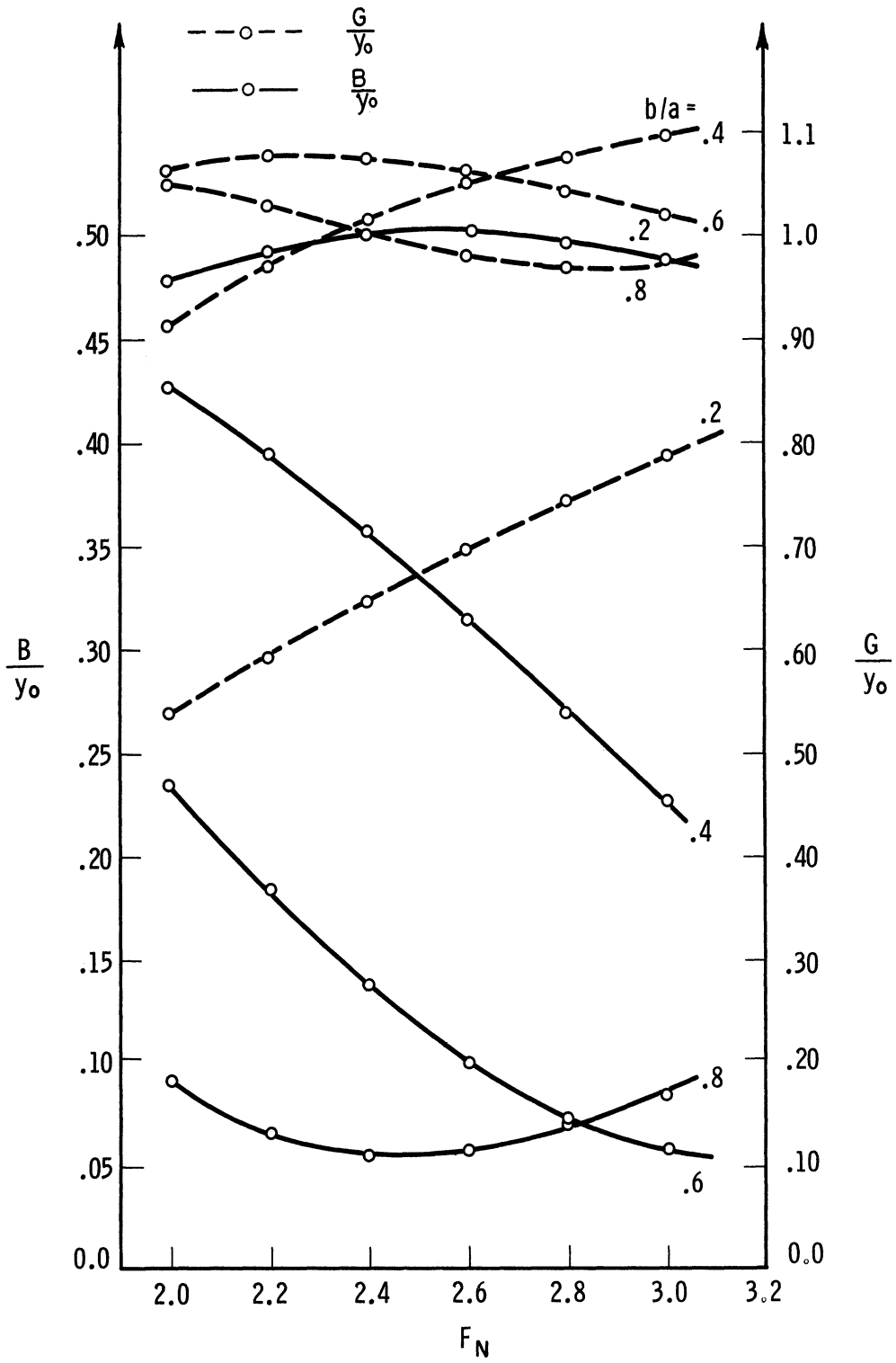

Fig. 9(a) Aperture admittance above (2,0) mode cutoff (F_N = 2.0 - 3.0) (F_N = 1.0 at cutoff). (a) $\mu_r = \epsilon_r = 1.0$.

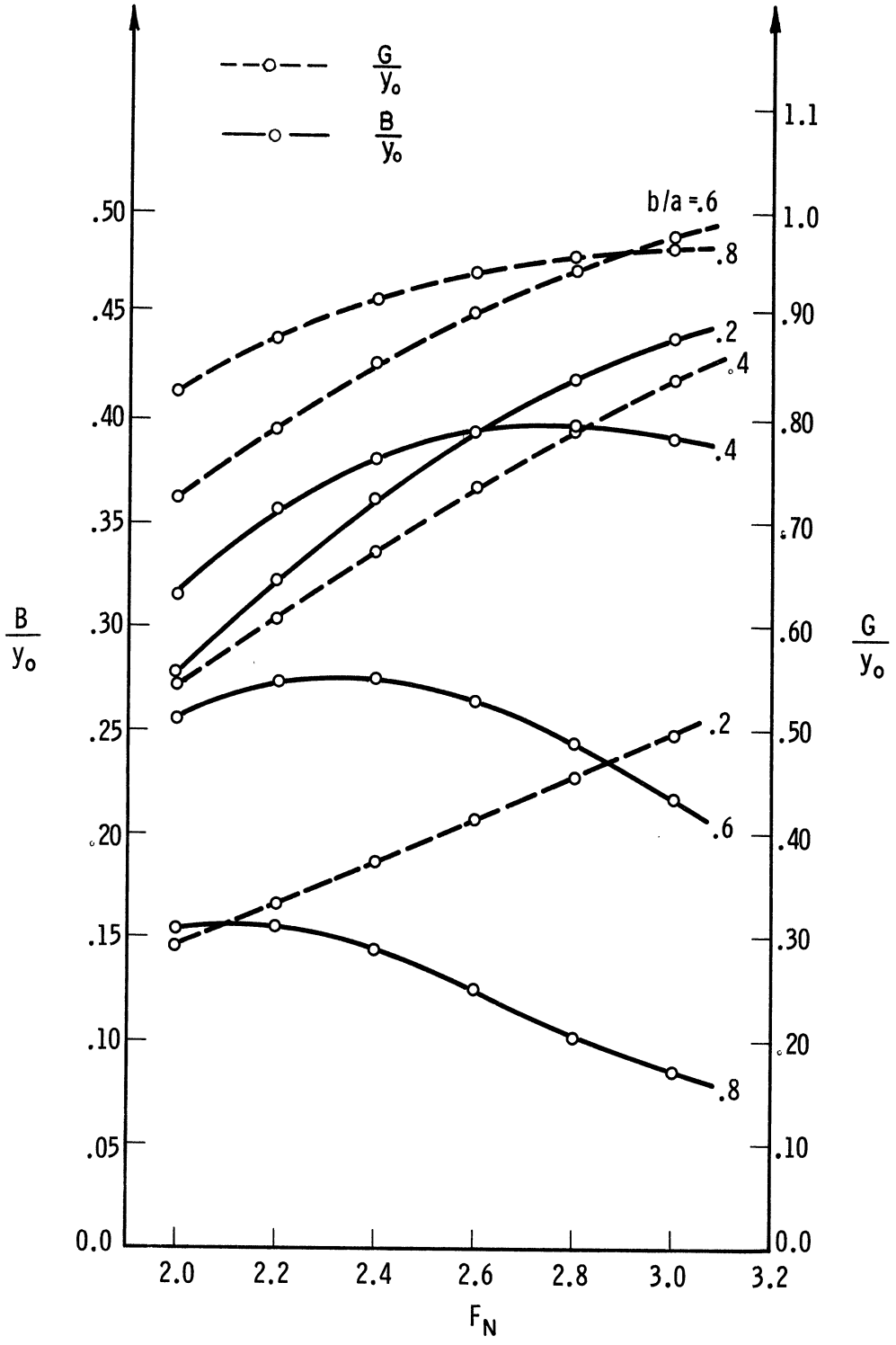

Fig. 9(b) Aperture admittance above (2, 0) mode cutoff (F_N = 2.0 - 3.0) (F_N = 1.0 at cutoff). (b) $\mu_r = \epsilon_r = 1.5$.

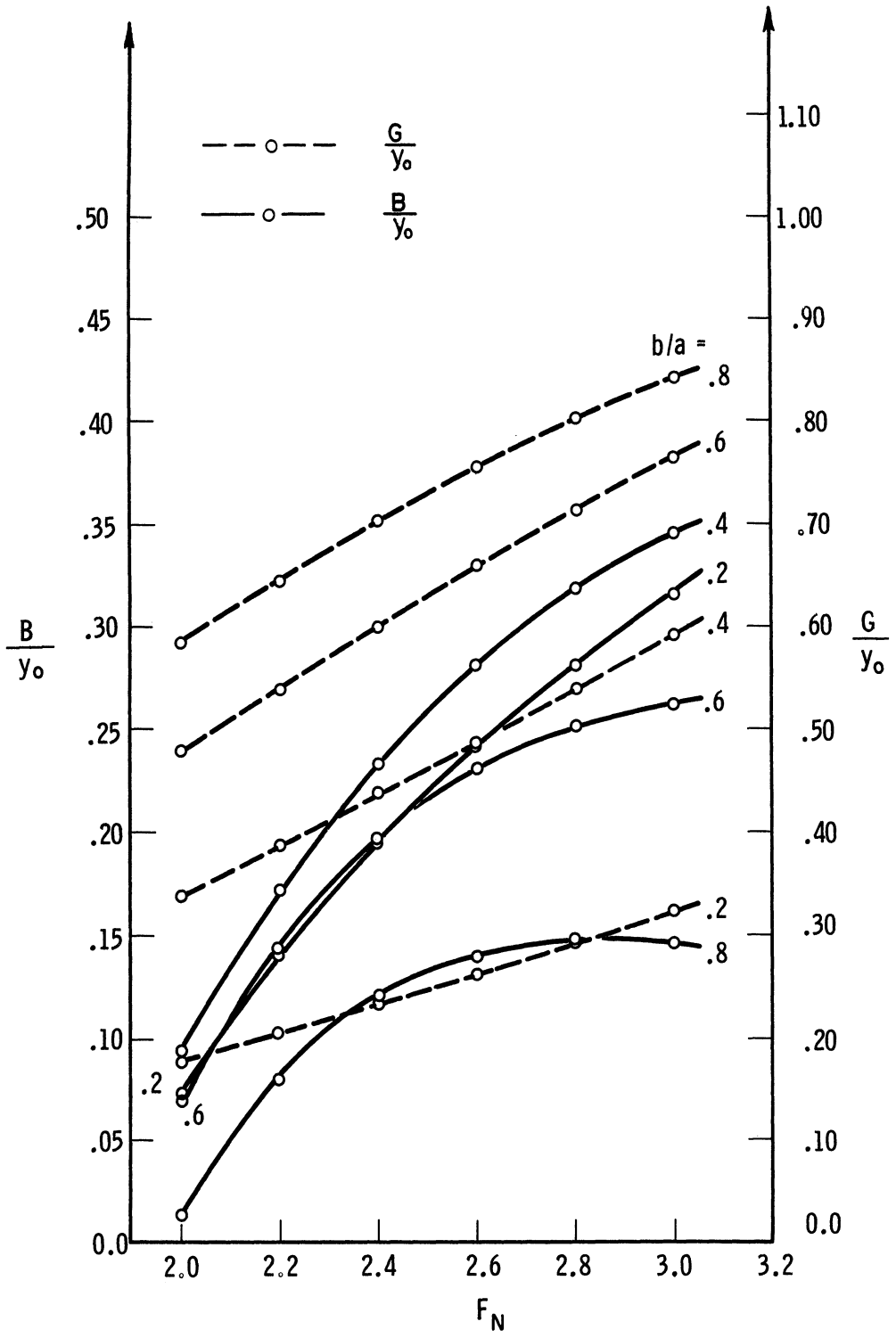

Fig. 9(c) Aperture admittance above (2, 0) mode cutoff (F_N = 2.0 - 3.0) (F_N = 1.0 at cutoff). (c) $\mu_r = \epsilon_r = 2.0$.

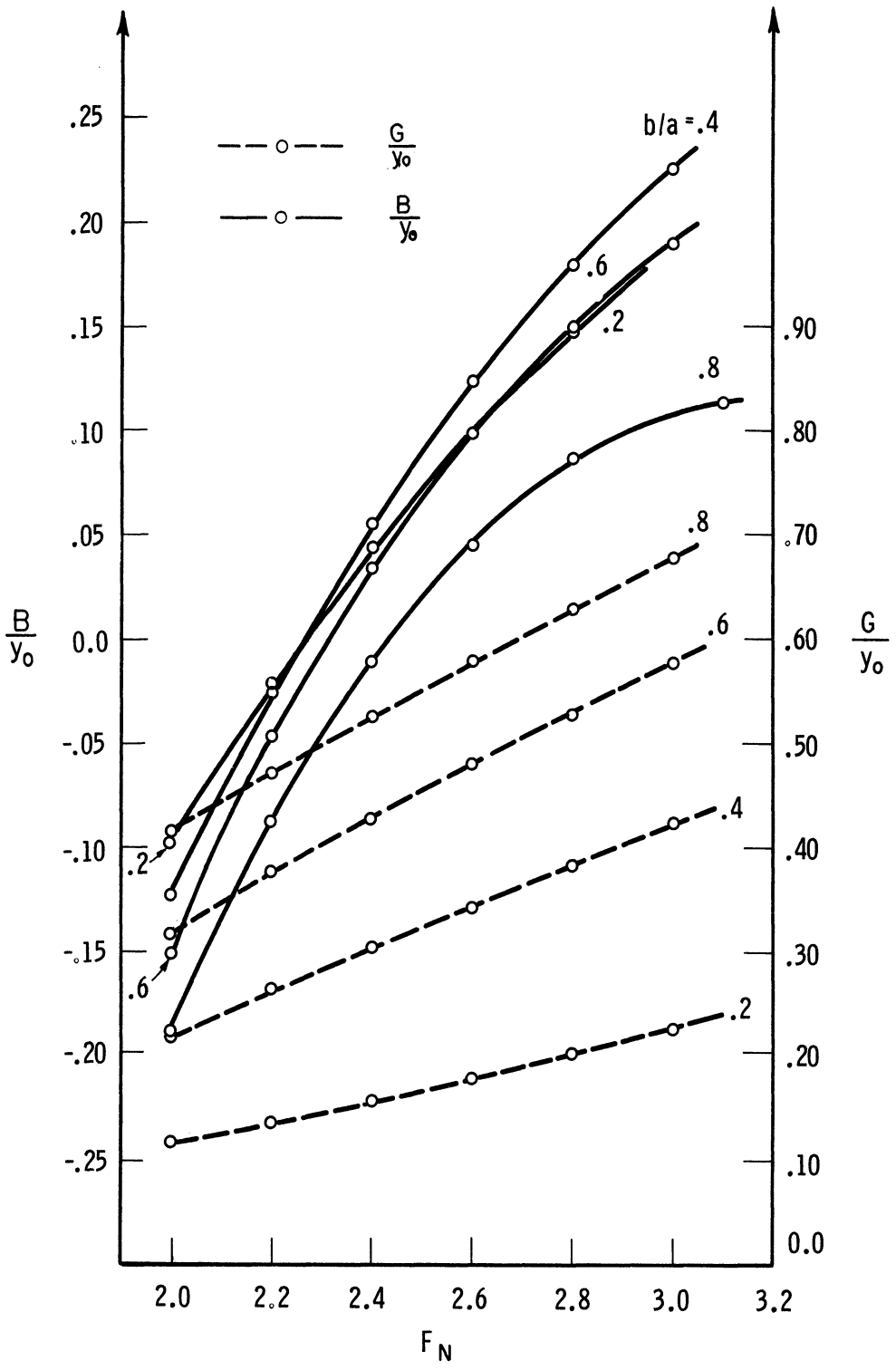

Fig. 9(d) Aperture admittance above (2, 0) mode cutoff (F_N = 2.0 - 3.0) (F_N = 1.0 at cutoff). (d) $\mu_r = \epsilon_r = 2.5$.

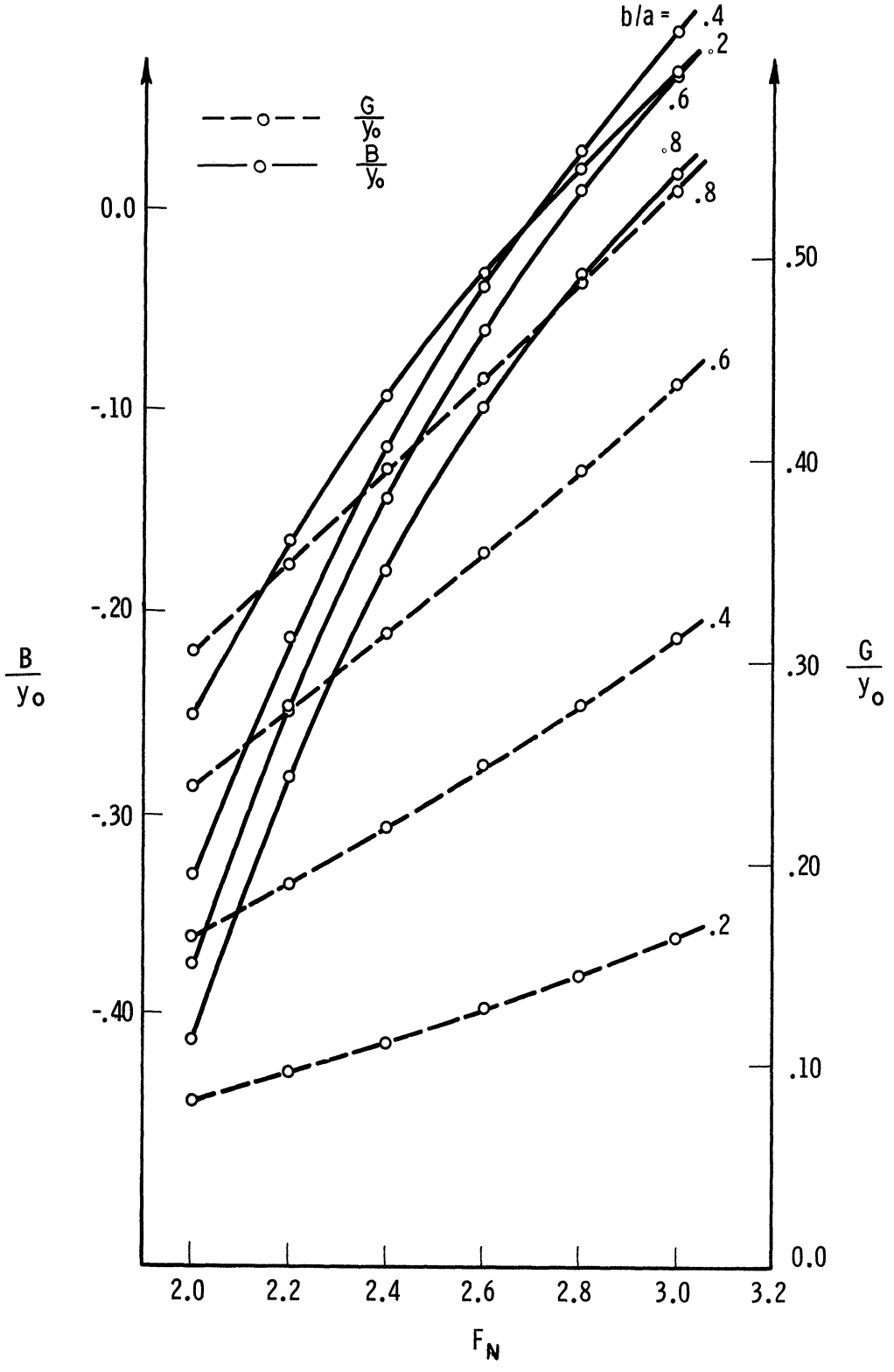

Fig. 9(e) Aperture admittance above (2, 0) mode cutoff (F_N = 2.0 - 3.0) (F_N = 1.0 at cutoff). (e) $\mu_r = \epsilon_r = 3.0$.

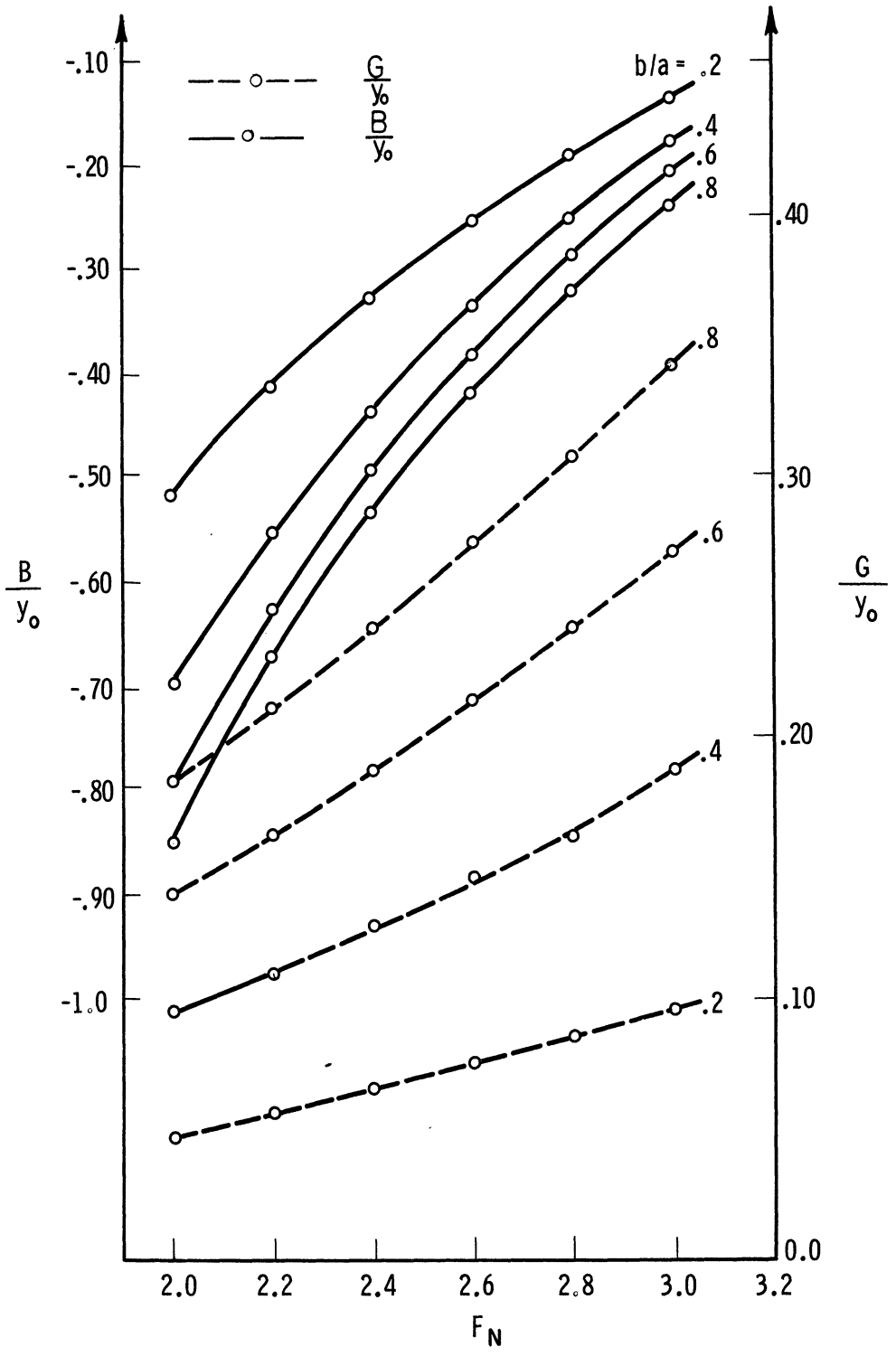

Fig. 9(f) Aperture admittance above (2, 0) mode cutoff (F_N = 2.0 - 3.0) (F_N = 1.0 at cutoff). (f) $\mu_r = \epsilon_r = 4.0$.

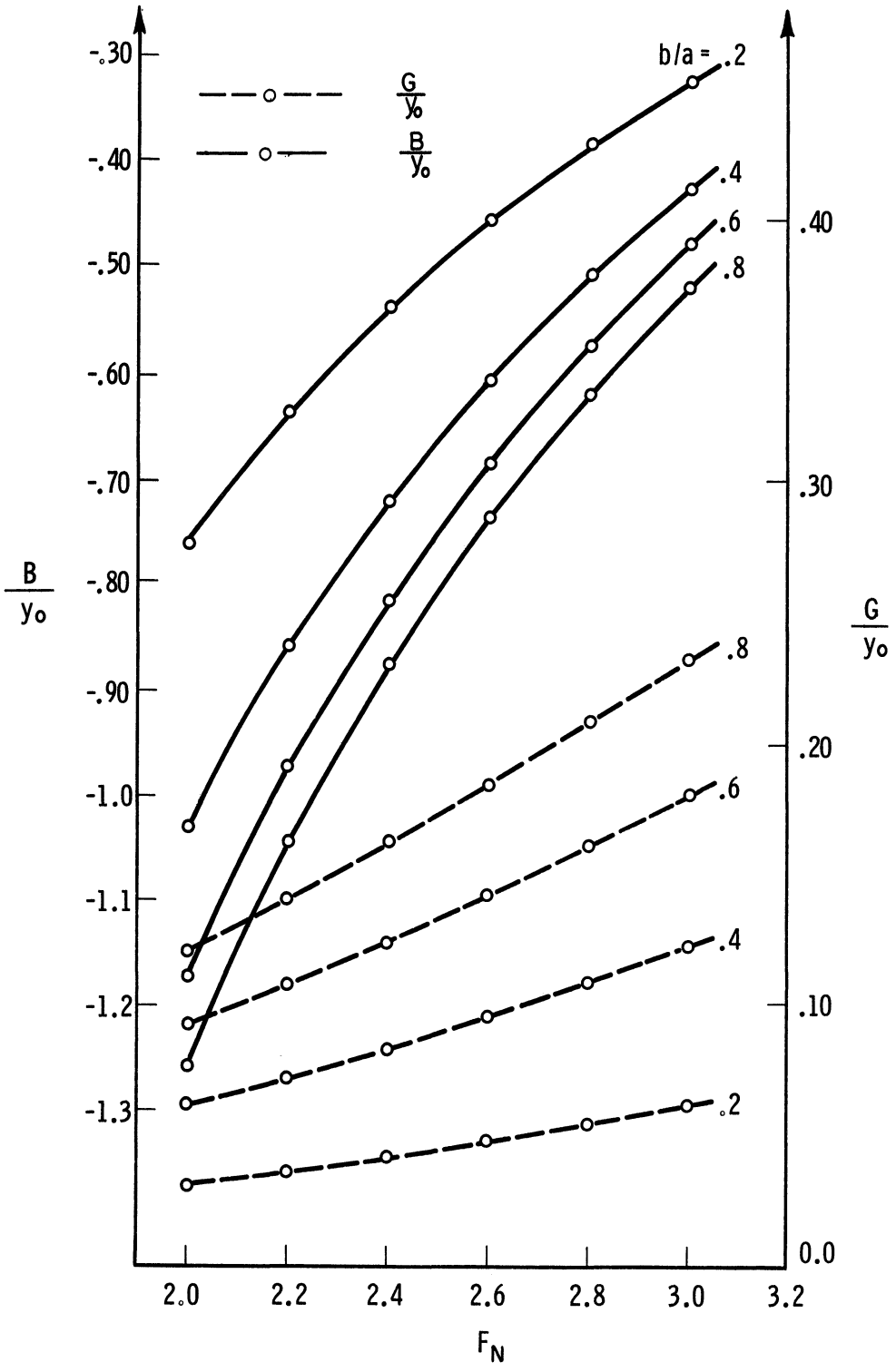

Fig. 9(g) Aperture admittance above (2, 0) mode cutoff (F_N = 2.0 - 3.0) (F_N = 1.0 at cutoff). (g) $\mu_r = \epsilon_r = 5.0$.

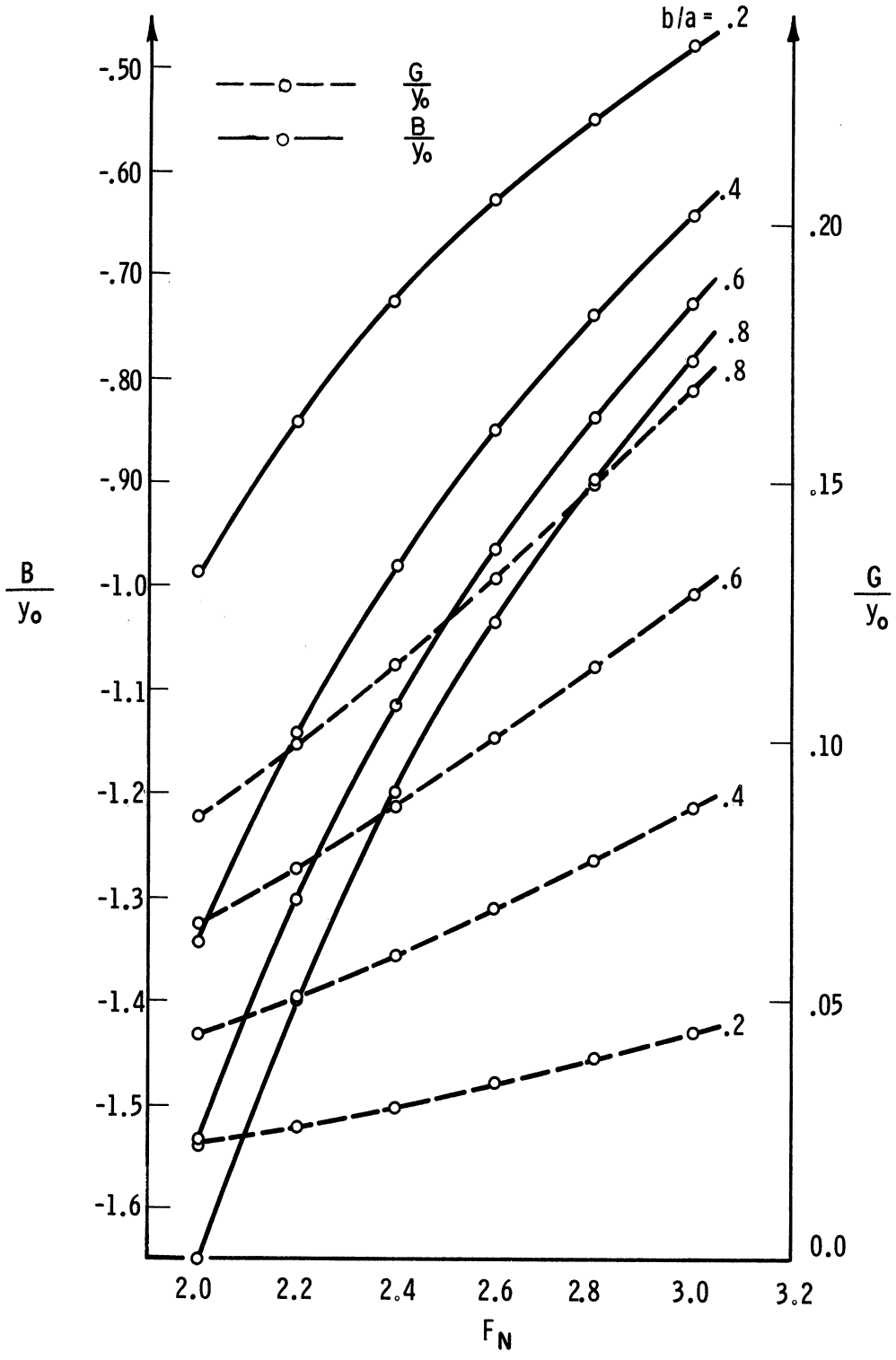

Fig. 9(h) Aperture admittance above (2, 0) mode cutoff (F_N = 2.0 - 3.0) (F_N = 1.0 at cutoff). (h) $\mu_r = \epsilon_r = 6.0$.

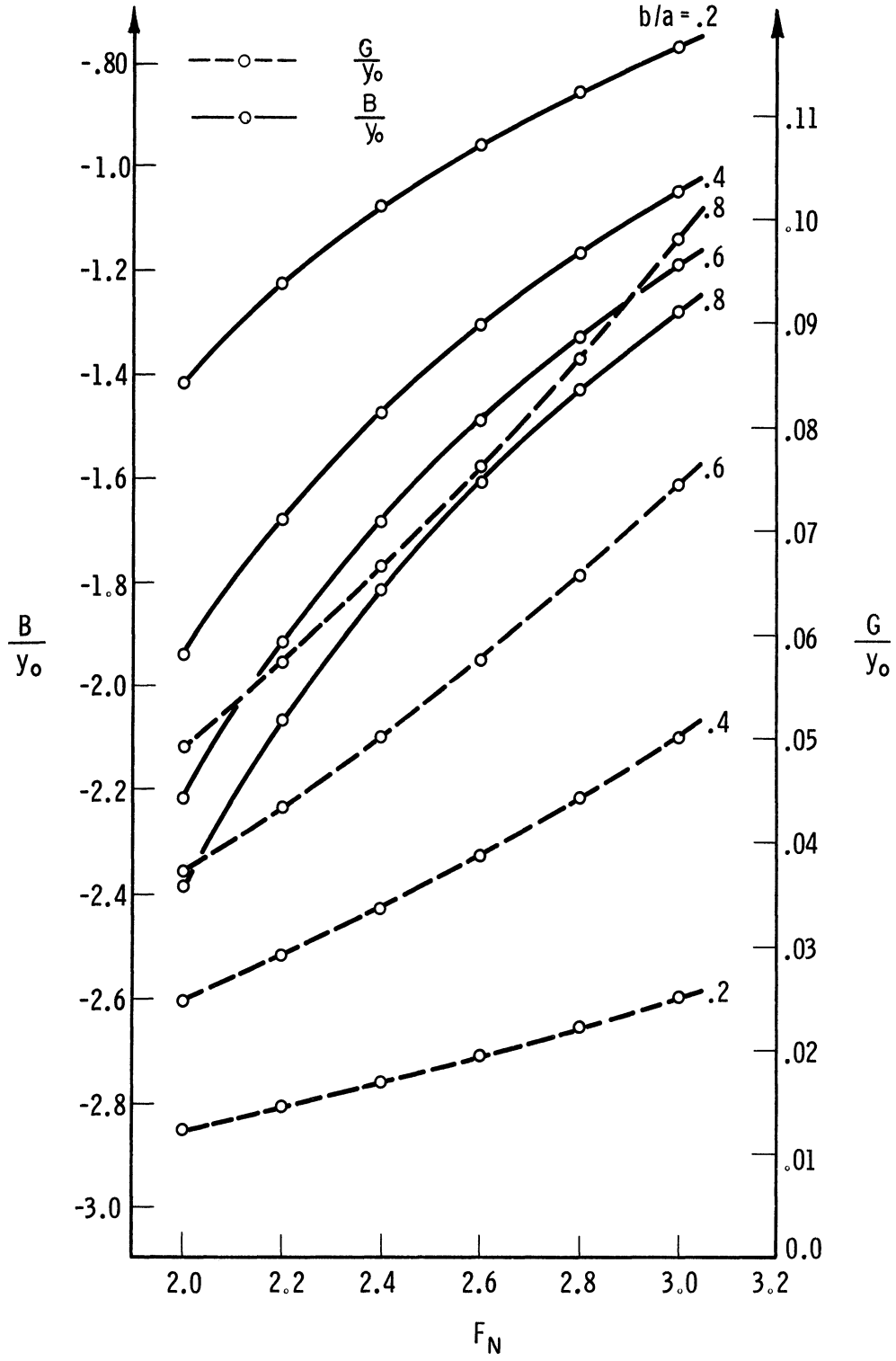

Fig. 9(i) Aperture admittance above (2, 0) mode cutoff (F_N = 2.0 - 3.0) (F_N = 1.0 at cutoff). (i) $\mu_r = \epsilon_r = 8.0$.

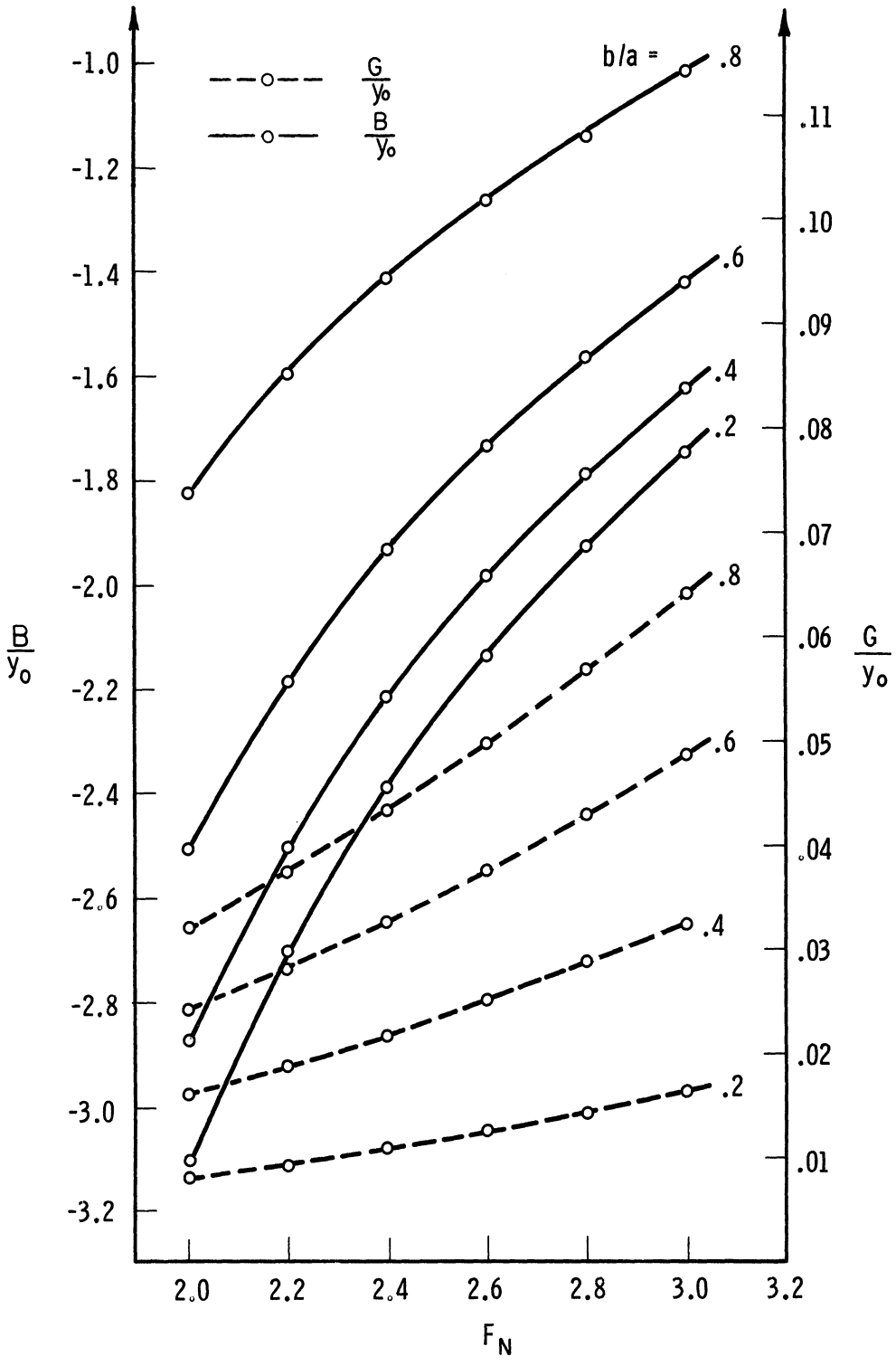

Fig. 9(j) Aperture admittance above (2, 0) mode cutoff (F_N = 2.0 - 3.0) (F_N = 1.0 at cutoff). (j) $\mu_r = \epsilon_r$ = 10.0.

CHAPTER 4

HIGHER ORDER MODES

4.1 Introduction

In Chapter 2, the first (dominant mode) approximation was manipulated into a form from which computation could be made. In this chapter an infinite sum of modes with unknown coefficients is substituted for the unknown aperture field $E_x(x,y)$. The condition of stationarity is used to derive an infinite set of equations in the unknown coefficients, and a corresponding infinite series for the admittance Y/Y_o in terms of the unknown coefficients A_{mn} and known quadruple integral functions C_{fghl}. The quadruple integral functions C_{fgmn} are reduced to double integral form suitable for computation. In the process, it is shown that C_{fghl} is zero if either $(f+h)$ or $(g+\ell)$ is odd. As a result, it can be shown that certain modes, namely those modes forbidden by symmetry, do not affect the admittance calculation. Finally, computation of the higher order corrections to the admittance for the (3, 0), (1, 2) and (3, 2) modes yield corrections of the order of 2 percent.

4.2 Higher Order Mode Coefficients

In this section, the aperture field $E_x(x,y)$ is expressed as an infinite sum of modes with unknown coefficients. The condition of stationarity applied to the input admittance Y/Y_o yields an infinite set of simultaneous linear equations in the unknown mode coefficients. Substituting this expression back in the admittance formulation yields an equation for the admittance in terms of the unknown coefficients.

In Chapter 2, the following expression for the normalized aperture admittance was derived:

$$\frac{Y}{Y_o} = \frac{G}{Y_o} + \frac{jB}{Y_o} = \frac{-ab\mu_r \int_0^a \int_0^b \int_0^a \int_0^b E_x(x,y)\, E_x(\xi,\eta)\, G_1(x,y,\xi,\eta)\, dx\, dy\, d\xi\, d\eta}{2\Gamma_{10} \left[\int_0^a \int_0^b E_x(x,y) \sin \frac{\pi y}{a}\, dx\, dy \right]^2} \quad . \quad (4.1)$$

Let

$$E_x(x,y) = \sin\frac{\pi y}{a} + \sum_{m=1}^{\infty}\sum_{n=0}^{\infty}{}' A_{mn} \sin\frac{m\pi y}{a}\cos\frac{n\pi x}{b} \tag{4.2}$$

Consider the integral in the denominator:

$$\int_0^a\int_0^b E_x(x,y)\sin\frac{\pi y}{a}\,dx\,dy = \frac{ab}{2}$$

$$\frac{Y}{Y_o} = \frac{G}{Y_o} + \frac{jB}{Y_o} = \frac{-2\mu_r}{\Gamma_{10}ab}\,[\,① + ② + ③ + ④\,] \tag{4.3}$$

where

$$① = \int_0^a\int_0^b\int_0^a\int_0^b \sin\frac{\pi y}{a}\sin\frac{\pi\eta}{a}\,G_1(x,y,\xi,\eta)\,dx\,dy\,d\xi\,d\eta$$

$$② = \int_0^a\int_0^b\int_0^a\int_0^b \sin\frac{\pi y}{a}\sum_{m=1}^{\infty}\sum_{n=0}^{\infty}{}' A_{mn}\sin\frac{m\pi\eta}{a}\cos\frac{n\pi\xi}{b}\,G_1(x,y,\xi,\eta)$$

$$dx\,dy\,d\xi\,d\eta$$

$$③ = \int_0^a\int_0^b\int_0^a\int_0^b \sin\frac{\pi\eta}{a}\sum_{m=1}^{\infty}\sum_{n=0}^{\infty}{}' A_{mn}\sin\frac{m\pi y}{a}\cos\frac{n\pi x}{b}\,G_1(x,y,\xi,\eta)$$

$$dx\,dy\,d\xi\,d\eta$$

$$④ = \int_0^a\int_0^b\int_0^a\int_0^b \sum_{m=1}^{\infty}\sum_{n=0}^{\infty}{}' A_{mn}\sin\frac{m\pi\eta}{a}\cos\frac{n\pi\xi}{b}\sum_{m=1}^{\infty}\sum_{n=0}^{\infty}{}'$$

$$A_{mn}\sin\frac{m\pi y}{a}\cos\frac{n\pi x}{b}\,G_1(x,y,\xi,\eta)\,dx\,dy\,d\xi\,d\eta$$

$$① = C_{1010} \tag{4.4}$$

where

$$C_{fgh\ell} = \int_0^a\int_0^b\int_0^a\int_0^b \sin\frac{f\pi y}{a}\cos\frac{g\pi x}{b}\sin\frac{h\pi\eta}{a}\cos\frac{\ell\pi\xi}{b}\left(\frac{\partial^2}{\partial y^2} + k_o^2\right)\frac{e^{-jk_o r}}{2\pi r}\,dx\,dy\,d\xi\,d\eta$$

$$C_{h\ell fg} = C_{ngf\ell} \tag{4.5}$$

② + ③ are identical since $G_1(x, y, \xi, \eta)$ is symmetrical in (y, η) and (x, ξ).

$$② + ③ = 2 \sum_{h=1}^{\infty} \sum_{\ell=0}^{\infty'} A_{h\ell} C_{10h\ell} \qquad \text{(changing subscripts from m, n to h, } \ell\text{)} . \tag{4.6}$$

$$④ = \frac{ab}{4\mu_r} \sum_{f=1}^{\infty} \sum_{g=0}^{\infty'} \frac{A_{fg}^2 \epsilon_{fg}}{\Gamma_{fg}} \left(k^2 - \frac{f^2\pi^2}{a^2}\right) + \sum_{f=1}^{\infty} \sum_{g=0}^{\infty'} \sum_{h=1}^{\infty} \sum_{\ell=0}^{\infty'} A_{fg} A_{h\ell} C_{fgh\ell} \tag{4.7}$$

$$\frac{Y}{Y_o} = \frac{-2\mu_r}{\Gamma_{10} ab} \left[C_{1010} + 2 \sum_{h=1}^{\infty} \sum_{\ell=0}^{\infty'} A_{h\ell} C_{10h\ell} + \frac{ab}{4\mu_r} \sum_{f=1}^{\infty} \sum_{g=0}^{\infty'} A_{fg}^2 \frac{\epsilon_{fg}}{\Gamma_{fg}} \left(k^2 - \frac{f^2\pi^2}{a^2}\right) \right.$$

$$\left. + \sum_{f=1}^{\infty} \sum_{g=0}^{\infty'} \sum_{h=1}^{\infty} \sum_{\ell=0}^{\infty'} A_{fg} A_{h\ell} C_{fgh\ell} \right] \tag{4.8}$$

The property of stationarity implies $\partial Y / \partial A_{mn} = 0$.

$$\frac{\partial}{\partial A_{mn}} \left(2 \sum_{h=1}^{\infty} \sum_{\ell=0}^{\infty'} A_{h\ell} C_{10h\ell} \right) = \frac{\partial}{\partial A_{mn}} (2 A_{mn} C_{10mn}) = 2 C_{10mn} \tag{4.9}$$

$$\frac{\partial}{\partial A_{mn}} \left(\sum_{f=1}^{\infty} \sum_{g=0}^{\infty'} \sum_{h=1}^{\infty} \sum_{\ell=0}^{\infty'} A_{fg} A_{h\ell} C_{fgh\ell} \right) = 2 \sum_{f=1}^{\infty} \sum_{g=0}^{\infty'} A_{fg} C_{fgmn} \tag{4.10}$$

because of symmetry of $C_{fgh\ell}$ $(C_{fgh\ell} = C_{h\ell fg})$

$$\frac{\partial Y}{\partial A_{mn}} = \frac{2\mu_r}{\Gamma_{10} ab} \left[2 C_{10mn} + 2 A_{mn} \frac{ab \epsilon_{mn}}{4\mu_r \Gamma_{mn}} \left(k^2 - \frac{m^2\pi^2}{a^2}\right) + 2 \sum_{f=1}^{\infty} \sum_{g=0}^{\infty'} A_{fg} C_{fgmn} \right] = 0 \tag{4.11}$$

$$C_{10mn} + A_{mn} D_{mn} + \sum_{f=1}^{\infty} \sum_{g=0}^{\infty'} A_{fg} C_{fgmn} = 0 \tag{4.12}$$

where

$$D_{mn} = \left(\frac{b}{a}\right) \frac{\epsilon_{mn}}{4\mu_r \Gamma_{mn}} \left(k^2 a^2 - m^2 \pi^2\right)$$

This represents an infinite set of simultaneous linear equations in the unknown coefficients A_{mn}. The solution for any specific A_{mn} is therefore the quotient of two infinite determinants. The above condition on the unknown coefficients contains terms similar to those in the expression for Y above. Changing subscripts from mn to hℓ, multiplying by $A_{h\ell}$ and summing over hℓ, we obtain

$$\sum_{h=1}^{\infty} \sum_{\ell=0}^{\infty}{}' A_{h\ell} C_{10h\ell} + \sum_{h=1}^{\infty} \sum_{\ell=0}^{\infty}{}' A_{h\ell}^2 D_{h\ell} + \sum_{f=1}^{\infty} \sum_{g=0}^{\infty}{}' \sum_{h=1}^{\infty} \sum_{\ell=0}^{\infty}{}' A_{fg} A_{h\ell} C_{fgh\ell} = 0 \tag{4.13}$$

Substitution of the above equation into Eq. (4.8) simplifies the expression for Y/Y_o.

$$\frac{Y}{Y_o} = -\frac{2\mu_r}{\Gamma_{10}ab} \left[C_{1010} + \sum_{h=1}^{\infty} \sum_{\ell=0}^{\infty}{}' A_{h\ell} C_{10h\ell} \right] = \frac{G}{Y_o} + \frac{jB}{Y_o}$$

$$= -\frac{2\mu_r}{\Gamma_{10}ab} \left[C_{1010} + \sum_{m=1}^{\infty} \sum_{n=0}^{\infty}{}' A_{mn} C_{10mn} \right] \tag{4.14}$$

This formula represents an equation for Y/Y_o in terms of the unknown coefficients A_{mn} and the known functions C_{10mn}. Now the coefficients must be determined by the conditions placed on them by the equation

$$C_{10mn} + A_{mn} D_{mn} + \sum_{m=1}^{\infty} \sum_{n=0}^{\infty}{}' A_{fg} C_{fgmn} = 0 \ .$$

Expanding: [SEE EQUATION ON PAGES 80-81]

Some of the terms in the expansion are zero. From symmetry considerations, it can be seen that:

$$A_{2n} = A_{4n} = A_{6n} = \ldots = 0 \tag{4.16}$$

$$A_{m1} = A_{m3} = A_{m5} = \ldots = 0 \tag{4.17}$$

$$A_{0n} = 0 \tag{4.18}$$

$$A_{11}(D_{11}+C_{1111}) + A_{12}C_{1211} + \ldots + A_{1n}C_{1n11} + A_{20}C_{2011} + A_{21}C_{2111} + \ldots + A_{2n}C_{2n11}$$

$$A_{11}C_{1112} + A_{12}(D_{12}+C_{1212}) + \ldots + A_{1n}C_{1n12} + A_{20}C_{2012} + A_{21}C_{2112} + \ldots + A_{2n}C_{2n12}$$

.
.

$$A_{11}C_{111n} + A_{12}C_{121n} + \ldots + A_{1n}(D_{1n}+C_{1n1n}) + A_{20}C_{201n} + A_{21}C_{211n} + \ldots + A_{2n}C_{2n1n}$$

$$A_{11}C_{1120} + A_{12}C_{1220} + \ldots + A_{1n}C_{1n20} + A_{20}(D_{20}+C_{2020}) + A_{21}C_{2120} + \ldots + A_{2n}C_{2n20}$$

$$A_{11}C_{1121} + A_{12}C_{1221} + \ldots + A_{1n}C_{1n21} + A_{20}C_{2021} + A_{21}(D_{21}+C_{2121}) + \ldots + A_{2n}C_{2n21}$$

.
.

$$A_{11}C_{112n} + A_{12}C_{122n} + \ldots + A_{1n}C_{1n2n} + A_{20}C_{202n} + A_{21}C_{212n} + \ldots + A_{2n}(D_{2n}+C_{2n2n})$$

.
.
.
.

$$A_{11}C_{11n0} + A_{12}C_{12n0} + \ldots + A_{1n}C_{1nn0} + A_{20}C_{20n0} + A_{21}C_{21n0} + \ldots + A_{2n}C_{2nn0}$$

$$A_{11}C_{11n1} + A_{12}C_{12n1} + \ldots + A_{1n}C_{1nn1} + A_{20}C_{20n1} + A_{21}C_{21n1} + \ldots + A_{2n}C_{2nn1}$$

.
.
.
.

$$A_{11}C_{11nn} + A_{12}C_{12nn} + \ldots + A_{1n}C_{1nnn} + A_{20}C_{20nn} + A_{21}C_{21nn} + \ldots + A_{2n}C_{2nnn}$$

$$
\begin{aligned}
&+ \ldots + \ldots + A_{n0}C_{n011} + A_{n1}C_{n111} && + \ldots + A_{nn}C_{nn11} && = 0 \\
&+ \ldots + \ldots + A_{n0}C_{n012} + A_{n1}C_{n112} && + \ldots + A_{nn}C_{nn12} && = -C_{1012} \\
&+ \ldots + \ldots + A_{n0}C_{n01n} + A_{n1}C_{n11n} && + \ldots + A_{nn}C_{nn1n} && = -C_{101n} \\
&+ \ldots + \ldots + A_{n0}C_{n020} + A_{n1}C_{n120} && + \ldots + A_{nn}C_{nn20} && = 0 \\
&+ \ldots + \ldots + A_{n0}C_{n021} + A_{n1}C_{n121} && + \ldots + A_{nn}C_{nn21} && = 0 \\
&+ \ldots + \ldots + A_{n0}C_{n02n} + A_{n1}C_{n12n} && + \ldots + A_{nn}C_{nn2n} && = 0 \\
&+ \ldots + \ldots + A_{n0}(D_{n0}+C_{n0n0}) + A_{n1}C_{n1n0} && + \ldots + A_{nn}C_{nn0} && = -C_{10n0} \\
&+ \ldots + \ldots + A_{n0}C_{n0n1} + A_{n1}(D_{n1}+C_{n1n1}) && + \ldots + A_{nn}C_{nnn1} && = -C_{10n1} \\
&+ \ldots + \ldots + A_{n0}C_{n0nn} + A_{n1}C_{n1nn} && + \ldots + A_{nn}(D_{nn}+C_{nnnn}) && = -C_{10nn}
\end{aligned}
\qquad (4.15)
$$

The method of solution of these equations involves truncation of the infinite matrix. The solution will be accurate only insofar as the terms included represent the dominant terms in the aperture field.

Several specific truncations will now be carried out

1. Two Modes--(1, 0) and (m, n)

$$C_{10mn} + A_{mn}D_{mn} + A_{mn}C_{mnmn} = 0$$

$$A_{mn} = - \frac{C_{10mn}}{C_{mnmn} + D_{mn}} \tag{4.19}$$

$$\frac{Y}{Y_o} = - \frac{2\mu_r}{\Gamma_{10}ab} \left[C_{1010} - \frac{C_{10mn}^2}{C_{mnmn} + D_{mn}} \right] = \frac{Y_{10}}{Y_o} + \frac{Y_{mn}}{Y_o} \tag{4.20}$$

$$\frac{Y_{mn}}{Y_o} = \frac{2\mu_r}{\Gamma_{10}ab} \left[\frac{C_{10mn}^2}{C_{mnmn} + D_{mn}} \right] \tag{4.21}$$

2. Three Modes--(1, 0), (m, n), (m', n')

$$A_{mn}(C_{mnmn} + D_{mn}) + A_{m'n'}(C_{m'n'mn}) = - C_{mn10}$$

$$A_{mn}(C_{mnm'n'}) + A_{m'n'}(C_{m'n'm'n'} + D_{m'n'}) = - C_{m'n'10}$$

$$A_{mn} = \frac{C_{m'n'mn}C_{m'n'10} - C_{mn10}(C_{m'n'm'n'} + D_{m'n'})}{\Delta} \tag{4.22}$$

$$A_{m'n'} = \frac{C_{mnm'n'}C_{mn10} - C_{m'n'10}(C_{mnmn} + D_{mn})}{\Delta} \tag{4.23}$$

where

$$\Delta = (C_{mnmn} + D_{mn})(C_{m'n'm'n'} + D_{m'n'}) - C_{m'n'mn}^2$$

$$\frac{Y}{Y_o} = -\frac{2\mu_r}{\Gamma_{10}ab}\left(C_{1010} + A_{mn}C_{mn10} + A_{m'n'}C_{m'n'10}\right) = \frac{Y_{10}}{Y_o} + \frac{Y_{mn}}{Y_o} + \frac{Y_{m'n'}}{Y_o} \quad (4.24)$$

Thus Y/Y_o has been reduced, in Eqs. (4.21) and (4.24), to expressions depending only on the quadruple integrals $C_{fgh\ell}$.

4.3 Reduction of Quadruple Integral Forms

The $C_{fgh\ell}$ terms will now be reduced to general double integral form. In the process, it will be shown that C_{mn10} is zero if m is even or n is odd, and that $C_{mnm'n'}$ is zero if (m-m') or (n-n') is odd. The calculations for the first form will be carried out in detail; the results for the other forms will be given without derivation. Finally some of the double integral forms are evaluated by computer. Calculations involving the (3,0), (1,2), and (3,2) modes are carried out, yielding corrections of the order of 2 percent to the input admittance Y/Y_o calculated assuming the dominant mode.

$$C_{mnm'n'} = \int_o^a \int_o^b \int_o^a \int_o^b \sin\frac{m\pi y}{a} \cos\frac{m\pi x}{b} \sin\frac{m'\pi\eta}{a} \cos\frac{n'\pi\xi}{b} \left(k_o^2 - \frac{\partial^2}{\partial y\,\partial\eta}\right) \frac{e^{-jk_o r}}{2\pi r}\, dx\, dy\, d\xi\, d\eta \quad (4.25)$$

$$C_{mnm'n'} = \frac{1}{4a^2} \int_o^a \int_o^b \int_o^a \int_o^b \left[\cos\frac{\pi}{b}(nx - n'\xi) + \cos\frac{\pi}{b}(nx + n'\xi)\right]$$

$$\left[D_{mm'} \cos\frac{\pi}{a}(my - m'\eta) - C_{mm'} \cos\frac{\pi}{a}(my + m'\eta)\right]$$

$$\frac{e^{-jk_o r}}{2\pi r}\, dx\, dy\, d\xi\, d\eta \quad (4.26)$$

where

$$C_m = k_o^2 a^2 + m\pi^2$$

$$D_m = k_o^2 a^2 - m\pi^2$$

$$r = \sqrt{(x-\xi)^2 + (y-\eta)^2} = \sqrt{\sigma^2 + \lambda^2}$$

let

$$y - \eta = \lambda \qquad x - \xi = \sigma$$

$$y + \eta = \mu + a \qquad x + \xi = b + \nu$$

In this case we do not have any symmetry in the integrand (Appendix A).

$$f(\lambda, \sigma, \mu, \nu) \neq f(\pm\lambda \pm \sigma, \pm\mu, \pm\nu)$$

$$\cos \frac{\pi}{b}(nx \pm n'\xi) = \cos \frac{\pi}{2b}[(n \pm n')b + (n \pm n')\nu + (n \mp n')\sigma]$$

$$\cos \frac{\pi}{a}(my \pm m'\eta) = \cos \frac{\pi}{2a}[(m \pm m')a + (m \pm m')\mu + (m \mp m')\lambda]$$

$$C_{mnn'n'} = \frac{1}{16a^2} \int\int\int\int \left\{\cos \frac{\pi}{2b}[(n-n')b + (n-n')\nu + (n+n')\sigma] + \cos \frac{\pi}{2b}[(n+n')b + (n+n')\nu + (n-n')\sigma]\right\}$$

$$\left\{D_{mm'} \cos \frac{\pi}{2a}[(m-m')a + (m-m')\mu + (m+m')\lambda] - C_{mm'} \cos \frac{\pi}{2a}[(m+m')a + (m+m')\mu + (m-m')\lambda]\right\} \frac{e^{-jk_o\sqrt{\sigma^2+\lambda^2}}}{2\pi\sqrt{\sigma^2+\lambda^2}}\, d\nu\, d\mu\, d\sigma\, d\lambda$$

where

$$\int\int\int\int = \int_0^a \int_0^b \int_{-(a-\lambda)}^{a-\lambda} \int_{-(b-\sigma)}^{b-\sigma} + \int_0^a \int_{-b}^{0} \int_{-(a-\lambda)}^{a-\lambda} \int_{-(b+\sigma)}^{b+\sigma} + \int_{-a}^{0} \int_0^b \int_{-(a+\lambda)}^{a+\lambda} \int_{-(b-\sigma)}^{b-\sigma} + \int_{-a}^{0} \int_{-b}^{0} \int_{-(a+\lambda)}^{(a+\lambda)} \int_{-(b+\sigma)}^{(b+\sigma)}$$

(see Appendix A).

$$C_{mnm'n'} = \frac{b}{4a\pi^2} \left\{\int_0^a \int_0^b G_1(\sigma)\, F_1(\lambda)\, d\sigma\, d\lambda + \int_{-a}^{0} \int_0^b G_1(\sigma)\, F_2(\lambda)\, d\sigma\, d\lambda + \int_0^a \int_{-b}^{0} G_2(\sigma)\, F_1(\lambda)\, d\sigma\, d\lambda + \int_{-a}^{0} \int_{-b}^{0} G_2(\sigma)\, F_2(\lambda)\, d\sigma\, d\lambda\right\} \qquad (4.27)$$

where

$$G_1(\sigma) = \left\{\left(\frac{1}{n-n'}\right)\left[\sin \frac{n'\pi\sigma}{b} \cos(n-n')\pi - \sin \frac{n\pi\sigma}{b}\right] - \left(\frac{1}{n+n'}\right)\left[\sin \frac{n'\pi\sigma}{b} \cos(n+n')\pi + \sin \frac{n\pi\sigma}{b}\right]\right\}$$

$$G_2(\sigma) = \left\{ \left(\frac{1}{n-n'}\right) \left[\sin \frac{n\pi\sigma}{b} \cos(n-n')\pi - \sin \frac{n'\pi\sigma}{b}\right] + \left(\frac{1}{n+n'}\right) \left[\sin \frac{n\pi\sigma}{b} \cos(n+n')\pi + \sin \frac{n'\pi\sigma}{b}\right]\right\}$$

$$F_1(\lambda) = \left\{ \frac{D_{mm'}}{m-m'} \left[\sin \frac{m'\pi\lambda}{a} \cos(m-m')\pi - \sin \frac{m\pi\lambda}{a}\right] + \frac{C_{mm'}}{m+m'} \left[\sin \frac{m'\pi\lambda}{a} \cos(m+m')\pi + \sin \frac{m\pi\lambda}{a}\right]\right\}$$

$$F_2(\lambda) = \left\{ \frac{D_{mm'}}{m-m'} \left[\sin \frac{m\pi\lambda}{a} \cos(m-m')\pi - \sin \frac{m'\pi\lambda}{a}\right] - \frac{C_{mm'}}{m+m'} \left[\sin \frac{m\pi\lambda}{a} \cos(m+m')\pi + \sin \frac{m'\pi\lambda}{a}\right]\right\}$$

If $m-m'$ is even $\quad F_1(\lambda) = -F_2(\lambda)$

If $m-m'$ is odd $\quad F_1(\lambda) = F_2(\lambda)$

If $n-n'$ is even $\quad G_1(\sigma) = -G_2(\sigma)$

If $n-n'$ is odd $\quad G_1(\sigma) = G_2(\sigma)$

Since all integrands are odd in σ and λ

$$C_{mnm'n'} = \frac{b}{4\pi^2 a} \left\{ \int_0^a \int_0^b G_1(\sigma) F_1(\lambda)\, d\sigma\, d\lambda - \int_0^a \int_0^b G_1(\sigma) F_2(\lambda)\, d\sigma\, d\lambda \right.$$

$$\left. - \int_0^a \int_0^b G_2(\sigma) F_1(\lambda)\, d\sigma\, d\lambda + \int_0^a \int_0^b G_2(\sigma) F_2(\lambda)\, d\sigma\, d\lambda \right\}$$

If $m-m'$ is odd:

The first and second integrals cancel

The third and fourth integrals cancel

If $n-n'$ is odd:

The first and third integrals cancel

The second and fourth integrals cancel

$$C_{mnm'n'} = 0 \quad \text{if} \quad \begin{cases} 1. \ (m-m') \text{ or } (n-n') \text{ is odd, and} \\ 2. \ m \neq m' \text{ and } n \neq n' \end{cases} \tag{4.28}$$

We have noted before that the only modes excited by the geometry of Fig. 3(a) are those with

m odd and n even. If (m-m') or (n-n') is odd, then either the (m,n) mode or the (m',n') mode must be a forbidden mode. If (m-m') and (n-n') are both even:

$$C_{mnm'n'} = \left(\frac{1}{\pi^2 a}\right)\frac{4}{(n^2-n'^2)(m^2-m'^2)} \int_o^a \int_o^b \left[n' \sin\frac{n'\pi\sigma}{b} - \sin\frac{n\pi\sigma}{b}\right]$$

$$\left[mD_{m'^2} \sin\frac{m'\pi\lambda}{a} - m'D_{m^2} \sin\frac{m\pi\lambda}{a}\right] \frac{e^{-jk_o r}}{2\pi r} \, d\sigma \, d\lambda$$

$$= \frac{2}{\pi^3}\left(\frac{b^2}{a}\right) \frac{1}{(n^2-n'^2)(m^2-m'^2)} \int_o^1 \int_o^1 [n' \sin n'\pi y - n \sin n\pi y]$$

$$[mD_{m'^2} \sin m'\pi x - m'D_{m^2} \sin m\pi x] \frac{e^{-jk_o a\sqrt{x^2+\delta^2 y^2}}}{\sqrt{x^2+\delta^2 y^2}} \, dx \, dy$$

(where $\delta = b/a$) (4.29)

$$\text{for} \begin{cases} (m-m') \text{ even} \\ (n-n') \text{ even} \\ n \neq n' \\ m \neq m' \end{cases}$$

As a result of the above calculations:

$$C_{mn10} = 0 \quad \text{if} \begin{cases} 1. \ m \text{ is even or } n \text{ is odd, and} \\ 2. \ m \neq 1 \text{ and } n \neq 0 \end{cases} \tag{4.30}$$

$$C_{mn10} = -\left(\frac{b^2}{a}\right) \frac{2}{n\pi^3(m^2-1)} \int_o^1 \int_o^1 \sin n\pi y [mD_1 \sin \pi x - D_{m^2} \sin m\pi x] \frac{e^{-jk_o a\sqrt{x^2+\delta^2 y^2}}}{\sqrt{x^2+\delta^2 y^2}} \, dx \, dy \tag{4.31}$$

$$\text{if} \begin{cases} 1. \ m \text{ is odd and } n \text{ is even, and} \\ 2. \ m \neq 1, \ n \neq 0 \end{cases}$$

The results of similar calculations yield:

$$C_{mnmn'} = \int_0^a \int_0^b \int_0^a \int_0^b \sin\frac{m\pi y}{a} \cos\frac{n\pi x}{b} \sin\frac{m\pi\eta}{a} \cos\frac{n'\pi\xi}{b} \left(k_o^2 - \frac{\partial^2}{\partial y\,\partial\eta}\right) \frac{e^{-jk_o r}}{2\pi r}\, dx\,dy\,d\xi\,d\eta$$

$$C_{mnmn'} = 0 \quad \text{if} \quad \begin{cases} 1. & (n-n') \text{ is odd, and} \\ 2. & m \neq 0 \end{cases} \tag{4.32}$$

$$C_{mnmn'} = \frac{b^2}{a} \frac{1}{m\pi^3} \frac{1}{(n-n')(n+n')} \int_0^1 \int_0^1 [n' \sin n'\pi y - n \sin n\pi y]$$

$$[m\pi(1-x) D_{m^2} \cos m\pi x + C_{m^2} \sin m\pi x] \frac{e^{-jk_o a\sqrt{x^2+\delta^2 y^2}}}{\sqrt{x^2+\delta^2 y^2}}\, dx\,dy \tag{4.33}$$

$$\text{if} \quad \begin{cases} 1. & (n-n') \text{ is even, and} \\ 2. & m \neq 0, \quad n \neq n' \end{cases} \tag{4.34}$$

$$C_{mnmn'} = 0 \quad \text{if} \quad m = 0 \tag{4.35}$$

$$C_{1n10} = 0 \quad \text{if} \quad n \text{ is odd} \tag{4.36}$$

$$C_{1n10} = -\frac{b^2}{a}\left(\frac{1}{n\pi^3}\right) \int_0^1 \int_0^1 \sin n\pi y[\pi D_1(1-x)\cos\pi x + C_1 \sin\pi x] \frac{e^{-jk_o a\sqrt{x^2+\delta^2 y^2}}}{\sqrt{x^2+\delta^2 y^2}}\, dx\,dy \tag{4.37}$$

if n is even

$$C_{mnm'n} = \int_0^a \int_0^b \int_0^a \int_0^b \sin\frac{m\pi y}{a} \cos\frac{n\pi x}{b} \sin\frac{m'\pi\xi}{a} \cos\frac{n\pi\xi}{b} \left(k_o^2 - \frac{\partial^2}{\partial y\,\partial\eta}\right) \frac{e^{-jk_o r}}{2\pi r}\, dx\,dy\,d\xi\,d\eta$$

$$C_{mnm'n} = 0 \quad \text{if} \quad \begin{cases} 1. & (m-m') \text{ is odd, and} \\ 2. & n \neq 0 \end{cases} \tag{4.38}$$

$$C_{mnm'n} = \left(\frac{b^2}{a}\right) \frac{2}{n\pi^2 (m+m')(m-m')} \int_0^1 \int_0^1 [n\pi(1-y)\cos n\pi y - \sin n\pi y]$$

$$[mD_{m'^2} \sin m'\pi x - m'D_{m^2} \sin m\pi x] \frac{e^{-jk_o a\sqrt{x^2+\delta^2y^2}}}{\sqrt{x^2+\delta^2y^2}} \, dx\, dy \qquad (4.39)$$

if
1. (m-m') is even, and
2. $n \neq 0$, $m \neq m'$

$C_{m0m'0}$ = 0 if (m-m') is odd

$$= \left(\frac{b^2}{a}\right) \frac{2}{\pi^2} \frac{1}{(m+m')(m-m')} \int_0^1 \int_0^1 (1-y)\,[mD_{m'^2} \sin m'\pi x - m'D_{m^2} \sin m\pi x]$$

$$\frac{e^{jk_o a\sqrt{x^2+\delta^2y^2}}}{\sqrt{x^2+\delta^2y^2}} \, dx\, dy \qquad (4.40)$$

if
1. (m-m') is even, and
2. $m \neq m'$

C_{m010} = 0 if m is even (4.41)

$$= \left(\frac{b^2}{a}\right) \frac{2}{\pi^2(m^2-1)} \int_0^1 \int_0^1 (1-y)\,[mD_1 \sin \pi x - D_{m^2} \sin m\pi x] \frac{e^{-jk_o a\sqrt{x^2+\delta^2y^2}}}{\sqrt{x^2+\delta^2y^2}} \, dx\, dy \qquad (4.42)$$

if m is odd

$$C_{mnmn} = \int_0^a \int_0^b \int_0^a \int_0^b \sin \frac{m\pi y}{a} \cos \frac{n\pi x}{b} \sin \frac{m\pi \eta}{a} \cos \frac{n\pi \xi}{b} \left(-\frac{\partial^2}{\partial y\, \partial \eta}\right) \frac{e^{-jk_o r}}{2\pi r} \, dx\, dy\, d\xi\, d\eta$$

$$+ \int_0^a \int_0^b \int_0^a \int_0^b \sin \frac{m\pi y}{a} \cos \frac{n\pi x}{b} \sin \frac{m\pi \eta}{a} \cos \frac{n\pi \xi}{b} (k_o^2) \frac{e^{-jk_o r}}{2\pi r} \, dx\, dy\, d\xi\, d\eta \qquad (4.43)$$

$$= \left(\frac{b^2}{a}\right) \frac{1}{2mn\pi^3} \int_0^1 \int_0^1 [n\pi(1-y) \cos n\pi y - \sin n\pi y]$$

$$\left[m\pi(1-x)\,D_{m^2}\cos m\pi x + C_{m^2}\sin m\pi x\right]\ \frac{e^{-jk_o a\sqrt{x^2+\delta^2y^2}}}{\sqrt{x^2+\delta^2y^2}}\ dx\,dy$$

if $m\neq 0,\ n\neq 0$ (4.44)

C_{mnmn} may have a finite value even though (m, n) is a forbidden mode.

$$C_{m0m0} = \int_0^a\int_0^b\int_0^a\int_0^b \sin\frac{m\pi y}{a}\sin\frac{m\pi\eta}{a}\left(-\frac{\partial^2}{\partial y\,\partial\eta}+k_o^2\right)\frac{e^{-jk_o r}}{2\pi r}\,dx\,dy\,d\xi\,d\eta \qquad (4.45)$$

$$C_{m0m0} = \left(\frac{b^2}{a}\right)\frac{1}{m\pi^2}\int_0^1\int_0^1 (1-y)\left[m\pi(1-x)\,D_{m^2}\cos m\pi x + C_{m^2}\sin\frac{m\pi x}{b}\right]$$

$$\frac{e^{-jk_o a\sqrt{x^2+\delta^2y^2}}}{\sqrt{x^2+\delta^2y^2}}\ d\sigma\,d\lambda \qquad (4.46)$$

if $m\neq 0$.

$$C_{0mn'n'} = \lim_{m\to 0}\int_0^a\int_0^b\int_0^a\int_0^b \sin\frac{m\pi y}{a}\sin\frac{m'\pi\eta}{a}\cos\frac{n\pi x}{b}\cos\frac{n\pi\xi}{b}\left(k_o^2-\frac{\partial^2}{\partial y\,\partial\eta}\right)\frac{e^{-jk_o r}}{2\pi r}\,dx\,dy\,d\xi\,d\eta$$

$$|C_{0nm'n'}| \le \lim_{m\to 0}\left\{-\frac{mm'\pi^2}{a^2}\int_0^a\int_0^b\int_0^a\int_0^b \frac{1}{2\pi r}\,dx\,dy\,d\xi\,d\eta\right.$$

$$\left. + k_o^2\int_0^a\int_0^b\int_0^a\int_0^b (m\pi)\,\frac{1}{2\pi r}\,dx\,dy\,d\xi\,d\eta\right\} \qquad \left|\sin\frac{m\pi y}{a}\right| \le \frac{m\pi y}{a} \le m\pi$$

$$\le \lim_{m\to 0}\left\{m\left(k_o^2-\frac{m'\pi^2}{a^2}\right)\int_0^a\int_0^b\int_0^a\int_0^b \frac{1}{2\pi r}\,dx\,dy\,d\xi\,d\eta\right\}$$

$$= 0$$

$$C_{0nm'n'} = 0 = C_{mn0n'} \qquad (4.47)$$

We have shown that

$$C_{mnm'n'} = 0 \quad \text{if} \quad \begin{cases} 1. & (m-m') \text{ or } (n-n') \text{ is odd, and} \\ 2. & m \neq m' \text{ and } n \neq n' \end{cases}$$

$$C_{mnmn'} = 0 \quad \text{if} \quad \begin{cases} 1. & (n-n') \text{ is odd, and} \\ 2. & m \neq 0 \end{cases}$$

$$C_{0nmn'} = 0$$

$$C_{mnm'n} = 0 \quad \text{if} \quad \begin{cases} 1. & (m-m') \text{ is odd, and} \\ 2. & n \neq 0 \end{cases}$$

$$C_{m0m'0} = 0 \quad \text{if} \quad m-m' \text{ is odd}$$

$$C_{mnmn} \neq 0 \text{ for } (m \neq 0) \text{ even if m, n is a forbidden mode.}$$

Therefore

$$C_{mnm'n'} = 0 \text{ if } (m-m') \text{ or } (n-n') \text{ is odd} \tag{4.48}$$

Using the general formulas (4.28 through 4.46) developed above:

$$C_{3030} = \left(\frac{b^2}{a}\right) \frac{1}{3\pi^2} \int_0^1 \int_0^1 (1-y)[3\pi(1-x) D_9 \cos 3\pi x + C_9 \sin 3\pi x] \frac{e^{-jk_o a\sqrt{x^2+\delta^2y^2}}}{\sqrt{x^2+\delta^2y^2}} \, dx\, dy \tag{4.49}$$

$$C_{3010} = \left(\frac{b^2}{a}\right) \frac{1}{4\pi^2} \int_0^1 \int_0^1 (1-y)[3D_1 \sin \pi x - D_9 \sin 3\pi x] \frac{e^{-jk_o a\sqrt{x^2+\delta^2y^2}}}{\sqrt{x^2+\delta^2y^2}} \, dx\, dy \tag{4.50}$$

$$C_{1210} = -\left(\frac{b^2}{a}\right)\left(\frac{1}{2\pi^3}\right) \int_0^1 \int_0^1 \sin 2\pi y[\pi D_1(1-x) \cos \pi x + C_1 \sin \pi x] \frac{e^{-jk_o a\sqrt{x^2+\delta^2y^2}}}{\sqrt{x^2+\delta^2y^2}} \, dx\, dy \tag{4.51}$$

$$C_{1212} = \left(\frac{b^2}{a}\right) \frac{1}{4\pi^3} \int_0^1 \int_0^1 [2\pi(1-y)\cos 2\pi y - \sin 2\pi y]\,[\pi D_1(1-x)\cos \pi x + C_1 \sin \pi x]$$

$$\frac{e^{-jk_o a\sqrt{x^2+\delta^2 y^2}}}{\sqrt{x^2+\delta^2 y^2}}\, dx\, dy \qquad (4.52)$$

$$C_{3232} = \left(\frac{b^2}{a}\right) \frac{1}{12\pi^3} \int_0^1 \int_0^1 [2\pi(1-y)\cos 2\pi y - \sin 2\pi y]\,[3\pi(1-x) D_9 \cos 3\pi x + C_9 \sin 3\pi x]$$

$$\frac{e^{-jk_o a\sqrt{x^2+\delta^2 y^2}}}{\sqrt{x^2+\delta^2 y^2}}\, dx\, dy \qquad (4.53)$$

$$C_{3210} = -\left(\frac{b^2}{a}\right)\left(\frac{1}{8\pi^3}\right) \int_0^1 \int_0^1 \sin 2\pi y[3D_1 \sin \pi x - D_9 \sin 3\pi x]\, \frac{e^{-jk_o\sqrt{x^2+\delta^2 y^2}}}{\sqrt{x^2+\delta^2 y^2}}\, dx\, dy \qquad (4.54)$$

The above formulas (4.49 - 4.54) were used to calculate by computer the higher order corrections to the admittance for the specific case ($\mu_r = 1$, $\epsilon_r = 10$, $b/a = .5$, $F_N = 1.5$). Results are shown in Table 1. The largest correction is 2.1 percent of the corresponding dominant mode term.

Dominant Mode Approximation

$$\frac{Y_{10}}{Y_o} = .041 - j.31$$

Higher Order Mode Correction Using Two Modes

(1,0) and (1,2) : $\frac{Y_{12}}{Y_o}$	$= .000116 - j.00602$
(1,0) and (3,0) : $\frac{Y_{30}}{Y_o}$	$= -.000628 + j.00636$
(1,0) and (3,2) : $\frac{Y_{32}}{Y_o}$	$= .0000145 - j.000135$

Table 1. Higher order mode calculations.

4.4 Effect of Forbidden Modes

It is shown in this section that forbidden modes (m even or n odd) do not affect the calculation of admittance and that the Rayleigh-Ritz procedure yields coefficient values of zero for all forbidden modes. Consider the variational expression for the normalized admittance with the addition of one higher mode:

$$\frac{Y}{Y_o} = -\frac{2\mu_r}{\Gamma_{10} ab}\left[C_{1010} - \frac{C_{mn10}^2}{C_{mnmn} + D_{mn}}\right] = \frac{Y_{10}}{Y_o} + \frac{Y_{mn}}{Y_o} \qquad (4.20)$$

where

$$\frac{Y_{mn}}{Y_o} = \frac{2\mu_r}{\Gamma_{10} ab}\left[\frac{C_{mn10}^2}{C_{mnmn} + D_{mn}}\right]$$

for m even or n odd, the higher order correction Y_{mn}/Y_o will be zero if the denominator is nonzero.

$$D_{mn} = \frac{b}{a}\,\frac{\epsilon_{mn}(k^2a^2 - m^2\pi^2)}{2\mu_r\sqrt{\frac{m^2\pi^2}{a^2} + \frac{n^2\pi^2}{b^2} - k^2}}\,, \qquad \left.\begin{array}{l} \text{Im } C_{mnmn} < 0 \ (ka < \pi) \\ \text{Im } C_{mnmn} > 0 \ \left(\pi^2 < k^2a^2 < \frac{m^2\pi^2}{a^2} + \frac{n^2\pi^2}{b^2}\right) \\ \text{Im } C_{mnmn} < 0 \ \left(k^2a^2 > \frac{m^2\pi^2}{a^2} + \frac{n^2\pi^2}{b^2}\right) \end{array}\right\} \text{shown in Chapter 5}$$

There are five ranges of interest:

(1) $ka < m\pi$

$$\begin{cases} D_{mn} \text{ negative and real} \\ I_m\, C_{mnmn} < 0 \end{cases} \quad D_{mn} + C_{mnmn} \neq 0$$

(2) $ka = \pi$

$$\begin{cases} \text{as } ka \longrightarrow \pi \text{ from the left} \\ D_{mn} \longrightarrow 0 \\ \text{Im } C_{mnmn} \longrightarrow -\infty \end{cases} \quad \begin{cases} \text{as } ka \longrightarrow \pi \text{ from the right} \\ D_{mn} \longrightarrow 0 \\ \text{Im } C_{mnmn} \longrightarrow +\infty \end{cases} \quad D_{mn} + C_{mnmn} \neq 0$$

(3) $ka > m\pi$

$$k^2a^2 < \frac{m^2\pi^2}{a^2} + \frac{n^2\pi^2}{b^2}$$

$$\begin{cases} D_{mn} \text{ positive and real} \\ \text{Im } C_{mnmn} > 0 \end{cases} \quad D_{mn} + C_{mnmn} \neq 0$$

(4) $k^2a^2 = \frac{m^2\pi^2}{a^2} + \frac{n^2\pi^2}{b^2}$

$$\begin{cases} \text{as } k^2a^2 \longrightarrow \frac{m^2\pi^2}{a^2} + \frac{n^2\pi^2}{b^2} \text{ from the left} \\ D_{mn} \longrightarrow +\infty \\ \text{Im } C_{mnmn} \longrightarrow +\infty \end{cases} \quad \begin{cases} \text{as } k^2a^2 \longrightarrow \frac{m^2\pi^2}{a^2} + \frac{n^2\pi^2}{b^2} \text{ from the right} \\ D_{mn} \longrightarrow -j\infty \\ \text{Im } C_{mnmn} \longrightarrow -\infty \end{cases} \quad D_{mn} + C_{mnmn} \neq 0$$

(5) $k^2a^2 > \frac{m^2\pi^2}{a^2} + \frac{n^2\pi^2}{b^2}$

$$\begin{cases} D_{mn} \text{ is negative imaginary} \\ \text{Im } C_{mnmn} < 0 \end{cases} \quad D_{mn} + C_{mnmn} \neq 0$$

Therefore the denominator is nonzero, and A_{mn}, Y_{mn}/Y_o are all zero for m even or n odd.

In fact, the analysis can be generalized. Consider a finite or infinite set of allowed modes (aa'), (bb'), ..., (ff') and one forbidden mode (m'n') with mode coefficients

$$A_{aa'}, A_{bb'} \cdots A_{ff'}, A_{m'n'}$$

In addition let:

$$D_{fgmn} = C_{fgmn} + D_{mn} \qquad \begin{pmatrix} f = m \\ g = n \end{pmatrix}$$

$$= C_{fgmn} \qquad \text{(otherwise)}$$

Equation (4. 15) reduces to

$$\sum_{1}^{\infty} \sum_{0}^{\infty} A_{fg} D_{fgmn} = C_{mn10} \tag{4.55}$$

Expanding Eq. (4. 55) yields, in matrix form:

$$\begin{bmatrix} D_{aa'aa'} & D_{bb'aa'} & \cdots & D_{ff'aa'} & D_{m'n'aa'} \\ D_{aa'bb'} & D_{bb'bb'} & \cdots & D_{ff'bb'} & D_{m'n'bb'} \\ \vdots & \vdots & & \vdots & \vdots \\ D_{aa'ff'} & D_{bb'ff'} & \cdots & D_{ff'ff'} & D_{m'n'ff'} \\ D_{aa'm'n'} & D_{bb'm'n'} & \cdots & D_{ff'm'n'} & D_{m'n'm'n'} \end{bmatrix} \begin{bmatrix} A_{aa'} \\ A_{bb'} \\ \vdots \\ A_{ff'} \\ A_{m'n'} \end{bmatrix} = \begin{bmatrix} C_{10aa'} \\ C_{10bb'} \\ \vdots \\ C_{10ff'} \\ C_{10m'n'} \end{bmatrix} \tag{4.56}$$

where:

$$D_{aa'm'n'} = D_{bb'm'n'} = D_{ff'm'n'} = C_{10m'n'} = D_{m'n'aa'} = D_{m'n'bb'} = D_{m'n'ff'} = 0$$

Thus all the coefficients D_{fgmn} in the bottom row and in the last column of the square matrix are zero, with the exception of $D_{m'n'm'n'}$. In addition the term C_{10mn} in the last row of the column matrix on the right hand side of (4. 56) is zero.

Using Cramer's rule to solve (4. 56)

$$A_{m'n'} = \frac{1}{\Delta} \begin{vmatrix} D_{aa'aa'} & D_{bb'aa'} & \cdots & D_{ff'aa'} & C_{10aa'} \\ D_{aa'bb'} & D_{bb'bb'} & \cdots & D_{ff'bb'} & C_{10bb'} \\ . & . & & . & . \\ . & . & & . & . \\ . & . & & . & . \\ D_{aa'ff'} & D_{bb'ff'} & \cdots & D_{ff'ff'} & C_{10ff'} \\ 0 & 0 & & 0 & 0 \end{vmatrix} = \frac{0}{\Delta} \qquad (4.57)$$

where Δ = the determinant of the square matrix in (4. 56).

Expanding the determinant

$$\Delta = D_{m'n'm'n'} \begin{vmatrix} D_{aa'aa'} & D_{bb'aa'} & \cdots & D_{ff'aa'} \\ D_{aa'bb'} & D_{bb'bb'} & \cdots & D_{ff'bb'} \\ D_{aa'ff'} & D_{bb'ff'} & \cdots & D_{ff'ff'} \end{vmatrix} = D_{m'n'm'n'} \Delta_{a-f} \qquad (4.58)$$

$$A_{m'n'} = \frac{0}{D_{m'n'm'n'} \Delta_{a-f}} \qquad (4.59)$$

$$A_{ff'} = \frac{\begin{vmatrix} D_{aa'aa'} & D_{bb'aa'} & \cdots & D_{10aa'} \\ D_{aa'bb'} & D_{bb'bb'} & \cdots & D_{10bb'} \\ D_{aa'ff'} & D_{bb'ff'} & \cdots & D_{10ff'} \end{vmatrix}}{D_{m'n'm'n'} \Delta_{a-f}} \qquad (4.60)$$

The coefficient $A_{ff'}$ has the same value as would be obtained from the Rayleigh-Ritz procedure if the forbidden mode (m'n') were not present. The coefficient $A_{m'n'}$ of the forbidden mode is zero except, perhaps, at zeros of the determinant Δ_{a-f}. But, if the determinant Δ_{a-f} were zero, this would imply that the set of simultaneous linear equations for the allowed modes were linearly dependent and thus had no unique solution. Since the mode coefficient $A_{m'n'}$ is zero and $C_{10m'n}$ is also zero, the term $A_{m'n'}C_{10m'n'}$ contributed to the dominant mode admittance by the forbidden mode is zero.

It is possible to generalize further. Consider an infinite set of allowed modes and an infinite set of forbidden modes. The matrix of the coefficients may be partitioned into two submatrices, one containing only allowed mode terms and the other containing only forbidden mode terms.

$$\begin{bmatrix} A & 0 \\ 0 & F \end{bmatrix} \begin{bmatrix} A_{allowed} \\ A_{forbidden} \end{bmatrix} = \begin{bmatrix} C_{10mm} \\ 0 \end{bmatrix} \tag{4.61}$$

where: $A_{allowed}$ = allowed mode coefficients

$A_{forbidden}$ = forbidden mode coefficients

A = submatrix of $D_{fgh\ell}$ terms associated with the allowed modes

F = submatrix of $D_{fgh\ell}$ terms associated with the forbidden modes.

Now it is possible to write separate matrix equations for the allowed and the forbidden modes. The allowed mode coefficients ($A_{allowed}$) will be independent of the forbidden modes and the forbidden mode coefficients will all be zero if the matrix equations for the forbidden mode coefficients are linearly independent.

Several facts concerning the higher order mode coefficients and their use in the Rayleigh-Ritz procedure have been pointed out.

(a) If a forbidden mode with an undetermined coefficient is added to a finite or infinite set of allowed modes whose coefficients have already been determined by the Rayleigh-Ritz procedure:

(1) The coefficient of the forbidden mode as determined by the Rayleigh-Ritz procedure is zero.

(2) The dominant mode admittance is unchanged from its value as determined from the set of allowed modes.

It is evident that, in the limit, as the number of modes included approaches a complete orthogonal set, the mode coefficients will approach their actual values and the mode coefficients for the forbidden modes will all approach zero. However, it is not evident, without the above derivation, that the Rayleigh-Ritz process yields a zero value for the forbidden mode coefficients at every step of the process, whether a finite or infinite number of modes is considered.

CHAPTER 5

GENERALIZATION OF THE VARIATIONAL ANALYSIS

5.1 Other LSE Modes Incident

Consider the configuration of Fig. 3(a) with an arbitrary one of the higher modes incident from the left.

Fields in Waveguide:

$$\Pi_1^* = -\frac{1}{j\omega\mu}\left[\left(\frac{e^{-\Gamma_{fg}z} - R_{fgfg}e^{\Gamma_{fg}z}}{\Gamma_{fg}}\right)\sin\frac{f\pi y}{a}\cos\frac{g\pi x}{b} + \sum_{m=1}^{\infty}\sum_{n=0}^{\infty}{}' \frac{A_{mn}}{\Gamma_{mn}}\sin\frac{m\pi y}{a}\cos\frac{n\pi x}{b}\,e^{\Gamma_{mn}z}\right] \tag{5.1}$$

Fields in Half-Space:

$$\Pi_2^* = -\frac{1}{2\pi j\omega\mu_o}\int_o^a\int_o^b E_x(\xi,\eta)\,\frac{e^{jk_o r}}{r}\,d\xi\,d\eta \tag{5.2}$$

where R_{fgfg} = self-reflection coefficient for (f,g) mode and where the prime on the double summation indicates that the (f,g) term has been removed.

$E_{x1} = E_{x2}$ at z = 0:

$$(1+R_{fgfg})\sin\frac{f\pi y}{a}\cos\frac{g\pi x}{b} - \sum_{m=1}^{\infty}\sum_{n=0}^{\infty}{}' A_{mn}\sin\frac{m\pi y}{a}\cos\frac{n\pi x}{b} = E_x(x,y)$$

multiplying by $\sin\frac{f\pi y}{a}\cos\frac{g\pi x}{b}$ and integrating over the aperture:

$$(1+R_{fgfg}) = \frac{4\epsilon_{fg}}{ab}\int_o^a\int_o^b E_x(x,y)\sin\frac{f\pi y}{a}\cos\frac{g\pi x}{b}\,dx\,dy \tag{5.3}$$

Multiplying by $\sin \frac{m'\pi y}{a} \cos \frac{n'\pi x}{b}$ where either $(m' \neq f)$ or $(n' \neq g)$ and integrating over the aperture:

$$A_{mn} = -\frac{4\epsilon_{mn}}{ab} \int_0^a \int_0^b E_x(x,y) \sin \frac{m\pi y}{a} \cos \frac{n\pi x}{b} \, dx \, dy \tag{5.4}$$

$\underline{H_{y1} = H_{y2} \text{ at } z = 0:}$

$$\frac{1}{j\omega\mu} \left(\frac{\partial^2}{\partial y^2} + k^2 \right) \left[\left(\frac{1 - R_{fgfg}}{\Gamma_{fg}} \right) \sin \frac{f\pi y}{a} \cos \frac{g\pi x}{b} + \sum_{m=1}^{\infty} \sum_{n=0}^{\infty}{}' \frac{A_{mn}}{\Gamma_{mn}} \sin \frac{m\pi y}{a} \cos \frac{n\pi x}{b} \right]$$

$$= \frac{1}{2\pi j\omega\mu_o} \left[\int_0^a \int_0^b E_x(\xi,\eta) \left(\frac{\partial^2}{\partial y^2} + k_o^2 \right) \frac{e^{-jk_o r}}{2\pi r} \, d\xi \, d\eta \right]$$

$$= \frac{1}{j\omega\mu} \left[- \left(\frac{1 - R_{fgfg}}{\Gamma_{fg}} \right) \Gamma_{mo}^2 \sin \frac{f\pi y}{a} \cos \frac{g\pi x}{b} \right.$$

$$- \sum_{m=1}^{\infty} \sum_{n=0}^{\infty}{}' \frac{4\epsilon_{mn}}{ab\Gamma_{mn}} \int_0^a \int_0^b E_x(\xi,\eta) \sin \frac{m\pi\eta}{a} \cos \frac{n\pi\xi}{b} \left(\frac{\partial^2}{\partial y^2} + k_o^2 \right)$$

$$\left. \sin \frac{m\pi y}{a} \cos \frac{n\pi x}{b} \, d\xi \, d\eta \right]$$

$$\int_0^a \int_0^b E_x(\xi,\eta) \, G_1(x,y,\xi,\eta) = -\frac{(1 - R_{fgfg}) \, \Gamma_{mo}^2}{\mu_r \Gamma_{fg}} \sin \frac{f\pi y}{a} \cos \frac{g\pi x}{b} \tag{5.5}$$

where

$$G_1(x,y,\xi,\eta) = \left[\left(\frac{\partial^2}{\partial y^2} + k_o^2 \right) \frac{e^{-jk_o r}}{2\pi r} + \left(\frac{\partial^2}{\partial y^2} + k^2 \right) \sum_{m=1}^{\infty} \sum_{n=0}^{\infty}{}' \frac{4\epsilon_{mn}}{ab\mu_r \Gamma_{mn}} \right.$$

$$\left. \sin \frac{m\pi\eta}{a} \cos \frac{n\pi\xi}{b} \sin \frac{m\pi y}{a} \cos \frac{n\pi x}{b} \right]$$

multiplying by $E_x(x,y)$ and integrating over the aperture:

$$\frac{(1 - R_{fgfg}) \, \Gamma_{fo}^2}{\mu_r \, \Gamma_{fg}} = -\frac{\int_0^a \int_0^b \int_0^a \int_0^b E_x(x,y) \, E(\xi,\eta) \, G_1(x,y,\xi,\eta) \, dx \, dy \, d\xi \, d\eta}{\int_0^a \int_0^b E_x(x,y) \sin \frac{f\pi y}{a} \cos \frac{g\pi x}{b} \, dx \, dy} \tag{5.6}$$

$$\frac{1-R_{fgfg}}{1+R_{fgfg}} = -\left(\frac{\Gamma_{fg}}{\Gamma_{fo}^2}\right)\frac{\mu_r ab}{4\epsilon_{fg}} \frac{\int_0^a\int_0^b\int_0^a\int_0^b E_x(x,y)\, E_x(\xi,\eta)\, G_1(x,y,\xi,\eta)\, dx\, dy\, d\xi\, d\eta}{\left[\int_0^a\int_0^b E_x(x,y)\sin\frac{f\pi y}{a}\cos\frac{g\pi x}{b}\, dx\, dy\right]^2}$$

$$= \frac{Y_{fg}}{Y_o} = \frac{G_{fg}}{Y_o} + \frac{jB_{fg}}{Y_o} \qquad (5.7)$$

Assume

$$E_x(x,y) = \sin\frac{f\pi y}{a}\cos\frac{g\pi x}{b}$$

$$\frac{Y_{fg}}{Y_o} = -\frac{\Gamma_{fg}}{\Gamma_{fo}^2}\frac{\mu_r ab}{4\epsilon_{fg}} \frac{\int_0^a\int_0^b\int_0^a\int_0^b \sin\frac{f\pi y}{a}\cos\frac{g\pi x}{b}\sin\frac{f\pi\eta}{a}\cos\frac{g\pi\xi}{b}\left(\frac{\partial^2}{\partial y^2}+k_o^2\right)\frac{e^{-jk_o r}}{2\pi r}\, dx\, dy\, d\xi\, d\eta}{\left[\int_0^a\int_0^b \sin^2\frac{f\pi y}{a}\cos^2\frac{g\pi x}{b}\, dx\, dy\right]^2}$$

$$= -\left(\frac{\Gamma_{fg}}{\Gamma_{fo}^2}\right)\frac{\mu_r 4\epsilon_{fg}}{ab}\int_0^a\int_0^b\int_0^a\int_0^b \sin\frac{f\pi y}{a}\cos\frac{g\pi x}{b}\sin\frac{f\pi\eta}{a}\cos\frac{g\pi\xi}{b}\left(\frac{\partial^2}{\partial y^2}+k_o^2\right)$$

$$\frac{e^{-jk_o\sqrt{x^2+\delta^2y^2}}}{2\pi\sqrt{x^2+\delta^2y^2}}\, dx\, dy\, d\xi\, d\eta$$

$$= -\frac{4\mu_r\epsilon_{fg}}{ab}\left(\frac{\Gamma_{fg}}{\Gamma_{fo}^2}\right)C_{fgfg} \qquad (5.8)$$

where

$$C_{fgfg} = \frac{b^2}{a}\frac{1}{2mn\pi^3}\int_0^1\int_0^1 [n\pi(1-y)\cos n\pi y - \sin n\pi y]\,[m\pi(1-x)D_m^2\cos m\pi x + C_{m^2}\sin m\pi x]$$

$$\frac{e^{-jk_o\sqrt{x^2+\delta^2y^2}}}{\sqrt{x^2+\delta^2y^2}}\, dx\, dy$$

if $(m \neq 0)$, $(n \neq 0)$

$$C_{fofo} = \frac{b^2}{a} \frac{1}{m\pi^2} \int_0^1 \int_0^1 (1-y)[m\pi(1-x) D_{m^2} \cos m\pi x - c_{m^2} \sin m\pi x] \frac{e^{-jk_o r}}{r} dx\, dy$$

$$\frac{\Gamma_{fg}}{\Gamma_{fo}^2} = \frac{\sqrt{\frac{f^2\pi^2}{a^2} + \frac{g^2\pi^2}{b^2} - k^2}}{\left(\frac{f^2\pi^2}{a^2} - k^2\right)}$$

The expression for the input admittance of the higher modes is similar to that of the dominant mode. The dependence on μ_r, ϵ_r is similar. In all cases, the normalized input admittance is equal to μ_r times an integral which is a function only of the product $\mu_r \epsilon_r$.

The form of the admittance function (Eq. 5.8) brings out several interesting points concerning the LSE (longitudinal section electric) modes. Consider the pole-zero pattern of the admittance functions. If $g \neq 0$, the real and imaginary parts of the admittance have zeros at cutoff for the (f, g) mode and poles at cutoff for the (f, o) mode. If $g = 0$, the real and imaginary parts of the admittance have poles at cutoff for the (f, o) mode. If $g = 0$, the real and imaginary parts of the admittance have poles at cutoff for the (f, o) mode.

This type of behavior is characteristic of LSE modes. Consider an $(LSE)_y$ type mode.

$$\Pi_y^* = \frac{1}{-j\omega\mu\Gamma_{mn}} \sin\frac{m\pi y}{a} \cos\frac{n\pi x}{b} e^{\pm\Gamma_{mn}z}$$

$$E_x = (\mp) \sin\frac{m\pi y}{a} \cos\frac{n\pi x}{b} e^{\pm\Gamma_{mn}z}$$

$$E_y = 0$$

$$E_z = -\left(\frac{n\pi}{b}\right) \sin\frac{m\pi y}{a} \sin\frac{n\pi x}{b} e^{\pm\Gamma_{mn}z}$$

$$H_x = +\frac{1}{j\omega\mu\Gamma_{mn}} \frac{nm\pi^2}{ab} \cos\frac{m\pi y}{a} \sin\frac{n\pi x}{b} e^{\pm\Gamma_{mn}z}$$

$$H_y = -\frac{\left(k^2 - \frac{m^2\pi^2}{a^2}\right)}{j\omega\mu\Gamma_{mn}} \sin\frac{m\pi y}{a} \cos\frac{n\pi x}{b} e^{\pm\Gamma_{mn}z}$$

$$H_z = \mp \frac{\frac{m\pi}{a}}{j\omega\mu} \cos\frac{m\pi y}{a} \cos\frac{n\pi x}{b} e^{\pm\Gamma_{mn} z}$$

The only two components which contribute to power flow in the longitudinal (z) direction are E_x and H_y. These field components are related by the factor $\Gamma_{mo}^2 / j\omega\mu\Gamma_{mn}$.

$$H_y = \frac{\Gamma_{mo}^2}{j\omega\mu\Gamma_{mn}} E_x \tag{5.9}$$

Thus for $(LSE)_y$ modes, there are two critical frequencies (besides $\omega = 0$) at which the ratio of E_x to H_y has a pole or zero, namely (m,n) cutoff and (m,o) cutoff. The fact that there is a pole at (m,o) cutoff is interesting because this does not occur for the ordinary TM and TE modes. This behavior is related to the fact that the waveguide is restricted in the x and y but not in the z direction. The poles and zeros in the ratio of H_y to E_x are identical to those occurring in the admittance functions Y_{fgfg}.

The behavior of TE and LSE modes at the critical frequencies is compared below:

TE Modes ($m \neq 0$)

$f \to \infty$	$f \to fc(m,n)$	$f \to fc(m,o)$	$f \to 0$
$E_x \to \infty$	$E_x \to$ const	$E_x \to$ const	$E_x \to 0$
$E_y \to \infty$	$E_y \to$ const	$E_y \to$ const	$E_y \to 0$
$H_x \to \infty$	$H_x \to 0$	$H_x \to$ const	$H_x \to$ const
$H_y \to \infty$	$H_y \to 0$	$H_y \to$ const	$H_y \to$ const
$H_z \to$ const	$H_z \to$ const	$H_z \to$ const	$H_z \to$ const

LSE Modes ($m \neq 0$)

$f \to \infty$	$f \to fc(m,n)$	$f \to fc(m,o)$	$f \to 0$
$E_x \to$ const	$E_x \to$ const	$E_x \to$ const	$E_x \to$ const
$E_z \to$ const	$E_z \to$ const	$E_z \to$ const	$E_z \to$ const
$H_x \to 0$	$H_x \to \infty$	$H_x \to$ const	$H_x \to \infty$
$H_y \to$ const	$H_y \to \infty$	$H_y \to 0$	$H_y \to \infty$
$H_z \to 0$	$H_z \to$ const	$H_z \to$ const	$H_z \to \infty$

We note that the behavior of the LSE and TE modes as $f \longrightarrow 0$ is similar. The magnetic fields are predominant and the excitation of an LSE or TE mode in the aperture from a probe source can be considered as a problem of simple magnetic coupling. At infinity, the fields are predominantly transverse for both the LSE and TE modes. At (m,n) cutoff, the electric fields are predominant for the TE modes and the magnetic fields are predominant for the LSE modes.

5.2 Below Cutoff Considerations

We have limited the range of experimental verification of our results to a frequency range where only the dominant mode propagates. There are several practical reasons for this:

1. Standing wave patterns are hopelessly confused when more than one mode propagates, although this could possibly be remedied by a mode filter.

2. Special techniques would be required to accurately determine below cutoff behavior. Below cutoff the standing wave pattern can be represented as:

$$E_x = \sin \frac{\pi y}{a} e^{-\Gamma_{10} z} (1 + A_{mn} e^{2\Gamma_{10} z}) \tag{5.10}$$

where A_{mn} is the complex aperture reflection coefficient for the (m,n) mode.

The rapid increase of the $e^{-\Gamma_{10} z}$ term away from the aperture (for z negative) and the rapid decay of the $A_{mn} e^{\Gamma_{10} z}$ term tends to mask the effects of A_{mn}.

However, the theoretical results for the dominant mode reflection coefficient are valid outside the frequency range where only the dominant mode propagates as long as the assumption of dominant mode aperture field is valid. In most cases, this assumption would appear to be a valid one. The results of some below cutoff calculations of normalized aperture admittance are shown in Fig. 8(a)-(h). These calculations are useful for calculating the admittance of a loaded waveguide with an iris in the aperture plane as noted in Chapter 3.

It is noted that, in the curves of Fig. 8, the imaginary part of the admittance goes to zero at zero frequency and that the real part of the admittance approaches a finite value. This can be explained by the following argument:

Consider incident and reflected dominant mode waves in a rectangular waveguide opening out into an infinite ground plane at z = 0 (Fig. 3)

Incident:

$$E_x = \sin \frac{\pi y}{a} e^{-\Gamma_{10} z}$$

$$H_y = \frac{\sqrt{\frac{\pi^2}{a^2} - k^2}}{j\omega\mu} \sin \frac{\pi y}{a} e^{-\Gamma_{10} z} \qquad (5.11)$$

Reflected:

$$E_x = R \sin \frac{\pi y}{a} e^{+\Gamma_{10} z}$$

where R is the dominant mode aperture reflection coefficient

$$R = R_r - jR_i$$

$$H_y = -\frac{R\sqrt{\frac{\pi^2}{a^2} - k^2}}{j\omega\mu} \sin \frac{\pi y}{a} e^{+\Gamma_{10} z} \qquad (5.12)$$

The total power radiated is

$$P = 1/2 \ \mathrm{Re} \int_0^a \int_0^b E_x H_y^* \, dx \, dy$$

$$= \frac{\sqrt{\frac{\pi^2}{a^2} - k^2}}{\omega\mu} \frac{ab}{2} (R_i) \qquad (ka < \pi) \qquad (5.13)$$

$$= \frac{\sqrt{k^2 - \frac{\pi^2}{a^2}}}{\omega\mu} \frac{ab}{4} (1 - |R|^2) \qquad (ka > \pi) \qquad (5.14)$$

Thus the total power radiated below cutoff depends only on the imaginary part of the reflection coefficient.

$$\frac{Y}{Y_o} = \frac{1-R}{1+R} = \frac{G}{Y_o} + j \frac{B}{Y_o}$$

$$R_i = \frac{+2B}{[(1+G)^2 + B^2]} \qquad G = \frac{[(1-R_r^2) - R_i^2]}{(1+R_r)^2 + R_i^2} \qquad (5.15)$$

$$R_r = \frac{[(1-G^2) - B^2]}{[(1+G)^2 + B^2]} \qquad B = \frac{2R_i}{(1+R_r)^2 + R_i^2} \qquad (5.16)$$

If B goes to zero, then R_i and the radiated power also go to zero. Thus the roles of G and B are interchanged below cutoff, the power radiated being proportional to B rather than G. In particular, G may go to zero without the radiated power going to zero. In order for the power radiated to be positive, R_i must be positive and B must be positive. Similarly, if we consider incident and reflected waves of the higher order modes:

$$P = \frac{ab}{4\epsilon_{fg}} \frac{1}{\omega\mu} \frac{\Gamma_{fo}^2}{\Gamma_{fg}} [R_{fgfg(i)}] \qquad (k < f\pi/a) \tag{5.17}$$

$$= \frac{ab}{4\epsilon_{fg}} \frac{1}{\omega\mu} \frac{\beta_{fo}^2}{\Gamma_{fg}} [-R_{fgfg(i)}] \qquad \left(\frac{f^2\pi^2}{a^2} < k^2 < \frac{f^2\pi^2}{a^2} + \frac{g^2\pi^2}{b^2}\right) \tag{5.18}$$

$$= \frac{ab}{8\epsilon_{fg}} \frac{1}{\omega\mu} \frac{\beta_{fo}^2}{\Gamma_{fg}} [1 - |R_{fgfg}|^2] \qquad \left(k^2 > \frac{f^2\pi^2}{a^2} + \frac{g^2\pi^2}{b^2}\right) \tag{5.19}$$

where

$$R_{fgfg} = R_{fgfg(r)} - j R_{fgfg(i)}$$

$$R_{fgfg(r)} > 0. \qquad (k > f^2\pi^2/a^2 + g^2\pi^2/b^2) \tag{5.20}$$

This last condition can be derived from the equivalent circuit representation. Since the net radiated power will always be greater than zero except at (f, g) cutoff and (f, 0) cutoff, the following conditions on the quadruple integral forms C_{fgfg} may be stated:

Below (f, 0) cutoff

$$\text{Im } C_{fgfg} \leq 0 \tag{5.21}$$

Between (f, 0) cutoff and (f, g) cutoff

$$\text{Im } C_{fgfg} \geq 0 \tag{5.22}$$

Above (f, g) cutoff

$$\text{Im } C_{fgfg} \leq 0 \tag{5.23}$$

where Im C_{fgfg} is equal to the imaginary part of C_{fgfg}. The conditions (5.20) through (5.23) have been used in Chapter 4 to show that the denominator of the mode coefficients is nonzero.

5.3 Superposition of LSE_x and LSE_y Solutions

Stratton[73] and others have shown that an arbitrary field in a homogeneous source free region can be expressed as the sum of three vector potential functions. Applying this to the Π and Π^* Hertzian potential functions leads to the well known fact that an arbitrary field can be expressed in terms of a Π_i^* and a Π_i vector function where i = x, y, or z, yielding, respectively, LSE_x and LSH_x modes, LSE_y and LSH_y modes, and TM and TE modes in rectangular waveguide. It is possible to show that an arbitrary field can be expressed in terms of other combinations of Π and Π^* vectors for both rectangular waveguides and for other cylindrical geometries. Consider an infinite rectangular waveguide (Fig. 10) excited by sources to the right of z = 0, which give rise to an infinite number of, for instance, TM and TE modes with arbitrary coefficients. Utilizing equivalence principles, the effect of the sources may be taken into account by introducing new sources at z = 0. Two alternative representations are:[74]

1. an electric current $\underline{J}_s = \hat{n} \times \underline{H}_{tangential}$ backed by a magnetic conductor.
2. a magnetic current $\underline{M}_s = \underline{E}_{tangential} \times \hat{n}$ backed by an electric conductor.

Using image theory, these representations may be replaced with

1. an infinite array of electric current sources in the plane z = 0.
2. an infinite array of magnetic current sources in the plane z = 0.

The problem is now reduced to a homogeneous boundary value problem. The $\underline{\Pi}$ and $\underline{\Pi}^*$ Hertzian potentials, or the $\underline{A}$ and $\underline{F}$ vector potentials, may be found by direct integration.

$$\underline{A} = \frac{1}{4\pi} \iiint_{\text{sources}} \frac{J e^{-jkr}}{r} \, dv$$

$$\underline{F} = \frac{1}{4\pi} \iiint_{\text{sources}} \frac{M e^{-jkr}}{r} \, dv$$

where r = distance from source to field point

The result is:

1. Π_x and Π_y vectors--resulting from the electric current representation, or
2. Π_x^* and Π_y^* vectors--resulting from the magnetic current representation.

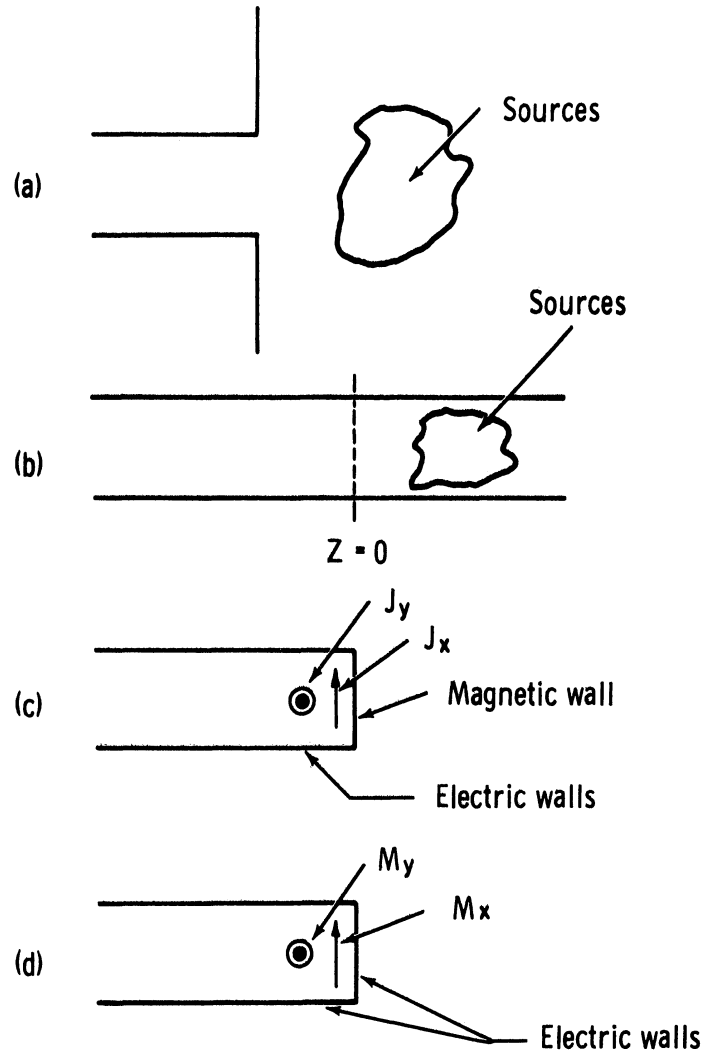

Fig. 10. Equivalent representations.

Thus an arbitrary field in rectangular waveguide can be expressed in terms of (1) transverse Π vectors or (2) transverse Π^* vectors. Increasing the number of sides of the waveguide does not invalidate the results, since all of the images are transverse magnetic or electric currents in the $z = 0$ plane. Thus the results apply to a polygonal waveguide, and, in the limit, to an arbitrary cylindrical waveguide. However, if we attempt to extend the results to nonuniform waveguides, the images will include longitudinal as well as transverse Π and Π^* components.

An immediate result is that the waveguide problem of Fig. 3(a) can be generalized to take into account any mode incident including LSH as well as LSE modes. The incident (m, n) mode may be broken up into a linear combination of a $\Pi_y^*(m, n)$ mode and a $\Pi_x^*(m, n)$

mode and the problem may be solved as a superposition of two problems of the type investigated in Chapters 1-4.

As a matter of fact, there are fifteen different possible combinations of π and/or π^* vector potential functions which can be used as complete representations of the field in a source free rectangular waveguide. There are six basic mode types generated by π_x, π_y, π_z, π_x^*, π_y^*, π_z^* vector potential functions. If we consider the TM-TE combination as a basic complete orthogonal set, it can be shown that a combination of any two of the six mode types will also be a complete orthogonal set. This can be accomplished by actually solving for the mode coefficients of each combination in terms of the TM-TE coefficients to show that the representations are completely equivalent.

5.4 The Dual Problem

The problem dual to that of Fig. 3(a) yields some information of interest concerning the effects of permeability and permittivity on input admittance.

Consider the geometry of Fig. 3(a) with the metal walls replaced with magnetic walls, and with a dominant mode wave incident from the left.

The solution to Eq. 2.6 of Chapter 2, appropriate to the magnetic walls, is:

$$\psi = \sin k_y y \cos k_x x$$

The field representations in Region No. 1 (waveguide) and Region No. 2 (half-space) are:

$$\Pi_{1y} = \frac{1}{j\omega\epsilon}\left[\frac{\left(e^{-\Gamma_{10}z} - R_m e^{\Gamma_{10}z}\right)}{\Gamma_{10}} \frac{\sin \pi y}{a} + \sum_{m=1}^{\infty}\sum_{n=0}^{\infty} \frac{A_{mn}}{\Gamma_{mn}} \sin \frac{m\pi y}{a} \cos \frac{n\pi x}{b} e^{\Gamma_{mn}z}\right] \tag{5.24}$$

where: R_m is the dominant mode reflection coefficient for H_x.

Region 2

$$\Pi_{2y} = -\frac{1}{2\pi j\omega\epsilon_o} \int_0^a \int_0^b H_x(\xi,\eta) \frac{e^{-jk_o r}}{r} \, d\xi \, d\eta \tag{5.25}$$

Using an analysis parallel to that of Chapter 2:

$$\frac{1-R_m}{1+R_m} = -\frac{ab\epsilon_r}{2\Gamma_{10}} \frac{\int_0^a \int_0^b \int_0^a \int_0^b H_x(x,y)\, G_{1m}(x,y,\xi,\eta)\, H_x(\xi,\eta)\, dx\, dy\, d\xi\, d\eta}{\left[\int_0^a \int_0^b H_x(x,y) \sin\frac{\pi y}{a}\, dx\, dy\right]^2} \tag{5.26}$$

where

$$G_{1m}(x,y,\xi,\eta) = \left[\left(\frac{\partial^2}{\partial y^2} + k_o^2\right)\left(\frac{e^{-jk_o r}}{2\pi r}\right) + \left(\frac{\partial^2}{\partial y^2} + k^2\right) \sum_{m=1}^{\infty} \sum_{n=0}^{\infty}{}' \frac{4\epsilon_{mn}}{ab\epsilon_r \Gamma_{mn}} \sin\frac{m\pi y}{a} \cos\frac{n\pi x}{b} \sin\frac{m\pi\eta}{a} \cos\frac{n\pi\xi}{b}\right]$$

For a dominant mode approximation to the aperture field, (5.26) reduces to an expression directly proportional to ϵ_r.

Consider R_e, the dominant mode reflection coefficient for E_y:

$$R_e = -R_m$$

$$\frac{1-R_m}{1+R_m} = \frac{1+R_e}{1-R_e}$$

Thus the electric field reflection coefficient is directly proportional to μ_r for the electric wall problem and inversely proportional to ϵ_r for the magnetic wall problem.

5.5 The Vector Problem

A variational expression for the vector problem will now be derived for the problem of Fig. 3(a). Methods used will be similar to those of Chapter 2 except (1) two simultaneous integral equations in $E_x(x,y)$ and $E_y(x,y)$ will be used and (2) an additional step is required to produce a variational expression.

Consider the problem of Fig. 3a. A variational expression will be found for the input admittance. Methods used will be similar to those of Chapter 2 except (1) two simultaneous integral equations in $E_x(xy)$ and $E_y(xy)$ will be found and (2) an additional step is required to produce a stationary expression.

The representations of the fields in Region No. 1 (waveguide) and Region No. 2 (half-space) are as follows:

Region No. 1

$$\Pi^*_{1y} = -\frac{1}{j\omega\mu}\left[\frac{e^{-\Gamma_{10}z} - R\,e^{\Gamma_{10}z}}{\Gamma_{10}}\sin\frac{\pi y}{a} + \sum_{m=1}^{\infty}\sum_{n=0}^{\infty}{}' \frac{A_{mn}}{\Gamma_{mn}}\sin\frac{m\pi y}{a}\cos\frac{n\pi x}{b}\,e^{\Gamma_{mn}z}\right]\Bigg\}\ \text{LSE}_y\ \text{Modes}$$

(5.27)

$$\Pi^*_{1x} = -\frac{1}{j\omega\mu}\left[-\sum_{m=1}^{\infty}\sum_{n=2}^{\infty}\frac{B_{mn}}{\Gamma_{mn}}\cos\frac{m\pi y}{a}\sin\frac{n\pi x}{b}\,e^{\Gamma_{mn}z}\right]\Bigg\}\ \text{LSE}_x\ \text{Modes}$$

For the allowed modes, m is odd and n is even.

Region No. 2

$$\Pi^*_{2y} = -\frac{1}{2\pi j\omega\mu_o}\int_0^a\int_0^b E_x(\xi,\eta)\,\frac{e^{-jk_o r}}{r}\,d\xi\,d\eta$$

$$\Pi^*_{2x} = -\frac{1}{2\pi j\omega\mu_o}\int_0^a\int_0^b -E_y(\xi,\eta)\,\frac{e^{-jk_o r}}{r}\,d\xi\,d\eta \qquad (5.28)$$

Equating E_x components at z = 0 yields an equation for A_{mn}. Equating E_y components at z = 0 yields an equation for B_{mn}. Equating H_y components and substituting for A_{mn} and B_{mn} yields the first integral equation. Proceeding as in Chapter 2 (multiplying the integral equation by $E_x(xy)$ and integrating over the aperture) yields an expression for $\frac{1-R}{1+R}$ which is not stationary. It can be made stationary by adding a second integral equation to the numeration of $\frac{1-R}{1+R}$. The second integral equation is obtained by equating H_x components at z = 0, substituting for A_{mn} and B_{mn}, multiplying by $E_y(x, y)$ and integrating over the aperture. The resultant integral equation has a left hand side equal to zero. This equation is added to the numerator (quadruple integral) of the previously obtained expression for $\frac{1-R}{1+R}$. The result is

(SEE NEXT PAGE FOR EQUATION 5.29)

where:

$G_1(x, y, \xi, \eta)$ is defined as in Chapter 2 [Eq. (2.30)].

$$\frac{1-R}{1+R} = -\frac{\mu_r ab}{2\Gamma_{10}}$$

$$\cdot \frac{\int_0^a \int_0^b \int_0^a \int_0^b \left[E_x(\xi,\eta)\, G_1(x,y,\xi,\eta)\, E_x(x,y) + E_y(\xi,\eta)\, G_4(x,y,\xi,\eta)\, E_y(x,y) + E_x(\xi,\eta)\, \left[G_2(x,y,\xi,\eta) + G_3(x,y,\xi,\eta)\right] E_y(x,y)\right] dx\, dy\, d\xi\, d\eta}{\left[\int_0^a \int_0^b E_x(x,y)\, \sin\frac{\pi y}{a}\, dx\, dy\right]^2} \qquad (5.29)$$

$$G_2(x,y,\xi,\eta) = -\left(\frac{\partial^2}{\partial x \partial y}\right)\left[\frac{e^{-jk_o r}}{2\pi r} + \sum_{m=1}^{\infty}\sum_{n=2}^{\infty} \frac{4}{ab\Gamma_{mn}\mu_r} \cos\frac{m\pi y}{a} \sin\frac{n\pi x}{b} \cos\frac{m\pi\eta}{a} \sin\frac{n\pi\xi}{b}\right] \tag{5.30}$$

$$G_3(x,y,\xi,\eta) = -\left(\frac{\partial^2}{\partial x \partial y}\right)\left[\frac{e^{-jk_o r}}{2\pi r} + \sum_{m=1}^{\infty}\sum_{n=0}^{\infty}{}' \frac{4\epsilon_{mn}}{ab\mu_r\Gamma_{mn}} \sin\frac{m\pi y}{a} \cos\frac{n\pi x}{b} \sin\frac{m\pi\eta}{a} \cos\frac{n\pi\xi}{b}\right] \tag{5.31}$$

$$G_4(x,y,\xi,\eta) = \left[\left(k_o^2 + \frac{\partial^2}{\partial x^2}\right)\left(\frac{e^{-jk_o r}}{2\pi r}\right) + \left(k^2 + \frac{\partial^2}{\partial x^2}\right)\sum_{m=1}^{\infty}\sum_{n=2}^{\infty} \frac{4}{ab\mu_r\Gamma_{mn}} \sin\frac{m\pi y}{a} \sin\frac{n\pi x}{b} \cos\frac{m\pi\eta}{a} \sin\frac{n\pi x}{b}\right] \tag{5.32}$$

This is a stationary expression for the input admittance. Reducing the ranges of integration appropriately will yield a stationary expression for the waveguide with compound iris. It is interesting to note that Eq. (5.29) reduces to Eq. (2.33) if $E_y(x,y)$ is set equal to zero.

5.6 Reaction Methods

In many of the problems investigated, the variational forms could have been derived using reaction methods. The methods of reaction theory simplify the derivation of stationary formulas for admittance, especially in complicated problems. One of the general stationary forms developed in connection with the reaction methods yields some additional information concerning the dependence of the admittance on μ_r and ϵ_r.

Harrington[75] has developed a general expression for the input admittance of a junction of two waveguides of arbitrary cross section. If the waveguide on the right approaches half-space as a special case, Eq. 8-128 of Ref. 75 becomes (using the notation of Harrington and Marcuvitz):

$$\frac{1-\Gamma}{1+\Gamma} = \frac{Y}{Y_o} = \frac{\iint_{\text{aperture}} E \times H \cdot ds + \sum\sum V_i^2 Y_i}{V_o^2 Y_o^-} \tag{5.33}$$

where: $\sum\sum V_i^2 Y_i$ indicates a sum over all modes except the mode incident from the left, whose mode admittance is Y_o^- and whose reflection coefficient is Γ.

If there is no iris in the aperture then the assumption of incident mode field in the aperture will drop out, by orthogonality, the terms of the infinite sum $\sum\sum V_i^2 Y_i$, leaving only the integral over the aperture, which depends on the free space size of the aperture, the form of the aperture field E, and the Green's function relationship between E and H. The dependence of Y/Y_0 on μ_r and ϵ_r derives solely, then, from the factor $1/Y_0^-$, the modal impedance of the incident mode.

The dependence of Y/Y_0 on μ_r and ϵ_r is then as follows:

Incident Mode	Dependence of Y/Y_0 on μ_r and ϵ_r
TE or LSE	μ_r
TM or LSH	$1/\epsilon_r$
TEM	$\sqrt{\frac{\mu_r}{\epsilon_r}}$

These three types of dependence give exactly the same type of behavior, in the following respect: Consider a material whose $\mu_r\epsilon_r$ product is fixed. As μ_r and ϵ_r are varied, μ_r, $1/\epsilon_r$, and $\sqrt{\mu_r/\epsilon_r}$ will all change by exactly the same factor. The process of optimizing the μ_r for a given $\mu_r\epsilon_r$ product is discussed in Chapter 7.

CHAPTER 6

EXPERIMENTAL RESULTS

6.1 Verification of Variational Results

In general, variational analyses have yielded accurate results, especially in interior problems. However, there are several considerations which make it desirable to obtain an accurate experimental verification of the results of Chapters 2 and 3.

1. Upper and lower bounds are not obtainable.

2. Field approximations may be less accurate than those used in similar interior problems

3. In some cases, poor results have been obtained in exterior scattering problems.[76] In addition, discrepancies have been noted in the literature in similar problems.[34]

4. In the case of the iris loaded radiator, two different approximations to aperture field have been used. To the author's knowledge, this type of calculation has not been checked experimentally.

An experimental check was made on the theoretical values (Fig. 5) of aperture admittance for the loaded waveguide radiator. Checks were made using Emerson and Cumming Stycast Hi-K with $\epsilon_r = 9.68$. The dielectric material was machined to fit into an x-band waveguide of dimensions .400 in. x.900 in. The waveguide was then mounted in a 2 ft. x 3 ft. ground plane which was mounted in a larger ground plane at one end of an anechoic chamber. Equipment used in the experiment is shown in Figs. 11 and 12. A sketch of the experimental arrangement in the anechoic chamber is shown in Fig. 13. Light absorbing pads were mounted around the 2 ft. x 3 ft. ground plane to simulate, as nearly as possible, an infinite ground plane.

A slot was machined in the dielectric to allow a probe to sample the field. Impedance was obtained by conventional slotted-line methods using an x-band slotted line and probe carriage. The geometry of the slotted dielectric insert is shown in Fig. 14. Because

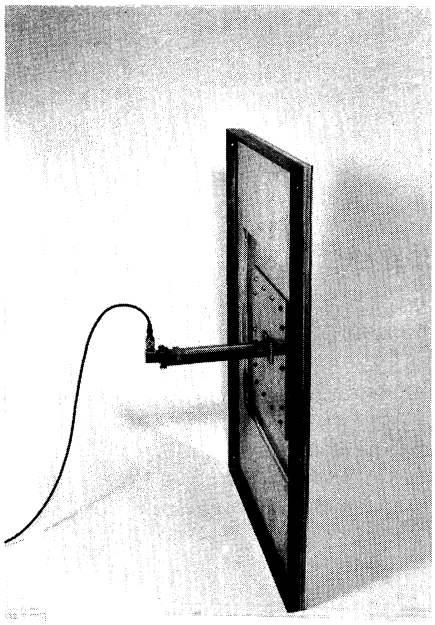

Fig. 11. Dielectric loaded waveguide radiator. (a) Side view.

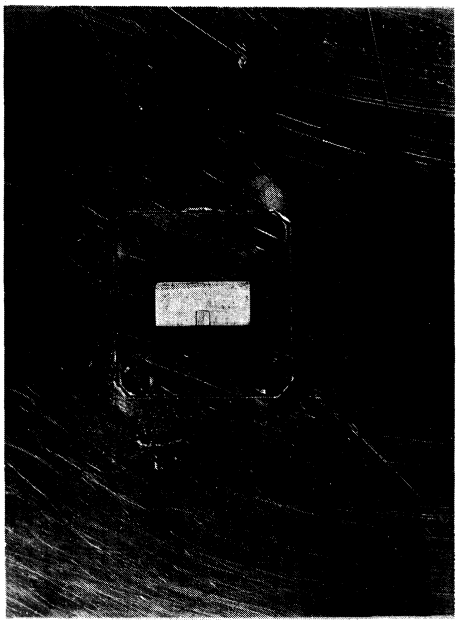

Fig. 11. Dielectric loaded waveguide radiator. (b) Front view.

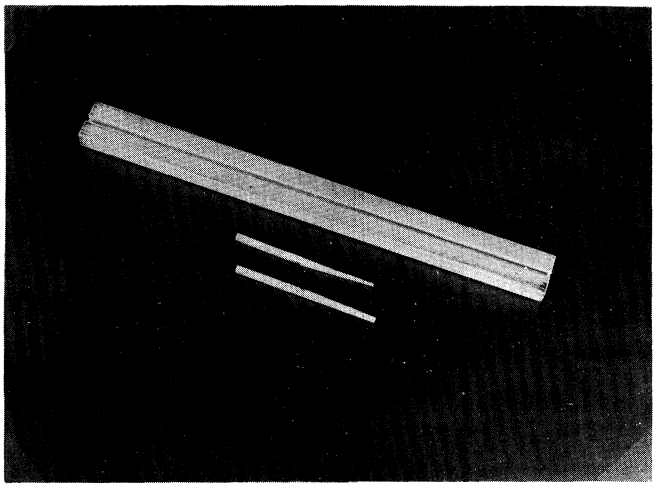

Fig. 12. Slotted dielectric and wedges.

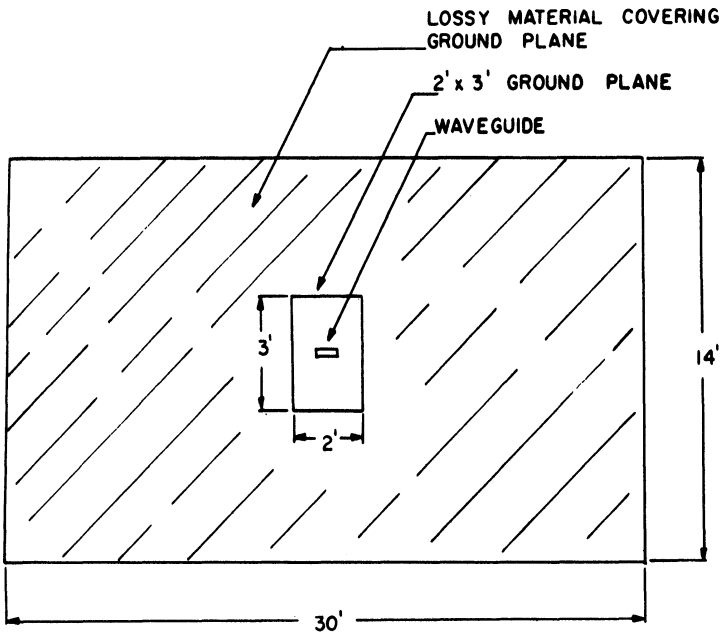

Fig. 13. Experimental arrangement.

of the slot, the geometry differs from the theoretical model. Tapered dielectric wedges (Fig. 12) were used in the slot to provide a measurement of the impedance of a geometry [Fig. 11(b)] more nearly corresponding to that of the theoretical calculations. Impedance was measured both with and without the wedges inserted. The tapered wedge constitutes a gradual transition from the rectangular dielectric cross section to the slotted dielectric cross section. The length of the taper is 1-1/2 in., or about a wavelength at $F_N = 1.5$. The effect of the taper section on the impedance measurement, which depends on the shunt susceptance at the ends of the taper and the transformation through the nonuniform taper section, is not precisely known. However, the admittance is uniquely determined by the value of the VSWR and the angle of the reflection coefficient. The taper introduces little reflection at frequencies where the taper length is appreciable compared to the guide wavelength. Near cutoff, the reflection introduced by the taper may become significant. At frequencies slightly above cutoff, the VSWR should correspond to that of the theoretical model. Similarly, the measured angle of the reflection coefficient depends only on the electrical length of the taper, if shunt susceptance at the ends of the taper is ignored. The electrical length of the taper is taken into account by a measurement of minimum position with a short on the waveguide.

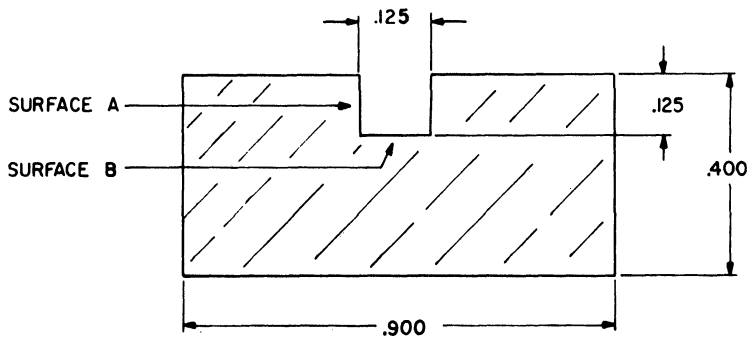

Fig. 14. Geometry of the dielectric insert.

Thus, the data with wedge represents a measurement of the admittance of a geometry identical to the theoretical model, with some inaccuracy expected near cutoff because of shunt susceptance and reflection introduced by the taper. The data without wedge represents a measurement of the admittance of a geometry differing from the theoretical model, with accuracy expected over the entire range of frequencies tested.

The presence of the slot in the dielectric modifies the cutoff wavelength as well as the equivalent circuit of the discontinuity. Unfortunately, the effect of the slot cannot be taken into account by perturbation formulas. The boundary conditions on E_x at the sides of the slot (surface A of Fig. 14) require continuity of E_x, while the boundary conditions at the bottom of the slot (surface B of Fig. 19) require continuity of $\epsilon\ E_x$. According to perturbation formulas, these two conditions would tend to change λ_g in different directions. However, we know that guide wavelength has approximately the form:

$$\lambda_g = \frac{\lambda_o}{\sqrt{\epsilon_{eff}}} \quad \frac{1}{\sqrt{1 - (f_c/f)^2}}$$

where

ϵ_{eff} = effective dielectric constant of the dielectric-guide and air-slot configuration. Two measurements of guide wavelength determine the two unknowns ϵ_{eff} and f_c.

Let

$$\left(\frac{\lambda_{01}}{\lambda_{g1}}\right)^2 \Bigg/ \left(\frac{\lambda_{02}}{\lambda_{g2}}\right)^2 = A \qquad (6.1)$$

Then

$$f_c = \frac{1 - A}{\frac{1}{f_1^2} - \frac{A}{f_2^2}} \tag{6.2}$$

Using this method, f_c was calculated using several measurements of guide wavelength and averaging the resultant values of f_c. This value of f_c was used in plotting the data without wedges. The cutoff frequency of the guide when completely loaded was used in plotting the data with the wedges. This cutoff frequency depends only on ϵ_r. ϵ_r was measured by completely filling the slotted line with dielectric material and measuring λ_g in the cutoff region bounded by the dielectric and the tapered metal slot of the slotted line.

In order to obtain accurate measurements of VSWR, a dial gauge was attached to the probe carriage and the double-minimum method was used. This improved the accuracy of the measurement of G somewhat, although the correction to G due to attenuation in the dielectric was as high as 50 percent in some cases. As a result, the G data are somewhat less accurate than the B data.

Results are shown in Fig. 15. The data with wedge agrees within a few percent with the theoretical data over most of the range of the data, with considerable divergence near cutoff as expected.

Experimental measurements of the aperture admittance of a loaded waveguide radiator with an iris in the aperture plane were made. $\epsilon_r = 3.9$ was used as the dielectric material. Figure 16 shows the experimental arrangement. All measurements were made with wedges. Figure 17 shows the results. Theoretical values were determined using the formulas of Chapter 3 and using The Waveguide Handbook[40] to determine the susceptance of the inductive and capacitive irises in an infinite waveguide. The experimental results of this section indicate accuracies comparable to those obtained in variational calculations for interior problems.

6.2 Measurements of Aperture Field

Measurements of the aperture field of a rectangular waveguide mounted in a ground plane were made for two different feed arrangements and both air and ferrite powder

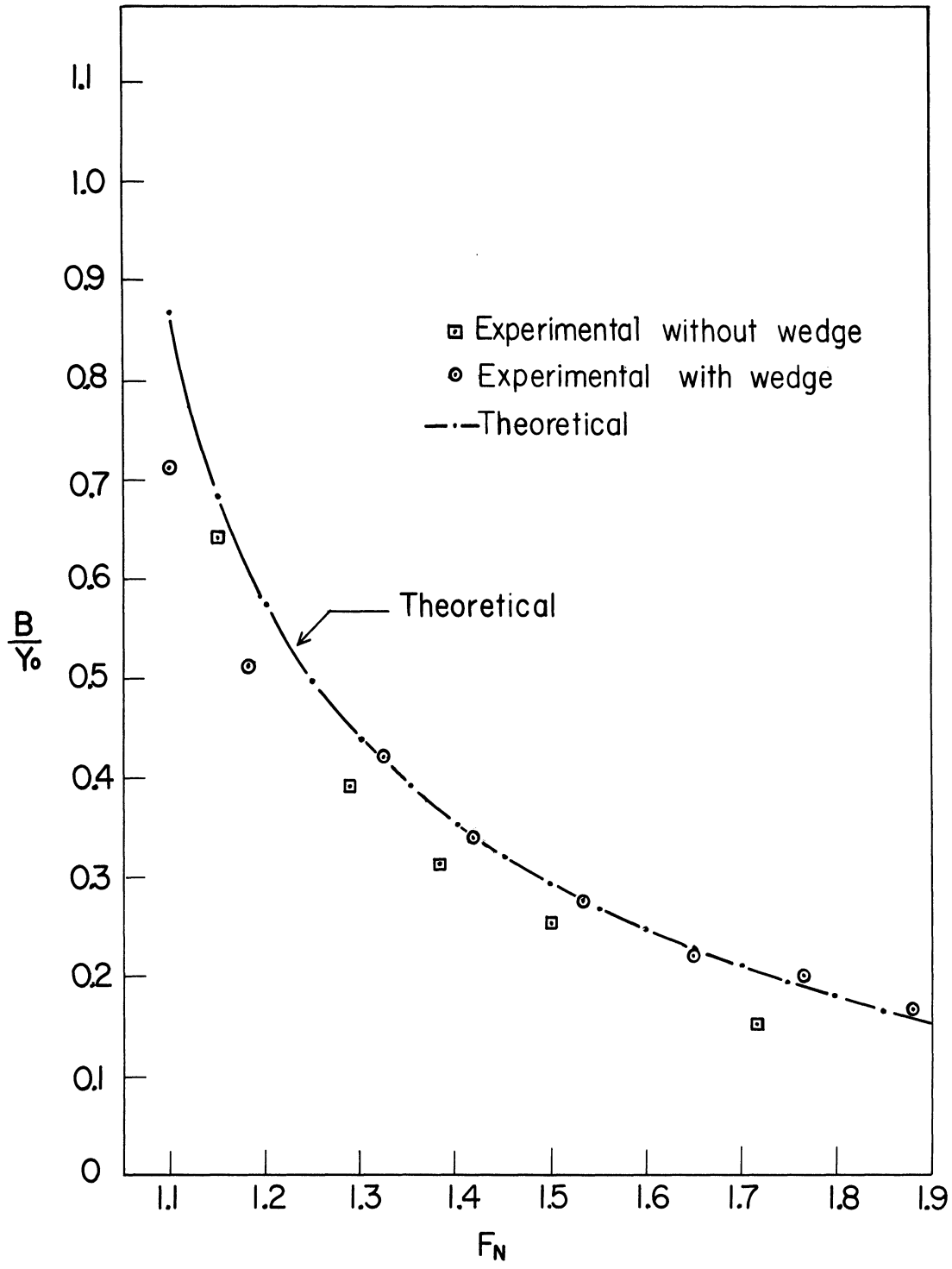

Fig. 15. Comparison of theoretical and experimental data for the loaded rectangular waveguide radiator.
(a) Susceptance - $\epsilon_r = 10$, $\mu_r = 1.0$, b/a = .444.

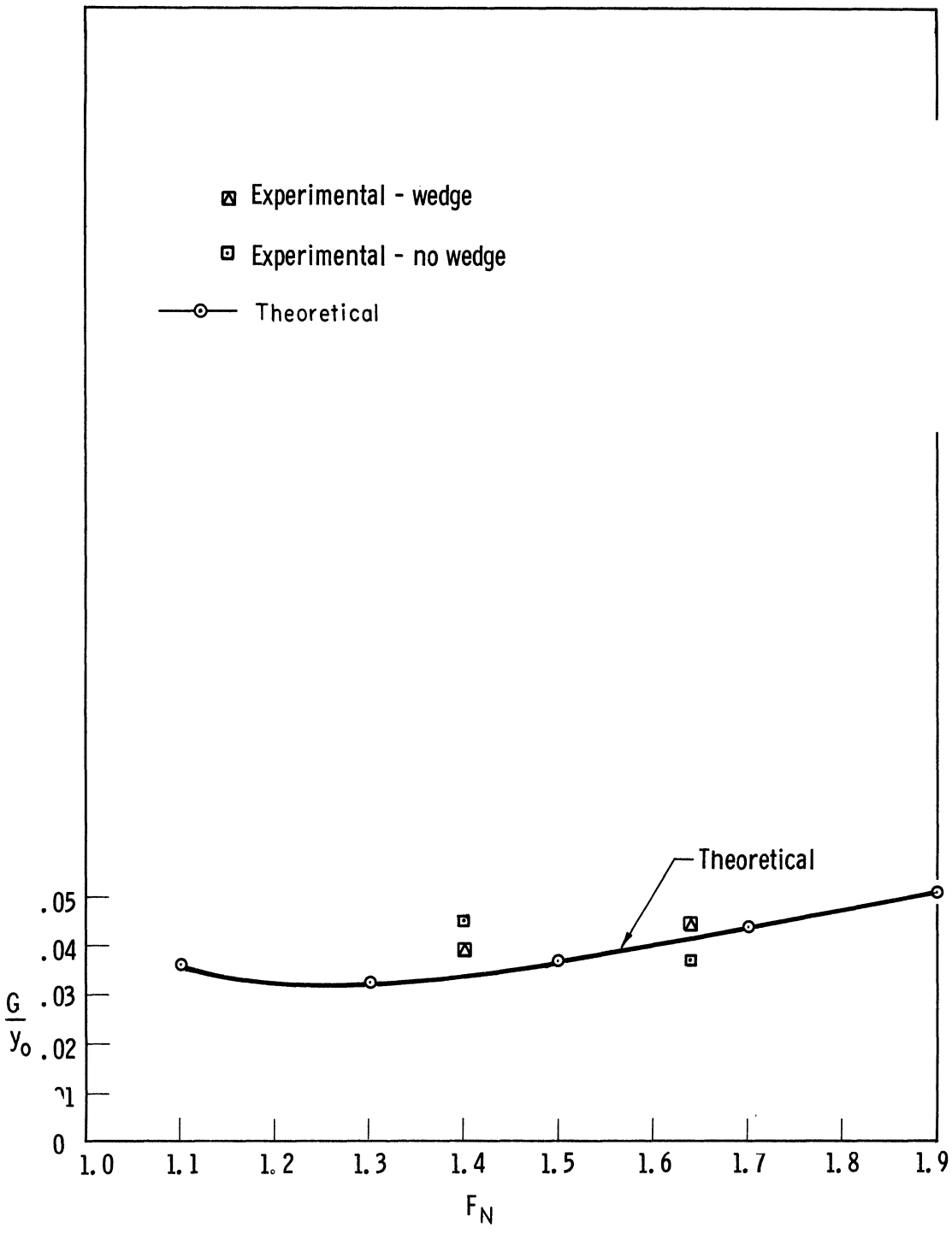

Fig. 15. Comparison of theoretical and experimental data for the loaded rectangular waveguide radiator.
(b) Conductance - $\epsilon_r = 10$, $\mu_r = 1.0$, b/a = .444.

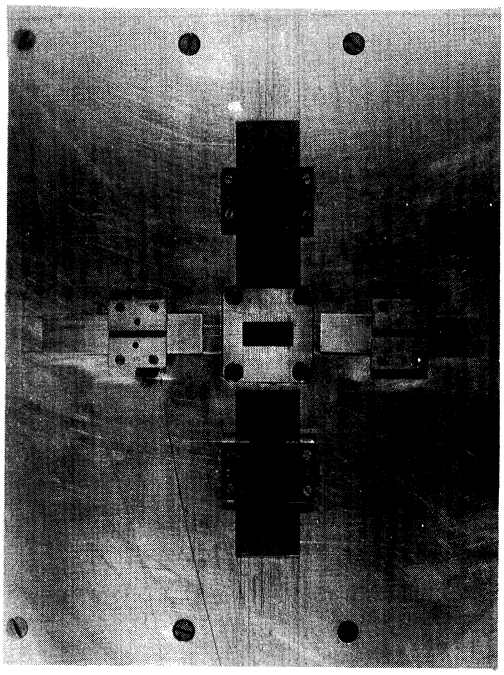

Fig. 16. Apparatus for measurement of the admittance of a loaded waveguide with a compound iris in the aperture plane.

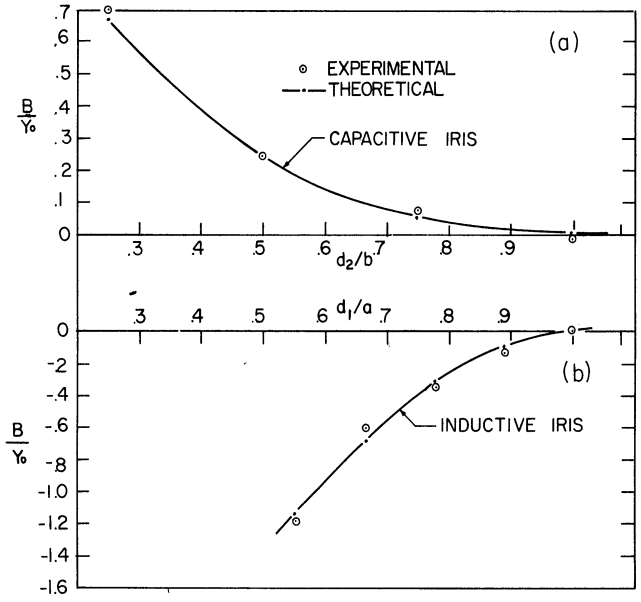

Fig. 17. Comparison of theoretical and experimental data for the loaded rectangular waveguide radiator with a capacitive or inductive iris in the paerture plane.

loading. The magnetic field H_z normal to the aperture plane was measured, using a shielded loop fed by a miniature rigid coaxial cable. The coaxial cable lies along the ground plane and is perpendicular to the electric field in the aperture. A two dimensional positioning apparatus with micrometer drive was used to position the probe in the aperture.

The complete field cannot be determined from H_z but the measurements give us some idea of the mode configuration. All of the TE modes could be determined from H_z measurements.

The size of the rectangular aperture was 12 in. x 13 in. The waveguide was 4 in. deep and was fed either by a cylindrical probe or a T-bar each located about 2-1/2 in. from the aperture. Figure 18 shows the coordinate system used and the actual cuts taken. Figure 19 shows the measurement system. The waveguide was mounted in a 3 ft. x 3 ft. ground plane. Measurements of ground plane currents indicated rapid decay away from the aperture and thus justified the use of a finite ground plane.

Figures 20(a) and (b) show the results. The fields are, in general, very similar to those that would result from a single dominant mode wave, although the presence of some $\sin \frac{3\pi y}{a}$ component is indicated by the steepness of the horizontal curve near $x = 0$ and the presence of some $\cos \frac{2\pi x}{b}$ component is indicated by the depression of the vertical curves near the center of the waveguide. There is not much difference between the cylindrical probe and T-bar feed arrangements. The T-bar horizontal measurements are more symmetric; this is reasonable since the T-bar is fixed but the probe may tend to slant. This same reason explains the unequal peaks in the horizontal cylindrical probe measurements. In the vertical measurements, there is little difference between the probe and T-bar feeds.

The deviations from dominant mode fields appear to be greater for the air loaded than for the material loaded case.

All of the curves fall rapidly at positions close to the waveguide walls. This is caused by the finite size of the loop. The average magnetic field threading the loop is measured rather than the magnetic field exactly at the coordinates. Thus, the power received by the antenna starts decreasing as soon as any part of the loop passes outside the aperture. The loop diameter is approximately 1/2 in.

Measurements were also made of the aperture field of an x-band (. 400 in. x . 900

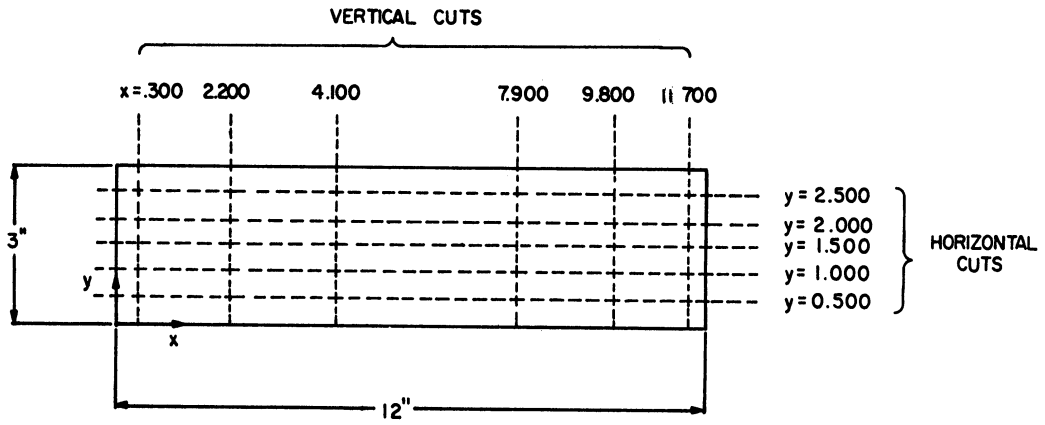

Fig. 18. Aperture coordinates for measurement of aperture field.

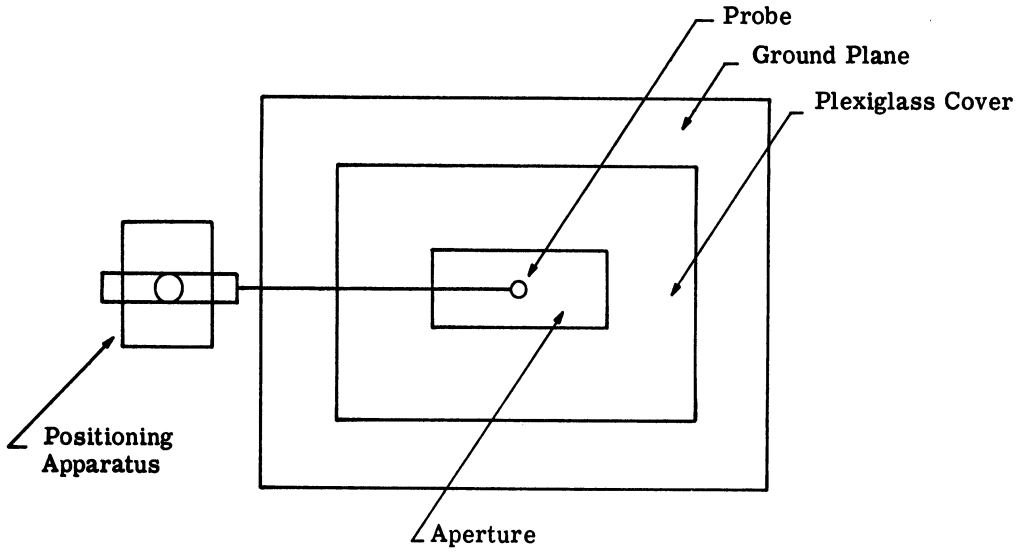

Fig. 19. Apparatus for measurement of aperture field.

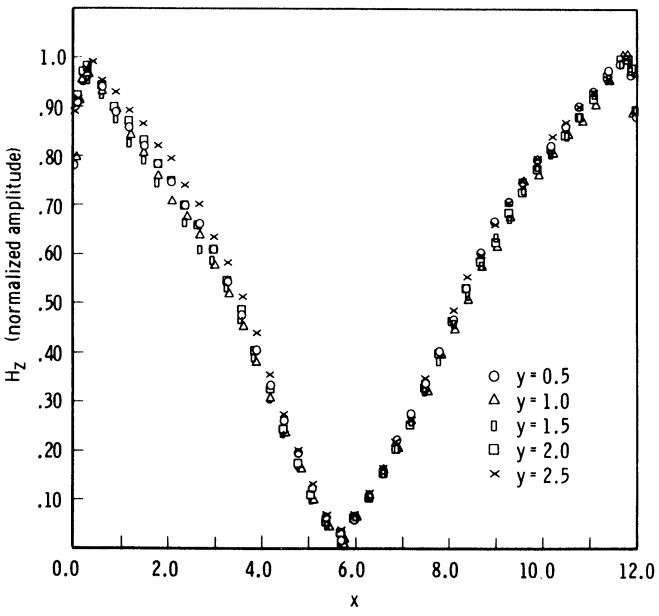

Fig. 20. Measurement of aperture field.

(a) T-bar feed - horizontal cuts, frequency - 324 Mcs (ferrite powder loaded).

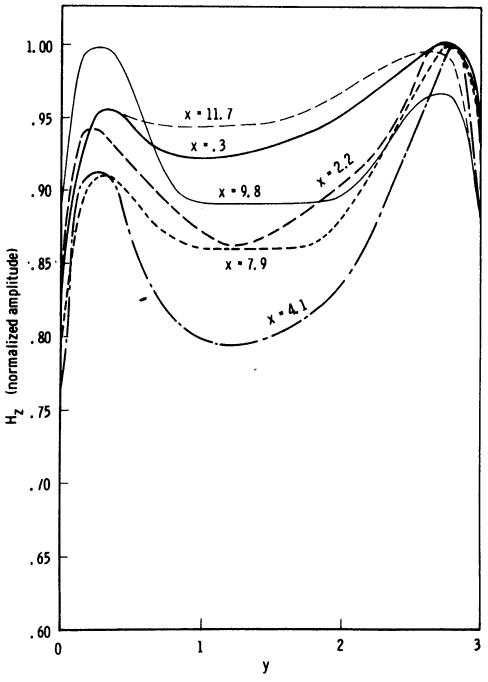

Fig. 20. Measurement of aperture field.

(b) T-bar feed - vertical cuts, frequency - 324 Mcs (ferrite powder loaded).

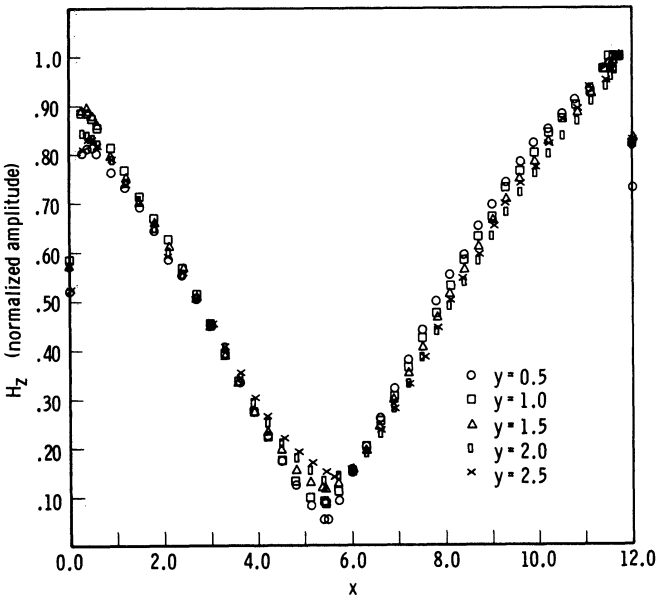

Fig. 20. Measurement of aperture field.

(c) Cylindrical probe feed - horizontal cuts, frequency - 324 Mcs (ferrite powder loaded).

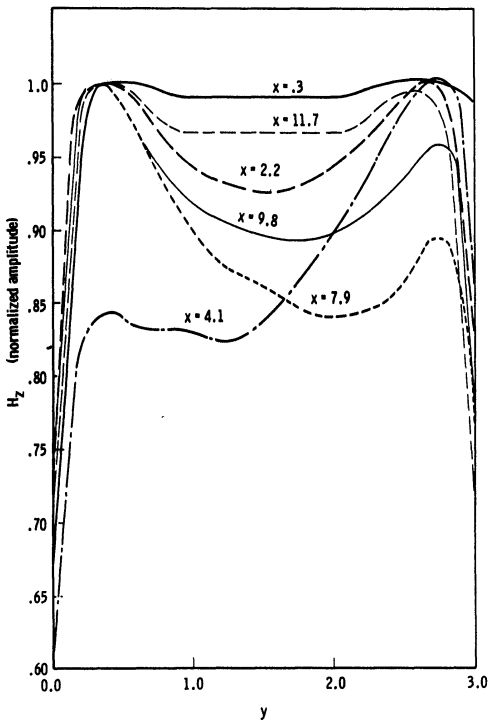

Fig. 20. Measurement of aperture field.

(d) Cylindrical probe feed - vertical cuts, frequency - 324 Mcs (ferrite powder loaded).

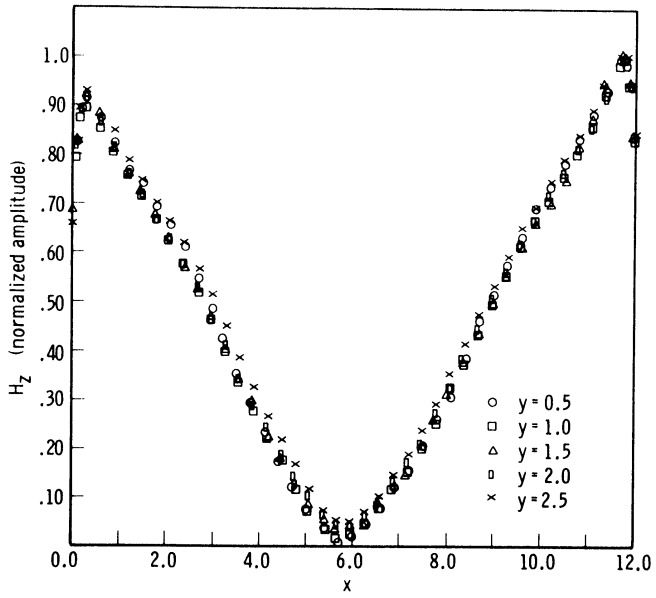

Fig. 20. Measurement of aperture field.

(e) Cylindrical probe feed - horizontal cuts, frequency - 735 Mcs (air loaded).

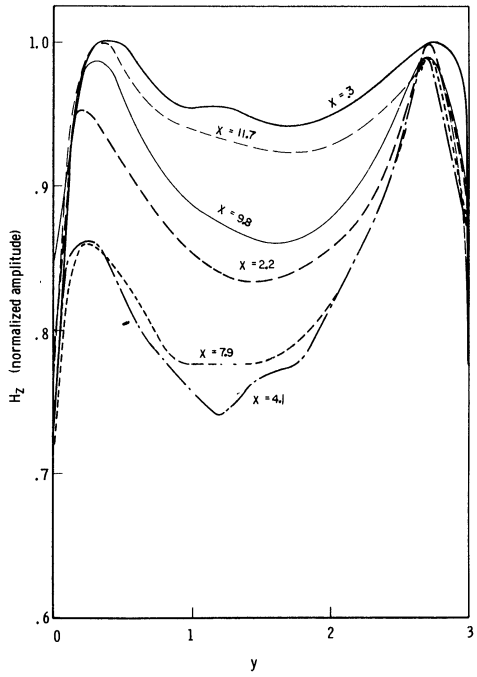

Fig. 20. Measurement of aperture field.

(f) Cylindrical probe feed - vertical cuts, frequency - 735 Mcs (air loaded).

in.) waveguide mounted in a ground plane and loaded with dielectric material (ϵ_r = 9.68, 12.18). Results were similar to those shown. Depression of the vertical curves was not noted because of the large size of the loop relative to the .400 in. dimension of the waveguide.

6.3 Experiments with Dielectric and Ferrite Loaded Cavity Slot Antennas

6.3.1 Introduction. A number of rectangular cavity slot antennas were constructed, using powdered ferrite, solid ferrite, and solid dielectric material. Experimental measurements of resonant frequency, efficiency bandwidth and beam pattern were performed and compared with theoretical predictions. Figure 21 shows three of these models, all operating at roughly the same frequency. Table No. 2 indicates the characteristics of these antennas, showing the size and weight reduction accomplished through the use of material loading as well as the price paid in terms of reduced bandwidth and efficiency.

	Size	Volume	Bandwidth With Flange		Bandwidth - No Flange		Efficiency	Directivity	Weight	Operating Frequency
			VSWR = 3.0	VSWR = 6.0	VSWR = 3.0	VSWR = 6.0				
Air Loaded Antenna	30" x 7½" x 10"	2250 cu. in.			64 Mc	90 Mc	90 %	5.8	25-3/4 pounds	300
Ferrite Powder Loaded Antenna	12" x 3" x 9"	144 cu. in.	22 Mc	50 Mc	20 Mc	36 Mc	65 %	5.0	16-3/4 pounds	320
Solid Ferrite Loaded Antenna	5" x 2" x 1½"	15 cu. in.	19 Mc	34 Mc	19 Mc	32 Mc	30 %	5.0	3.6 pounds	352

Table 2. Performance comparison of rectangular cavity-slot antennas.

Later sections of this chapter describe methods of predicting antenna characteristics using the basic variational data, each section being devoted to a single characteristic. Comparisons are made between theory and experiment. The characteristic of the materials used are shown in Table 3. The characteristics of the solid ferrite material was measured by the manufacturer using disk samples and standard slotted line measurement techniques. The listed characteristics of these measurements were also checked at The University of Michigan Solid State Laboratory. The listed characteristics of the dielectric are also those of the manufacturer. The characteristics of the ferrite powder have been approximately

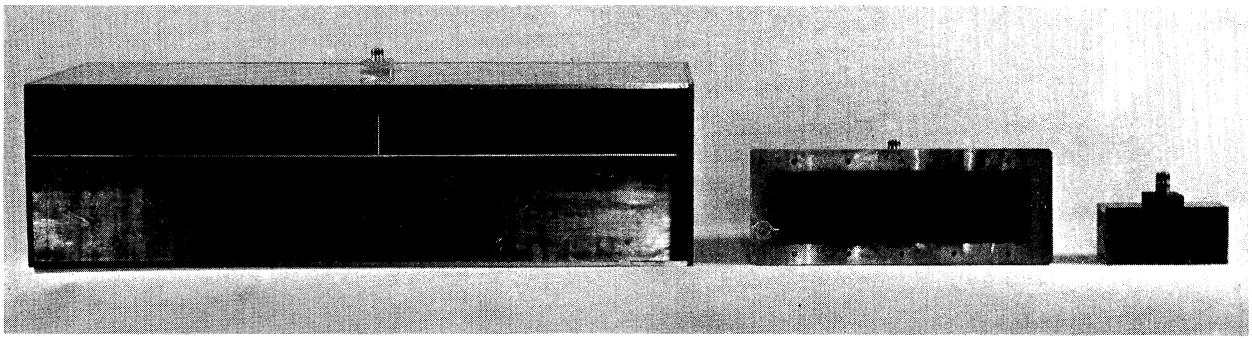

Fig. 21. Loaded cavity antennas.

Ferrite Powder $\mu'\epsilon' = 8.3$ $\mu' \approx 2.2$ $Q = \mu'/\mu'' = 30$ at 300 Mc
Solid Ferrite $\mu' = 6.63$ $\epsilon' = 12.6$ $Q = \mu'/\mu'' = 30$ at 300 Mc
Solid Dielectric $\epsilon' = 10$ $Q = \epsilon'/\epsilon''$, $Q > 1000$

Table 3. Characteristics of ferrite and dielectric material.

The $\mu_r\epsilon_r$ product was measured by loading a slotted slab line with ferrite powder material and measuring the distance between minimum positions in the air directly above the powder. The relative permeability was measured by standard techniques, but

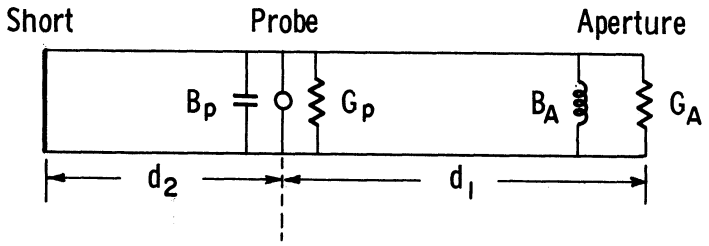

Transforming to the aperture:

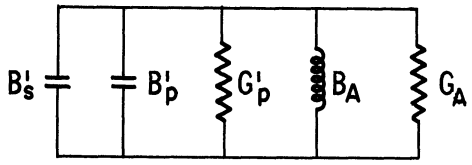

B'_s = Admittance of short

At resonance:

$$G'_p = G_A$$

$$B'_s + B'_p + B_A = 0$$

Fig. 22. Simplified equivalent circuit of a cavity slot antenna.

since the thickness of the sample could not be determined accurately, the data must be regarded as approximate.

6.3.2 Resonant Frequency. Utilizing the variational data and a simplified equivalent circuit (Fig. 22), it is possible to predict very accurately the resonant frequency of a ferrite material loaded rectangular cavity slot antenna. The resonant frequency, or the frequency at which the input reflection coefficient is minimum, is calculated simply by calculating the frequency at which the short susceptance transformed to the aperture plane (B'_s) is the negative of the aperture susceptance (B_A). The probe admittance is taken into account by perturbation calculations (Appendix C).

The short position required for resonance at a given frequency is calculated simply by reading off a Smith chart, the electrical distance (d_{res}/λ_g) from the complex conjugate of the aperture admittance to a short circuit. Similarly, for a given length, the frequency of resonance can be calculated either by trial and error, or by noting the frequency

at which the curves for d_{res}/λ_g and d_{act}/λ_g cross, where d_{act}/λ_g is defined as the actual electrical length of the cavity. Two examples are shown below:

Example 1--Solid dielectric loaded cavity

$$\mu_r = 1 \qquad \epsilon_r = 10$$

$$b = 3 \text{ in.}$$

$$a = 11\text{-}3/4 \text{ in.}$$

$$d = 3\text{-}3/4 \text{ in.}$$

$$\text{cutoff frequency} = 159 \text{ Mcs}$$

From computed data:

F_N	B/Y_o	G/Y_o	d_{res}/λ_g
1.95	-.125	.0279	.2700
2.00	-.115	.0290	.2685

By trial and error the frequency at which d is the proper length for resonance is 313 Mcs. At 313 Mcs:

$$\lambda_g = 35.35 \text{ cm} \qquad d = .2695\ \lambda_g$$

Perturbation correction: (Appendix C)

$$\text{Probe size} = 1/4 \text{ in. radius x } 1 \text{ in. length}$$

$$= .049 \text{ cu. in.}$$

$$abd = 132 \text{ cu. in.}$$

$$\frac{\omega-\omega_o}{\omega_o} = 2.43 \times 10^{-4}$$

The predicted resonant frequency is 313 Mcs. The actual resonant frequency is 316 Mcs. The error for this example is less than 1 percent.

Example 2--Solid ferrite loaded cavity

$$\mu_r = 6.63 \qquad \epsilon_r = 12.6$$

$$b = 2 \text{ in.}$$

$$a = 5 \text{ in.}$$

$$d = 1\text{-}1/2 \text{ in.}$$

$$\text{cutoff frequency} = 129.5 \text{ Mcs}$$

Interpolating from the data of Fig. 9:

F_N	G/Y_o	B/Y_o	d_{res}/λ_g	d_{act}/λ_g
2.6	$\approx .025$	-1.111	.384	.361
2.8	$\approx .025$	-1.011	.376	.392

Curves for d_{res}/λ_g and d_{act}/λ_g cross at $F_N = 2.715 \longrightarrow 351$ Mcs

Perturbation Correction:

$$\text{Probe size} = 1/4 \text{ in. radius x } 9/16 \text{ in. length}$$

$$= .0276 \text{ cu. in.}$$

$$\text{Size of Teflon plug below probe} = 1/4 \text{ in. radius x } 1\text{-}7/16 \text{ in. length}$$

$$= .0705 \text{ cu. in.}$$

$$\frac{\Delta\epsilon}{\epsilon} = -.794$$

$$abd = 15 \text{ cu. in.}$$

$$\frac{\omega - \omega_o}{\omega_o} = +.213\%$$

Predicted resonant frequency is 351.7 Mcs. Actual resonant frequency is 347 Mcs. The error for this example is 1.4 percent. It is interesting to note that the variational data are

valid at $F_N = 2.6$, which is well above cutoff frequency for the (2,0) mode.

The accuracy of these calculations suggests a new method of measuring dielectric constant, namely completely loading a rectangular cavity which is open on one end and utilizing variational data and a measurement of resonant frequency to determine dielectric constant. This method could also be used to determine either μ_r or ϵ_r if one were known.

Some of the advantages of this method would be:

1. The resonance is sharp, especially for electrically small cavities.

2. Measurement would not depend critically on wall losses; movable walls could be used for different size samples.

3. Sample preparation would involve only drilling a cylindrical hole in a rectangular block.

The theoretical data on admittance and perturbation effects could be refined further, using more accurate calculations and more extensive higher order mode data. Accuracies on the order of 1 percent or better for the determination of dielectric constant should be obtainable.

6.3.3 Bandwidth. For purposes of bandwidth calculation, several assumptions are made concerning the equivalent circuit of Fig. 22.

1. $B_p = 0$. The probe introduces no reactance into the cavity and does not, therefore, affect the bandwidth or efficiency of the antenna. The reactance of the probe is taken into account by perturbation calculations in the prediction of resonant frequency.

2. $G'_p = G_A$. The probe conductance is taken into account by assuming that, over the frequency range of operation, the probe conductance, when transformed by transmission line transformations to the aperture, is equal to the aperture conductance.

3. The use of transmission line calculations involves the assumption that higher order modes can be neglected. There are two sources of higher order modes in the cavity, namely, the probe and the aperture. In some cases, the distance from probe to aperture or probe to short is small in terms of guide wavelength, on the order of $\lambda_g/8$. The equivalent circuit calculations and transformations are theoretically valid only if all obstacles, and the point of observation of the impedance, are all separated by large distances.

The bandwidth is calculated using simple Smith chart techniques. Referring to Fig. 22, since $G'_p = G_A$, the total real part of the admittance at the aperture is $2G_A$. The

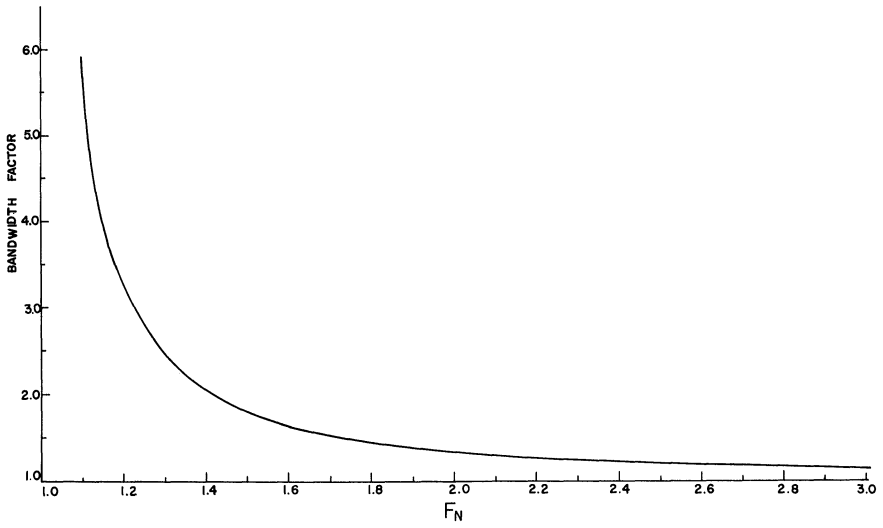

Fig. 23. Bandwidth factor.

total susceptance at the aperture ($B'_s + B_A$) is zero at resonance. The half power points, then, occur when $B'_s + B_A = 2G_A$. The behavior with frequency of B'_s and B_A is known. As the frequency moves off resonance, the change of B'_s with frequency can be calculated by transforming the short to the aperture. The behavior of B_A with frequency is known from the basic variational data (Fig. 5). Thus, the half power bandwidth can be calculated by trial and error. A single trial and linear correction were found to be accurate. The single trial might consist, for instance, of assuming that the changes in B_A and B'_p were equal, calculating the frequency at which the change in B'_p is equal to G_A, and then finding B_A from the variational data.

It should be noted that it is necessary to use a bandwidth conversion factor in the trial and error process to convert from a percentage change in λ_g to a percentage change in frequency. This bandwidth ratio is equal to:

$$\frac{1}{\lambda_g}\frac{d\lambda_g}{df} \Big/ \frac{1}{\lambda_o}\frac{d\lambda_o}{df} ,$$

which reduces to $F_N^2/F_N^2 - 1$. This bandwidth ratio is plotted in Fig. 23. It would be possible, of course, to transform all the admittances to the probe position and to assume that G_p was

constant, and to use the off resonance values of G_A rather than the value at resonance. It was found that this did not make an appreciable difference in the results.

The efficiency, of course, effects the bandwidth. This can be taken into account by assuming an additional lumped conductance at the aperture. This new conductance G_e will be equal to $G_A(P_L/P_R)$ where P_L/P_R is determined from efficiency calculations as described in the next section. The effect of this additional conductance will be to increase the bandwidth by the factor (1/efficiency).

Table 4 compares theoretical and experimental bandwidth data.

RESONANT FREQUENCY

	Theoretical	Experimental
Solid Dielectric Cavity	313 Mc	316 Mc
Solid Ferrite Cavity	351.7 Mc	347 Mc

Maximum Error = 1.3 %

HALF-POWER BANDWIDTH

	Frequency (Mc)	Theoretical	Experimental
Solid Dielectric Cavity	316	4.9 %	5.7 %
Solid Ferrite Cavity	352	8.0%	9.7 %
Powder Ferrite Cavity	320	12.6 %	15.6 %

Maximum Error = 19 %

EFFICIENCY

	Frequency (Mc)	Theoretical	Experimental	Experimental Method
Powder Ferrite Cavity	315	62.6%	66.5 %	R.T. + G.C.
Solid Ferrite Cavity	352	21 %	30.0 % *	G.C.

Table 4. Comparison of theoretical and experimental data.

*Only an approximate efficiency measurement was obtainable.

R.T. - Reflection techniques.

G.C. - Gain comparison.

6.3.4 Efficiency. A method of efficiency calculation is outlined in Appendix B. This method assumes a dominant mode only in the cavity, and utilizes the aperture admittance data and the material constants to calculate the efficiency. The analysis for one of the simpler cases (probe near aperture, low losses, magnetic losses only), was used and theoretical data for efficiency were calculated and compared with experimental results.

From Appendix B (Section B.3, Eq. B.28)

Magnetic volume losses only:

$$\text{Efficiency} = \frac{1}{1 + \frac{P_L}{P_R}}$$

$$\frac{P_L}{P_R} = \frac{\frac{\mu''}{\mu'}\left[k^2a^2\left(\frac{2d}{a}\right) + \frac{(k^2a^2 - 2\pi^2)\sin 2\beta_{10}d}{\sqrt{k^2a^2 - \pi^2}}\right]}{(1 - |R|^2)\sqrt{k^2a^2 - \pi^2}} \qquad (6.3)$$

where

d = length of cavity

R = complex aperture reflection coefficient

$$\beta_{10} = \frac{\sqrt{k^2a^2 - \pi^2}}{a}$$

Using the above formula, theoretical efficiency data was calculated for several cases. d was calculated using theoretical aperture admittance data. An example of efficiency calculation is shown below.

Example No. 1 - Efficiency of the powder ferrite loaded cavity antenna shown in Fig. 21.

$\mu_r\epsilon_r = 8.3$ $\mu_r = 2.2$ $\mu''/\mu' = .0290$

b = 3 in.

a = 11.75 in.

Frequency = 315 Mcs
Cutoff Frequency = 174.5 Mcs

$F_N = 1.805 = ka/\pi$

Interpolating from the data of Fig. 5:

$$\frac{B}{Y_o} = -.268 \qquad \frac{G}{Y_o} = .0746$$

$$1 - |R|^2 = .244$$

From a Smith chart plot of B/Y_o and G/Y_o:

$$2\beta_{10} d = 210^o$$

$$d/a = .388$$

$$P_L/P_r = .595$$

Efficiency = 62.6 percent

The measured efficiency was 66.5 percent. The measurements are described below.

Efficiency Measurements:

The efficiency of the ferrite powder loaded antenna shown in Fig. 21 was measured using reflection techniques.[70-72] The method is analogous to that described by Deschamps[73] for transmission-line components.

In the transmission-line method, the sample to be evaluated is placed in a transmission line. As a short circuit is moved on the output end, the impedance is measured on the input end. The locus of the impedance values is a circle on the Smith chart and is thus determined by three points. The efficiency is determined by four measurements, i.e., the three measurements using a short to determine the Smith chart circle and a measurement of impedance with the output terminated in its characteristic impedance.

Similarly, in the application of this method to antennas, the short circuit consists of a metal enclosure which reflects all of the energy back toward the input. In this method, at least three different sizes of enclosures are required to determine the circle on the Smith chart.

The tests described were made in an anechoic chamber. A flange was mounted on the rectangular cavity slot antenna and the flange was mounted in a large ground plane at

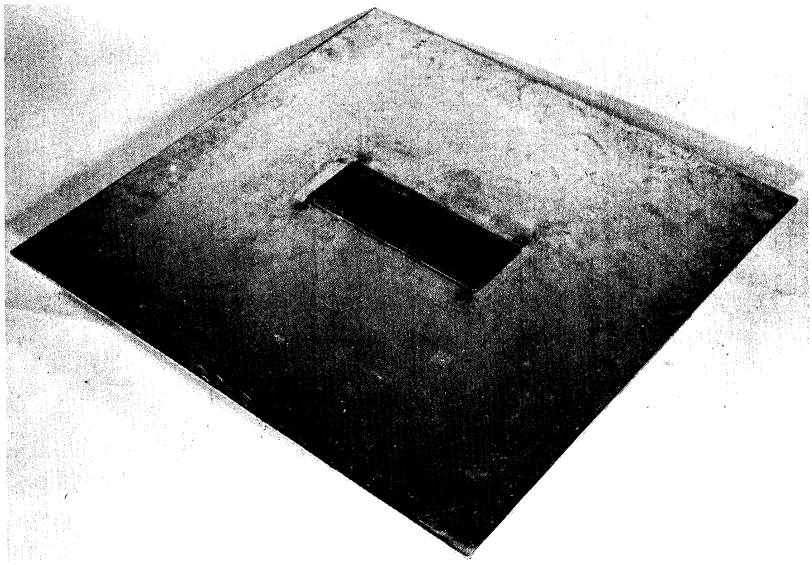

Fig. 24. Equipment for efficiency measurements.
(a) Antenna and flange.

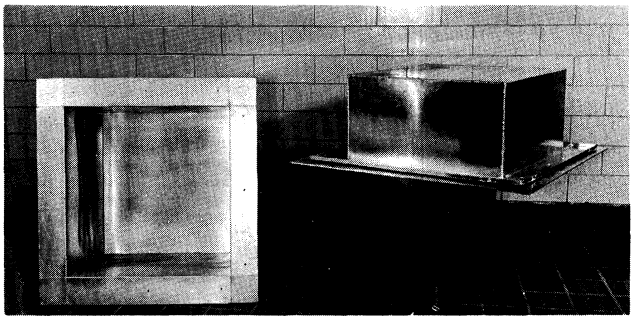

Fig. 24. Equipment for efficiency measurements.
(b) Aluminum "hats".

one end of the anechoic chamber. Four aluminum "hats" of different sizes were alternately placed over the aperture and bolted to the flange. The antenna, flange, and "hats" are shown in Fig. 24(a) and (b).

The Smith chart plot of efficiency is shown in Fig. 25. The figure shows efficiency calculated directly from the data and a corrected efficiency, which takes cable loss into account. The efficiency, as defined in Ref. 70 is equal to

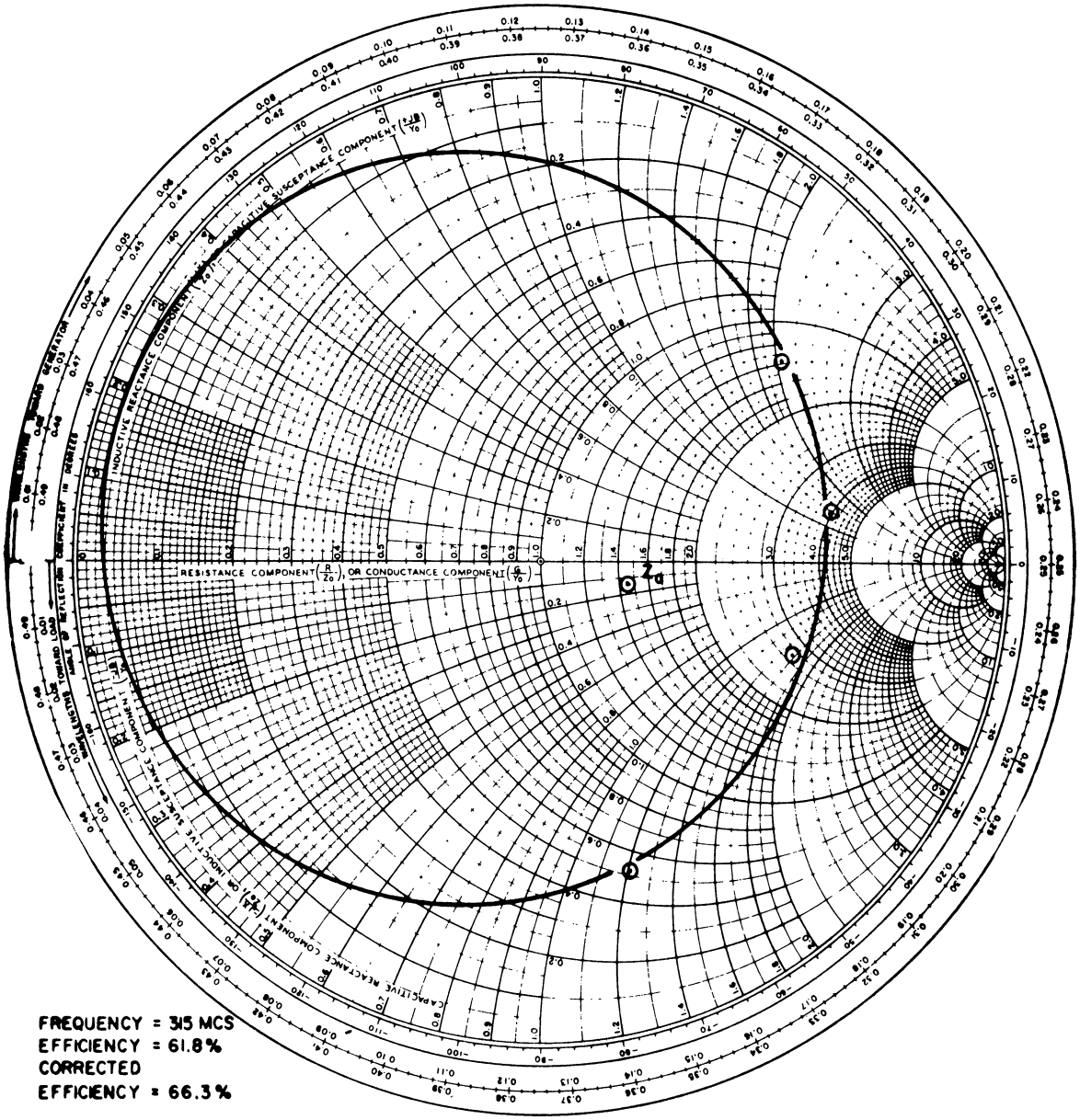

Fig. 25. Efficiency of the ferrite powder loaded cavity antenna shown in Fig. 21.

$$\frac{2D_1D_2}{(D_1 + D_2)(1 - D_3^2/R^2)}$$

where

D_1 = longest distance from Z_a to the edge of the circle.

D_2 = shortest distance from Z_a to the edge of the circle.

D_3 = distance from Z_a to center of the Smith chart.

R = radius of the Smith chart.

Z_a = impedance of the antenna in free space with an infinite ground plane.

For the measurement of Z_a, light lossy pads were placed on the ground plane and a large (10 ft. x 10 ft.) array of lossy pyramids was placed in front of the antenna in order to reduce reflections as much as possible, thereby simulating an infinite ground plane.

This method of efficiency measurement is generally regarded as a reliable one. However, a few limitations should be mentioned. The analogy to transmission-line methods is strictly correct only if a single radiating mode is excited. This assumption is realistic for electrically-small antennas but would not be expected to hold for electrically-large antennas. The method has sometimes been justified by the fact that the data points do, as predicted, lie on a circle. This is not a proof of the accuracy of the method; even if a perfect circle occurs, the location of Z_a can significantly affect the result.

It was desirable to have some check of the results by another method. Accordingly, the gain of the ferrite loaded antenna was compared to the gain of a larger air loaded antenna (Fig. 21) at the same frequency. The directivity of each antenna was calculated approximately from the E and H plane patterns. Relative efficiency was calculated from the following formulas.

$$\begin{aligned} (\text{gain})_1 &= (\text{directivity})_1\,(\text{efficiency})_1 \\ (\text{gain})_2 &= (\text{directivity})_2\,(\text{efficiency})_2 \end{aligned} \qquad (6.5)$$

$$\frac{(\text{efficiency})_2}{(\text{efficiency})_1} = \frac{(\text{gain})_2\,(\text{directivity})_1}{(\text{gain})_1\,(\text{directivity})_2}$$

The result was a relative efficiency of about 75 percent, as compared with an absolute efficiency of 66.5 as measured by reflection techniques. This data indicates good agreement since the efficiency of an air loaded waveguide radiator should be on the order of 90 percent. There are many sources of error in the gain comparison method and, as a result, it can be regarded as only a rough check on the reflection techniques. Table 4 shows a comparison of theoretical and experimental efficiency data. It was not possible to obtain a measurement of efficiency by reflection techniques for the solid ferrite antenna of Fig. 21 because only a small part of the Smith chart circle was defined.

6.3.5 Beam Patterns. The far field beam patterns of a loaded rectangular waveguide opening out into an infinite ground plane were calculated, assuming dominant mode fields. Figure 26(a) shows the coordinate system used. The E plane and H plane patterns are:

E Plane ($\phi = \pi/2$)

$$|E_\theta|^2 = \left(\frac{2}{k_o b}\right)^2 \left[\frac{\sin\left(\frac{k_o b \sin\theta}{2}\right)}{\sin\theta}\right]^2 \tag{6.6}$$

H Plane ($\phi = 0$)

$$|E_\phi|^2 = \left[\frac{\pi^2 \cos\left(\frac{k_o a \sin\theta}{2}\right)\cos\theta}{[\pi^2 - (k_o a \sin\theta)^2]}\right]^2 \tag{6.7}$$

The fields are normalized so that the maximum squared magnitude is unity.

It is noted that the E plane pattern depends only on the free space electrical size of b and that the H plane pattern depends only on the free space electrical size of a.

Figures 26(b) and 26(c) are plots from a computer program for Eqs. 6.6 and 6.7 showing the theoretical E and H plane patterns as functions of, respectively, $k_o b$ and $k_o a$. As the size of the aperture becomes electrically small, the pattern approaches that of a magnetic dipole oriented parallel to the broad wall of the waveguide. This agrees with the image theory concepts used in Chapter 2. Figure 27 compares experimental beam patterns of a

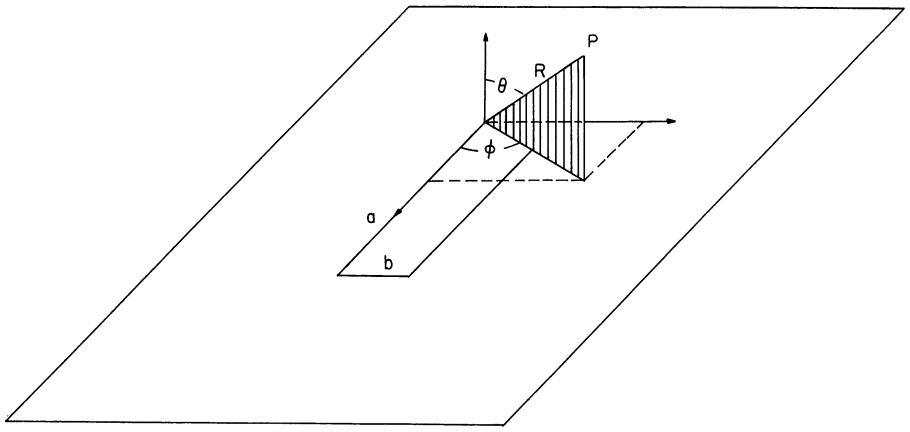

Fig. 26. Rectangular slot beam patterns.
(a) Coordinate system.

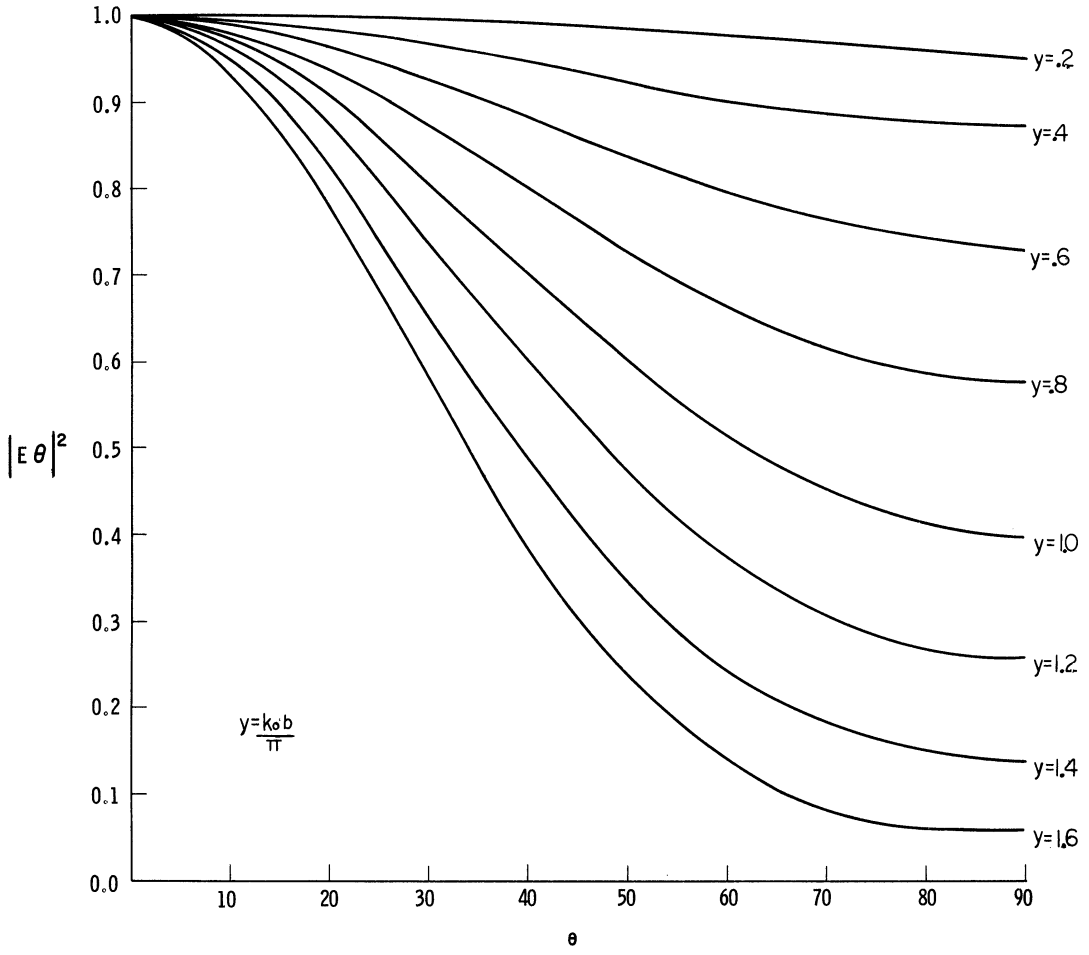

Fig. 26. Rectangular slot beam patterns.
(b) E plane pattern.

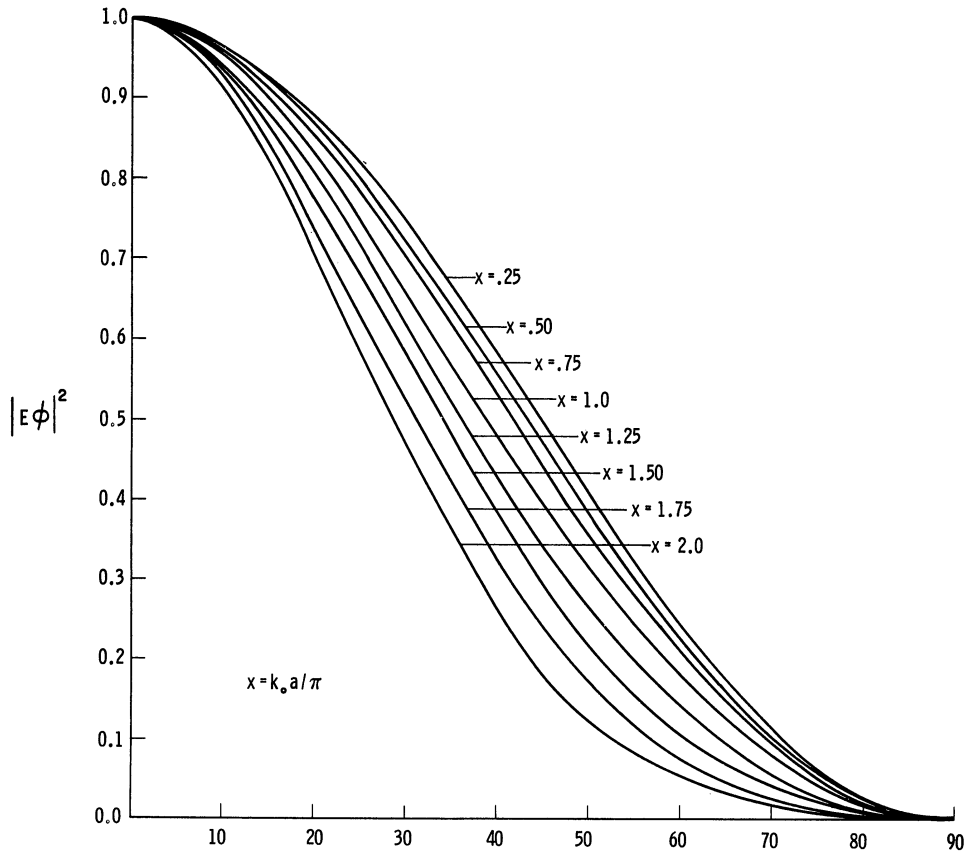

Fig. 26. Rectangular slot beam patterns.
(c) H plane pattern.

solid ferrite loaded rectangular cavity slot antenna mounted in a 3 ft. x 3 ft. ground plane with the corresponding theoretical patterns. Beam patterns are also shown for the same antenna without a flange. It is noted that the H plane patterns (with flange) show good agreement with the theoretical data, whereas the E plane patterns do not. These data show the same trends as that reported by Butson and Thompson[81] for electrically larger air loaded waveguide radiators with finite flanges. More accurate H plane results could probably be obtained using their approximate methods. It is noted further that the effect of physical asymmetries is more pronounced (note H plane pattern--no flange) for electrically small antennas without flanges than is the case either for small antennas with flanges or large antennas without flanges. These characteristics have been noted in other experiments by the author.

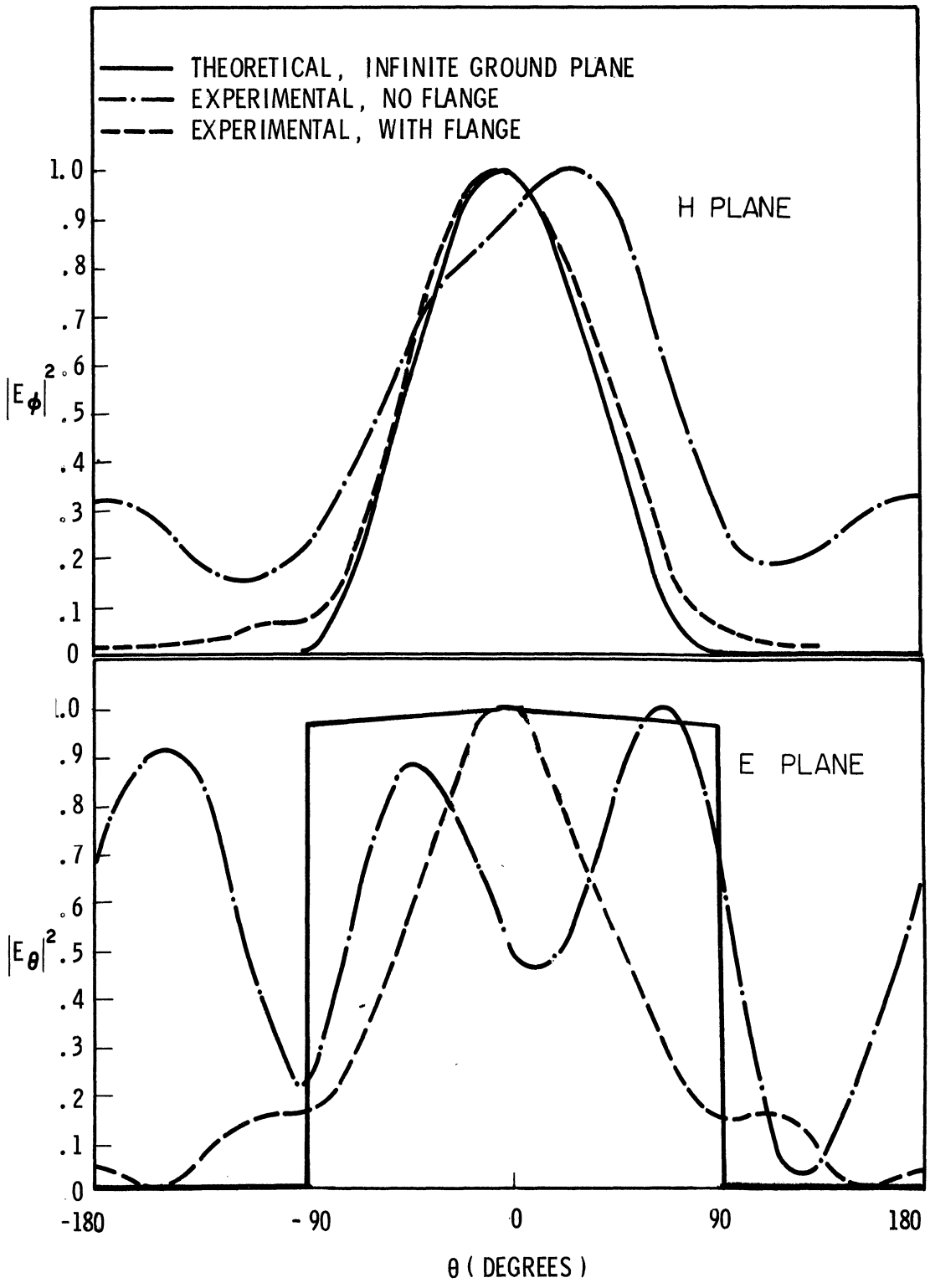

Fig. 27. Comparison of experimental and theoretical beam patterns.

6.3.6 Magnetically Tuned Antennas. Preliminary experimental data were obtained on the effects of magnetically tuning a ferrite loaded cavity antenna. The antenna size was 2" by 5" by $2\frac{1}{2}$" (same as the small antenna of figure--except that the length is $2\frac{1}{2}$" instead of $1\frac{1}{2}$"). The resonant frequency with no applied magnetic field was 243 Mcs. Applying a magnetic field parallel to the "b" dimension, with the pole pieces located at the center of the top and bottom walls, it was possible to change the resonant frequency from 243 to 320 Mcs. Magnetic field was approximately 400 gauss at 260 Mcs; 1000 gauss at 290 Mcs. The antenna was fairly well matched at each frequency. VSWR at resonant frequency varied from 1.50 to 1.80. The bandwidth for a VSWR of 3.0 was about 5 Mcs at all frequencies. The probe depth and probe position were not changed throughout the tests. Thus the device is automatically matched as the applied field and resonant frequency are changed. Efficiency is estimated at about 15 percent.

6.3.7 Transmission Line Tuning Effect. A critical experiment was performed to determine if comparable performance could be obtained with the ferrite material removed and a tuner inserted in the transmission line [Fig. 1(e)]. If this were possible then the ferrite loading would offer no advantage. The ferrite powder material was removed from an antenna of size 12" by 3" by 4". The probe was placed as close to the aperture as possible ($\frac{1}{2}$"), adjusted for optimum length, and a double stub tuner was inserted in the coaxial transmission line feed. Bandwidth was reduced by a factor greater than ten. Efficiency was also reduced by a factor greater than ten, judging from a comparison of field strength on the peak of the beam pattern.

CHAPTER 7

CONCLUSIONS AND RECOMMENDATIONS

7.1 Optimization of Antenna Characteristics

Several processes of optimization of bandwidth and efficiency are considered. The first three processes discussed are:

1. For a given $\mu_r \epsilon_r$ product and given size of aperture, what is the optimum μ_r?
2. For a given size of aperture, what is the optimum $\mu_r \epsilon_r$ product?
3. For a given "a" dimension, what is the optimum "b" dimension?

Only process (1) has a true optimum. Processes (2) and (3) have monotonic types of behavior which must be weighed qualitatively against other antenna characteristics.

Consider process (1). What are some of the factors that affect bandwidth and efficiency? Certainly the squared magnitude of the transmission coefficient ($|T|^2$), which is equal to $1 - |R|^2$, is of basic importance. $|T|^2$ represents the fraction of the power transmitted for a wave incident from $-\infty$. $|T|^2$ enters directly into the equations for efficiency [Eq. 6.3]. The maximum value of $|T|^2$ can be calculated.

$$\frac{1-R}{1+R} = \frac{Y}{Y_0} = G + jB$$

$$|T|^2 = 1 - |R|^2 = \frac{4G}{(1+G)^2 + B^2} \tag{7.1}$$

let $K = G/B$. For a given physical size of aperture, given $\mu_r \epsilon_r$, and given frequency, K will be constant since both G and B are proportional to μ_r.

$$|T|^2 = \frac{4KB}{(1 + KB)^2 + B^2}$$

Differentiating with respect to B:

$$\frac{d(T)^2}{dB} = 0 \quad \text{at} \quad B = \sqrt{\frac{1}{1 + K^2}}$$

The maximum value of T^2 is

$$\frac{2\sqrt{\frac{K^2}{1+K^2}}}{1+\sqrt{\frac{K^2}{1+K^2}}} \tag{7.3}$$

The maximum occurs at that value of μ_r which makes $B = \sqrt{1/(1+K^2)}$.

Figure 28 shows a plot of bandwidth and $1 - |R|^2$ as a function of μ_r for the following given characteristics

$$\mu_r \epsilon_r = 9$$

$$b/a = .3$$

$$F_N = 1.8$$

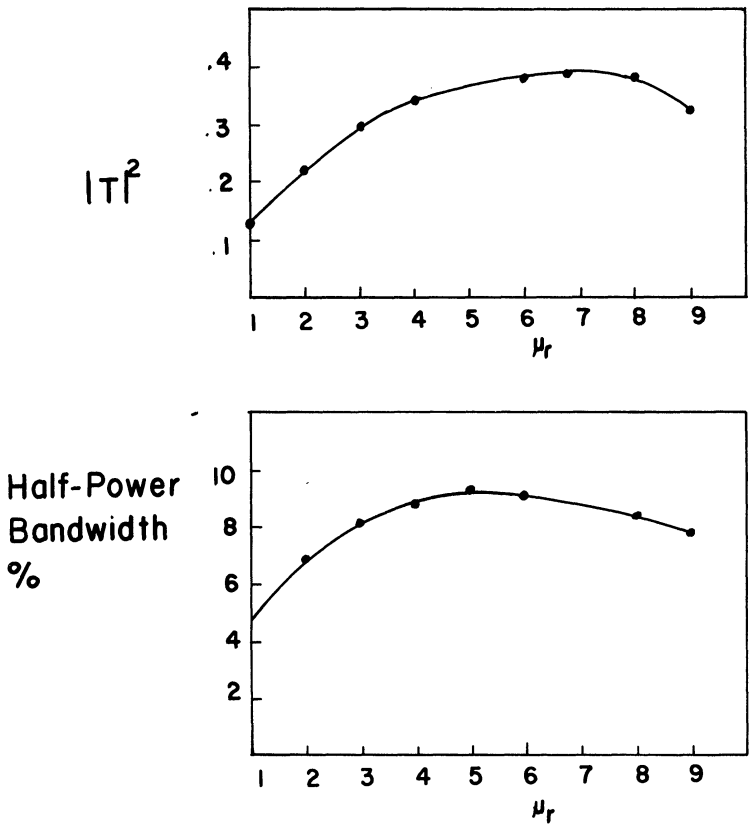

Fig. 28. Optimization of $|T|^2$ for fixed $\mu_r \epsilon_r$ product.

It is noted that the maximum value of $|T|^2$ occurs at $\mu_r = 6.8$ as predicted by Eq. 7.2. However, the maximum value of bandwidth occurs for $\mu_r = 5.0$. The reason for this is that, as μ_r increases, the electrical length of the cavity increases. This effect tends to decrease bandwidth and leads to a bandwidth maximum at a value of μ_r slightly less than the μ_r value for maximum $|T|^2$. This same discussion would also apply to the efficiency characteristics, since the increase in cavity length will increase losses. It is interesting to note that, according to Fig. 28, the maximum bandwidth is almost double that for the purely dielectric case ($\mu_r = 1$, $\epsilon_r = 9$). This is supported by the experimental data in Table 4 for the dielectric cavity and the powdered ferrite cavity. These antennas are exactly the same size and operate at almost exactly the same frequency.

Figure 29 summarizes the information on $|T|^2$. It is a plot of $|T|^2$ vs. B, with K as a parameter. Every plot of $|T|^2$ vs. μ_r (such as that of Fig. 28) will lie along one of the constant K curves. For a given aperture size, $\mu_r\epsilon_r$ product, and frequency, K can be determined from the variational data. Then, as μ_r varies the constant K curve describes the variation of $|T|^2$ and B. Thus the behavior of $|T|^2$ as a function of μ_r can be determined immediately from the curves of Fig. 29. Figure 30 shows a plot of optimum μ_r as a function of the product $\mu_r\epsilon_r$ for $ka/\pi = 1.9$. It is noted that the optimum value of μ_r decreases with increasing μ_r.

Consider optimization process (2). For a given size of aperture, what is the optimum $\mu_r\epsilon_r$ product? A check of the computed data for G and B reveals that, for a given aperture size and frequency, different values of $\mu_r\epsilon_r$ yield almost exactly the same values of K. This agrees with the asymptotic expression for 1/K or B/G (Eq. 2.67)

$$\frac{B}{G} \longrightarrow \frac{-\pi}{4}\,\frac{a}{b}\,\frac{F_1(\theta_1)}{\left(\frac{k_o a}{\pi}\right)^3}$$

This expression is independent of the $\mu_r\epsilon_r$ product and depends only on the free space electrical size of the aperture. This implies that a further optimization as in process (1) would yield identical values of $|T|^2$. However, as noted before, the bandwidth will depend not only on $|T|^2$, but also on the rate of change with frequency of the aperture admittance parameters B'_s, B_A, and G_A.

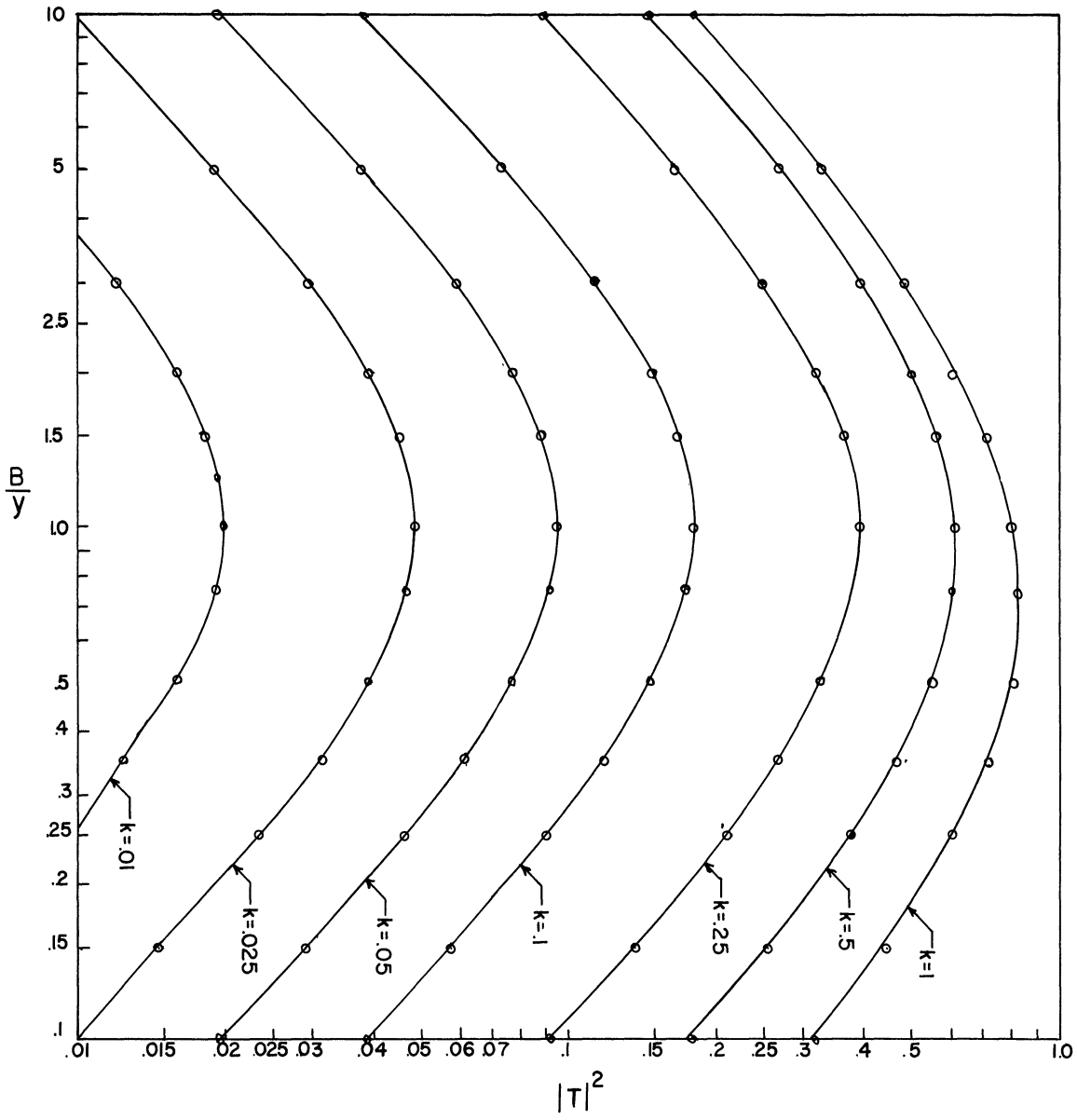

Fig. 29. $|T|^2$ vs. b/y.

B_A and G_A are proportional to $1/\sqrt{F_N^2 - 1}$ and change very rapidly with frequency near cutoff. The rate of change of B'_s with frequency is proportional to the bandwidth ratio plotted in Fig. 23. Thus, all parameters change very rapidly near cutoff and bandwidth improves monotonically as cutoff frequency is decreased by increasing the $\mu_r\epsilon_r$ product. Figure 31 shows a plot of bandwidth vs. $\mu_r\epsilon_r$ product for a fixed aperture size and operating frequency. For all points on the curve, μ_r is chosen for optimum $|T|^2$. The curve can be closely approximated by a curve of form: Bandwidth = K/Bandwidth factor of Fig. 23, (where K is a constant). It is noted that significant improvement in bandwidth can be obtained by using material with a high $\mu_r\epsilon_r$ product.

Figure 32 shows a plot of bandwidth vs. free space electrical size for a given ka/π. This curve shows the basic relationship between bandwidth and size reduction. The bandwidth decreases rapidly with size reduction as noted in Chapter 1 in connection with the spherical line analogy. The curve is plotted assuming 100 percent efficiency; actual bandwidths would be greater than those plotted by the factor $\left(\frac{1}{\text{efficiency}}\right)^3$. The data can be closely approximated by a curve of form: Bandwidth = $K\left(\frac{k_o a}{\pi}\right)$ where K is a constant. This agrees with Eq. 2.67.

Consider optimization process (3). For a given "a" dimension, what is the optimum "b" dimension? From Eq. 2.70, it is noted that K has roughly the dependence $(b/a)^{1/2}$. In addition the maximum value of $|T|^2$ approaches 2K (for small K). Thus $|T|^2$,

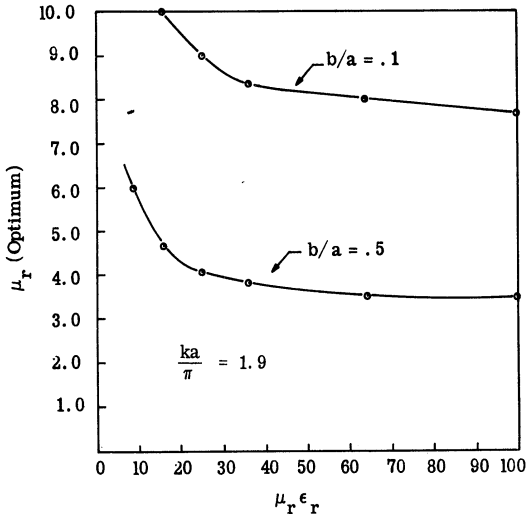

Fig. 30. Choice of μ_r for maximum $|T|^2$.

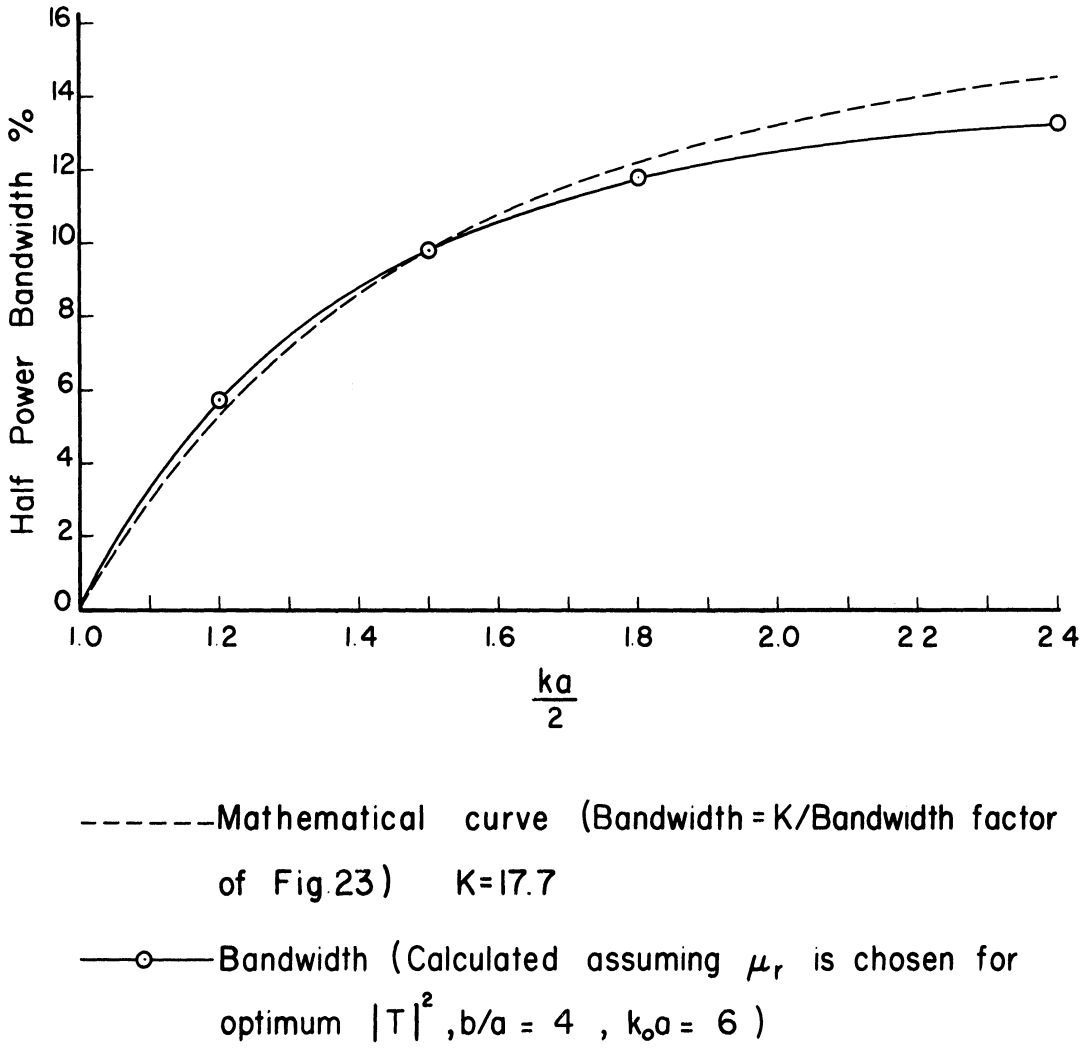

Fig. 31. Bandwidth of a rectangular cavity antenna (fixed size and frequency--variable $\mu_r \epsilon_r$ product).

which we have found to be roughly proportional to bandwidth and efficiency, has the approximate dependence $(b/a)^{1/2}$, indicating that the price paid for reduced "b" dimension is not very severe.

Several other types of optimization processes are considered below.

4. Optimization of $|T|^2$ for a given $\mu_r \epsilon_r$ product, given frequency, and a given physical configuration including an iris in the aperture plane.

$$Y = \underbrace{G_A + jB_A}_{\text{proportional to } \mu_r} \qquad \underbrace{+ j B_I}_{\text{independent of } \mu_r}$$

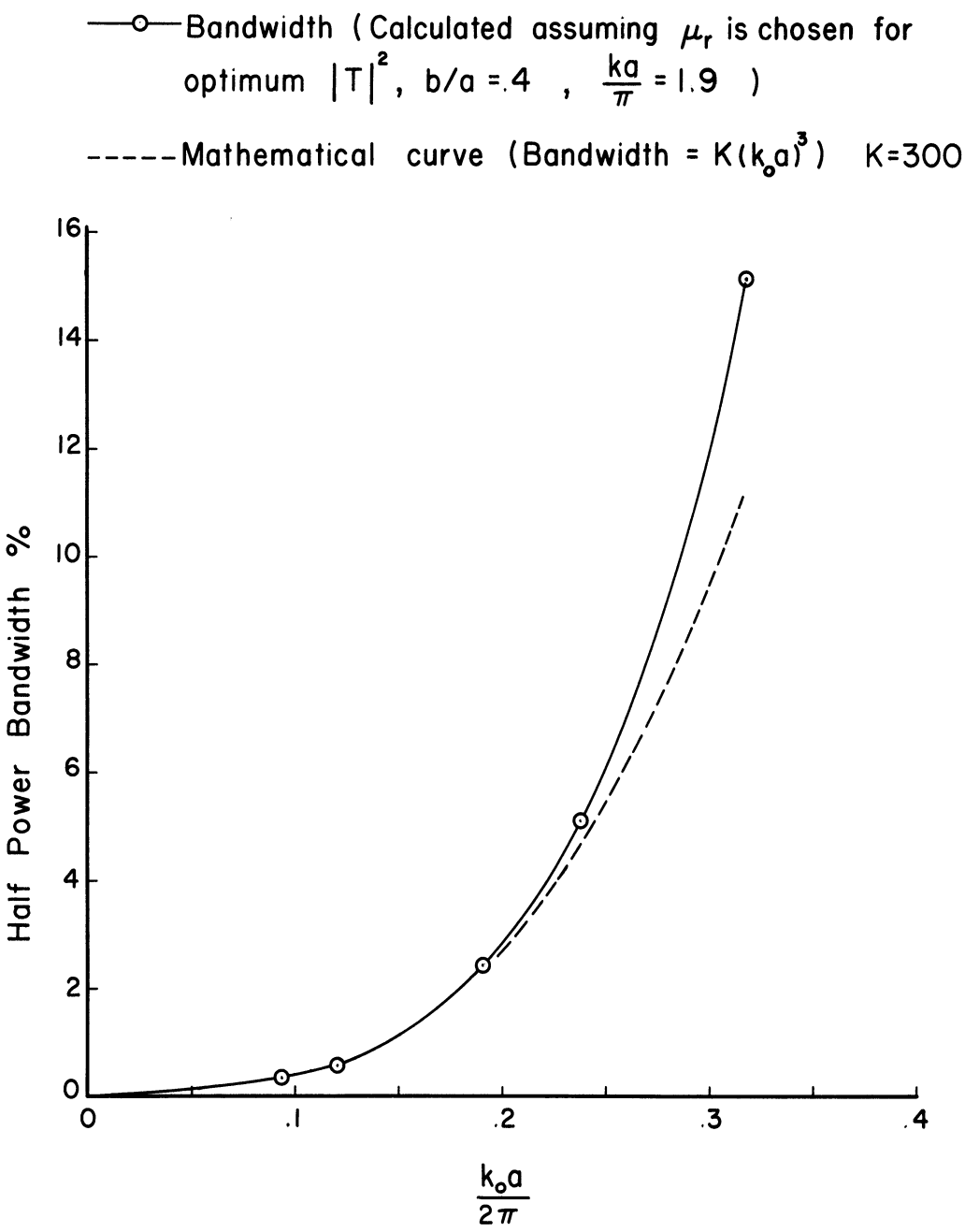

Fig. 32. Bandwidth of a rectangular cavity slot antenna (fixed ka/π and variable electrical size).

where

B_I = iris susceptance

= 1/2 susceptance of the same iris in an infinite waveguide.

$$|T|^2 = \frac{4G_A}{(1 + G_A)^2 + (B_A + B_I)^2} \tag{7.4}$$

let $K = G_A/B_A$

Then $|T|^2$ has a maximum of

$$\frac{2\sqrt{\frac{K^2(1+B_I^2)}{1+K^2}}}{1+2(1+B_I/K)\sqrt{\frac{K^2(1+B_I^2)}{1+K^2}}} \tag{7.5}$$

At the maximum:

$$B_A = \pm\sqrt{\frac{1+B_I^2}{1+K^2}} \approx \pm\sqrt{1+B_I^2} \quad \text{(small k)} \tag{7.6}$$

Only one of the two possibilities (±) corresponds to a realizable B_A.

Several optimization processes have been considered. Conditions for optimum $|T|^2$ have been derived under a number of different conditions. Because of the effect of the increase with μ_r of the electrical length of the cavity, the optimum efficiency and bandwidth values will occur at slightly lower values of μ_r.

An additional effect which is not included in the optimization process is that of the relative frequency sensitivity of some of the more complicated geometries such as that of the compound iris. Such factors will enter into the optimization process and effect the calculation of optimum bandwidth conditions. The analysis of Chapter 3 and the curves of Figs. 5, 8, 9 provide the necessary tools to carry out a more exact numerical optimization process for any given geometry. The approximate optimal condition derived in the section could serve as a starting point for such an analysis.

The optimization process (1), utilizing Fig. 29, can be applied to any other type of loaded slot antenna which satisfies the conditions that that aperture field may be represented approximately by the form of the incident mode. All that would be necessary would be to plot new variational data similar to that of Fig. 5, appropriate to the given geometry. Then, once K was determined from the variational data, the curves of Fig. 29 could be used to determine the optimum choice of μ_r.

7.2 Conclusions

This section will cover conclusions other than those concerned with optimization.

7.2.1 Basic Limitations of Electrically Small Antennas. The basic limitations on electrically small antennas, as discussed by Chu,[2] Wheeler,[16] and Harrington,[3] pose severe restrictions on antennas small compared with a free space wavelength.

There is no implication in this thesis that these basic limitations can be overcome. As a matter of fact, the analysis and experiment tend to emphasize in many different ways the severity of these restrictions. The factor K, which determines the applicable curve of Fig. 29, is determined solely by the free-space electrical size of the antenna. Thus, the maximum $|T|^2$ obtainable depends on the free-space electrical size of the antenna. Whether the maximum is actually attained depends on a proper choice of material. The data of Table 4 and Fig. 32 also show the reduction in bandwidth and efficiency accompanying a reduction in size.

7.2.2 Properties of Loaded Rectangular Cavity Antennas. The effort has been made, working within the basic limitations of electrically small antennas, to (a) accurately predict antenna characteristics and (b) to provide such optimization as may be possible. It has been shown that characteristics such as (1) resonant frequency (2) bandwidth, and (3) efficiency can be accurately predicted for the rectangular cavity slot antennas, using data obtained from variational methods in conjunction with simplified Smith chart techniques.

The normalized aperture admittance has been formulated for a number of similar problems including (a) dominant mode incident-scalar problem, (b) other modes incident-scalar problem, (c) dominant mode incident-scalar dual problem, (d) dominant mode incident-vector problem. In all cases it has been possible to show that, if the aperture electric field has approximately the form of the incident mode, then the normalized aperture admittance is proportional to μ_r.

The presence of an iris in the aperture complicates the dependence somewhat, introducing a lumped reactance which is one half of the reactance of the same iris in an infinite waveguide and which is independent of μ_r in addition to the complex normalized aperture admittance which is proportional to μ_r.

As a result of the dependence on μ_r, it is possible to optimize the bandwidth and efficiency characteristics by choosing material constants for maximum $|T|^2$, the squared magnitude of the transmission coefficient.

7.2.3 General Properties of Loaded Slot Antennas. Many of the characteristics of the rectangular cavity slot antenna may be carried over to a more general class of antennas, namely the class of loaded cavity slot antennas. The loaded cavity slot antenna is defined here as a section of uniform transmission line feeding a ground plane. The ground plane may be infinite, finite, and of any shape. A special case would be a loaded waveguide radiator with no ground plane attached, such as the antennas of Fig. 21. We can say, in general, that if two conditions are satisfied, the admittance functions will be directly proportional to μ_r, $1/\epsilon_r$, or $\sqrt{\mu_r/\epsilon_r}$ and that the ratio of B/G will be independent of relative permeability or permittivity. The two conditions are (1) the form of the aperture electric field must be roughly that of the incident field and (2) there must be no aperture plane iris. If either of these conditions are not satisfied, then the admittance will contain additional terms which will be independent of μ_r and ϵ_r. An example is the iris problem of Chapter 3, which yields an additional reactance term B_I which is independent of μ_r and ϵ_r. Similarly, if the aperture field is radically different in form from that of the incident wave, the infinite sum

$$\frac{\sum\sum V_i^2 Y_i}{V_o^2 Y_o} \quad 75$$

will yield an additional admittance term which, for a given $\mu_r\epsilon_r$ product, will be independent of μ_r, because of the factor (Y_i/Y_o). This additional term will be reactive if the mode (i) is cut off and resistive if the mode (i) is propagating.

As a result, for a given physical configuration, given frequency, and given $\mu_r\epsilon_r$ product, an optimum choice of materials is always possible for the general class of antennas referred to as cavity slot antennas.

The discussion and analysis has been limited to the case of a single incident mode. If a number of different modes are incident upon the aperture, each mode will have a different admittance and a different optimum. The over-all optimum may depend, for instance, on the relative strengths of the different modes. The experimental data seems to indicate

that, in the cases observed, the effect of higher modes is negligible, even in cases where several modes may propagate. One reason for this is certainly that the excitation is such as to launch predominantly the TE_{10} mode.

The generality of the conclusions suggests applications to other types of antennas. We have discussed a rectangular waveguide with a unidirectional radiation pattern. The conclusions also apply to a waveguide radiator whose cross section consists of a doubly connected region, such as a coaxial waveguide. One form of this antenna is the annular slot antenna, which is in common use.[33] The analysis implies that the characteristics of the annular slot antenna could be improved through an optimum choice of material constants. Variational data in the literature[31] could be readily adapted to such an antenna. There are some significant differences between the rectangular cavity slot antenna and the annular slot antenna which would perhaps, lead to different applications. The beam pattern of the rectangular cavity slot antenna is unidirectional, whereas the pattern of the annular slot is doughnut-shaped. A combination of these two patterns would give complete half plane coverage.

7.2.4 Variational Calculations. Several points concerning the mathematical techniques of variational calculations are noted. The use of variational calculations may be separated into three parts:

(a) The formulation of the variational expression and proof of stationarity.

(b) The reduction of the variational form to a form suitable for computation.

(c) The computation of results.

Numerous examples of variational expressions are available in the literature. Familiarity with similar forms often makes the process of deriving a variational expression and proving stationarity fairly simple.

The computation of results, although it is an essential part of the process and requires a thorough process of checking, is straightforward. Part (b), the reduction to a form suitable for computation, represents an important part of the calculations for those problems studied in this thesis. It is in this area that two contributions to mathematical techniques are made. They are concerned with:

(1) The use of two expressions for electric field in a single variational calculation.

(2) The effect of forbidden modes on the Rayleigh-Ritz procedure.

In addition, several interesting points are made concerning:

(3) The effect of assumptions concerning the scalar nature of a problem, and

(4) The evaluation of higher mode coefficients.

In Chapter 3, a variational expression was derived for the admittance, of a loaded rectangular waveguide radiator with an aperture plane iris. The expression consisted of two terms. It was not convenient to use the same form of the electric field in both expressions. A form $E_1(xy)$ was used in one term and a form $E_2(xy)$ was used in the other. This invalidated the proof of stationarity. Nevertheless, it was argued, by appealing to related variational expressions that each of the individual terms would be accurately evaluated. Experimental data from Chapter 6 indicates that accurate results are obtained in a particular problem (a loaded waveguide radiator with capacitive and inductive aperture plane irises).

It is shown in Section 5. 4 that the forbidden modes have no effect on the Rayleigh-Ritz process. The forbidden mode coefficients are zero and the contribution of the forbidden modes to the admittance is zero. This result is proven for a specific problem (the loaded rectangular waveguide radiator). This fact is primarily of mathematical interest, since one would probably exclude forbidden modes from a Rayleigh-Ritz process as a matter of course. If this fact is true in general and if, in addition, its inverse is true, namely that a zero coefficient implies that a mode is forbidden, then this fact could be used as a test for forbidden modes.

It has been shown in Chapter 5, in two particular examples, that the assumption of a scalar problem ($E_y = 0$) before forming a variational problem is no more serious than the same assumption after forming a variational expression for the vector problem. Very few vector problems have been treated in the literature. One reason for this is that the complexity of a vector problem is greater than that of a similar scalar problem by at least a factor of four. However, we need only a crude assumption for aperture field. In many vector problems a scalar field assumption is justified.

It has been noted, in connection with the evaluation of higher mode coefficients of the particular problem under study, that the quadruple integrals can be reduced to double

integral form and evaluated by methods similar to those used for the evaluation of the dominant mode approximation.

Gross approximations have been made in the analysis in order to apply the results of the problem of Fig. 7(a) to the configuration of Fig. 1(g). In view of these gross assumptions, the accuracy of the results is surprising.

7.2.5 Experimental Techniques.

Several brief conclusions may be made concerning experimental techniques. The use of wedged transition from the rectangular dielectric block to the slotted dielectric block has apparently yielded accurate admittance measurements. This conclusion must be hedged slightly since the agreement of the wedged data and the theoretical data has been used to conclude both (a) that the theoretical data is accurate and (b) the wedged transition admittance measurement method is accurate at frequencies slightly above cutoff.

A new method of measuring dielectric constant has been proposed (Section 6. 3. 2). This method has not been thoroughly investigated, but it is believed that it may offer some advantages over conventional techniques in (a) measurement accuracy, (b) sample preparation and (c) rapidity of measurement.

7.2.6 Very Small Antennas.

For very small antennas (antennas which are small compared with a material wavelength $\lambda_0/\sqrt{\mu_r\epsilon_r}$), certain conclusions can be drawn.

For a very small loop antenna, the magnetic field is proportional to $1/r^2$ whereas the electric field is proportional to $1/r^3$. Therefore energy storage is primarily in the magnetic field and the effects of dielectric loading are negligible. Similarly, for the very small electric dipole, the effects of magnetic loading are negligible. It has been noted that increasing ϵ_r decreases the radiation resistance of the very small loaded dipole, whereas increasing μ_r of the very small loop increases the radiation resistance of the loop. This may be explained in terms of the fact that induced polarization currents $\frac{\partial \rho}{\partial t}$ of the dipole oppose the currents on the conductor whereas the induced magnetization currents $\Delta \times M$ of the loop aid the currents on the conductor. For antennas large compared with a material wavelength, phase differences between induced currents and driving currents must be taken into account. As a result the above conclusions are invalid for antennas large compared with a material wavelength.

7.2.7 Summary.

What has been accomplished through the use of ferrite loading? The use of ferrite in a rectangular cavity slot antenna may be described in simple terms as an effective method of synthesizing the simusoidal aperture distribution, and one which permits accurate prediction of antenna characteristics. In addition, the use of material loading also reduces the reflection coefficient. An additional advantage in ferrite materials is that they may be tuned to change resonant frequency (Section 6.3.6). However, it should be emphasized that there may be other methods of accomplishing the same thing without ferrite loading. It is certainly not claimed that the results obtained cannot be obtained by any other method. It is claimed that the results show one method of obtaining significant size reduction at moderate expense in terms of bandwidth and efficiency.

The contributions of this thesis are outlined below.

1. The derivation of accurate simplified design techniques for rectangular cavity slot antennas and the optimization of antenna characteristics.

2. Two contributions to mathematical techniques for variational calculations.

   (a) Discussion and example of two forms of electric field in a single variational expression.

   (b) A proof that, in the problem at hand; the forbidden modes do not contribute to the admittance calculation.

3. General conclusions concerning the limitation and potentialities of loaded antennas.

4. Practical realization of several loaded cavity antennas of reduced size.

5. Two contributions to measurement techniques including:

   (a) The measurement of aperture admittance using a wedged transition.

   (b) A proposed new method of measuring dielectric constant.

7.3 Recommendations for Future Work

1. The accuracy of the bandwidth prediction could be improved by a complete solution of the coaxial probe to waveguide junction. The equivalent circuit could then be used in the same type of Smith chart calculation. It is also possible that a more sophisticated model of the junction, short of a complete solution, would improve the accuracy of bandwidth prediction.

2. The application of ferrite loading to traveling wave types of antennas shows some promise. Results of experiments on a loaded scimitar antenna are shown in Fig. 31. The scimitar has essentially a high pass characteristic. The low frequency cutoff is lowered by a factor of two or three in frequency. Bandwidth is essentially unaffected and efficiency is 80 percent. Similar results have been noted for tests on loaded spiral antennas.

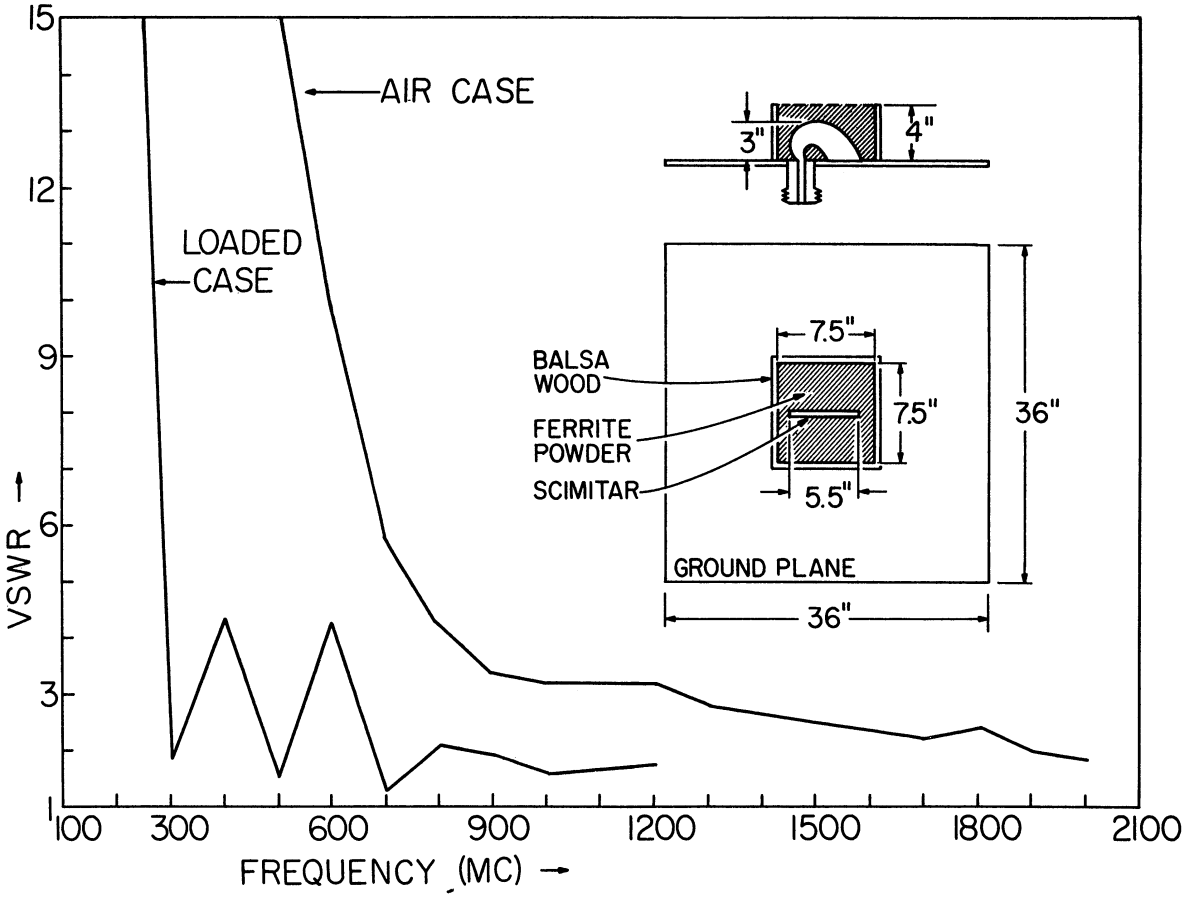

Fig. 33. A ferrite loaded scimitar antenna.

3. The preliminary experiments performed on the magnetically tuned slot antenna show promise. It is interesting to note that what has been accomplished is not only a change in the cavity resonance, but essentially automatic matching since it was not necessary to mechanically readjust the probe depth at each frequency. The bandwidth is very narrow, but this may have some inherent advantages in high rejection for off-resonant frequencies.

4. Directive antennas. Material loading may have some application to directive antennas. Certainly the decreased wavelength $\lambda_o / \sqrt{\mu_r \epsilon_r}$ may help to realize the required

supergain distribution; some progress has already been reported in increasing the gain of helices by dielectric loading.[82] Of course, the basic limitations of supergain antennas cannot be overcome. As an example consider a horn antenna of a given size. Material loading may facilitate the launching of the higher modes necessary for higher gain. If higher gain is attained, it must be accompanied by narrow bandwidth and low efficiency. The beam pattern of the horn antenna depends only on the aperture field. If material is added and the aperture field distribution is not changed, then the directivity will be exactly the same.

APPENDIX A

COORDINATE TRANSFORMATION

In Chapters 2-4, the following coordinate transformation is used extensively.

$$y - \eta = \lambda \qquad x - \xi = \sigma$$

$$y + \eta = a + \mu \qquad x + \xi = \nu + b$$

The purpose in transforming to sum and difference coordinates is to allow reduction of the quadruple integrals to double integrals. e^{jkr}/r cannot be integrated but the other terms of the $C_{mnm'n'}$ coefficients arising in Chapters 2 and 4 can be integrated. The transformation reduces e^{jkr}/r to a function of two rather than four variables.

This transformation consists of a 45^{o} rotation of coordinates, a reduction of scale, and a translation.

Consider the general coordinate rotation:

$$\mu'' = \eta \sin \theta + y \cos \theta$$

$$\lambda'' = -\eta \cos \theta + y \sin \theta$$

let $\theta = 45^{o}$

$$\mu'' = 1/\sqrt{2}\ [y + \eta]$$

$$\lambda'' = 1/\sqrt{2}\ [y - \eta]$$

Now perform the transformation

$$\left.\begin{aligned} \mu' &= \sqrt{2}\ \mu'' \\ \lambda' &= \sqrt{2}\ \lambda'' \end{aligned}\right\} \text{ reduction of scale}$$

$$\mu' = y + \eta$$

$$\lambda' = y - \eta$$

Now perform a translation along the μ' axis

$$\mu = \mu' - a$$

$$\lambda = \lambda'$$

This translation locates our coordinate system at the center of the area of integration and makes more readily apparent any symmetries which may exist.

These operations are shown in Fig. 4. Consider an integration over the square area of Fig. 4.

$$\int_0^a \int_0^a f(y,\eta)\, dy\, d\eta$$

$$dy\, d\eta = \frac{1}{2}\, d\mu\, d\lambda \quad \text{(because of the reduction of scale)}$$

$$\int_0^a \int_0^a f(y,\eta)\, dy\, d\eta = \frac{1}{2} \int_0^a \int_{-(a-\lambda)}^{a-\lambda} f(\mu,\lambda)\, d\mu\, d\lambda + \frac{1}{2} \int_{-a}^{0} \int_{-(a+\lambda)}^{a+\lambda} f(\mu,\lambda)\, d\mu\, d\lambda \qquad \text{(A. 1)}$$

If $f(\mu,\lambda)$ is even in μ and λ: $f(-\mu,\lambda) = f(\mu,-\lambda) = f(\mu,\lambda)$ then

$$\int_0^a \int_0^a f(y,\eta) = 2 \int_0^a \int_0^{a-\lambda} f(\mu,\lambda)\, d\mu\, d\lambda \qquad \text{(A. 2)}$$

The integration over the square area reduces to four equal integrations over a triangular area. Similarly, for the other half of the transformation

$$\int_0^b \int_0^b f(\xi,x)\, d\xi\, dx = \frac{1}{2} \int_0^b \int_{-(b-\sigma)}^{b-\sigma} f(\sigma,\nu)\, d\nu\, d\sigma + \frac{1}{2} \int_{-b}^{0} \int_{-(b+\sigma)}^{b+\sigma} f(\sigma,\nu)\, d\nu\, d\sigma \qquad \text{(A. 3)}$$

$$= 2 \int_0^b \int_0^{b-\sigma} f(\sigma,\nu)\, d\nu\, d\sigma \text{[if } f(\sigma,\nu) \text{ is even in } \sigma \text{ and } \nu\text{]} \qquad \text{(A. 4)}$$

Similarly

$$\int_0^a\int_0^b\int_0^a\int_0^b f(x,y,\xi,\eta)\,dx\,dy\,d\xi\,d\eta = \frac{1}{4}\int_0^a\int_0^b\int_{-(a-\lambda)}^{a-\lambda}\int_{-(b-\sigma)}^{b-\sigma} f(\nu,\mu,\sigma,\lambda)\,d\nu\,d\mu\,d\sigma\,d\lambda$$

$$+\frac{1}{4}\int_0^a\int_{-b}^{0}\int_{-(a-\lambda)}^{a-\lambda}\int_{-(b+\sigma)}^{b+\sigma} f(\nu,\mu,\sigma,\lambda)\,d\nu\,d\mu\,d\sigma\,d\lambda$$

$$+\frac{1}{4}\int_{-a}^{0}\int_0^b\int_{-(a+\lambda)}^{a+\lambda}\int_{-(b-\sigma)}^{b-\sigma} f(\nu,\mu,\sigma,\lambda)\,d\nu\,d\mu\,d\sigma\,d\lambda \qquad \text{(A. 5)}$$

$$+\frac{1}{4}\int_{-a}^{0}\int_{-b}^{0}\int_{-(a+\lambda)}^{a+\lambda}\int_{-(b+\sigma)}^{b+\sigma} f(\nu,\mu,\sigma,\lambda)\,d\nu\,d\mu\,d\sigma\,d\lambda$$

$$= \int_0^a\int_0^b\int_0^{a-\lambda}\int_{-(b-\sigma)}^{b-\sigma} f(\nu,\mu,\sigma,\lambda)\,d\nu\,d\mu\,d\sigma\,d\lambda + \int_0^a\int_{-b}^{0}\int_0^{a-\lambda}\int_{-(b+\sigma)}^{b+\sigma} f(\nu,\mu,\sigma,\lambda)\,d\nu\,d\mu\,d\sigma\,d\lambda \qquad \text{(A. 6)}$$

[if $f(\nu,\mu,\sigma,\lambda)$ is even in μ and λ]

$$= \int_0^a\int_0^b\int_{-(a-\lambda)}^{a-\lambda}\int_0^{b-\sigma} f(\nu,\mu,\sigma,\lambda)\,d\nu\,d\mu\,d\sigma\,d\lambda + \int_{-a}^{0}\int_0^b\int_{-(a+\lambda)}^{a+\lambda}\int_0^{b-\sigma} f(\nu,\mu,\sigma,\lambda)\,d\nu\,d\mu\,d\sigma\,d\lambda \qquad \text{(A. 7)}$$

[if $f(\nu,\mu,\sigma,\lambda)$ is even in ν and σ]

$$= 4\int_0^a\int_0^b\int_0^{a-\lambda}\int_0^{b-\sigma} f(\nu,\mu,\sigma,\lambda)\,d\nu\,d\mu\,d\sigma\,d\lambda \qquad \text{(A. 8)}$$

if $f(\nu,\mu,\sigma,\lambda)$ is even in ν,μ,σ,λ.

APPENDIX B

EFFICIENCY OF A RECTANGULAR CAVITY SLOT RADIATOR

B. 1 General Formulation

The efficiency of a rectangular cavity slot radiator has been analyzed, assuming an attenuated dominant mode only in the cavity and utilizing the reflection coefficient at the aperture which has been evaluated by variational techniques in Chapter 2. An electric current sheet source exciting the dominant mode is located at the probe position [Fig. 33(a) and (b)]. The source may also be assumed to be magnetic current, in which case the complex constant A, which determines the fields in Region No. 2, will have a different value. The electric current source gives rise to a discontinuity in H_y whereas the magnetic current source produces a discontinuity in E_x. The radiated power is calculated by integrating Poynting's vector across the aperture. The formulation takes into account magnetic and electric volume losses and wall losses with certain simplifications resulting in special cases.

The fields are represented in terms of a Hertzian vector potential of magnetic type in Regions No. 1 and No. 2

$$\Pi_1^* = \frac{-1}{j\omega\mu}\left[\frac{e^{-\Gamma_{10}z} - R\,e^{\Gamma_{10}z}}{\Gamma_{10}}\right]\sin\frac{\pi y}{a}\cdot\hat{y} \qquad \text{(B. 1)}$$

$$\Pi_2^* = \frac{-A}{j\omega\mu}\left[\frac{e^{-\Gamma_{10}z'} + e^{\Gamma_{10}z'}}{\Gamma_{10}}\right]\sin\frac{\pi y}{a}\cdot\hat{y} \qquad \text{(B. 2)}$$

$$J_s = J_0 \sin\frac{\pi y}{a}\cdot\hat{x} \qquad \text{electric current}$$

or

$$M_s = M_0 \sin\frac{\pi y}{a}\cdot\hat{y} \qquad \text{magnetic current}$$

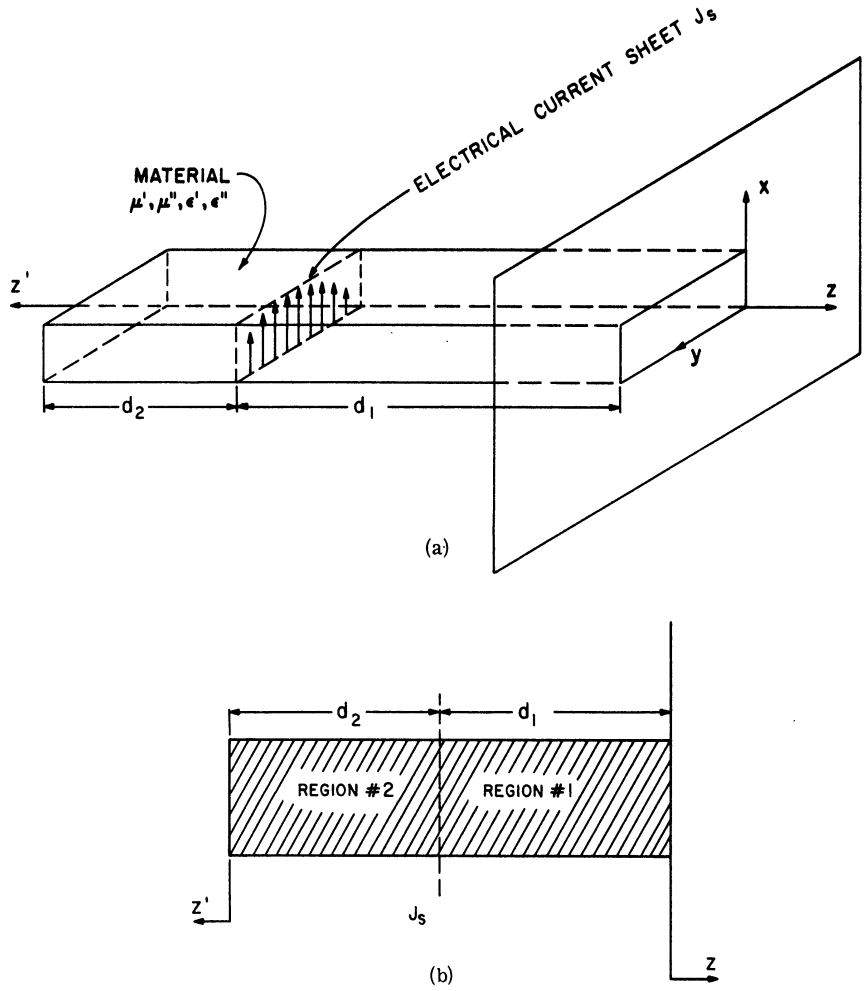

Fig. 34. Model for efficiency calculations.

where

R is the complex dominant mode reflection coefficient evaluated in Chapter two.

Efficiency

$$\text{time average power radiated} = \overline{P}_r = \text{Re} \int_0^a \int_0^b E_x H_y^* \, dx \, dy$$

(evaluated at z = 0)

time average power dissipation in the cavity

$$= \overline{P}_L = \iiint_{\text{cavity}} \omega\epsilon''|E|^2 \, dv + \iiint_{\text{cavity}} \omega\mu''|H|^2 \, dv$$

$$+ R_s \iiint_{\text{walls}} |H|^2 \, da$$

where E and H are rms values,

$$\epsilon = \epsilon' - j\epsilon''$$

$$\mu = \mu' - j\mu''$$

R_s = surface resistivity

$$\text{efficiency} = \frac{\overline{P}_r}{\overline{P}_r + \overline{P}_L} \quad \frac{1}{1 + \frac{\overline{P}_L}{\overline{P}_r}} \tag{B. 3}$$

since we are concerned with the ratio $\overline{P}_L/\overline{P}_r$, it is immaterial whether we use peak or rms values in the above equations.

Solving for the Fields in Regions No. 1 and No. 2

$$|E_{x1}|^2 = \sin^2 \frac{\pi y}{a} \left[e^{-2\alpha 10^z} + |R|^2 e^{2\alpha 10^z} + 2|R| \cos (2\beta 10^z + \theta_r) \right] \tag{B. 4}$$

$$|H_{y1}|^2 = \left| \frac{k^2 a^2 - \pi^2}{\omega\mu a^2} \right|^2 \sin^2 \frac{\pi y}{a} \frac{1}{\Gamma_{10}{}^2}$$

$$\left[e^{-2\alpha 10^z} + |R|^2 e^{2\alpha 10^z} - 2|R| \cos (2\beta 10^z + \theta_r) \right]$$

$$H_{z1}{}^2 = \left| \frac{\pi}{a\omega\mu} \right|^2 \cos^2 \frac{\pi y}{a}$$

$$\left[e^{-2\alpha 10^z} + |R|^2 e^{2\alpha 10^z} + 2|R| \cos (2\beta 10^z + \theta_r) \right]$$

Region No. 1

$$E_{x2}^{\ 2} = |A|^2 \sin^2 \frac{\pi y}{a} \left[e^{-2\alpha_{10} z'} + e^{2\alpha_{10} z'} - 2 \cos 2\beta_{10} z' \right]$$

$$H_{y2}^{\ 2} = \left| \frac{k^2 a^2 - \pi^2}{\omega \mu a^2} \right|^2 \frac{|A|^2}{|\Gamma_{10}|^2} \sin^2 \frac{\pi y}{a} \left[e^{-2\alpha_{10} z'} + e^{2\alpha_{10} z'} + 2 \cos 2\beta_{10} z' \right]$$

$$H_{z2}^{\ 2} = \left| \frac{\pi}{a\omega\mu} \right|^2 |A|^2 \cos^2 \frac{\pi y}{a} \left[e^{-2\alpha_{10} z'} + e^{2\alpha_{10} z'} - 2 \cos 2\beta_{10} z' \right]$$

(B. 5)

Region No. 2

where: Subscript one vectors are zero in region two and vice versa.

$$R = R\, e^{j\theta_r}$$

$$\Gamma_{10} = \alpha_{10} + j\beta_{10}$$

Value of A

Applying boundary conditions at the source:

Electric Current Source:

$$E_{x1}]_{z = -d_1} = E_{x2}]_{z' = -d_2}$$

$$A = \left[\frac{e^{+\Gamma_{10} d_1} + R\, e^{-\Gamma_{10} d_1}}{e^{+\Gamma_{10} d_2} - e^{-\Gamma_{10} d_2}} \right]$$

$$|A|^2 = \frac{e^{+2\alpha_{10} d_1} + |R|^2\, e^{-2\alpha_{10} d_1} + 2\,|R| \cos(2\beta_{10} d_1 - \theta_r)}{e^{+2\alpha_{10} d_2} + e^{-2\alpha_{10} d_2} - 2\,|R| \cos(2\beta_{10} d_2)} \tag{B. 6}$$

$$= \left.\frac{\cosh 2\alpha_{10} d + \cos(2\beta_{10} d - \theta_r)}{\cosh 2\alpha_{10} d - \cos(2\beta_{10} d)}\right\} \text{ if} \begin{cases} |R|^2 = 1 \\ d_1 = d_2 = d \end{cases} \tag{B. 7}$$

The value J_0 may be derived by applying boundary conditions on tangential H.

Radiated Power:

$$\text{Radiated power} = \text{Re} \iint_{\text{aperture}} (E_x \cdot H_y^*) \cdot \hat{z}\, dx\, dy \tag{B. 8}$$

$$E_x = (1+R) \sin \frac{\pi y}{a} \tag{B. 9}$$

$$H_y^* = \left(\frac{k^2 a^2 - \pi^2}{a^2}\right)^* \left(\frac{1}{j\omega\mu}\right)^* \left(\frac{1-R^*}{\Gamma_{10}^*}\right) \sin \frac{\pi y}{a}$$

$$\text{Radiated power} = \text{Re} \left[(1+R)(1-R^*) \left(\frac{k^2 a^2 - \pi^2}{a^2}\right)^* \left(\frac{+1}{j\omega\mu^*}\right) \frac{1}{\Gamma_{10}^*}\right] \frac{ab}{2} \tag{B. 10}$$

where: * indicates complex conjugate except when used with Π^*.

$$\Gamma_{10}^* = \frac{1}{a} \left[\sqrt{\pi^2 - k^2 a^2}\right]^*$$

$$(\omega\mu a)^* = (ka) \left[\sqrt{\frac{\mu}{\epsilon}}\right] \left[\frac{\mu^*}{\mu}\right]$$

R = complex aperture reflection coefficient

$$ka = k_0 a \sqrt{(\mu_r' \epsilon_r' - \mu_r'' \epsilon_r'') - j(\mu_r' \epsilon_r'' + \mu_r'' \epsilon_r')}$$

$$\mu_r = \mu_r' - j\mu_r''$$

$$\epsilon_r = \epsilon_r' - j\epsilon_r''$$

$$\mu = \mu_r \mu_o$$

$$\epsilon = \epsilon_r \epsilon_o$$

It should be noted that the proper definition of the square roots must be chosen so that all the quantities have the correct physical significance. Γ_{10} is in the first quadrant, $(\omega\mu a)^*$ and ka are in the fourth quadrant for a time dependence $e^{j\omega t}$.

$$\text{Efficiency} = \frac{\bar{P}_r}{\bar{P}_r + \bar{P}_L}$$

$$\text{where } \bar{P}_L = \omega\epsilon'' \iiint_{\text{cavity}} |E_x|^2 \, dv + \omega\mu'' \iiint_{\text{cavity}} \left[|H_y|^2 + |H_z|^2\right] dv \qquad \text{(B. 11)}$$

$$+ R_s \iint_{\text{walls}} |H_{tang}|^2 \, da$$

The following integration formulas are useful:

$$\int_o^{-d} \left[e^{-2\alpha_{10} z} + |R|^2 e^{2\alpha_{10} z} \pm 2 R \cos(2\beta_{10} z + \theta) \right] dz$$

$$= \frac{1}{2\alpha_{10}} \left[|R|^2 e^{-2\alpha_{10} d} + (1 - |R|^2) \right] \mp \qquad \text{(B. 12)}$$

$$\frac{|R|}{\beta_{10}} \left[\sin(2\beta_{10} d - \theta) + \sin\theta_r \right]$$

$$\int_o^{-d} \left[e^{-2\alpha_{10} z} + e^{2\alpha_{10} z} \pm 2 \cos 2\beta_{10} z \right] dz$$

$$= \frac{1}{2\alpha_{10}} \left[e^{-2\alpha_{10} d} - e^{2\alpha_{10} d} \right] \mp \frac{1}{\beta_{10}} \sin 2\beta_{10} d \qquad \text{(B. 13)}$$

$$= \frac{-\sinh 2\beta_{10} d}{\alpha_{10}} \mp \frac{\sin 2\beta_{10} d}{\beta_{10}}$$

Magnetic Volume Losses

$$\omega\mu'' \iiint_{\text{cavity}} \left[|H_{y1}|^2 + |H_{y2}|^2 + |H_{z1}|^2 + |H_{z2}|^2\right] dv$$

$$= ① + ② + ③ + ④ \qquad \text{(B. 14)}$$

$$\omega\mu''a = |ka| \cdot \left|\sqrt{\frac{\mu}{\epsilon}}\right| \cdot \left|\frac{\mu''}{\mu}\right|$$

$$|\Gamma_{10}|^2 = \frac{1}{a^2}\left|k^2a^2 - \pi^2\right|$$

$$|\omega\mu a| = |ka|\left|\sqrt{\frac{\mu}{\epsilon}}\right|$$

$$① = \frac{\left|k^2a^2 - \pi^2\right| \cdot \left|\sqrt{\frac{\epsilon}{\mu}}\right| \cdot \left|\frac{\mu''}{\mu}\right|}{|ka|} \frac{b}{2}$$

$$\left\{\frac{1}{2\alpha_{10}}\left[-|R|^2 e^{-2\alpha_{10}d_1} + e^{2\alpha_{10}d_1} - (1 - |R|^2)\right] - \frac{|R|}{\beta_{10}}\left[\sin(2\beta_{10}d_1 - \theta_r) + \sin\theta_r\right]\right\}$$

$$② = \frac{|A|^2 \cdot \left|k^2a^2 - \pi^2\right| \cdot \left|\sqrt{\frac{\epsilon}{\mu}}\right| \cdot \left|\frac{\mu''}{\mu}\right|}{|ka|} \frac{b}{2}\left\{\frac{+\sinh 2\alpha_{10}d_2}{\alpha_{10}} + \frac{\sin 2\beta_{10}d_2}{\beta_{10}}\right\}$$

$$③ = \frac{\pi^2 \left|\sqrt{\frac{\epsilon}{\mu}}\right| \cdot \left|\frac{\mu''}{\mu}\right|}{|ka|} \frac{b}{2} \left\{\frac{\left[-|R|^2 e^{-2\alpha_{10}d_1} + e^{2\alpha_{10}d_1} - (1 - |R|^2)\right]}{2\alpha_{10}}\right.$$

$$\left. + \frac{|R|}{\beta_{10}}\left[\sin(2\beta_{10}d_1 - \theta_r) + \sin\theta_r\right]\right\}$$

$$④ = \frac{|A|^2 \pi^2 \left|\sqrt{\frac{\epsilon}{\mu}}\right| \cdot \left|\frac{\mu''}{\mu}\right|}{|ka|} \frac{b}{2}\left\{\frac{+\sinh 2\alpha_{10}d_2}{\alpha_{10}} - \frac{\sin 2\beta_{10}d_2}{\beta_{10}}\right\}$$

Electric Volume Losses

$$\omega\epsilon''a = |ka| \cdot \left|\sqrt{\frac{\epsilon}{\mu}}\right| \cdot \left|\frac{\epsilon''}{\epsilon}\right|$$

$$\omega\epsilon'' \iiint \left[|E_{x1}|^2 + |E_{x2}|^2 \right] dv$$

$$= |ka| \cdot \left|\sqrt{\frac{\epsilon}{\mu}}\right| \cdot \left|\frac{\epsilon''}{\epsilon}\right| \frac{b}{2} \left\{ \frac{1}{2\alpha_{10}} \left[- |R|^2 e^{-2\alpha_{10} d_1} + e^{2\alpha_{10} d_1} - (1 - |R|^2) \right] \right.$$

$$+ \frac{|R|}{\beta_{10}} \left[\sin (2\beta_{10} d_1 - \theta_r) + \sin \theta_r \right]$$

$$\left. + |A|^2 \left[\frac{\sinh 2\alpha_{10} d_1}{\alpha_{10}} - \frac{\sin 2\beta_{10} d_1}{\beta_{10}} \right] \right\} \qquad \text{(B. 15)}$$

Resistivity Losses

$$R_s \iint_{\text{wall}} |H_{tang}|^2$$

$$= 2R_s \iint_{\text{top wall}} \left[|H_{y1}|^2 + |H_{y2}|^2 + |H_{z1}|^2 + |H_{z2}|^2 \right] dy\, dz$$

$$+ 2R_s \iint_{\text{side wall}} \left[|H_{z1}|^2 + |H_{z2}|^2 \right] dx\, dz + R_s \iint_{\text{back wall}} |H_{z2}|^2 \, dx\, dy$$

$$= \left[① + ② + ③ + ④ \right] + \left[⑤ + ⑥ \right] + \left[⑦ \right] \qquad \text{(B. 16)}$$

$$① = \frac{aR_s \left| k^2 a^2 - \pi^2 \right| \cdot \left| \frac{\epsilon}{\mu} \right|}{\left| k^2 a^2 \right|} \left\{ \frac{1}{2\alpha_{10}} \left[- |R|^2 e^{-2\alpha_{10} d_1} + e^{2\alpha_{10} d_1} - (1 - |R|^2) \right] \right.$$

$$\left. - \frac{|R|}{\beta_{10}} \left[\sin (2\beta_{10} d_1 - \theta_r) + \sin \theta_r \right] \right\}$$

$$② = \frac{|A|^2 \, aR_s \left| k^2 a^2 - \pi^2 \right| \cdot \left| \frac{\epsilon}{\mu} \right|}{\left| k^2 a^2 \right|} \left\{ \frac{+ \sinh 2\alpha_{10} d_2}{\alpha_{10}} + \frac{\sin 2\beta_{10} d_2}{\beta_{10}} \right\}$$

$$③ = \frac{\pi^2 \, aR_s \left|\frac{\epsilon}{\mu}\right|}{|k^2 a^2|} \left\{ \frac{1}{2\alpha_{10}} \left[- |R|^2 \, e^{-2\alpha_{10} d_1} + e^{2\alpha_{10} d_1} - (1 - |R|^2) \right] + \frac{|R|}{\beta_{10}} \left[\sin (2\beta_{10} d_1 - \theta_r) + \sin \theta_r \right] \right\}$$

$$④ = \frac{|A|^2 \, \pi^2 \, aR_s \left|\frac{\epsilon}{\mu}\right|}{|k^2 a^2|} \left\{ \frac{+ \sinh 2\alpha_{10} d_2}{\alpha_{10}} - \frac{\sin 2\beta_{10} d_2}{\beta_{10}} \right\}$$

$$⑤ = \frac{2\pi^2 \, bR_s \left|\frac{\epsilon}{\mu}\right|}{|k^2 a^2|} \left\{ \frac{1}{2\alpha_{10}} \left[- |R|^2 \, e^{-2\alpha_{10} d_1} + e^{2\alpha_{10} d_1} - (1 - |R|^2) \right] + \frac{|R|}{\beta_{10}} \left[\sin (2\beta_{10} d_1 - \theta_r) + \sin \theta_r \right] \right\}$$

$$⑥ = \frac{|A|^2 \, 2\pi^2 \, bR_s \left|\frac{\epsilon}{\mu}\right|}{|k^2 a^2|} \left\{ \frac{+ \sinh 2\alpha_{10} d_2}{\alpha_{10}} - \frac{\sin 2\beta_{10} d_2}{\beta_{10}} \right\}$$

$$⑦ = \frac{2|A|^2 \, ab |k^2 a^2 - \pi^2| \left|\frac{\epsilon}{\mu}\right|}{|ka|^2}$$

B. 2 Efficiency Using High Q Material

Certain simplifications to the above formulation can be made in some cases. If the loss tangent of the material is small enough so that $e^{\alpha_{10} d_1}$, $e^{\alpha_{10} d_2}$ are nearly unity, then the cavity fields can be represented by unattenuated exponentials for purposes of calculating losses in the cavity. The power radiated can be calculated simply by multiplying the power flow in the incident wave by $(1 - |R|^2)$. The problem will be reformulated using these assumptions. It should be noted that the assumption of unattenuated exponentials will hold if the loss tangent is sufficiently low even in cases where a low efficiency may result due to the high reflection coefficient. In Sections B. 2 and B. 3, μ, ϵ, k are assumed to be real as used in the equations. For purposes of calculation, μ may be replaced by μ', ϵ by ϵ', and k by $\omega\sqrt{\mu'\epsilon'}$ in Eqs. B. 17 through B. 30.

$$|E_{x1}|^2 = \sin^2 \frac{\pi y}{a} \left[1 + |R|^2 + 2|R| \cos (2\beta_{10} z + \theta_r) \right] \qquad \text{(B. 17)}$$

$$|H_{y1}|^2 = \frac{(k^2a^2 - \pi^2)}{k^2a^2} \frac{\epsilon}{\mu} \sin^2 \frac{\pi y}{a}$$

$$\left[1 + |R|^2 - 2|R| \cos (2\beta_{10} z + \theta_r)\right]$$

$$H_{z1}{}^2 = \frac{\pi^2}{k^2a^2} \frac{\epsilon}{\mu} \cos^2 \frac{\pi y}{a}$$

$$\left[1 + |R|^2 + 2|R| \cos (2\beta_{10} z + \theta_r)\right]$$

Region No. 1

$$|E_{x2}|^2 = 2|A|^2 (1 - \cos 2\beta_{10} z') \sin^2 \frac{\pi y}{a}$$

$$|H_{y2}|^2 = 2|A|^2 \frac{(k^2a^2 - \pi^2)}{k^2a^2} \frac{\epsilon}{\mu} (1 + \cos 2\beta_{10} z') \sin^2 \frac{\pi y}{a}$$

$$|H_{z2}|^2 = 2|A|^2 \frac{\pi^2}{k^2a^2} \frac{\epsilon}{\mu} (1 - \cos 2\beta_{10} z') \cos^2 \frac{\pi y}{a}$$

Region No. 2

(B. 18)

Radiated Power

$$\text{Radiated power} = \left[1 - |R|^2\right] \frac{\sqrt{k^2a^2 - \pi^2}}{ka} \sqrt{\frac{\epsilon}{\mu}} \frac{ab}{2} = P_R \qquad \text{(B. 19)}$$

Electric Volume Losses

$$\omega\epsilon'' \iiint \left[|E_{x1}|^2 + |E_{x2}|^2\right] dv$$

$$= ka \sqrt{\frac{\epsilon}{\mu}} \frac{\epsilon''}{\epsilon} \frac{ab}{2} \left\{ - (1 + |R|^2) \frac{d_1}{a} + \frac{|R|}{\sqrt{k^2a^2 - \pi^2}} \left[\sin (2\beta_{10} d_1 - \theta_r) + \sin \theta_r\right] \right\}$$

$$+ |A|^2 ka \sqrt{\frac{\epsilon}{\mu}} \frac{\epsilon''}{\epsilon} ab \left\{ \frac{d_2}{a} - \frac{\sin 2\beta_{10} d_2}{2\sqrt{k^2a^2 - \pi^2}} \right\} \qquad \text{(B. 20)}$$

Magnetic Volume Losses

$$\omega\mu'' \iiint |H_{y1}|^2 + |H_{y2}|^2 + |H_{z1}|^2 + |H_{z2}|^2 \, dv = ① + ② + ③ + ④ \qquad \text{(B. 21)}$$

$$① = \frac{(k^2a^2 - \pi^2)}{ka}\sqrt{\frac{\epsilon}{\mu}}\,\frac{\mu''}{\mu}\,\frac{ab}{2}\left\{(1 + |R|^2)\,\frac{d_1}{a} + \frac{|R|}{\sqrt{k^2a^2 - \pi^2}}\left[\sin(2\beta_1 d_1 - \theta_r) + \sin\theta_r\right]\right\}$$

$$② = |A|^2\,\frac{k^2a^2 - \pi^2}{ka}\sqrt{\frac{\epsilon}{\mu}}\,\frac{\mu''}{\mu}\,ab\left\{\frac{d_2}{a} + \frac{\sin 2\beta_{10} d_2}{2\sqrt{k^2a^2 - \pi^2}}\right\}$$

$$③ = \frac{\pi^2}{ka}\sqrt{\frac{\epsilon}{\mu}}\,\frac{\mu''}{\mu}\,\frac{ab}{2}\left\{(1 + |R|^2)\,\frac{d_1}{a} + \frac{|R|}{\sqrt{k^2a^2 - \pi^2}}\left[\sin(2\beta_{10} d_1 - \theta_r) + \sin\theta_r\right]\right\}$$

$$④ = |A|^2\,\frac{\pi^2}{ka}\sqrt{\frac{\epsilon}{\mu}}\,\frac{\mu''}{\mu}\,ab\left\{\frac{d_2}{a} - \frac{\sin 2\beta_{10} d_2}{2\sqrt{k^2a^2 - \pi^2}}\right\}$$

Surface Resistivity Losses

$$2R_s \iint_{\text{top wall}} \left[|H_{y1}|^2 + |H_{y2}|^2 + |H_{z1}|^2 + |H_{z2}|^2\right] dy\,dz$$

$$+ 2R_s \iint_{\text{side wall}} \left[|H_{z1}|^2 + |H_{z2}|^2\right] dx\,dz + R_s \iint_{\text{back wall}} |H_{y2}|^2\,dx\,dy$$

$$= ① + ② + ③ + ④ + ⑤ + ⑥ + ⑦ \qquad \text{(B. 22)}$$

$$① = R_s\,\frac{(k^2a^2 - \pi^2)}{k^2a^2}\,\frac{\epsilon}{\mu}\,a^2\left\{(1 + |R|^2)\,\frac{d_1}{a} - \frac{|R|}{\sqrt{k^2a^2 - \pi^2}}\left[\sin(2\beta_{10} d_1 - \theta_r) + \sin\theta_r\right]\right\}$$

$$② = 2|A|^2\,R_s\,\frac{(k^2a^2 - \pi^2)}{k^2a^2}\,\frac{\epsilon}{\mu}\,a^2\left\{\frac{d_2}{a} + \frac{\sin 2\beta_{10} d_2}{2\sqrt{k^2a^2 - \pi^2}}\right\}$$

$$③ = R_s\,\frac{\pi^2}{k^2a^2}\,\frac{\epsilon}{\mu}\,a^2\left\{(1 + |R|^2)\,\frac{d_1}{a} + \frac{|R|}{\sqrt{k^2a^2 - \pi^2}}\left[\sin(2\beta_1 d_1 - \theta_r) + \sin\theta_r\right]\right\}$$

$$④ = 2|A|^2\,R_s\,\frac{\pi^2}{k^2a^2}\,\frac{\epsilon}{\mu}\,a^2\left\{\frac{d_2}{a} - \frac{\sin 2\beta_{10} d_2}{2\sqrt{k^2a^2 - \pi^2}}\right\}$$

$$⑤ = 2R_s\,\frac{\pi^2}{k^2a^2}\,\frac{\epsilon}{\mu}\,ab\left\{(1 + |R|^2)\,\frac{d_1}{a} + \frac{|R|}{\sqrt{k^2a^2 - \pi^2}}\left[\sin(2\beta_{10} d_1 - \theta_r) + \sin\theta_r\right]\right\}$$

$$⑥ = 4|A|^2 R_s \frac{\pi^2}{k^2a^2} \frac{\epsilon}{\mu} ab \left\{ \frac{d_2}{a} - \frac{\sin 2\beta_{10} d_2}{2\sqrt{k^2a^2 - \pi^2}} \right\}$$

$$⑦ = 2|A|^2 \frac{(k^2a^2 - \pi^2)}{k^2a^2} \cdot \frac{\epsilon}{\mu} \cdot ab$$

B. 3 Efficiency with Probe Near Aperture

If the probe is located near the aperture, the problem can be simplified to a single region. Let

$$\left.\begin{aligned} \Pi_y^* &= \frac{1}{\beta_1} \left(\frac{-1}{j\omega\mu} \right) \cos \beta_{10} z' \sin \frac{\pi y}{a} \\ |E_x|^2 &= \sin^2 \beta_{10} z' \sin^2 \frac{\pi y}{a} \\ |H_y|^2 &= \frac{(k^2a^2 - \pi^2)}{k^2a^2} \left(\frac{\epsilon}{\mu} \right) \cos^2 \beta_{10} z' \sin^2 \frac{\pi y}{a} \\ |H_z|^2 &= \frac{\pi^2}{k^2a^2} \left(\frac{\epsilon}{\mu} \right) \sin^2 \beta_{10} z' \cos^2 \frac{\pi y}{a} \end{aligned}\right\} \quad \text{(B. 23)}$$

$$\text{Radiated power} = (1 - |R|^2) \operatorname{Re} \int_0^a \int_0^b E_x H_y^* \, dx \, dy = (1 - |R|^2) \frac{ab}{8} \frac{\sqrt{k^2a^2 - \pi^2}}{ka} \sqrt{\frac{\epsilon}{\mu}} = \overline{P}_r \quad \text{(B. 24)}$$

Electric Volume Losses

$$\omega\epsilon'' \iiint_{\text{cavity}} \sin^2 \beta_{10} z \sin^2 \frac{\pi y}{a} \, dv = \omega\epsilon'' \frac{a^2 b}{8} \left[\frac{2d}{a} - \frac{\sin^2 \beta_{10} d}{\sqrt{k^2a^2 - \pi^2}} \right] \quad \text{(B. 25)}$$

Magnetic Volume Losses

$$\omega\mu'' \iiint_{\text{cavity}} \left[|H_y|^2 + |H_z|^2 \right] dv = \frac{\omega\mu''}{k^2a^2} \frac{a^2 b}{8} \frac{\epsilon}{\mu} \cdot \left[k^2a^2 \left(\frac{2d}{a} \right) + \frac{\sin 2\beta_{10} d}{\sqrt{k^2a^2 - \pi^2}} (k^2a^2 - 2\pi^2) \right] \quad \text{(B. 26)}$$

Resistive Wall Losses

$$R_s \iint_{\text{all walls}} |H_{tang}|^2 \, dA = \frac{R_s}{k^2a^2} \frac{a^2}{4} \frac{\epsilon}{\mu} \left[\frac{2d}{a} \left(k^2a^2 + \frac{2b}{a} \pi^2 \right) + \frac{\sin 2\beta_{10} d}{\sqrt{k^2a^2 - \pi^2}} \left(k^2a^2 - 2\pi^2 - 2\pi^2 \frac{b}{a} \right) + \frac{2b}{a} (k^2a^2 - \pi^2) \right] \quad \text{(B. 27)}$$

For Magnetic Volume Losses Only:

$$\frac{\overline{P}_L}{\overline{P}_r} = \frac{\mu''}{\mu'} \frac{\left[k^2a^2 \left(\frac{2d}{a} \right) + \frac{\sin 2\beta_{10} d}{\sqrt{k^2a^2 - \pi^2}} (k^2a^2 - 2\pi^2) \right]}{(1 - |R|^2) \sqrt{k^2a^2 - \pi^2}} \quad \text{(B. 28)}$$

For Electric Volume Losses Only:

$$\frac{\overline{P}_L}{\overline{P}_r} = \left(\frac{\epsilon''}{\epsilon'} \right) \frac{k^2a^2 \left[\frac{2d}{a} - \frac{\sin 2\beta_{10} d}{\sqrt{k^2a^2 - \pi^2}} \right]}{(1 - |R|^2) \sqrt{k^2a^2 - \pi^2}} \quad \text{(B. 29)}$$

For Resistive Wall Losses Only:

$$\frac{\overline{P}_L}{\overline{P}_r} = \frac{.00531 R_s \sqrt{\frac{\epsilon_r}{\mu_r}} \left(\frac{a}{b} \right) \left[\frac{2d}{a} \left(k^2a^2 + \frac{2b}{a} \pi^2 \right) + \frac{\sin 2\beta_{10} d}{\sqrt{k^2a^2 - \pi^2}} \left(k^2a^2 - 2\pi^2 - 2\pi^2 \frac{b}{a} \right) \right.}{ka (1 - |R|^2) \sqrt{k^2a^2 - \pi^2}} \quad \text{(B. 30)}$$

$$\left. + \frac{2b}{a} (k^2a^2 - \pi^2) \right]$$

In Eqs. B. 17 through B. 30 μ may be replaced with μ', ϵ with ϵ' and k with $\omega\sqrt{\mu'\epsilon'}$ for purposes of calculation.

APPENDIX C

PERTURBATIONAL CALCULATIONS

The effect of a coaxial feed structure on the resonant frequency of a loaded rectangular cavity slot antenna can be calculated utilizing perturbational formulations. A simplified approach which treats the antenna as a resonant cavity is discussed.

Perturbation techniques for calculating the percentage shift in resonant frequencies of cavities due to small changes in material loading or deformation of cavity walls are well known.[83, 84] The loaded rectangular cavity slot antenna may be considered as a resonant cavity since the magnitude of the aperture reflection coefficient is nearly unity for electrically small antennas. A more accurate method would be to assume a two region model with a current sheet source as in Appendix B, but this degree of sophistication is unnecessary since the shift in resonant frequency is very small in most cases. Figure 34 shows the model employed, which is a rectangular cavity resonant in the lowest (TE_{101}) mode with a perturbation caused either by the insertion of a cylindrical metal probe or by the material perturbation of a cylindrical section of material. The shift in resonant frequency may be calculated from the following formulas.[85]

Metal Probe

$$\frac{\omega - \omega_o}{\omega_o} = \frac{\iiint_{\text{probe}} \left(\mu|H_o|^2 - \epsilon|E_o|^2\right) dv}{\iiint_{\text{cavity}} \left(\mu|H_o|^2 + \epsilon|E_o|^2\right) dv} \qquad \text{(C. 1)}$$

Material Perturbation

$$\frac{\omega - \omega_o}{\omega_o} = - \frac{\iiint_{\text{cavity}} \left(\Delta\epsilon|E_o|^2 + \Delta\mu|H_o|^2\right) dv}{\iiint_{\text{cavity}} \left(\mu|H_o|^2 + \epsilon|E_o|^2\right) dv} \qquad \text{(C. 2)}$$

where

E_o and H_o are the unperturbed fields,

$\Delta\epsilon, \Delta\mu$ are the changes in material constants,

$\Delta\epsilon, \Delta\mu$ are positive for an increase in material constants,

$\Delta\epsilon, \Delta\mu$ are negative for a decrease in material constants.

$$|E_o|^2 = |E_x|^2 = \sin^2 \frac{\pi z}{d} \sin^2 \frac{\pi y}{a}$$

$$|H_o|^2 = |H_y|^2 + |H_z|^2$$

$$|H_y|^2 = \frac{(k^2a^2 - \pi^2)}{k^2a^2} \left(\frac{\epsilon}{\mu}\right) \cos^2 \frac{\pi z}{d} \sin^2 \frac{\pi y}{a}$$

$$|H_z|^2 = \frac{\pi^2}{k^2a^2} \left(\frac{\epsilon}{\mu}\right) \sin^2 \frac{\pi z}{d} \cos^2 \frac{\pi y}{a}$$

Assuming that the fields are constant over the region of perturbation, these formulas reduce to:

Metal Probe

$$\frac{\omega - \omega_o}{\omega_o} = \frac{2V}{abd} \left[\cos^2 \frac{2\pi d_1}{d} - \frac{\pi^2}{k^2a^2} \cos^2 \frac{\pi d_1}{d}\right] \qquad \text{(C. 3)}$$

$$= -\frac{2V}{abd} \quad \left(d_1 \approx \frac{d}{2}\right)$$

where V is the volume of the probe.

Material Perturbation

$$\frac{\omega - \omega_o}{\omega_o} = -\frac{2V}{abd} \left[\frac{(k^2a^2\pi^2)}{k^2a^2} \left(\frac{\Delta\mu}{\mu}\right) \cos^2 \frac{\pi d_1}{d} + \frac{\Delta\epsilon}{\epsilon} \sin^2 \frac{\pi d_1}{d}\right] \qquad \text{(C. 4)}$$

If the perturbation consists of the removal of a cylindrical section of material, leaving an

air space:

$$\frac{\omega - \omega_o}{\omega_o} = \frac{2V}{abd}\left[\frac{(k^2a^2 - \pi^2)}{k^2a^2}\left(1 - \frac{1}{\mu_r}\right)\cos^2\frac{\pi d_1}{d} + \left(1 - \frac{1}{\epsilon_r}\right)\sin^2\frac{\pi d_1}{d}\right]$$

where V is the volume of the air space.

$$= \frac{2V}{abd}\left[1 - \frac{\pi^2}{k^2a^2}\cos^2\frac{\pi d_1}{d}\right] \qquad \text{(for large } \mu_r\epsilon_r\text{)}$$

$$= \frac{2V}{abd} \quad (d_1 \approx d_2)$$

It is interesting to note that the effects of a probe and an air space of equal size cancel, the probe decreasing the resonant frequency by 2V/abd and the air space increasing the resonant frequency by the same amount.

APPENDIX D

NOTE ON MATHEMATICAL STEPS REQUIRING FURTHER JUSTIFICATION

Throughout Chapters 2, 3, and 4 certain mathematical steps have been made which cannot be justified in terms of the Riemann integral formulation. Among these are:

(a) interchange of the order of integration

(b) interchange of the order of integration and differentiation

(c) integration by parts.

Because of the singularity $e^{-jk_o r}/r$ occurring in the integrands, these steps cannot be justified by theorems of Riemann integration which require continuity of the integrand. However, the singularity is absolutely integrable, which means that we could discard a small area about the origin and justify the steps by theorems of Riemann integration. It would be preferable to formulate the problem in terms of the Lebesgue integral, for which some of the steps could be justified immediately. For example, Fubini's theorem permits the interchange of the order of integration if the integrand is absolutely integrable. Singularities of this type often occur in boundary value problems, because of the idealized nature of the sources assumed. In Chapter 2, the singularity occurs because of the idealized magnetic current sources, which after imaging, consist of a thin current sheet in free space. If the problem were formulated in terms of distributed volume sources similar to any realizable source system, the singularities would not occur.

REFERENCES

1. N. Marcuvitz, The Waveguide Handbook, Vol. 10 of The Radiation Laboratory Series, McGraw-Hill Book Co., N. Y., 1950., p. 47.

2. L. J. Chu, "Physical Limitations of Omni-Directional Antennas," J. Appl. Phys., 19, Dec. 1948, pp. 1163-1175.

3. R. F. Harrington, Time Harmonic Electromagnetic Fields, McGraw-Hill, N. Y., 1961.

4. J. A. M. Lyon, A. T. Adams, and R. M. Kalafus, "Analysis of the Miniaturization of Resonant and Non-Resonant Antennas Utilizing High "Q" Materials," Transactions NEC, 1962.

5. Proceedings of the Symposium on Microminiaturization of Electronic Assemblies, Hayden Book Company, Inc., N. Y., 1958.

6. S. A. Schelkunoff, "A Mathematical Theory of Linear Arrays," Bell System Tech. J. 22, Jan 1943, pp. 80-107.

7. W. W. Hansen, Notes on Microwaves, MIT Radiation Laboratory Report T-2.

8. C. J. Bouwkamp and N. G. de Bruijn, The Problem of Optimum Antenna Current Distribution, Phillips Research Reports, Vol. 1, 1946, pp. 135-158.

9. H. J. Riblet, "Note on the Maximum Directivity of an Antenna," IRE Proceedings, May 1948, pp. 620-623.

10. T. T. Taylor, "A Discussion of the Maximum Directivity of an Antenna," IRE Proceedings, Sept. 1948, pp. 1134-1135.

11. S. Ramo and J. R. Whinnery, Fields and Waves in Modern Radio, John Wiley and Sons, N. Y., 1953.

12. S. A. Schelkunoff and Harold Friis, Antennas - Theory and Practice, John Wiley and Sons, N. Y., 1952.

13. J. D. Kraus, Antennas, McGraw-Hill, N. Y., 1950, p. 348.

14. W. W. Hansen and J. R. Woodyard, "A New Principle in Directional Antenna Design," IRE Proceedings, Vol. 26, March 1938, pp. 333-345.

15. L. B. Felsen and N. Marcuvitz, "Slot Coupling of Rectangular and Spherical Waveguides," J. Appl. Phys., June 1953, pp. 755-770.

16. H. A. Wheeler, "Fundamental Limitations of Small Antennas," IRE Proceedings, Dec. 1947, pp. 1479-1484.

17. M. H. Cohen, "On the Bandwidth of Cavity Antennas," J. Appl. Phys., May 1954, pp. 582-587.

18. R. H. Barfield and R. E. Burgess, "Small Aerials in Dielectric Media," Wireless Engineer, Aug. 1948, pp. 246-253.

19. W. J. Polydoroff, High Frequency Magnetic Materials - Their Characteristics and Principal Applications, John Wiley and Sons, N. Y., 1960.

20. D. G. Kiely, Dielectric Aerials, Methuen and Co., Ltd., London, 1953.

21. R. C. Hansen, "Two Famous Inventions," Microwave J., Aug. 1961, p. 15.

22. M. Islam, "A Theoretical Treatment of Low-Frequency Loop Antennas with Permeable Cores," IRE Trans. PGAP, March 1963, pp. 162-169.

23. R. E. Burgess, "Iron-Cored Loop Receiving Aerial," Wireless Engineer, June 1946, pp. 172-178.

24. J. Herman, "Thin Wire Loop and Thin Biconical Antennas in Finite Media," Diamond Ord. Fuze Lab. Tech. Rept. No. TR-462, May 1957.

25. O. R. Cruzan, "Radiation Properties of a Thin Wire Loop Antenna Fmbedded in a Spherical Medium," IRE Trans. PGAP, Oct 1959, pp. 345-352.

26. Saburo Adachi, "Impedance Characteristics of a Uniform Current Loop Having a Spherical Core," Ohio State Univ. Res. Foun. Rept. No. 662-26, April 1959.

27. C. T. Tai, "Radiation From a Uniform Circular Loop Antenna in the Presence of a Sphere," Stanford Res. Inst. Tech. Rept. No. 32, 1952.

28. D. M. Grimes, "Miniaturized Resonant Antenna Using Ferrites," J. Appl. Phys., Vol. 29, No. 3, March 1958, p. 401.

29. C. Polk, "Resonance and Supergain Effects in Small Ferromagnetically or Dielectrically Loaded Biconical Antennas," IRE Trans. PGAP, Dec 1959.

30. L. Lewin, Advanced Theory of Waveguides, Iliffe and Sons, Ltd., London, 1951.

31. H. Levine and C. H. Papas, "Theory of the Circular Diffraction Antenna," J. Appl. Phys., Jan 1951, pp. 29-43.

32. C. T. Tai, "Application of a Variational Principle to Biconical Antennas," J. Appl. Phys., Nov 1949, pp. 1076-1084.

33. J. W. Galejs and T. W. Thompson, "Admittance of a Cavity-Backed Annular Slot Antenna," IRE Trans. PGAP, Nov 1962, pp. 671-678.

34. J. W. Galejs, "Admittance of a Rectangular Slot Which is Backed by a Rectangular Cavity," IRE Trans. PGAP, March 1963, pp. 119-126.

35. J. E. Storer, Variational Solution to the Problem of the Symmetrical Cylindrical Antenna, Cruft Lab. Rept. TR 101, Harvard Univ., 1952.

36. M. H. Cohen, T. H. Crowley, and C. A. Levis, The Aperture Admittance of a Rectangular Waveguide Radiating Into Half Space, Ohio State Univ. Res. Foun. Rept. 339-22 of Nov 1951.

37. V. H. Rumsey, "Traveling Wave Slot Antennas," J. Appl. Phys., Nov 1953, pp. 1358-1365.

38. M. H. Cohen, "The Normal Modes of Cavity Antennas," Doctoral Dissertation, Ohio State Univ., 1952.

39. C. A. Levis, "Variational Calculations of the Impedance Parameters of Coupled Antennas," Doctoral Dissertation, Ohio State Univ., 1956.

40. J. S. S. Kerr, "The Radiation Impedance of a Flanged Rectangular Waveguide," Doctoral Dissertation, Univ. of Ill., 1951.

41. C. C. Nash, "The Input Impedance of a Rectangular Aperture Antenna," Doctoral Dissertation, Univ. of Ill., 1949.

42. N. Marcuvitz, op. cit., p. 184.

43. V. Counter, Miniature Cavity Antennas, Microwave Laboratory, Stanford Univ., Rept. No. 105, Jan 1950.

44. R. J. Tector, The Cavity Backed Slot Antenna, Electrical Engineering Research Lab., University of Illinois, Technical Report. No 26.

45. H. M. Barlow and J. Brown, "Radio Surface Waves," Oxford Univ. Press, 1962.

46. H. Levine and J. Schwinger, "On the Radiation of Sound from an Unflanged Circular Pipe," Phys. Rev., Feb 1948, pp. 383-406.

47. B. Noble, Methods Based on the Wiener-Hopf Technique, Pergamon Press, Inc., N. Y., 1953.

48. L. A. Vajnshtehn, Propagation in Semi-Infinite Waveguides, Six papers translated by J. Schmoys, New York Univ., Inst. of Math. Sci., Rept. No. EM-63.

49. F. P. Brownell and D. E. Kendall, "Miniaturized Cavity Fed Slot Antennas," 1960 WESCON Records, Part 1, pp. 158-166.

50. F. E. Butterfield, "Dielectric Sheet Radiators," IRE Trans. PGAP, Oct 1954, pp. 152-158.

51. C. W. Morrow and J. L. Moore, "High-Dielectric Rod Antenna Arrays for UHF," Electronics, Feb 1960, pp. 60-62.

52. K. E. Niebuhr and E. H. Scheibe, Surface Wave Dielectric Disc Antenna, Univ. of Wisc. Internal Rept., Contract No. DA-36-039- sc-71158.

53. W. Rotman, Metal Clad, Progressive-Phase, Dielectric Antennas, Air Force Cambridge Research Center, Rept. No. E 5081, Nov 1951.

54. R. W. Wagner, The Dielectric Plate Antenna, USASRDL Rept. No. 2240, Fort Monmouth, New Jersey.

55. K. G. Balmain, The Radiation Pattern of a Dipole on a Finite Dielectric Sheet, Elec. Eng. Res. Lab., Univ. of Ill., Tech. Rept. No. 41, Aug 1959.

56. J. W. Eberle, C. A. Levis, and D. McCoy, "The Flared Slot: A Moderately Directive Flush Mounted Broad Band Antenna," IRE Trans. PGAP, Sept 1960, pp. 461-468.

57. B. T. Stephenson and C. H. Walter, "Endfire Slot Antennas," IRE Trans. PGAP, Oct 1954, pp. 152-158.

58. Special Issue on Electromagnetic Waves in the Earth, IRE Trans. PGAP, May 1963.

59. L. Lewin, op. cit., p. 123.

60. B. B. Baker and E. T. Copson, The Mathematical Theory of Huygens Principle, Oxford Clarendon Press, 1939, p. 157.

61. R. F. Harrington, op. cit.

62. Ibid., p. 98.

63. L. Lewin, op. cit., p. 124.

64. Ibid., p. 126.

65. Ibid., p. 126.

66. Ibid., p. 90, Eq. (4.39).

67. Ibid., p. 96, Eq. (4.52).

68. Ibid., p. 91.

69. D. S. Saxon, Notes on Lectures by Julian Schwinger, "Discontinuities in Waveguides."

70. R. F. Harrington, op. cit., Ch. 8.

71. R. E. Collin, Field Theory of Guided Waves, McGraw-Hill Book Co., N. Y., 1960, p. 349.

72. Ibid., p. 351.

73. J. A. Stratton, Electromagnetic Theory, McGraw-Hill Book Co., N. Y., 1941, p. 393.

74. R. F. Harrington, op. cit., p. 108.

75. Ibid., p.

76. C. L. Dolph, "A Saddle Point Characterization of the Schwinger Stationary Points in Exterior Scattering Problems," J. Soc. Ind. Appl. Math., Sept 1957, pp. 89-104.

77. Interim Engineering Report of Research on Miniature Zero Drag Broadband Tunable Cavity Antennas - 1 July to 30 Sept., 1953, Univ. of Oklahoma Res. Inst., Contract No. AF 33(038) - 10405.

78. C. F. Arantz, Measurement of Efficiency of Small Linearly Polarized Antennas by Reflection Coefficients, Aerial Reconnaisance Lab., Wright Air Development Center, Wright Patterson AFB, Ohio, March 1958.

79. D. E. Royal, Efficiency Measurements Using Reflection Techniques, Ramo-Wooldridge, March 1959.

80. G. A. Deschamps, "Determination of Reflection Coefficients and Insertion Loss of a Wave-Guide Junction," JAP, 24, No. 8, Aug 1953, p. 1046.

81. P. C. Butson and G. T. Thompson, "The Effect of Flanges on the Radiation Patterns of Waveguides and Sectoral Horns," IEE Proceedings, July 1959, pp. 422-426.

82. V. P. Shestopalov, A. A. Bulgakov and B. M. Bulgakov, "Theoretical and Experimental Investigations of Helix-Dielectric Aerials," Radiotekhnika i elektronika, Vol. 6, No. 7, 1961, pp. 1136-1145.

83. R. F. Harrington, op. cit., Chap. 7.

84. A. D. Berk, "Variational Principles for Electromagnetic Resonators and Waveguides," IRE Trans. PGMIT, April 1956, pp. 104-110.

85. R. F. Harrington, op. cit., p. 319.

DISTRIBUTION LIST

	Copies
DDC, Cameron Station, Arlington VA, 22314	5
AFAL (AVWE), Weight-P	
AFAL (AVWE), Wright-Patterson AFB, Ohio 45433	5
AFCRL (CRRD), L. G. Hanscom Field, Bedford, Massachusetts, 01731	1
AFBMD (Technical Library), Air Force Unit Post Office, Los Angeles 45, California	1
NASA, Attn: Librarian, Langley AFB, Va, 23265	1
NASA, Goddard Space Flight Center, Antenna Section, Code 523, Greenbelt, Maryland	1
AFEL (RALTM), Griffiss AFB, New York 13442	1
U. S. Naval Research Laboratory, Attn: Dr. A. E. Marston, Code 5250, Washington, D. C. 20370	1
Commanding Officer, Diamond Ordnance Fuse Laboratories, Attn: 240, Washington, D. C.	1
Director, U. S. Navy Electronics Laboratory, Attn: Library, San Diego, California 92152	1
National Bureau of Standards, Department of Commerce, Attn: Dr. A. G. McNish, Washington, D. C.	1
Scientific and Technical Information Facility, Attn: NASA Representative (SAK/DL), P. O. Box 5700, Bethesda, Maryland 20014	2
Adams-Russell Company, 280 Bear Hill Road, Attn: Library (Antenna Section), Waltham 54, Massachusetts	1
Aero Geo Astro Corporation, Attn: Security Officer, Edsall and Lincolnia Blvd., Alexandria, Virginia	1
Airborne Instruments Labs., Inc., Attn: Librarian (Antenna Section), Walt Whitman Road, Melville, Long Island, New York	1
American Electronic Labs., Inc., P. O. Box 552 (Antenna Section, Colmar, Pennsylvania	1
American Systems, Inc., Attn: Technical Library (Antenna Section), 1625 E. 126th Street, Hawthorne, California	1
Andrew Alfred Consulting Engineers, Attn: Librarian (Antenna Section), 299 Atlantic Avenue, Boston 10, Massachusetts	1
Bell Aircraft Corporation, Attn: Technical Library (Antenna Section), Buffalo 5, New York	1

DISTRIBUTION LIST (Cont.)

	Copies
Bell Telephone Labs., Inc., Attn: Librarian (Antenna Section), Whippany, New Jersey	1
Bendix Radio Division of Bendix Aviation Corporation, Attn: Technical Library (For Dept. 462-4), E. Joppa Road, Baltimore 4, Maryland	1
Bendix Corporation, Research Division, Attn: Technical Library (Antenna Section), P. O. Box 5115, Detroit 35, Michigan	1
Boeing Airplane Company, Attn: Technical Library, M/F Antenna Systems Staff Unit, 3801 S. Oliver, Wichita, Kansas	1
Boeing Airplane Company, Aero Space Division, Attn: Technical Library, M/F Antenna and Radomes Unit, Seattle, Washington	1
Collins Radio Company, Attn: Technical Library (Antenna Section), Cedar Rapids, Iowa	1
Convair, Attn: Technical Library (Antenna Section), Pomona, California	1
Convair, Fort Worth Division, Attn: Technical Library (Antenna Section), Grants Lane, Fort Worth, Texas	1
Dalmo Victor Company, Attn: Technical Library (Antenna Section), 1515 Industrial Way, Belmont, California	1
Dorne and Margolin, Inc., Attn: Technical Library (Antenna Section), 29 New York Avenue, Westbury, Long Island, New York 11591	1
Douglas Aircraft Co., Inc., Attn: Technical Library (Antenna Section), 3000 Ocean Park Blvd., Santa Monica, California	1
Dynatronics, Inc., Attn: Technical Library (Antenna Section), P. O. Box 2566, Orlando, Florida	1
General Electric Company, Electronics Laboratory, Attn: Technical Library, Electronics Park, Syracuse, New York	1
General Precision Lab., Division of General Precision, Inc., Attn: Technical Library (Antenna Section), 63 Bedford Road, Pleasantville, New York	1
Georgia Institute of Technology, Engineering Experiment Station, Attn: Technical Library, M/F Electronics Division, Atlanta 13, Georgia	1
Goodyear Aircraft Corporation, Attn: Technical Library, M/F Dept. 474, 1210 Massilon Road, Akron 15, Ohio	1
Granger Associates, Attn: Technical Library (Antenna Section) 1601 California Avenue, Palo Alto, California	1
Grumman Aircraft Engineering Corp., Attn: Technical Library, M/F Avionics Engineering, Bethpage, New York	1

DISTRIBUTION LIST (Cont.)

	Copies
Electronic Communications, Inc., Research Division, Attn: Technical Library, 1830 York Road, Timonium, Maryland	1
The Hallicrafters Company, Attn: Technical Library (Antenna Section), 4401 W. Fifth Avenue, Chicago 24, Illinois	1
Hoffman Laboratories, Inc., Attn: Technical Library (Antenna Section), Los Angeles 7, California	1
John Hopkins University, Applied Physics Laboratory, 8621 Georgia Ave., Silver Springs, Maryland	1
Hughes Aircraft Corporation, Attn: Technical Library (Antenna Section), Florence and Teal Street, Culver City, California	1
University of Illinois, Attn: Technical Library, (Dept. of Electrical Engineering), Urbana, Illinois	1
ITT Laboratories, Attn: Technical Library (Antenna Section), 500 Washington Avenue, Nutley 10, New Jersey	1
Jasik Laboratories, Attn: Librarian (Antenna Section), 100 Shames Drive, Westbury, New York	1
Lincoln Laboratories, Massachusetts Institute of Technology, Attn: Document Room, P. O. Box 73, Lexington 73, Massachusetts	1
Ling Temco Aircraft Corporation, Temco Aircraft Division, Attn: Librarian (Antenna Lab), Garland, Texas	1
Litton Industries, Attn: Technical Library (Antenna Section), 4900 Calvert Road, College Park, Maryland	1
Lockheed Missile and Space Division, Attn: Technical Library (M/F Dept. --58-42, Plant 1, Bldg. 130), Sunnyvale, California	1
The Martin Company, Attn: Technical Library (Antenna Section), P. O. Box 179 (Mail T-38), Denver 1, Colorado	1
The Martin Company, Attn: Charles L. Dans (T-38), P. O. Box 179, Denver 1, Colorado	1
The Martin Company, Attn: Technical Library (M/F Microwave Laboratory), Box 5837, Orlando, Florida	1
The Martin Company, Attn: Technical Library (Antenna Section), Baltimore 3, Maryland	1
W. L. Maxson Corporation, Attn: Technical Library (Antenna Section), 460 West 34th Street, New York 1, New York	1
McDonnell Aircraft Corporation, Attn: Technical Library (Antenna Section), Box 516, St. Louis 66, Missouri	1
Melpar, Inc., Attn: Technical Library (Antenna Section), 3000 Arlington Blvd., Falls Church, Virginia	1

DISTRIBUTION LIST (Cont.)

	Copies
University of Michigan, Aeronautical Research Laboratory, Willow Run, Ypsilanti, Michigan	1
Mitre Corporation, Attn: Technical Library (M/F Elec. Warfare Department D-21), Middlesex Turnpike, P. O. Box 208, Bedford, Massachusetts	1
New Mexico State University, Attn: Technical Library (M/F Antenna Department), P. O. Box 548, University Park, New Mexico	1
North American Aviation, Inc., Attn: Technical Library (M/F Engineering Dept.), 4300 E. Fifth Street, Columbus 16, Ohio	1
Autonetics, Division of North American Aviation, Inc., Attn: Technical Library (M/F Antenna Dept.), 9150 E. Imperial Way, Downer, California	1
North American Aviation, Inc., Attn: Technical Library (M/F Dept. 56), International Airport, Los Anteles 9, California	1
Northrop Aircraft Corporation, NORAIR Division, Attn: Technical Information (M/F 3125-31), 3901 N. Broadway, Hawthorne, California 90250	1
Ohio State University Research Foundation, Attn: Technical Library (M/F Antenna Laboratory), 1314 Kinnear Road, Columbus 12, Ohio	1
Philco Corporation, Government and Industrial Division, Attn: Technical Library (M/F Antenna Section), 4700 Wissachickon Avenue, Philadelphia 44, Pennsylvania	1
Radiation, Inc., Attn: Technical Library (M/F Antenna Section), Drawer 37, Melbourne, Florida	1
Radio Corporation of America, Attn: Technical Library (M/F Antenna Laboratory), Route 62, Burlington, Massachusetts	1
Radio Corporation of America, Missile and Surface Radio Division, Attn: H. J. Schrader, Moorestown, New Jersey	1
Radioplane Company, Attn: Librarian (M/F Aerospace Lab), 8000 Woodly Avenue, Van Nuys, California	1
Ramo-Wooldridge Corporation, Attn: Librarian (Antenna Lab), Canoga Park, California	1
Rand Corporation, Attn: Librarian (Antenna Lab), 1700 Main Street, Santa Monica, California	1
Rantec Corporation, Attn: Librarian (Antenna Lab), 23999 Ventura Blvd., Calabasas, California	1
Raytheon Company, Missile and Space Division, Attn: Technical Library (Antenna Section), P. O. Box 636, Santa Barbara, California	1

DISTRIBUTION LIST (Cont.)

	Copies
Raytheon Electronics Corporation, Attn: Librarian (Antenna Lab), 1089 Washington Street, Newton, Massachusetts	1
Raytheon Electronics Corporation, Attn: Librarian (Antenna Lab), Boston Post Road, Box 110, Wayland, Massachusetts	1
Republic Aviation Corporation, Applied Research and Development Div., Attn: Librarian (Antenna Lab), Farmingdale, New York	1
Sylvania Electronic System, Attn: Librarian (Mountain View Operations), P. O. Box 188, Mountain View, California	1
Sylvania Electronic System, Attn: Librarian (M/F Antenna and Microwave Lab), 100 First Street, Waltham 54, Massachusetts	1
Technical Research Group, Attn: Librarian (Antenna Section), 2 Aerial Way, Syosset, New York	1
Texas Instruments, Inc., Attn: Librarian (Antenna Lab), 600 Lemmon Avenue, Dallas 9, Texas	1
A. S. Thomas, Inc., Attn: Librarian (Antenna Lab), 355 Providence Highway, Westwood, Massachusetts	1
Westinghouse Electric Corporation, Air Arms Division, Attn: Librarian (Antenna Lab), P. O. Box 1693, Mail Stop 1299, Baltimore 3, Maryland	1
Wheeler Laboratories, Inc., Attn: Librarian (Antenna Lab), P. O. Box 561, Smithtown, New York	1